University of Strathclyde
Department of Physics

Submitted in partial fulfilment of the requirements for the degree of Doctor of Philosophy

Nonlinear Optical Effects in Cold Atomic Gases

James A. McKelvie

supervised by

Dr. G. R. M. Robb

September 20, 2016

This thesis is the result of the author's original research. It has been composed by the author and has not been previously submitted for examination which has led to the award of a degree.

SIGNED:

DATE:

Contents

List of Figures

Published material

- J. A. McKelvie, and G. R. M. Robb, Two-Photon Collective Atomic Recoil Lasing. *Atoms*, 3(4):495-508, 2015
- Enhancement of Collective Atomic Recoil Lasing by Electromagnetically Induced Transparency, poster presented at the Institute of Physics (IOP) Photon12 conference, Durham (UK), 2012

Acknowledgements

Firstly, I would like to express my sincere gratitude to my supervisor, Dr. Gordon Robb, for his support, motivation, knowledge, and endless patience. I would also like to thank my fellow Ph.D. students for the many stimulating discussions and for all the fun we have had in the last few years. I would like to thank my friends for helping keep me grounded and reminding me to step away from the keyboard once in a while. Last but not the least, I would like to thank my parents, Katrina and Michael Flaherty, for supporting me in more ways than I can count throughout my studies, the writing of this thesis and my life in general.

Science is not about building a body of known 'facts'. It is a method for asking awkward questions and subjecting them to a reality-check, thus avoiding the human tendency to believe whatever makes us feel good.

Terry Pratchett

Abstract

In this thesis the Collective Atomic Recoil Laser (CARL) model of Bonifacio et al., which described CARL by two-level atoms, is extended to describe three-level atoms with ladder and Λ energy level configurations. It is shown that, in contrast to the case of two-level atoms where the CARL instability is quenched at high pump rates with significant atomic excitation, CARL instabilities involving 3-level atoms can persist at high pump rates due to transitions between the populated states being dipole forbidden. It is also demonstrated for the ladder configuration that, when the system is operated in the two-photon superfluorescent regime, introduction of centre of mass motion and atomic bunching result in symmetry breaking in the sign of detuning from field-atom resonance. CARL instabilities involving three-level atoms with Λ energy level configurations are investigated for two distinct cases : in the first the two ground states are degenerate, whereas in the second the ground states are non-degenerate. It is demonstrated that in the degenerate case, it is possible to decouple the atomic centre of mass motion from the internal atomic degrees of freedom. It is also demonstrated that for the non-degenerate case it is possible for the the atomic motion to be decoupled from the atomic coherence but not the atomic population. The population difference remains constant throughout the interaction, so the population inversion acts as a parameter in the equation for the force experienced by the atoms. Consequently, for both the degenerate and non-degenerate Λ configurations, CARL instabilities can occur at higher pump intensities than for the case of two-level atoms.

Chapter 1

Introduction

1.1 Background

1.1.1 Optical Forces

1.1.1.1 History

The idea that light may exert a force upon matter is by no means a recent one. As early as the 17th Century, the noted mathematician and astronomer Johannes Kepler was taken by the notion that the light of the sun may be responsible for the direction of a comet's tail as it travels through the solar system. After observing Halley's Comet in 1607 he wrote that

> "The direct rays of the Sun strike upon it [the comet], penetrate its substance, draw away with them a portion of this matter, and issue thence to form the track of light we call the tail . . . In this manner the comet is consumed by breathing out is own tail"

Almost a century later, in his 1704 book "Opticks: or, a treatise of the reflexions, refractions, inflexions and colours of light" [5], Newton posited that light may consist of tiny masses travelling at incredible speed. He queried

> "Are not the gross bodies and light convertible into one another, and may not bodies receive much of their activity from the particles of light which enter their composition?"

In 1873 James Clerk Maxwell published his treatise on electricity and magnetism [6] in which he stated

> "In a medium in which waves are propagated there is a pressure in the direction normal to the wave, and numerically equal to the energy contained in unit of volume."

Maxwell's treatise is one of a number of signposts on the path to understanding not only light, but optical forces as well. Said understanding advanced another step when, in 1889, Oliver Heaviside published a derivation for the force affecting a charged particle moving through a field, referred to now as the Lorentz force. Another step occurred in 1901 when Lebedev [7] published his observation of light pressure on macroscopic objects.

By the twentieth century steps forward occurred at greater speed and by only 1903 Nichols and Hull [8] provided understanding of how light could exert force upon matter. Einstein's 1917 paper "The Quantum Theory of Radiation" [9] introduced the concept that upon absorbing a photon of energy hf, an atom experiences a matching momentum "kick" of $\frac{hf}{c}$ in the direction which the photon was travelling.

The first experimental demonstration of light exerting force upon the motion of atoms was made by O. R. Frisch in 1933 [10] when he deflected a beam of sodium atoms using light from a sodium lamp.

The invention of the laser in the 1960's greatly enhanced the intensity of optical sources available. Coupled with cooling techniques which allowed for atoms to remain in a vaporous state[11], radiation forces became a useful experimental tool.

By 1970 Ashkin [12] had successfully used optical forces to trap micron sized particles with a pair of counterpropagating, focussed beams of laser light. He continued research into trapping using optical forces, proposing and demonstrating new trap geometries in 1978 [13] and in 1980 [14].

In 1975 Hänsch and Schawlow published a paper theorising that the same forces responsible for optical trapping could, for certain optical frequency de-

tunings, be repurposed for cooling atoms using laser light [15]. Such "Doppler Cooling" as it would come to be known, was experimentally realised in 1985 by Chu et al. [16].

In the years since, numerous papers have been published with results related to optical forces. Topics covered by such papers range from new cooling schemes [16, 17], methods for atomic clocks [18, 19], optically trapping and manipulating bacteria & viruses without damage [20] and even measurement of the force generated by a single RNA polymerase enzyme pulling itself along a DNA molecule [21].

More complete histories of the subject may be found in papers such as [22, 23, 24].

1.1.1.2 Optical scattering force

The optical scattering force can be easily understood by considering the small momentum "kicks" which an atom receives when it absorbs or emits a photon.

As was mentioned previously with regards to Einstein's Quantum Theory of Radiation, a photon has a momentum $\hbar k$, where $\hbar = {}^{h}/_{2\pi}$, h is Planck's constant and k is the wavenumber of the photon. If an atom absorbs a photon, it must also absorb the "kick" of that photons momentum, i.e. a stationary atom would be moved very slightly in the direction that the photon was travelling. Similarly, when a photon is emitted from an excited atom, the photon leaves with the same characteristic photonic momentum. From simple conservation of momentum, the atom must experience a small momentum kick opposite to the direction of the departing photon.

Figure 1.1 provides a simple visual interpretation of the optical scattering force process. In the case of a laser incident upon a sample of atoms, where the frequency of the laser is close to some resonant transition of the atoms, many photons may be absorbed and subsequently re-emitted as seen in Figure 1.1(a)&(b). When absorbing, the atoms will always receive a momentum kick along the direction of propagation for the laser beam. The photons spontaneously emitted from the excited atoms may be ejected in any direction, giving corresponding

momentum kicks opposite to the direction of photonic ejection, as demonstrated in Figure 1.1(c)&(d). Averaged over many absorption/emission events, the momentum kicks from spontaneous emission average out to zero. The momentum kicks from the absorbed photons, however, will provide a net force in the direction of propagation for the laser beam. As the optical scattering force requires that photons be absorbed by the atoms, it is a dissipative effect which results in heating of the atoms[25].

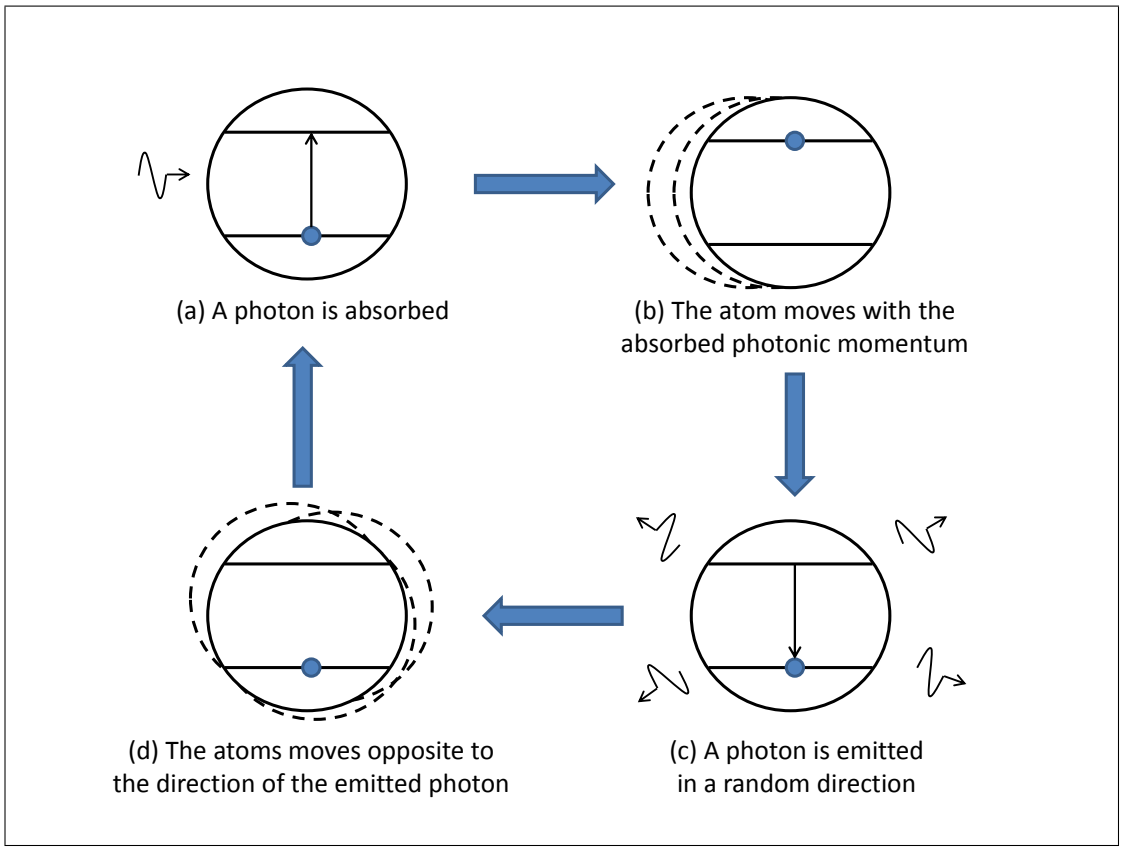

Figure 1.1: Simplified Optical Scattering Force Diagram [1]. The basic steps of the scattering force: (a) An atom absorbs a photon (b) When the atom absorbs the photon, the photon's momentum is added to that of the atom (c) The absorbed photon is re-emitted (d) The emitted photon gives the atom a momentum "kick" in the direction opposite to the direction in which it was emitted.

1.1.1.3 Optical dipole gradient force

The optical dipole gradient force, sometimes referred to as the "optical gradient force", the "gradient force" or the "dipole force", is a coherent (dispersive) optical force.

The force experienced by an atom due to the dipole force can be understood through analogy with a simple lens [26]. If a laser beam with a gaussian intensity distribution is red detuned relative to an energy level transition within an atom upon which it is incident, then the lens in the analogy is convex. Such a situation is shown in Figure 1.2(a).

In this analogy the "lens", initially some distance away from the intensity maxima of the incident light beam, focusses the light and thereby changes the direction in which the photons travel. By refracting the photons away from the optical beam the lens must, by conservation of momentum, experience a force towards the optical beam. When the lens reaches the central intensity peak of the optical beam, as can be seen in Figure 1.2(b), the forces resulting from changing the direction of the photons balance out.

If the light field is instead blue detuned with respect to the atom upon which it is incident, then the analogy can be repeated with a concave lens instead, as in Figure 1.2(c). As before, the lens alters the path the light takes. However, for a convex lens the photons are redirected towards the light beam, thus the lens experiences a force counter to this and is ejected from the optical beam.

Being proportional to the gradient of optical intensity, hence the aforementioned name "gradient force", the dipole force can occur as a result of intensity peaks in standing waves as well as the guassian beams described previously. Figure 1.3 illustrates how the intensity peaks of a standing wave result in periodic bunching of vaporous atoms.

For the case of a laser with gaussian intensity profile acting upon a positive (converging) lens, this means that the focussing of the beam moves the lens to the region of highest intensity[24].

A more rigorous description of the dipole force can be found in Metcalf and Van der Straten's "Laser Cooling and Trapping" (1999) [27] or in Gordon and

Ashkin's "Motion of atoms in a radiation trap" (1980)[26],

In the event that the population becomes entirely inverted and the atom is in the excited state, then the direction of the dipole force is reversed. For a red detuned laser the dipole force acts to force atoms with inverted populations away from regions of high intensity. Similarly, a blue detuned laser attracts inverted population atoms into regions of high intensity[22].

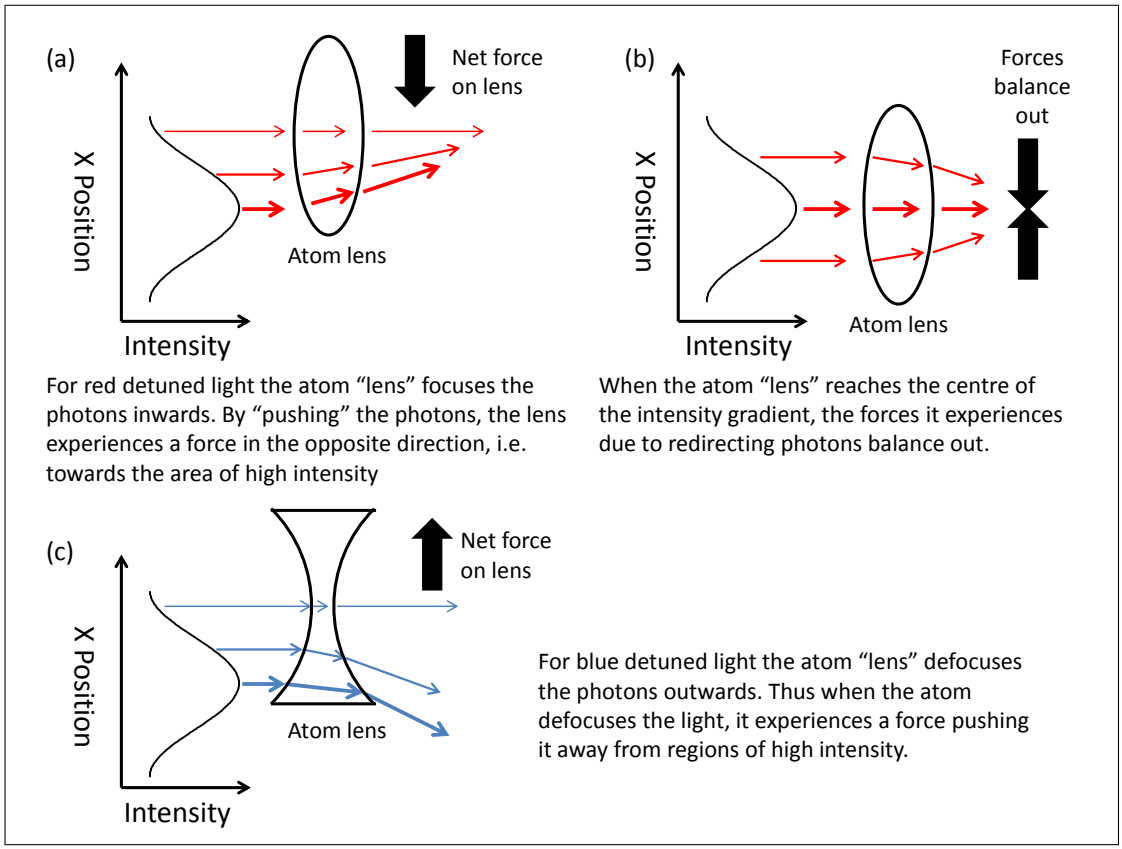

Figure 1.2: Simplified Dipole Force Atomic Lens Explanation

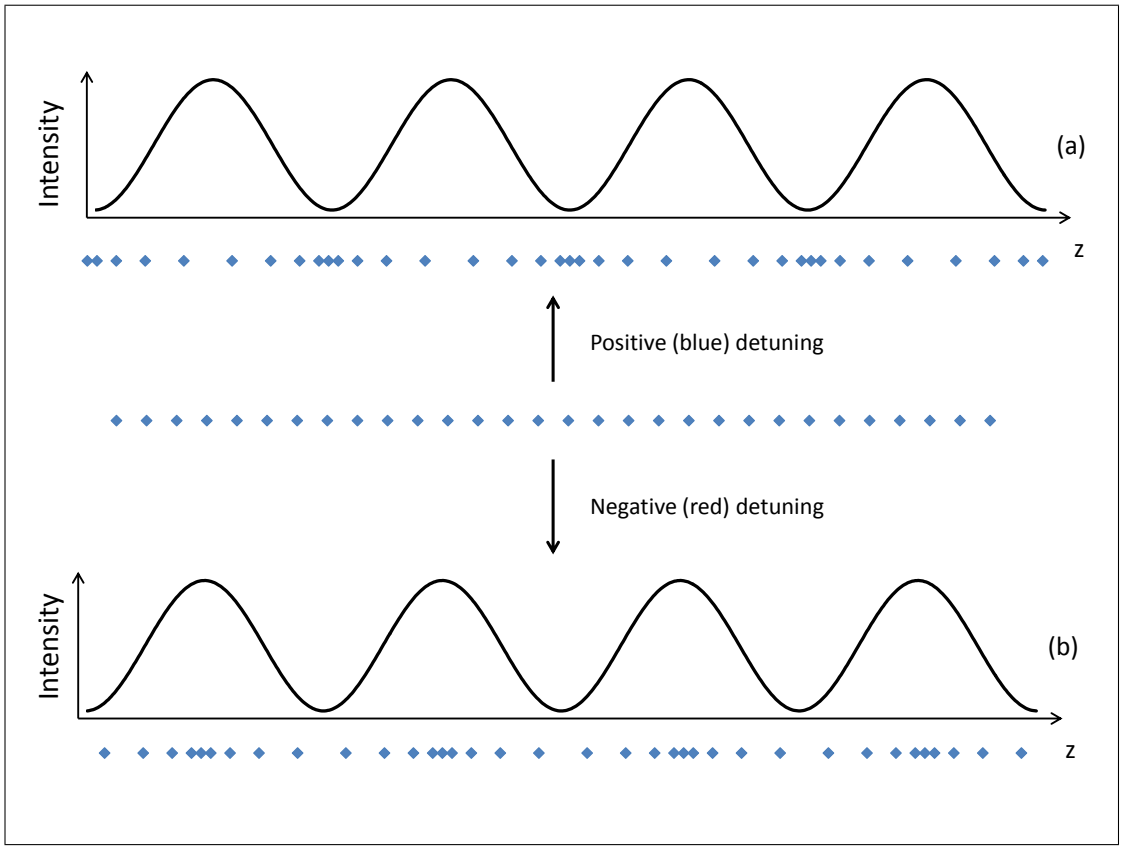

Figure 1.3: Simplified Dipole Force Diagram for (a) Positive "blue" detuning, in which atoms are drawn to areas of minimum intensity and for (b) Negative "red" detuning, in which atoms are drawn to areas of maximum intensity.

1.1.1.4 Example applications of optical forces

For a laser with a Gaussian intensity profile incident upon an atom, the atom will experience an intensity gradient orthogonal to the direction of propagation of the optical beam. If the frequency of the laser is tuned below a transition in the atom, then the optical dipole gradient force draws the atom towards the centre of the beam. If the beam is then focussed so that there exists a minimum "waist" for the beam, then there should exist a point where the pull of the optical dipole gradient force towards the intensity maximum at the beam waist balances against the scattering force of the laser. Such a system allows for the trapping and movement of atoms with only a single laser beam and is commonly referred to as "Optical tweezers".

Although the system described here uses atoms, optical tweezers have been shown to work on a multitude of matter, ranging from simple atoms, to long chain molecules, DNA chains all the way up to macrosized objects such as glass beads suspended in liquid [14, 22]. In the case of larger objects the forces involved can be understood more simply through ray diagrams.

When an atom travels towards an optical field, it "perceives" the frequency of the light as being higher than if the atom was stationary. If such an optical field is a laser source tuned below some resonance in the atom, then the atom is more likely to undergo a scattering event. When the atom first absorbs a photon from the optical field it receives a small momentum "kick" in the direction opposite its travel path. The subsequently emitted photon may be sent off in any direction, averaging out the emission "kicks" over many scattering events to a net zero. The result is a net force in the direction the laser travels. An atom travelling along a single axis between two such lasers set counterpropagating with one another would ultimately experience a loss of momentum, and thus kinetic energy, along that axis. This process would be independent of the atom travelling in the co- or counter-propagating direction as, due to Doppler shifting of the laser frequency, scattering events would be more likely to occur in the direction the atom was travelling. With three such paired counterpropagating lasers, one for each axis, atoms could be cooled solely through such scattering events. This process is

referred to as "Doppler Cooling".

1.1.2 Non-linear Optical Effects

While optical forces and the effects resulting from them result from the external degrees of freedom atoms possess, there are also many non-linear optical effects which result from an atom's internal degrees of freedom.

1.1.2.1 Optical Bistability

If a system wherein light is incident upon matter possesses more than one stable intensity value for the output optical field for a given input intensity of the optical field then such a system may be described as being optically multistable. Optical bistability is a subset of such nonlinear systems where there exist two possible stable output intensities for the optical field for one given input intensity. It was Szöke [28] who, in 1969, first considered that bistable states may be produced using optical feedback. That research was later extended by Gibbs in 1976 [29].

Optical bistability may arise as a result of one of two processes. The first, absorptive bistability, results from saturability of the absorbing material. The equation for the absorption coefficient for a two level saturable absorber can be taken to be

$$\alpha = \frac{\alpha_0}{1 + \frac{I}{I_s}} \tag{1.1.2.1}$$

where α is the absorption coefficient, α_0 is the unsaturated absorption coefficient, I is the intensity of the field in the material and I_s is the saturation intensity [30].

Considering a two level saturable absorber inside an optical cavity. It is easy to see that as the intensity of the light being pumped into the cavity increases, the value of the absorption coefficient decreases. As a result, the intensity of the light escaping the cavity increases. However, the process does not produce exactly the same result in reverse. Consider the optical output intensity vs. optical input intensity diagram shown in Figure 1.4. When the optical input intensity is slowly

increased from zero to point (a), the output intensity shows a gradual increase as a result. When the input intensity reaches point (b), the absorber becomes saturated, the optical beam passes through the absorber almost unhindered and the output intensity increases sharply. Increasing the input intensity further produces a commensurate increase in the output field along the "upper branch" of the system.

When the input intensity is lowered once again to the point (c) the material does not immediately desaturate. Consequently the optical output intensity does not decrease back to the same value it had at point (b). Instead, when the input intensity is decreased the output intensity proceeds along the aforementioned "upper branch" until it reaches point (d). At point (d) there is no longer sufficient energy being put into the system for the absorber to remain saturated, thus the output intensity drops to the point (a) once more as the absorber proceeds to "block" the passage of the input optical beam. Figure 1.4 demonstrates then a hysteresis curve where there exists a region in where the output intensity may have one of two values for a given input intensity.

The second method for achieving bistability is known as dispersive bistability. In this second process the system operates far detuned from resonance, so the absorption coefficient is typically considered to be negligibly small ($\alpha \approx 0$). Instead, the physical phenomena which causes bistability is a nonlinear dependence of the refractive index n upon the input intensity of the optical field. Whilst the underlying phenomena may be different, the mechanism remains much the same. It is the delay of the material responding to a diminishing input intensity which results in a higher output intensity.

More thorough explanations of bistable processes may be found in Lugiato 1984 [31] or Collins & Wasmundt 1980 [2].

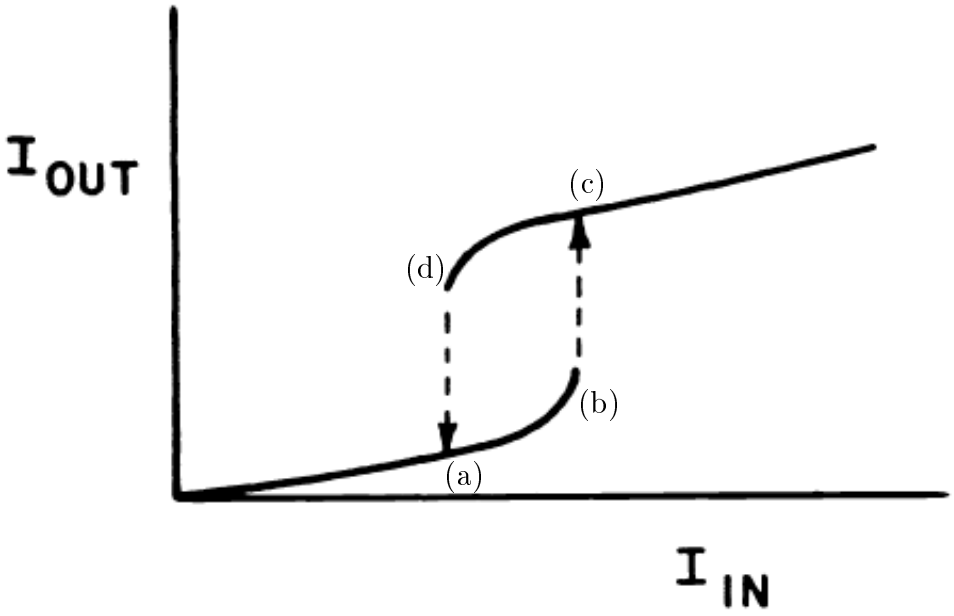

Figure 1.4: Simplified Optical Bistability Hysteresis Curve from [2].

1.1.2.2 Two Photon Absorption

The next nonlinear optical effect to be considered, one which forms in part the basis for a result in Chapter 3, is that of two photon absorption.

Consider the simplified case wherein a laser of frequency ω interacts with a cold atom which has internal energy levels $|1\rangle$, $|2\rangle$ & $|3\rangle$ in a ladder formation and is initially in level $|1\rangle$, the ground state. Such a configuration is shown in Figure 1.5.

The frequencies associated with the transitions between each of the three energy levels are given by $\omega_{21} = \omega_2 - \omega_1$, $\omega_{32} = \omega_3 - \omega_2$ and $\omega_{31} = \omega_3 - \omega_1$. If the frequency ω of the laser light is close to that of the transition frequency ω_{21} then the single photon atom-light detuning, defined as $\Delta_a = \omega - \omega_{21}$, will have a small value. In this case the atom can absorb the photon and become excited from the ground state $|1\rangle$ to the intermediate state $|2\rangle$.

If, however, the single photon detuning is large then the photon is unlikely to be absorbed and the population of state $|2\rangle$ will be negligible.

It is possible though for the single photon detunings Δ_a and $\Delta_b = \omega - \omega_{32}$ to be large but for the two photon detuning $\Delta_{ab} = 2\omega - \omega_{31}$ to be small or, as in Figure 1.5, zero. In such a scenario, the atom may absorb two photons of frequency ω and acquire population in state $|3\rangle$. This process is known as two-photon absorption. The two photon absorption rate is proportional to the product of the photonic flux for each photon [32]. For the degenerate scenario described above the two photon absorption rate is therefore proportional to the square of the photonic flux.

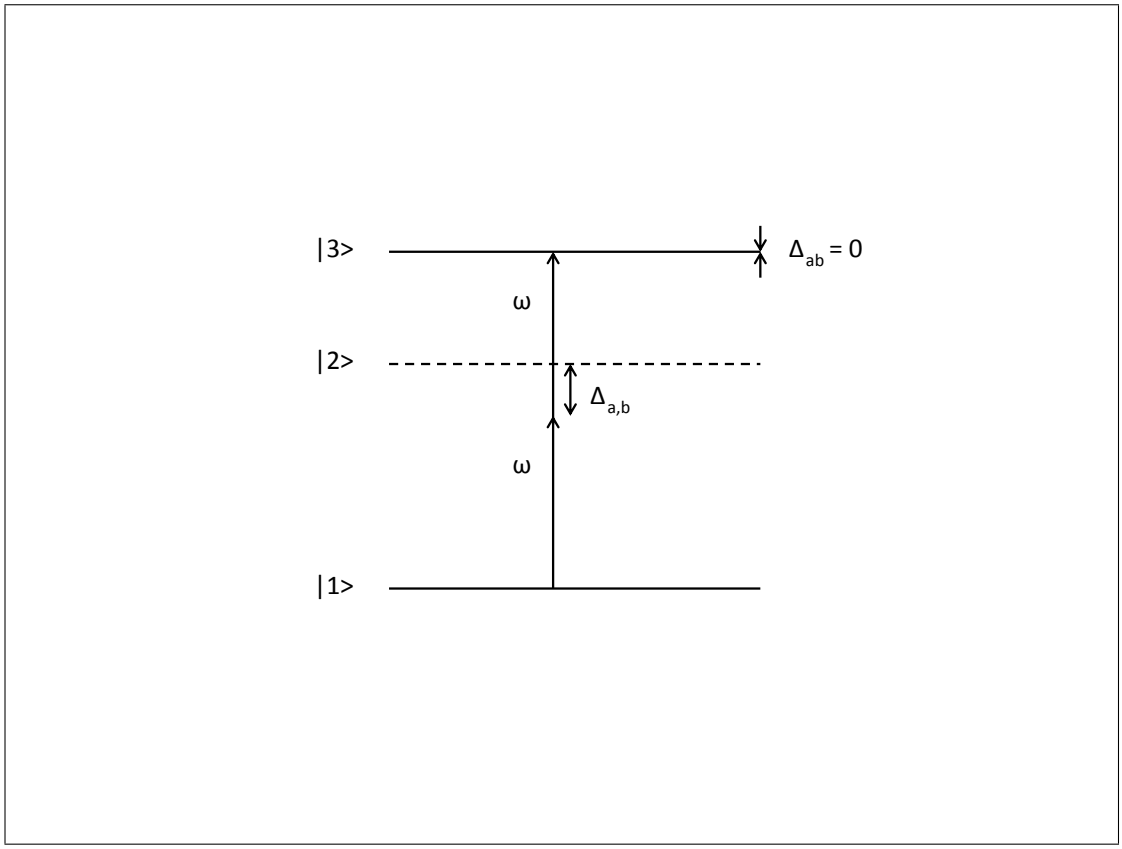

Figure 1.5: Simplified Energy Level Diagram for Two-Photon Absorption

1.1.2.3 Superradiance and Superfluorescence

The traditional picture of fluorescence from a gas of atoms assumes that each atom radiates independently. The excited state population decays exponentially by spontaneous emission with a characteristic timescale, $\tau_{spontaneous}$, proportional to the inverse of the the atomic transition's decay rate γ. The field emitted by the fluorescing system is proportional to the number of atoms, N. This behaviour is visualised in Figure 1.6(a). The typical argument made to justify this picture is that the atoms are sufficiently distanced from each other that any effect a neighbouring atom may have upon an atom's probability of emitting a photon should be negligible.

This is not always the case, as Dicke describes in his 1954 paper [33]. He argues that every atom is coupled to a common radiation field and thus may not be treated as being independent. In his paper he describes, for the first time, the nonlinear optical process known as Superradiance. Under certain conditions, a sample of N atoms which have been coherently pumped to an excited state may decay cooperatively. As the emission intensity is proportional to the square of the emission amplitude, to which each atom contributes, the maximum intensity of the superradiant pulse is proportional to the square of the number of atoms, N^2.

Superfluorescence is a similar but differentiable optical process first described in [34], though some literature refers to the processes of superradiance and superfluorescence interchangeably [3]. In a superfluorescent system the atoms are again pumped to the excited state, their populations inverted, but there exists no initial macroscopic dipole. Instead, ordinary fluorescent emission initiates the process and the system of atoms "spontaneously creates correlations"[35]. The spontaneously formed dipole then radiates a light pulse with maximum intensity proportional to the square of the number of emitting atoms, N^2, as in superradiance.

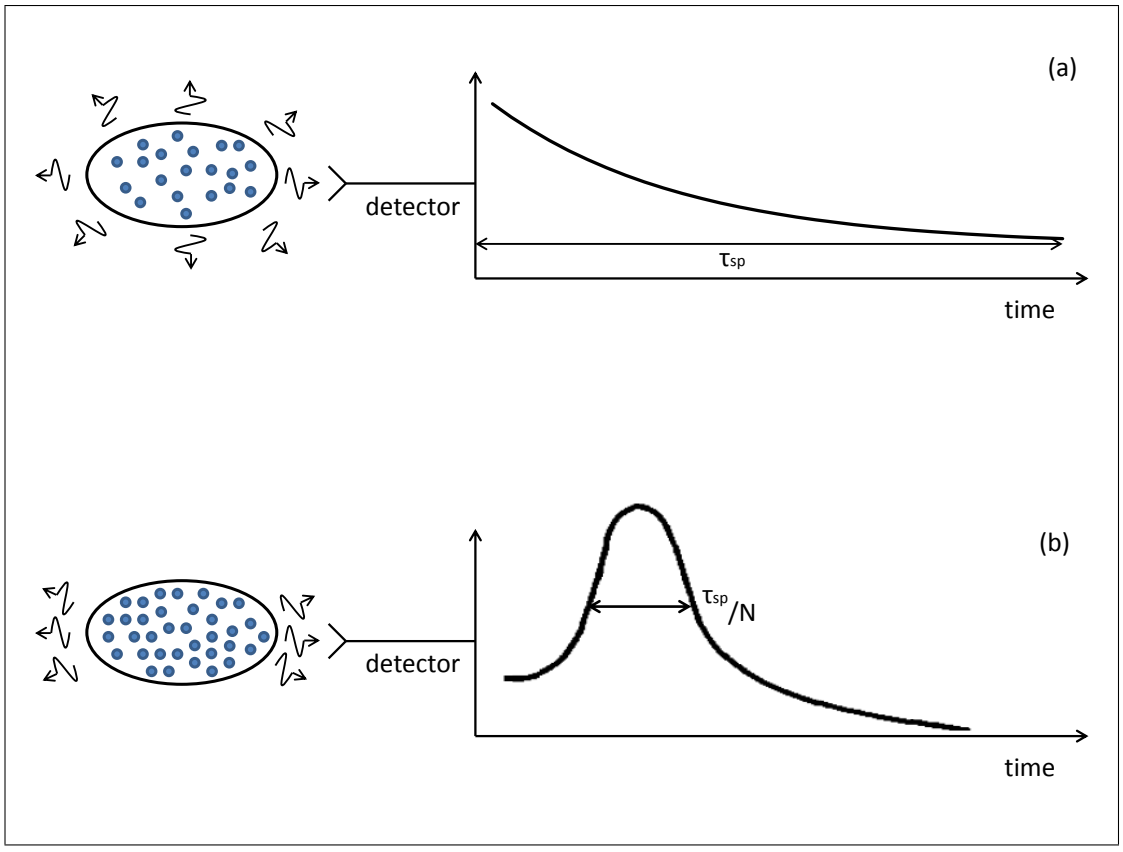

Figure 1.6: Radiated intensity vs. time for (a) Ordinary fluorescence (b) Superfluorescence. Adapted from an image in [3]

1.2 Thesis layout

In Chapter 2 the Maxwell-Bloch equations for a cloud of cold two level atoms are derived. First, equations are produced describing the evolution of the internal degrees of freedom of two level atoms as they respond to a single uniform plane electromagnetic wave. Those equations are then used to demonstrate Rabi oscillations in the atomic population and the variation of susceptibility with field-atom detuning. Second, an equation is produced which governs the evolution of a single applied field coupled to the internal degrees of freedom of the atom. It is demonstrated that, for certain parameter values, the system is optically bistable. Finally, the two level Maxwell-Bloch equations are expanded to describe the evolution of the internal degrees of freedom of the atoms and their centre of mass motion under the stimulus of two counterpropagating optical fields which evolve in time. In this form the equations are used to model an instability known as Collective Atomic Recoil Lasing.

In Chapter 3 the Maxwell-Bloch equations are expanded to describe the internal and centre of mass motional degrees of freedom of a cloud of atoms with a three level internal energy structure in a ladder configuration. The three level ladder equations are utilised to investigate two non-linear optical processes.

For the first of the two processes, two-photon CARL, two noteworthy expressions are derived. The first expression describes the required pump intensity for the population to saturate (i.e. for a significant proportion of the population to shift to the excited state). This relation allows for two regimes to be defined: The weak pump limit, where the population remains unsaturated; and the strong pump limit, wherein a significant proportion of the atomic population is excited. The second equation describes the expected gain in the probe beam in the weak pump limit. The expressions are used to compare the system in the two pump limits. It is demonstrated that, contrary to the case of two level CARL, in two-photon CARL the instability survives the transition to the strong pump regime.

The second process investigated is that of two-photon superfluorescence. It is demonstrated that, as was the case for single photon fluorescence [36], introduc-

tion of centre of mass motion and atomic bunching results in symmetry breaking in the sign of detuning from field-atom resonance. When the emitting atoms are stationary, the two-photon SF pulse is independent of the sign of detuning. When centre of mass motion is included, the atoms bunch at maxima (minima) of intensity when the field is red (blue) detuned from field-atom resonance. When the atoms bunch at the maxima of optical standing wave intensity, the optical pulse is enhanced over the case in which the atoms bunch at the point of intensity minima, wherein the optical pulse is retarded.

Chapter 4 contains a derivation of Maxwell-Bloch equations for the alternate three level Λ (lambda) atomic energy level configuration. Two variations of the Λ configuration are considered: a case where the two lower energy levels are degenerate, referred to as the degenerate Λ configuration, and a case where the two lower energy levels are not degenerate, the non-degenerate Λ configuration.

In the degenerate configuration it is demonstrated that for certain field-atom detunings it is possible to decouple the atomic centre of mass equations from the internal atomic degrees of freedom. An expression is then produced for the gain which may be expected of the system when operating in the degenerate Λ configuration.

In the non-degenerate configuration it is shown that there exist values field-atom detuning in which the atomic motion becomes decoupled from the atomic coherence but not the atomic population. Although the population does not decouple from the atomic motion, it remains constant at its initial value and acts as a parameter more than a variable.

In both the energy level configurations described in Chapter 4, the bunching force becomes divorced from the detrimental effects of the evolution of the atomic population. Discussion is given to the advantages of operating CARL in a gas of three level atoms with a Λ energy configuration over CARL in a system of two level atoms.

Chapter 5 summerises the results produced throughout the thesis and concludes with possible future work which may stem from the results presented here.

Chapter 2

Two level Collective Atomic Recoil Lasing

2.1 Collective Atomic Recoil Lasing

Collective Atomic Recoil Lasing (CARL), is a nonlinear effect which combines both external and internal degrees of atomic freedom. In simplest terms, CARL can be understood as follows: consider a gas of ultracold (microKelvin) ground state atoms being illuminated by a laser light source. If the frequency ω of the laser light is close to, but sufficiently detuned from, a transition between the ground state $|1\rangle$ and an excited energy state $|2\rangle$ within the atom, then the light may be scattered from the atomic sample.

If some of the light is scattered in the direction exactly opposing that of the incoming laser light, then a weak standing wave exists. As has been explained in Section 1.1.1.3, for a negative (red) detuning the dipole force results in atoms moving towards areas of high light intensity, so the standing wave results in a weak bunching of the atoms with a periodic spacing of $\lambda/2$.

The periodic bunching results in a cooperative backscattering of the incident laser field, which in turn results in a stronger standing wave and even tighter periodic bunching. This exponential bunching and backscattering is the heart of the CARL gain mechanism. Figure 2.1 shows a simplified representation of the CARL mechanism and the backscattering described above.

First suggested by Bonifacio and De Salvo[37], CARL has been described as "unifying the physics of traditional lasers and Free Electron Lasers" (FEL)[38]. Though the theory for CARL was published in 1994 it was almost ten years later that Kruse et al. [4] produced the first unambiguous experimental proof of the CARL instability. While previous experiments into collective atomic recoil had been undertaken, most notably by Hemmer et al. [39], Courtois et al. [40], and Lippi et al. [41], the authors were unable to demonstrate conclusively that the gain in the optical probe beam was due to an atomic density grating, the hallmark of the CARL instability, or a population/coherence grating.

The optical forces described in Chapter 1 have an insignificant effect upon thermal velocities of atoms around room temperature. Experiments involving systems of high intensity light sources, such as lasers, incident upon ultracold (microKelvin) matter, allows for optical forces to have a significant effect on atomic motion. In such systems, the long coherence times of an atom's or molecule's centre-of-mass motion may allow for interesting regimes of collective behaviour, such as CARL.

Throughout this thesis, the term CARL is used as a shorthand label to describe collective atomic instabilities involving the simultaneous growth of periodic atomic bunching on the scale of incident optical fields with gain in an optical output field. It should be noted, however, that in the literature there exist other names for processes similar to that of CARL, such as Recoil-Induced Resonances [40], or Superradiant Rayleigh Scattering [42, 25].

Many studies, both theoretical and experimental, have been performed on such CARL-like interactions, involving the mechanical effect of light on cold atoms, for example instabilities involving self-organisation [25, 38, 4, 42, 43, 44, 45, 46, 47, 48, 49, 50, 51, 52, 53, 54, 55, 56, 57, 58, 59], collective cooling [60, 61, 62], and optomechanical transverse pattern formation [63, 64, 65, 66, 67].

CARL has been proposed for a number of applications, including a tunable source of high frequency light [68, 69], or as a method for bunching atoms in a particle beam [68, 69].

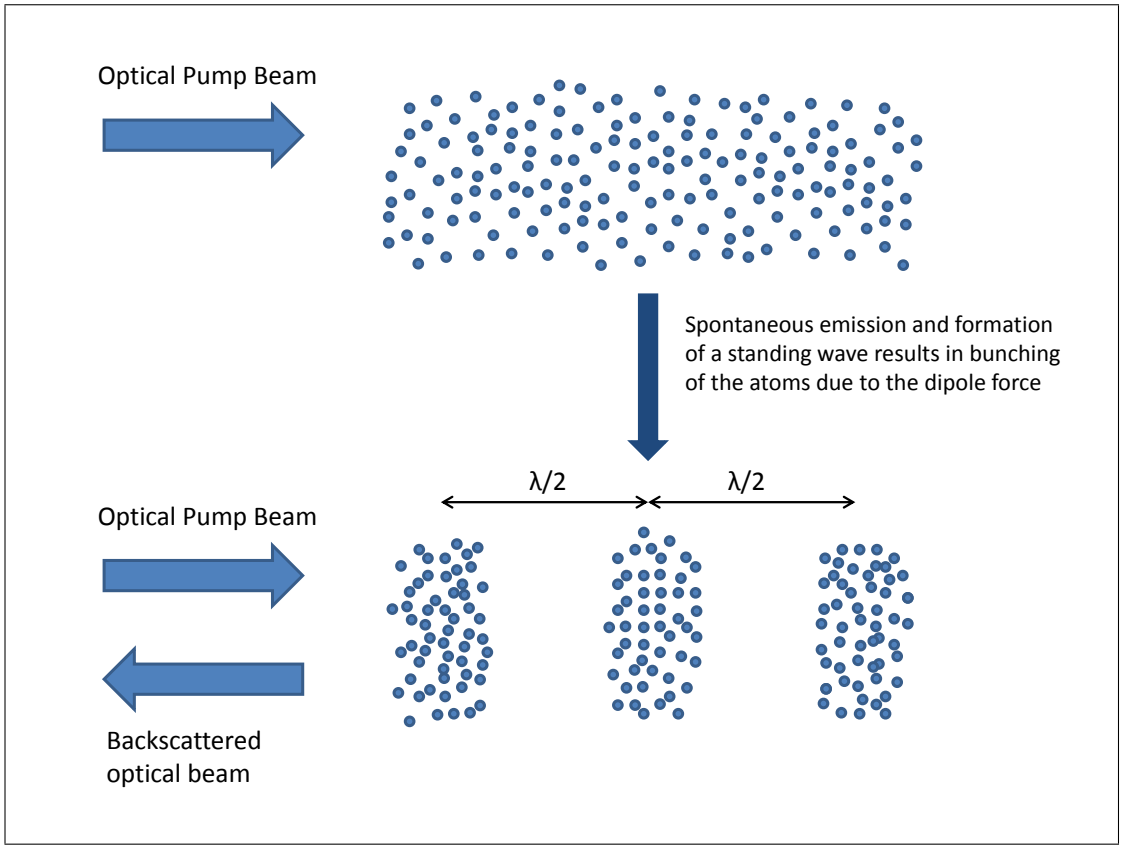

Figure 2.1: Simplified CARL Bunching and Backscattering Diagram

2.2 Derivation of the Bloch Equations

The first step in producing equations to model the CARL instability is the derivation of the governing equations for the internal degrees of freedom of the atoms in the system. These are referred to as the Bloch equations. The following derivation is reproduced from [70] as a means of introducing the notation and terminology used throughout this thesis.

The discrete states of quantised degrees of freedom in matter may be described by the quantum mechanical wavefunction ψ and the Hamiltonian operator H. The Hamiltonian's discrete eigenvalues define the set of energy levels. The eigenfunctions corresponding to those energy levels are the basis states. For the unperturbed state, the Hamiltonian may be written as H_0. The energy levels E_j are given by $\hbar\omega_j$ with the assumption made that the eigenstate which corresponds to that energy given by ψ_j, so that

$$H_0\psi_j = \hbar\omega_j\psi_j, \qquad j = 1, ..., N \tag{2.2.0.1}$$

and the eigenstates $\{\psi_j\}$ form a complete, orthonormal basis

$$\int \psi_j^*\psi_k \, d\vec{R} = \delta_{j,k}\,, \tag{2.2.0.2}$$

where $\delta_{j,k}$ is the Kronecker Delta,

$$\delta_{j,k} = \begin{cases} 1, & \text{if j = k} \\ 0, & \text{if j} \neq \text{k} \end{cases} \tag{2.2.0.3}$$

In cases where the photon flux is sufficiently large the electric field may be treated as being classical, and the system as a whole may be described semiclassically.

When a near chromatic light source of frequency ω is applied to a material (in the unperturbed state) which has an energy level transition frequency of $\omega_{jk} = \frac{E_j - E_k}{\hbar}$ which is close to that of the applied electric field, photons from the light source striking the atoms may then be absorbed. Such photonic absorption allows the electrons of those atoms to access higher energy states.

If the atoms are considered to consist of an electron orbiting a nucleus, and the electron coordinate with respect to the nucleus is denoted by $\vec{R}$, then:

- In the unperturbed ground state, the wavefunction is spherically symmetric and localized around a radius $|\vec{R}| = R_0$.
- In the perturbed state, the electron cloud is distorted in the direction of the electric field and an effective electric dipole is induced in the material.

The dipole induced by the applied light source oscillates and, as all classical oscillating dipoles do, radiates electromagnetic waves. It can be expected then that the induced dipoles (oscillating and emitting radiation), act to modify the electric field.
The derivation of the Bloch equations begins with the calculation of the polarisation vector. The polarisation vector may be considered to be the sum of the dipole moments of each atom in the system

$$\vec{P} = \sum_j \vec{d}_j \delta(r - r_j)\,, \tag{2.2.0.4}$$

where the dipole moment induced by the field in the jth atom, $\vec{d}_j$, is given by

$$\vec{d}_j = e \int \vec{R}\psi\psi^* \, d\vec{R} \tag{2.2.0.5}$$

In the above, $\vec{R}$ is the radius, $\vec{P}$ is the polarization vector, and e is the charge of an electron.

2.2.1 Step 1: Schrödinger's Equation

It is assumed that the wavefunction $\psi(\vec{R}, t)$ satisfies Schrödinger's Equation

$$i\hbar\frac{\partial\psi}{\partial t} = H\psi\,, \tag{2.2.1.1}$$

where the Hamiltonian H is the sum of the unperturbed Hamiltonian and the perturbed vector potential

$$H = H_0 + \delta V\,. \tag{2.2.1.2}$$

The perturbation potential δV, ordinarily be given by $\delta V = -e\int \vec{E}.d\vec{R}$, may instead be written as $\delta V = -e\vec{E}.\vec{R}$ as $\vec{E}(\vec{r}, t)$ changes very little over atomic distances as measured by R. The Hamiltonian then takes the form

$$H = H_0 - e\vec{E}.\vec{R} \tag{2.2.1.3}$$

where $\vec{E}$ is treated as approximately constant over interatomic distances $|\vec{R}|$. The perturbation potential δV is considered to be much smaller than the potential $V_0(\vec{R})$ of the unperturbed Hamiltonian H_0 for the laser intensities considered here. As the atoms are considered to possess no chemical bonds, neither vibrations nor rotations around chemical bonds play any role within the system. As a result, the potential $V_0(\vec{R})$ due to the the unperturbed Hamiltonian is considered to be simply the Coulomb potential.

2.2.2 Step 2: The Unperturbed States

Schrödinger's equation can be solved by assuming that the wavefunction $\psi(\vec{R},t)$ may be written as

$$\psi(\vec{R},t) = \sum_{j=1}^{N} a_j(t)\psi_j(\vec{R}) \tag{2.2.2.1}$$

where the $\psi_j(\vec{R})$ terms are the unperturbed states and the $a_j(t)$ terms are time dependent probability amplitudes. This equation simply describes how a time dependence factor is applied to the wavefunction.

The unperturbed states can be arranged to have the properties that

$$\int \vec{R}\,\psi_j(\vec{R})\,d\vec{R} = 0 \tag{2.2.2.2}$$

and

$$\int \vec{R}\,\psi_j\,\psi_j^*\,d\vec{R} = 0 \tag{2.2.2.3}$$

Which means that the expectation value of the position is zero, the states are spherically symmetric around the atomic centre of mass.

If $H = H_0$, then it can be written that

$$a_j(t) = a_j(0)e^{-i\omega_j t} \tag{2.2.2.4}$$

2.2.3 Step 3: The Polarization

As previously stated, the polarization or dipole moment, for a single atom is given by

$$\vec{d} = e \int \vec{R}\, \psi\, \psi^* d\vec{R} \tag{2.2.3.1}$$

Using (2.2.2.1) to expand the wave functions gives

$$\vec{d} = e \int \vec{R} \left(\sum_{j=1}^{N} a_j(t) \psi_j(\vec{R}) \right) \left(\sum_{k=1}^{N} a_k^*(t) \psi_k^*(\vec{R}) \right) d\vec{R} \tag{2.2.3.2}$$

The probability amplitude terms $a_{j,k}(t)$ are independent of $\vec{R}$ and may therefore be extracted from the integral leaving

$$\vec{d} = \sum_{j,k=1}^{N} a_j(t) a_k^*(t)\ \ e \int \vec{R}\, \psi_k^*(\vec{R})\, \psi_j(\vec{R})\, d\vec{R} \tag{2.2.3.3}$$

The time dependent density matrix elements are defined as

$$\rho_{jk} = a_j a_k^* \tag{2.2.3.4}$$

And the time independent dipole matrix terms are defined as

$$\vec{p}_{jk} = e \int \vec{R}\, \psi_j^*\, \psi_k\, d\vec{R} \tag{2.2.3.5}$$

So the dipole moment for a single atom is therefore

$$\begin{aligned} \vec{d} &= \sum_{j,k} \rho_{jk}\, \vec{p}_{kj} \\ &= Trace(\vec{p}\rho) \end{aligned} \tag{2.2.3.6}$$

i.e. the polarization per atom is given by the trace of the matrix multiplication of $\vec{p}$ and ρ.

It is preferable to work with density matrix elements $\rho_{jk}(t)$ rather than probability amplitudes $a_j(t)$ as density matrix elements may be directly tied to physical observables.

The diagonal terms of the density matrix, ρ, (i.e., where j=k) give the occupational probability of a particular quantum state. The off-diagonal terms of the density matrix relate directly to the coherence associated with a given transition.

In order for a particular dipole transition to occur, its corresponding dipole transition matrix element must be nonzero (i.e. for a transition from level j to level k, $\vec{p}_{jk}$ must be nonzero). The strength of the transition is determined by the magnitude of this quantity. As a result, all diagonal terms $\vec{p}_{jj}$ are zero. Off-diagonal terms may also be zero, indicating that direct transitions between those two levels are forbidden. These transition restrictions are referred to as *Selection Rules*. Having obtained equation (2.2.3.6) it can be seen that the next step to obtaining the polarisation vector is to produce equations for the density matrix elements ρ_{jk} for an atom [71].

2.2.4 Step 4: The "Raw" Bloch Equations

The first step to deriving the raw Bloch equations is to produce an equation for the probability amplitudes. Consider initially equation (2.2.1.1):

$$i\hbar\frac{\partial\psi(\vec{R},t)}{\partial t} = H\psi(\vec{R},t)\,. \tag{2.2.4.1}$$

Into this both equation (2.2.1.3) and (2.2.2.1) are substituted to produce

$$i\hbar\frac{\partial}{\partial t}\left(\sum_{j=1}^{N} a_j(t)\psi_j(\vec{R})\right) = \left(H_0 - e\vec{E}.\vec{R}\right)\left(\sum_{j=1}^{N} a_j(t)\psi_j(\vec{R})\right)\,. \tag{2.2.4.2}$$

Multiplying out the brackets on both sides, substituting in equation (2.2.0.1) and then dividing through by $i\hbar$ gives

$$\sum_{j=1}^{N}\psi_j(\vec{R})\frac{\partial a_j(t)}{\partial t} = \sum_{j=1}^{N}\left(-i\omega_j\psi_j(\vec{R})a_j(t) + \frac{ie}{\hbar}\vec{E}\cdot\vec{R}\,a_j(t)\psi_j(\vec{R})\right)\,. \tag{2.2.4.3}$$

Multiplying both sides by $\psi_k^*(\vec{R})$ gives

$$\sum_{j=1}^{N}\psi_k^*(\vec{R})\psi_j(\vec{R})\frac{\partial a_j(t)}{\partial t} = \sum_{j=1}^{N}\left(-i\omega_j\psi_k^*(\vec{R})\psi_j(\vec{R})a_j(t) + \frac{ie}{\hbar}\vec{E}\cdot\vec{R}\,\psi_k^*(\vec{R})\psi_j(\vec{R})a_j(t)\right), \tag{2.2.4.4}$$

for k = 1,...,N. Integrating this equation with respect to $\vec{R}$ throughout means that, due to equation (2.2.0.2) the terms

$$\int\psi_j^*(\vec{R})\psi_k(\vec{R})\,d\vec{R} \tag{2.2.4.5}$$

are equal to 1 when $j = k$ and 0 when $j \neq k$. Therefore, any terms multiplied by the above integral may have any j subscripts replaced by k subscripts. Additionally, as the initial k subscripts may take any value between 1 and N whereas the j subscripts are being explicitly summed between 1 and N, any summations over j containing the above integral vanish as they are the sum of only one term.

Furthermore, (2.2.3.5) allows for the substitution of the dipole matrix element $\vec{p}_{kj}$ into the equation to give

$$\frac{\partial a_k(t)}{\partial t} = -i\omega_k a_k(t) + \frac{i\vec{E}}{\hbar} \cdot \sum_{j=1}^{N} \vec{p}_{kj} a_j(t)\,, \tag{2.2.4.6}$$

for k = 1,...,N. To avoid complications regarding subscripts in the formation of the equation for the evolution of the dipole matrix elements, the subscript j is replaced by l

$$\frac{\partial a_k(t)}{\partial t} = -i\omega_k a_k(t) + \frac{i\vec{E}}{\hbar} \cdot \sum_{l=1}^{N} \vec{p}_{kl} a_l(t)\,, \tag{2.2.4.7}$$

for k = 1,...,N . Equation (2.2.4.7) is the equation for the evolution of the probability amplitude. It can be seen from the definition of the density matrix elements, given by equation (2.2.3.5), that

$$\frac{\partial \rho_{jk}(t)}{\partial t} = a_k^*(t)\frac{\partial a_j(t)}{\partial t} + a_j(t)\frac{\partial a_k^*(t)}{\partial t}\,. \tag{2.2.4.8}$$

The equation for the evolution of the probability amplitudes can therefore be manipulated to produce an equation for the density matrix elements. Taking equation (2.2.4.7), replacing the subscript k with j and multiplying by $a_k^*(t)$ gives

$$a_k^*(t)\frac{\partial a_j(t)}{\partial t} = -i\omega_j a_j(t) a_k^*(t) + \frac{i\vec{E}}{\hbar} \cdot \sum_{l=1}^{N} \vec{p}_{jl} a_l(t) a_k^*(t), \tag{2.2.4.9}$$

for j = 1,...,N. Taking the complex conjugate of (2.2.4.7) and multiplying through by $a_j(t)$

$$a_j(t)\frac{\partial a_k^*(t)}{\partial t} = i\omega_k a_j(t) a_k^*(t) - \frac{i\vec{E}}{\hbar} \cdot \sum_{l=1}^{N} \vec{p}_{kl} a_j(t) a_l^*(t), \tag{2.2.4.10}$$

for k = 1,...,N. Summing these two equations gives

$$a_k^*(t)\frac{\partial a_j(t)}{\partial t} + a_j(t)\frac{\partial a_k^*(t)}{\partial t} = -i\omega_j a_j(t)a_k^*(t) + \frac{i\vec{E}}{\hbar}\cdot\sum_{l=1}^{N}\vec{p}_{jl}a_l(t)a_k^*(t) \quad (2.2.4.11)$$

$$+ i\omega_k a_j(t)a_k^*(t) - \frac{i\vec{E}}{\hbar}\cdot\sum_{l=1}^{N}\vec{p}_{kl}a_j(t)a_l^*(t)\,, \quad (2.2.4.12)$$

for j,k = 1,...,N. Applying the product rule to the left hand side, grouping terms on $ia_j(t)a_k^*(t)$ and using the substitution from (2.2.3.4) produces

$$\frac{\partial \rho_{jk}}{\partial t} = -i(\omega_j - \omega_k)\rho_{jk} + \frac{i\vec{E}}{\hbar}\cdot\sum_{l=1}^{N}\vec{p}_{jl}\rho_{lk} - \frac{i\vec{E}}{\hbar}\cdot\sum_{l=1}^{N}\vec{p}_{lk}\rho_{jl}\,. \quad (2.2.4.13)$$

The above equation describes the evolution of the atomic internal degrees of freedom in response to an applied electric field. However, it does not yet describe the decay of coherence between internal energy levels or the decay from upper population levels to lower levels through spontaneous emission. Such processes are encapsulated through the addition of homogeneous broadening terms $-\gamma_{jk}\rho_{jk}$.

In warm atomic samples the homogeneous broadening terms additionally describe a gradual loss of energy from the levels of interest to an effective heat bath of all other material states. The terms γ_{jj} in such a system would represent the decay rates due to irreversible losses to the heat bath of lower-energy states and terms γ_{jk} decay rates with additional contributions due to the elastic collisions between the atoms. For an ultracold atomic sample (typically on the order of a few microKelvins) as is considered here, however, losses due to collision are reduced to levels considered negligible and the population is assumed conserved, such that γ_{jj} & γ_{jk} represent only spontaneous emission and decay in the coherence, as stated above. With the homogeneous broadening terms added, the Bloch equations are given the form

$$\frac{\partial \rho_{jk}}{\partial t} = -(\gamma_{jk} + i\omega_{jk})\rho_{jk} + \frac{i\vec{E}}{\hbar}\left(\sum_{l=1}^{N}\vec{p}_{jl}\rho_{lk}\right) - \frac{i\vec{E}}{\hbar}\left(\sum_{l=1}^{N}\vec{p}_{lk}\rho_{jl}\right)\,, \quad (2.2.4.14)$$

where $\omega_{jk} = \omega_j - \omega_k$. It is clear from the above equation that the density matrix elements, as a result of their relation to $\vec{E}(\vec{R}, t)$, will likewise depend upon both position $\vec{R}$ and time t. The time taken for energy to be coherently transfered from an incident optical field to a system of atoms and back again is given by the inverse of the Rabi frequency, $T_{Rabi} = \omega_{Rabi}^{-1}$, where

$$\omega_{Rabi} = \frac{Ep}{\hbar} \tag{2.2.4.15}$$

is the Rabi frequency.

From equation (2.2.0.4) for the total polarisation of the system and equation (2.2.3.6), describing the expected polarisation of a single atom, the polarization field $\vec{P}$ is given by

$$\vec{P} = \sum_j Trace(\vec{p}\rho)\delta(r - r_j)\,, \tag{2.2.4.16}$$

i.e. the sum of the diagonal terms of the matrix multiplication of $\vec{p}$ and ρ for all the atoms in the system.

2.3 Stationary atoms interacting with a single static field

Having computed the general Bloch equations, it is an easy matter to attain equations governing the reaction of the atomic system to an applied field. Easier still as for this initially considered system it is assumed that the atoms are stationary, uniformly spaced and that the field does not evolve spatially.

2.3.1 Bloch equations

The electric field can be taken to be simply

$$\vec{E} = \vec{A}_a e^{-i\omega t} + \vec{A}_a^* e^{i\omega t} \tag{2.3.1.1}$$

where ω, the frequency of the optical field, is close to the energy level transition

frequency ω_{21}. It can be assumed, for simplicity's sake, that the electric field is linearly polarised in the direction, ê, so that

$$\vec{A}(x,y,z) = \hat{e}A(x,y,z) \tag{2.3.1.2}$$

and that the direction of the dipole moment is parallel to that of the electric field. The response of the dipole moment of an atom to such an applied field can then be assumed to be of the form

$$\vec{d} = \mu\left(\sigma e^{-i\omega t} + \sigma^* e^{i\omega t}\right)\hat{e} \tag{2.3.1.3}$$

From equation (2.2.3.6) the dipole moment for the system of two level atoms is

$$\begin{aligned}\vec{d} &= Trace(\vec{p}\rho) \\ &= Trace\left(\begin{bmatrix}\vec{p}_{11} & \vec{p}_{12}\\ \vec{p}_{21} & \vec{p}_{22}\end{bmatrix}\begin{bmatrix}\rho_{11} & \rho_{12}\\ \rho_{21} & \rho_{22}\end{bmatrix}\right) \qquad (2.3.1.4)\\ &= (\vec{p}_{11}\rho_{11} + \vec{p}_{12}\rho_{21} + \vec{p}_{21}\rho_{12} + \vec{p}_{22}\rho_{22}) \qquad (2.3.1.5)\end{aligned}$$

As has already been mentioned, the terms $\vec{p}_{jj}$ are all zero, so the dipole moment for a two level atom simplifies to

$$\vec{d} = (\vec{p}_{12}\rho_{21} + \vec{p}_{21}\rho_{12}) \tag{2.3.1.6}$$

As the phase of a complex $\vec{p}_{12}$ can be included in the density matrix element ρ_{12} there is no loss of generality in taking the dipole matrix element $\vec{p}_{21}$ to be real [70, p. 165]. It has already been assumed that the dipole moment is linearly polarised parallel to the field, so it may therefore be written that

$$\vec{p}_{12} = \vec{p}_{21} = p\hat{e} = \mu\hat{e} \tag{2.3.1.7}$$

Using the above in equation (2.3.1.6) leaves

$$\vec{d} = \mu(\rho_{12} + \rho_{21})\hat{e} \tag{2.3.1.8}$$

Upon comparison with (2.3.1.3), consistency requires that

$$\rho_{21} = \sigma_{21}e^{-i\omega t} \tag{2.3.1.9}$$

It is also important to note that, by its definition in equation (2.2.3.4),

$$\rho_{21} = \rho_{12}^{*}. \tag{2.3.1.10}$$

To obtain an equation for the coherence between levels $|2\rangle$ and $|1\rangle$, ρ_{21}, the values $j = 2$ and $k = 1$ are substituted into equation (2.2.4.14) to produce

$$\begin{aligned}\frac{\partial \rho_{21}}{\partial t} =& -(\gamma_{21} + i\omega_{21})\rho_{21} \\ &+ \frac{i\vec{E}}{\hbar} \cdot (\vec{p}_{21}\rho_{11} + \vec{p}_{22}\rho_{21}) \\ &- \frac{i\vec{E}}{\hbar} \cdot (\vec{p}_{11}\rho_{21} + \vec{p}_{21}\rho_{22})\end{aligned}$$

Once again, the terms $\vec{p}_{jj}$ are zero. Taking the dot product and making the substitution (2.3.1.7) gives

$$\frac{\partial \rho_{21}}{\partial t} = -(\gamma_{21} + i\omega_{21})\rho_{21} + \frac{i\mu E}{\hbar}(\rho_{11} - \rho_{22}) \ . \tag{2.3.1.11}$$

In a similar fashion, an expression for the population of the excited state, ρ_{22}, may be obtained by substituting $j = 2$ and $k = 2$ into (2.2.4.14), giving

$$\begin{aligned}\frac{\partial \rho_{22}}{\partial t} =& -(\gamma_{22} + i\omega_{22})\rho_{22} \\ &+ \frac{i\vec{E}}{\hbar} \cdot (\vec{p}_{21}\rho_{12} + \vec{p}_{22}\rho_{22}) \\ &- \frac{i\vec{E}}{\hbar} \cdot (\vec{p}_{12}\rho_{21} + \vec{p}_{22}\rho_{22})\end{aligned}$$

From its definition as $\omega_{jk} = \omega_j - \omega_k$ the frequency term ω_{22} must be zero. Taking the dot product, the equation becomes

$$\frac{\partial \rho_{22}}{\partial t} = -\gamma_{22}\rho_{22} + \frac{i\mu E}{\hbar}(\rho_{12} - \rho_{21}) \tag{2.3.1.12}$$

Using the same method the equation for the ground state population, ρ_{11}, can be shown to be

$$\frac{\partial \rho_{11}}{\partial t} = -\gamma_{11}\rho_{11} + \frac{i\mu E}{\hbar}(\rho_{21} - \rho_{12}) \tag{2.3.1.13}$$

The above expression governs the evolution of the population of the ground state, thus population cannot decay away from level $|1\rangle$ and γ_{11} is set to zero. The population of the system is considered to be closed, thus $\rho_{11} + \rho_{22} = 1$. Any population decaying from level $|2\rangle$ must therefore be introduced to level $|1\rangle$. This population growth is expressed in the above equation through the addition of the term $+\gamma_{22}\rho_{22}$. Equation (2.3.1.13) then becomes

$$\frac{\partial \rho_{11}}{\partial t} = \gamma_{22}\rho_{22} + \frac{i\mu E}{\hbar}(\rho_{21} - \rho_{12}) \tag{2.3.1.14}$$

The equations for the two population terms may then be combined to form one equation governing the evolution of the population as a whole, rather than solving two separate population rate equations. The term D is defined as

$$D = \frac{1}{2}(\rho_{11} - \rho_{22}) \tag{2.3.1.15}$$

When the value of ρ_{22} exceeds that of ρ_{11}, i.e. the atom is most likely found in the excited state, the population is considered to be inverted. The term D is therefore referred to as the *population inversion*. When population inversion occurs, D takes a negative value. From the above definition of the D, the equation for the evolution of the population inversion is simply

$$\frac{\partial D}{\partial t} = \frac{1}{2}\left(\frac{\partial \rho_{11}}{\partial t} - \frac{\partial \rho_{22}}{\partial t}\right)$$
$$= \gamma_{22}\rho_{22} + \frac{i\mu E}{\hbar}\left(\rho_{21} - \rho_{12}\right) \tag{2.3.1.16}$$

As has already been stated, the system does not decay from the ground state ρ_{11}. Furthermore, the system only decays from ρ_{22} to the ground. It is said that the system is closed, i.e. $\rho_{11} + \rho_{22} = 1$. Since it has already been defined that the relation between the population levels and the population inversion is $D = \frac{1}{2}(\rho_{11} - \rho_{22})$, it can be shown that

$$\rho_{11} = \frac{1}{2} + D, \qquad \rho_{22} = \frac{1}{2} - D \tag{2.3.1.17}$$

Using these substitutions in equation (2.3.1.16) produces

$$\frac{\partial D}{\partial t} = -\gamma_{22}\left(D - \frac{1}{2}\right) + \frac{i\mu E}{\hbar}\left(\rho_{21} - \rho_{12}\right) \tag{2.3.1.18}$$

Owing to its definition, and the fact that the system is closed, the value of D may only vary between $-1/2$ and $1/2$. The term $-\gamma_{22}\left(D - \frac{1}{2}\right)$ results in a constant loss of population from the excited state to the ground state. To keep the system active, energy must be supplied to it so that there exists some proportion of the population in the excited state. The constant energy supply pumping the system towards the excited state (towards a negative value of D) is captured in the equation by changing the term $\gamma_{22}\frac{1}{2}$ to the term $\gamma_{22}D^{eq}$, where D^{eq} represents the term which the population tends towards at equilibrium. When D^{eq} is set to $\frac{1}{2}$ then the population in the system experiences no population pumping and relaxes to the ground state. The expression for the population then takes the form,

$$\frac{\partial D}{\partial t} = -\gamma_{22}\left(D - D^{eq}\right) + \frac{i\mu E}{\hbar}\left(\rho_{21} - \rho_{12}\right) \tag{2.3.1.19}$$

Into the above equation are substituted the expression for the optical field (2.3.1.1)

and the expression for the coherences (2.3.1.9), leaving

$$\frac{\partial D}{\partial t} = -\gamma_{22}\left(D - D^{eq}\right) + \frac{i\mu}{\hbar}\left(\sigma_{21}e^{-i\omega t} - \sigma_{12}e^{i\omega t}\right)\left(A_a e^{-i\omega t} + A_a^* e^{i\omega t}\right) . \quad (2.3.1.20)$$

Multiplying out the brackets results in terms containing $e^{\pm 2i\omega t}$. The use of the Rotating Wave Approximation allows terms which vary as $e^{\pm ni\omega t}$ (for $n \geq 2$), to be neglected under the assumption that such rapidly oscillating terms average themselves out. Equation (2.3.1.20) is then left in the form

$$\frac{\partial D}{\partial t} = -\gamma_{22}\left(D - D^{eq}\right) + \frac{i\mu}{\hbar}\left(A_a^*\sigma_{21} - A_a\sigma_{12}\right) \quad (2.3.1.21)$$

Using (2.3.1.9) and (2.3.1.15) in equation (2.3.1.11) gives it the form

$$\frac{\partial}{\partial t}\left(\sigma_{21}e^{-i\omega t}\right) = -(\gamma_{21} + i\omega_{21})\sigma_{21}e^{-i\omega t} + \frac{2i\mu E}{\hbar}D\,. \quad (2.3.1.22)$$

The product rule may be applied to the left of this equation to give

$$\frac{\partial \sigma_{21}}{\partial t}e^{-i\omega t} - i\omega\sigma_{21}e^{-i\omega t} = -(\gamma_{21} + i\omega_{21})\sigma_{21}e^{-i\omega t} + \frac{2i\mu E}{\hbar}D \quad (2.3.1.23)$$

Multiplying both sides of the equation by $e^{i\omega t}$ then moving the term $-i\omega\sigma_{21}$ to group together terms with $i\sigma_{21}$ leaves

$$\frac{\partial \sigma_{21}}{\partial t} = -\left(\gamma_{21} - i\left(\omega - \omega_{21}\right)\right)\sigma_{21} + \frac{2i\mu E}{\hbar}De^{i\omega t}\,. \quad (2.3.1.24)$$

Defining the frequency difference between the optical field and the transition frequency between levels 2 and 1 as

$$\Delta_a = \omega - \omega_{21} \quad (2.3.1.25)$$

and substituting the equation (2.3.1.1) for the optical field E, gives

$$\frac{\partial \sigma_{21}}{\partial t} = -\left(\gamma_{21} - i\Delta_a\right)\sigma_{21} + \frac{2i\mu}{\hbar} D\left(A_a e^{-i\omega t} + A_a^* e^{i\omega t}\right) e^{i\omega t}\,. \tag{2.3.1.26}$$

Multiplying out the bracket and applying the Rotating Wave Approximation, which once again allows for the neglection of terms containing exponentials of the form $e^{\pm ni\omega t}$ (for $n \geq 2$), gives

$$\frac{\partial \sigma_{21}}{\partial t} = -\left(\gamma_{21} - i\Delta_a\right)\sigma_{21} + \frac{2i\mu}{\hbar} D A_a\,. \tag{2.3.1.27}$$

While the above equations can be numerically solved in their current form, it is convenient to utilize a series of scaling terms to rewrite the Maxwell-Bloch equations in a dimensionless scaled form. For this reason, and for consistency with later equations and results, the scaling terms

$$\tau = \omega_r \rho t \tag{2.3.1.28}$$

$$\bar{A}_a = -i\sqrt{\frac{2\epsilon_0}{n\hbar\omega\rho}} A_{a,b} \tag{2.3.1.29}$$

$$\Gamma = \frac{\gamma}{\omega_r \rho} \tag{2.3.1.30}$$

$$\bar{\Delta} = \frac{\Delta}{\omega_r \rho} \tag{2.3.1.31}$$

$$\omega_r = \frac{2\hbar k^2}{m} \tag{2.3.1.32}$$

$$\rho = \left(\frac{\omega \mu^2 n}{2\epsilon_0 \omega_r^2 \hbar}\right)^{\frac{1}{3}} \tag{2.3.1.33}$$

are introduced. The term τ is the scaled time variable, $\bar{A}_a$ is the scaled field variable, Γ is the scaled decay parameter, and $\bar{\Delta}$ is the scaled field-atom detuning. The scaling terms ω_r & ρ are the recoil frequency, which is related to the recoil temperature by the relation $T_r = \frac{\hbar\omega_r}{k_B}$, and the dimensionless scaling parameter ρ, which may be regarded as the number of photons per atom in the cavity respectively. In the above expressions m is the atomic mass, k is the wave number, and $n = \frac{N}{A\mathcal{L}}$ is the density of atoms in the cavity, where A is the cross sectional

sample area and $\mathcal{L}$ is the cavity length. One of the immediate advantages of the dimensionless form is that the parameter ρ may be related to the gain in the probe beam produced by the CARL instability. Applying the scaling terms (2.3.1.28) - (2.3.1.33) to equations (2.3.1.21) and (2.3.1.27) gives

$$\frac{\partial D}{\partial \tau} = -\Gamma_{22}\left(D - D^{eq}\right) + \rho\left(\bar{A}_a^* \sigma_{21} + \bar{A}_a \sigma_{12}\right) \tag{2.3.1.34}$$

$$\frac{\partial \sigma_{21}}{\partial \tau} = -\left(\Gamma_{21} - i\bar{\Delta}_a\right)\sigma_{21} - 2\rho D \bar{A}_a\,. \tag{2.3.1.35}$$

Equations (2.3.1.34) and (2.3.1.35) describe the evolution of a system of pumped two level atoms under the effect of a constant, nondepleting optical field, $\bar{A}_a$.

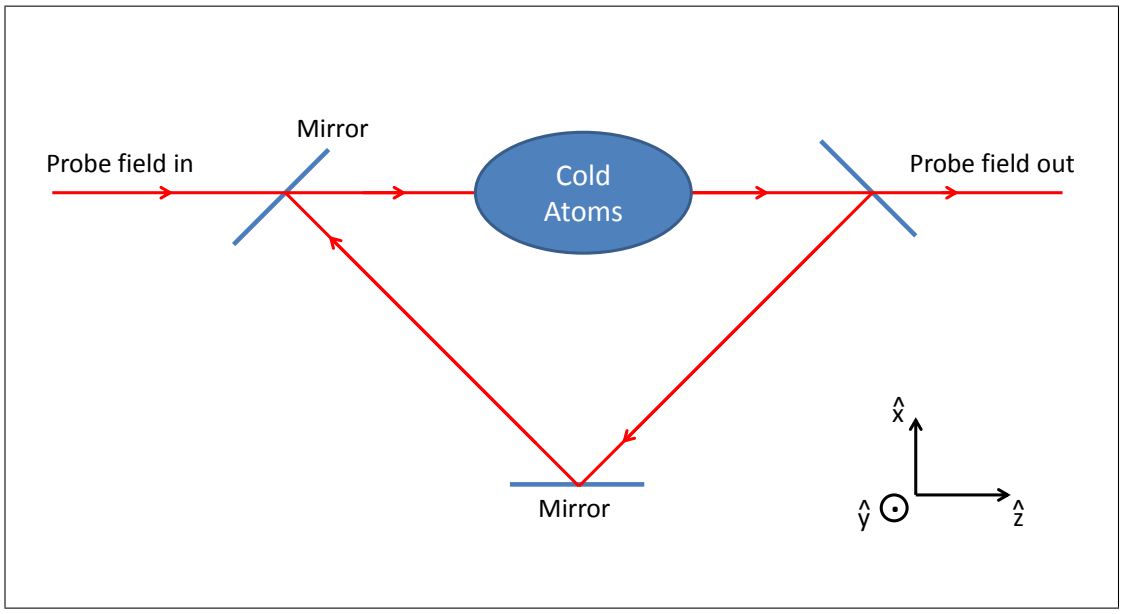

Figure 2.2: Simplified Single Field Cavity Structure Diagram

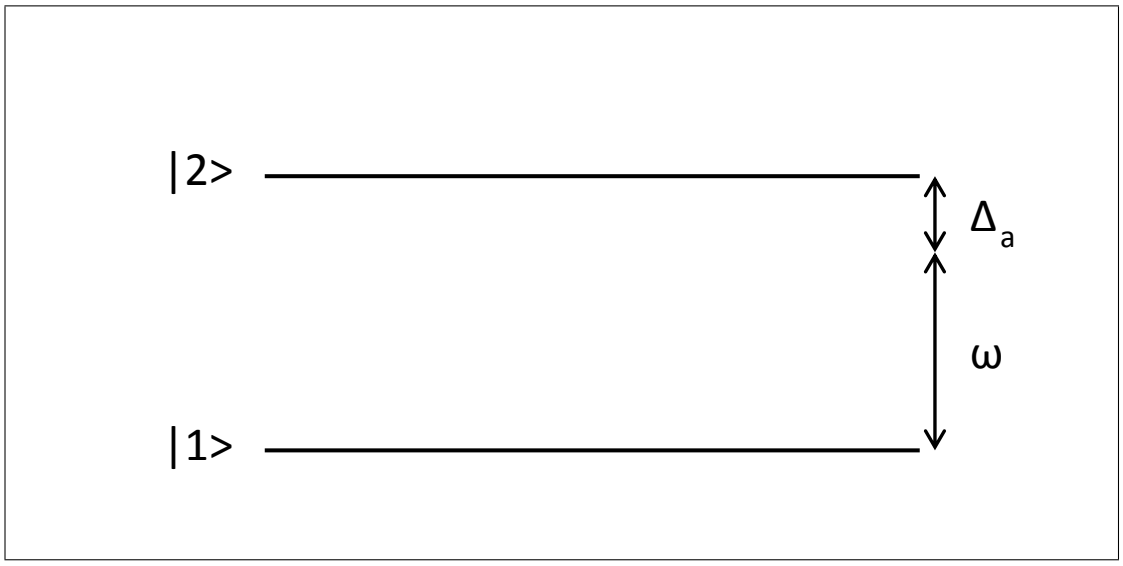

Figure 2.3: Simplified Two Level Energy Level Diagram

2.3.2 Rabi oscillations

As a step towards producing more complex simulations and verifying the accuracy of the computational methods chosen, a number of phenomena associated with a single field incident upon a sample of ultracold atoms will now be demonstrated. The first of these phenomena is that of Rabi oscillations.

2.3.2.1 Rabi oscillations at field-atom resonance

As previously stated in Section 2.2.4, the inverse of the Rabi frequency measures the time taken for energy to transfer from the field to the atoms and back. The population inversion, D, being a measure of atomic excitation, should therefore show correlation with the Rabi frequency. The oscillations in the population of a system such as the one being described currently are described as *Rabi oscillations* or *Rabi flopping*. Taking the governing equations (2.3.1.34) and (2.3.1.35), and setting $\Gamma_{21} = 0$, $\Gamma_{22} = 0$, $\bar{\Delta}_a = 0$, and $\sigma_{21}(t = 0) = 0$ reduces them to

$$\frac{\partial D}{\partial \tau} = \rho \left(\bar{A}_a^* \sigma_{21} + \bar{A}_a \sigma_{12} \right) \tag{2.3.2.1}$$

$$\frac{\partial \sigma_{21}}{\partial \tau} = -2\rho D \bar{A}_a \tag{2.3.2.2}$$

Taking $\frac{\partial}{\partial \tau}$ of equation (2.3.2.1) gives

$$\frac{\partial^2 D}{\partial \tau^2} = \rho \left(\bar{A}_a^* \frac{\partial \sigma_{21}}{\partial \tau} + \bar{A}_a \frac{\partial \sigma_{12}}{\partial \tau} \right) , \tag{2.3.2.3}$$

into which (2.3.2.2) may be substituted to give

$$\frac{\partial^2 D}{\partial \tau^2} = -4\rho^2 |\bar{A}_a|^2 D \, . \tag{2.3.2.4}$$

The above, using the substitution $\alpha = 4\rho^2 |\bar{A}_a|^2$, can be arranged to take the form

$$\frac{\partial^2 D}{\partial \tau^2} + \alpha^2 D = 0 \tag{2.3.2.5}$$

which is that of a simple harmonic oscillator of frequency α. As this equation

was obtained by neglecting and pumping or dampening terms for the system, the frequency of the oscillator should correspond to the undamped Rabi frequency, ω_{Rabi}, with a period given by

$$T_{Rabi} = \frac{2\pi}{\omega_{Rabi}} = \frac{\pi}{\rho \bar{A}_a} \,. \tag{2.3.2.6}$$

For a simple set of input values ($\rho \bar{A}_a = 3$) the expected period was $\pi/3$, which compares favourably to the output curve (a) in Figure 2.4.

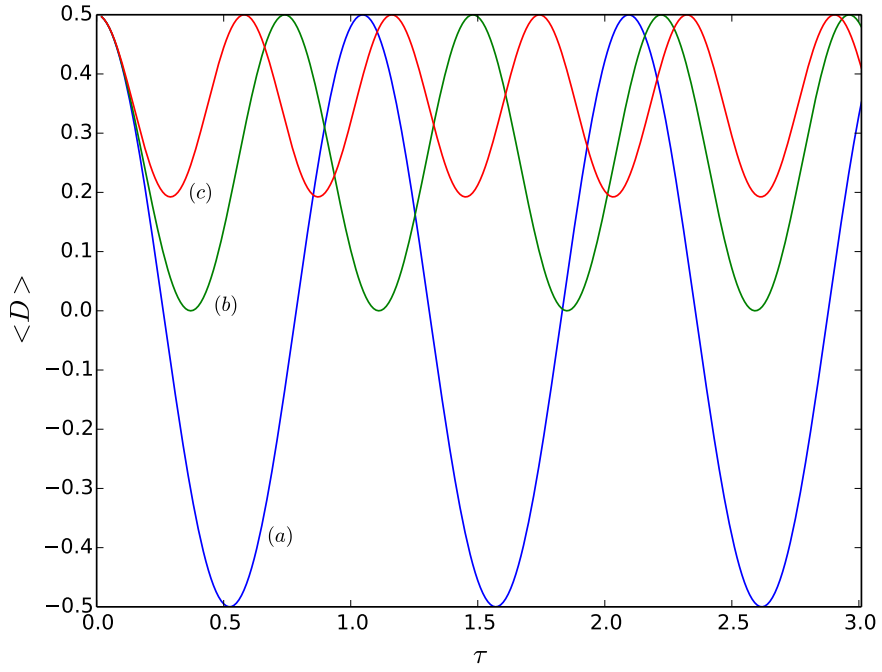

Figure 2.4: Population inversion vs. time for field-atom detunings, as described in (2.3.1.25), of (a) $\bar{\Delta}_a$=0 (No mismatch between frequencies), (b) $\bar{\Delta}_a$= 4, (c) $\bar{\Delta}_a$= 9.

2.3.2.2 Rabi oscillations including field-atom detuning

Relaxing the previous assumptions to allow for a mismatch between the frequency of the incident field and the atomic transition (i.e. ω and ω_{21} may possess different values, so that $\Delta_a \neq 0$) gives equation (2.3.1.35) the form

$$\frac{\partial \sigma_{21}}{\partial \tau} = i\bar{\Delta}_a \sigma_{21} - 2\rho D \bar{A}_a \,. \tag{2.3.2.7}$$

An expression for the evolution of D may be obtained by following a similar process as that for used in the previous section (i.e. differentiating the equation for the population inversion and substituting in for σ until the expression relies solely upon D). Including a detuning Δ_a, the expression for D may be shown to be

$$\frac{\partial^3 D}{\partial \tau^3} = -\left(\bar{\Delta}_a^2 + 4\rho^2 \bar{A}_a^2\right) \frac{\partial D}{\partial \tau} \,. \tag{2.3.2.8}$$

The period of a single Rabi oscillation should then be given by the expression

$$T_{Rabi} = \frac{2\pi}{\omega_{Rabi}} = \frac{2\pi}{\sqrt{\bar{\Delta}_a^2 + 4\rho^2 \bar{A}_a^2}} \,. \tag{2.3.2.9}$$

Keeping the value of the undampened Rabi frequency the same as for the resonant case, i.e. $\rho \bar{A}_a = 3$ but allowing the frequency to become detuned gives detuned Rabi periods of

$$T_{Rabi} = \frac{2\pi}{\sqrt{\Delta_a^2 + 4\frac{\mu^2 A_a^{R^2}}{\hbar^2}}} = \frac{2\pi}{\sqrt{(6)^2 + 4(3)^2}} \approx 0.74 \quad for\, \bar{\Delta}_a = 6$$
$$T_{Rabi} = \frac{2\pi}{\sqrt{\Delta_a^2 + 4\frac{\mu^2 A_a^{R^2}}{\hbar^2}}} = \frac{2\pi}{\sqrt{(9)^2 + 4(3)^2}} \approx 0.58 \quad for\, \bar{\Delta}_a = 9 \,.$$

These value sare consistent with the curves (b) and (c) in Figure 2.4, which were produced by numerically solving equations (2.3.1.34) and (2.3.1.35) for the values used above. As can be observed from Figure 2.4(c), even a small change in the value of the scaled detuning, $\bar{\Delta}_a$ (less than one order of magnitude) produces a significant decrease in the peak value of the population inversion.

2.3.3 Linear Susceptibility: Absorption and Dispersion

The next phenomenon to be demonstrated is that of the linear susceptibility of the atomic sample. The electric susceptibility, χ_e, is a quantity which indicates the degree of polarization which can be expected from a dielectric material in response to an applied electric field. The linear susceptibility is given by the equation

$$\vec{P} = \epsilon_0 \chi_e \vec{E} \tag{2.3.3.1}$$

[70, p. 167]. As the polarisation is given as the sum of the individual atomic coherence terms, the assumption is made that the susceptibility for a single atom may be written in scaled variables as

$$\sigma_{21} = i\bar{\chi}\bar{A}_a \ . \tag{2.3.3.2}$$

When the equation governing the evolution of the coherence, (2.3.1.35), reaches steady state, the derivative $\frac{\partial \sigma_{21}}{\partial \tau}$ is zero. When the equation is then adiabatically eliminated, then

$$\sigma_{21} = \frac{-2\rho \bar{A}_a D(\Gamma_{21} + i\bar{\Delta}_a)}{(\Gamma_{21}^2 + \bar{\Delta}_a^2)} \tag{2.3.3.3}$$

is obtained, where the field A_a has been assumed purely real. In a similar manner, the equation for the population difference may be adiabatically eliminated to give a steady state expression for D of

$$D = D^{eq} - \frac{\rho}{\Gamma_{22}}(\bar{A}_a^* \sigma_{21} + \bar{A}_a \sigma_{12}) \, . \tag{2.3.3.4}$$

By substituting the above expression for σ_{21} into the equation for the population inversion, an expression for D is obtained which no longer depends upon any other variables.

$$D = \frac{D^{eq}}{1 + \frac{4\rho^2 |\bar{A}_a|^2 \Gamma_{21}}{\Gamma_{22}(\Gamma_{21}^2 + \bar{\Delta}_a^2)}} \tag{2.3.3.5}$$

When the above expression for D at steady state is substituted back into the equation for the coherence, then a similar expression for σ_{21} is obtained which does not depend upon other variables.

$$\sigma_{21} = \frac{-2\rho\Gamma_{22}\bar{A}_a D^{eq}(\Gamma_{21} + i\Delta_a)}{(\Gamma_{22}(\Gamma_{21}^2 + \bar{\Delta}_a^2) + 4\rho^2\bar{A}_a^2\Gamma_{21})} \tag{2.3.3.6}$$

From the above and (2.3.3.2), it is trivial to obtain an expression for the scaled susceptibility of a single atom of

$$\bar{\chi} = \frac{2\rho\Gamma_{22}D^{eq}(-\Delta_a + i\Gamma_{21})}{(\Gamma_{22}(\Gamma_{21}^2 + \bar{\Delta}_a^2) + 4\rho^2\bar{A}_a^2\Gamma_{21})} \ , \tag{2.3.3.7}$$

where the real and imaginary components of the susceptibility correspond respectively to the dispersive and absorptive properties of the atom.

Figure 2.5 was produced using the same computation model as for section 2.3.2, i.e. numerically solving equations (2.3.1.21) and (2.3.1.27). Each point on the curves (a) and (b) was produced by running the model for a particular value of Δ_a until the system reached steady state, then plotting the imaginary and real components, respectively, of $\bar{\chi} = \frac{\sigma_{21}}{iA_a}$. The values used for Figure 2.5 were chosen solely to demonstrate the general shape of the absorptive and dispersive susceptibility curves, not to be representative of any particular atomic transition. As can be clearly seen, peak absorption occurs when there is zero detuning, i.e. the field is absorbed most readily when the frequency of the applied electric field exactly matches that of the energy level transition.

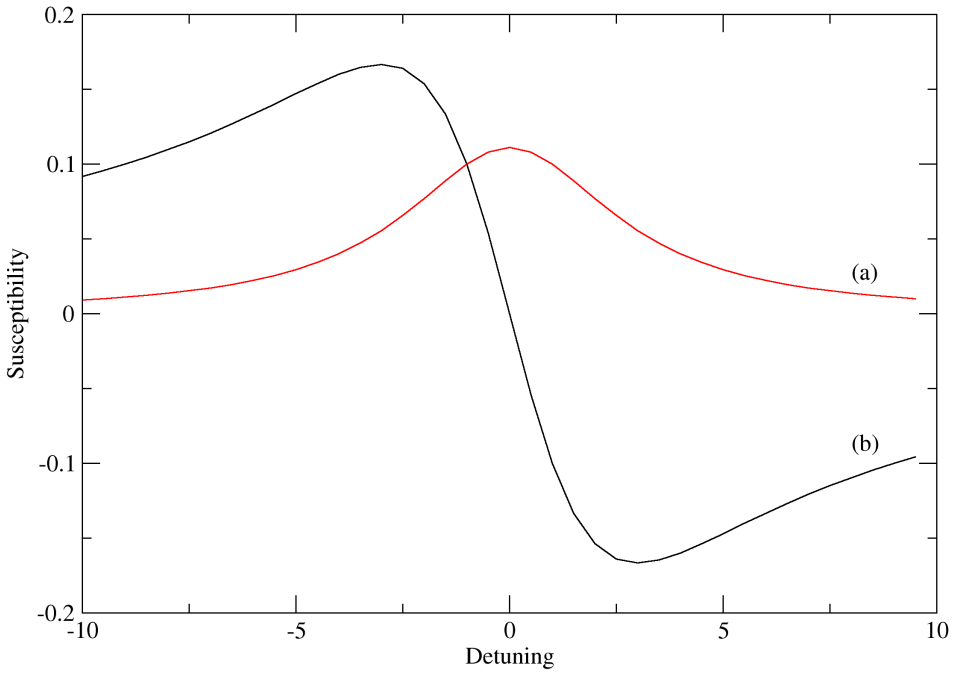

Figure 2.5: The (a) imaginary and (b) real components of $\bar{\chi}$ vs. $\bar{\Delta}_a$

2.4 Stationary atoms interacting with a single evolving field

The next advancement made to the model was to allow for temporal evolution of the optical field. In doing so it is shown that the model may become optically bistable for certain parameter values.

2.4.1 The Maxwell-Bloch equations

The governing equation for a singly polarized electric field is

$$\nabla^2\vec{E} - \frac{1}{c^2}\frac{\partial^2\vec{E}}{\partial t^2} = \frac{1}{\epsilon_0 c^2}\frac{\partial^2\vec{P}}{\partial t^2}\,, \tag{2.4.1.1}$$

that is Maxwell's wave equation in a nonlinear optical medium. Considering the optical field to be a mode of an optical cavity, such as the cavity shown in figure 2.2, then the electric field $\vec{E}$ can be written as

$$\vec{E} = \vec{A}_a(t)e^{i(kz-\omega t)} + \vec{A}_a^*(t)e^{-i(kz-\omega t)}\,. \tag{2.4.1.2}$$

It is assumed that any spatial variation of A_a or its complex conjugate are negligible and such may be described by the cavity mode rather than by terms in the wave equation. For the polarisation, $\vec{P}$, given by (2.2.0.4) to show consistency between (2.3.1.3) and (2.3.1.8) it must have the form

$$\vec{P} = \sum_j \left(\mu\left(\sigma_{21}e^{i(kz-\omega t)} + \sigma_{12}e^{-i(kz-\omega t)}\right)\hat{e}\right)\delta(r-r_j)\,. \tag{2.4.1.3}$$

Substituting (2.4.1.2) into the second term of 2.4.1.1 produces

$$\frac{\partial^2\vec{E}}{\partial t^2} = \left(\frac{\partial^2\vec{A}_a}{\partial t^2} - 2i\omega\frac{\partial\vec{A}_a}{\partial t} - \omega^2\vec{A}_a\right)e^{i(kz-\omega t)} + c.c.\,. \tag{2.4.1.4}$$

Since the only evolution of the field which is of concern is that which takes place in the z direction, the simplification of $\nabla^2 \approx \frac{\partial^2}{\partial z^2}$ gives the spatial derivative of the field to be

$$\frac{\partial^2 \vec{E}}{\partial z^2} = -k^2 \vec{A}_a e^{i(kz-\omega t)} + c.c. \tag{2.4.1.5}$$

Substituting (2.4.1.4) and (2.4.1.5) into the wave equation (2.4.1.1) results in the left hand of the equation taking the form

$$-k^2 \vec{A}_a e^{i(kz-\omega t)} - \frac{1}{c^2}\left(\frac{\partial^2 \vec{A}_a}{\partial t^2} - 2i\omega \frac{\partial \vec{A}_a}{\partial t} - \omega^2 \vec{A}_a\right) e^{i(kz-\omega t)} + c.c. \tag{2.4.1.6}$$

From the dispersion relation, $k = \frac{\omega}{c}$, so the terms $-k^2\vec{A}_a$ and $+\frac{\omega^2}{c^2}\vec{A}_a$ cancel, leaving

$$-\frac{1}{c^2}\left(\frac{\partial^2 \vec{A}_a}{\partial t^2} - 2i\omega \frac{\partial \vec{A}_a}{\partial t}\right) e^{i(kz-\omega t)} + c.c. \tag{2.4.1.7}$$

The Slowly Vary Envelope Approximation (SVEA) is the assumption that the wave packet evolves spatially and temporally slowly, so that $\frac{\partial^2 \vec{A}_a}{\partial t^2} << \omega \frac{\partial \vec{A}_a}{\partial t} << \omega^2 \vec{A}_a$, thus only the largest such term is considered. When this is applied, the left hand side of the equation reduces to

$$2i\frac{\omega}{c^2}\frac{\partial \vec{A}_a}{\partial t} e^{i(kz-\omega t)} + c.c.\ . \tag{2.4.1.8}$$

Substituting (2.4.1.3) into the right hand side of the wave equation gives

$$\begin{aligned} \frac{1}{\epsilon_0 c^2}\frac{\partial^2 \vec{P}}{\partial t^2} =& \frac{1}{\epsilon_0 c^2}\frac{\partial^2}{\partial t^2}\sum_j \vec{d}_j \delta(r - r_j(t)) \\ =& \frac{1}{\epsilon_0 c^2}\sum_j \frac{\partial^2 \vec{d}_j}{\partial t^2}\delta(r - r_j(t))\,. \end{aligned} \tag{2.4.1.9}$$

Substituting $\vec{d}_j = \mu\left(\sigma_{21}e^{i(kz-\omega t)} + \sigma_{12}e^{-i(kz-\omega t)}\right)\hat{e}$ into $\frac{\partial^2 \vec{d}_j}{\partial t^2}$ gives

$$\begin{aligned}\frac{\partial^2 \vec{d}_j}{\partial t^2} &= \frac{\partial^2}{\partial t^2}\left(\mu\left(\sigma_{21}e^{i(kz-\omega t)} + \sigma_{12}e^{-i(kz-\omega t)}\right)\hat{e}\right) \\ &= \mu\left(\left(\frac{\partial^2\sigma_{21}}{\partial t^2} - 2i\omega\frac{\partial\sigma_{21}}{\partial t} - \omega^2\sigma_{21}\right)e^{i(kz-\omega t)} + c.c.\right)\hat{e} \qquad (2.4.1.10)\end{aligned}$$

which, upon application of the SVEA, reduces to

$$\frac{\partial^2 \vec{d}_j}{\partial t^2} = -\mu\omega^2\left(\sigma_{21}e^{i(kz-\omega t)} + \sigma_{12}e^{-i(kz-\omega t)}\right)\hat{e}\,. \qquad (2.4.1.11)$$

Substituting this, equation (2.4.1.9) and (2.4.1.8) into the wave equation (2.4.1.1) gives

$$\begin{aligned}&2i\frac{\omega}{c^2}\frac{\partial \vec{A}_a}{\partial t}e^{i(kz-\omega t)} + c.c. \\ &= \frac{1}{\epsilon_0 c^2}\sum_j\Big(-\mu\omega^2\left(\sigma_{21}e^{i(kz-\omega t)} + \sigma_{12}e^{-i(kz-\omega t)}\right)\hat{e}\Big)\delta(r - r_j(t))\,. \qquad (2.4.1.12)\end{aligned}$$

To obtain an equation solely for the evolution of A_a, the above is multiplied by $e^{i(kz-\omega t)}$ and the Rotating Wave Approximation is applied, so that terms multiplied by $e^{\pm in\omega t}$ (for $n \geq 2$) may be neglected. Doing so reduces the above equation to

$$2i\frac{\omega}{c^2}\frac{\partial \vec{A}_a}{\partial t} = -\frac{1}{\epsilon_0 c^2}\sum_j\Big(\mu\omega^2\sigma_{21}\hat{e}\Big)\delta(r - r_j(t))\,. \qquad (2.4.1.13)$$

Integrating the above over the length, L, and incident area, A, of the atomic sample applies the Dirac delta function to the right hand side of the equation, giving

$$2i\frac{\omega}{c^2}\frac{\partial A_a}{\partial t}\hat{e} = -\frac{\mu\omega^2 n}{\epsilon_0 c^2}\left\langle\sigma_{21}\right\rangle\hat{e}\,. \qquad (2.4.1.14)$$

The right of the above has been multiplied by ${}^{N}/_{N}$, so that $n = N/AL$ and

$\langle \cdots \rangle = \frac{1}{N}\sum_j (\cdots)$ could be applied. When the dot product by $\hat{e}$ of both sides of the above expression is taken, the equation becomes

$$\frac{\partial A_a}{\partial t} = \frac{i\mu\omega_a n}{2\epsilon_0}\langle\sigma_{21}\rangle \ . \tag{2.4.1.15}$$

This equation describes the evolution of an idealized field, i.e. a field without losses due to mirror imperfections in the cavity. By assuming that the field amplitude A_a evolves on a timescale much longer than the time taken for a cavity round-trip ($\frac{\mathscr{L}}{c}$), the field losses can be represented by the introduction of a loss rate of $-TA_a$ per round trip, where $T = 1 - R$ is the mirror transmissivity [72]. The losses are described by

$$\left.\frac{\partial A_a}{\partial t}\right|_{losses} = -\frac{TA_a}{\mathscr{L}/c} = -\frac{cT}{\mathscr{L}}A_a = -\kappa A_a \,, \tag{2.4.1.16}$$

the detuning of the field from exact cavity resonance is described by

$$\left.\frac{\partial A_a}{\partial t}\right|_{detuning} = i(\omega - \omega_c)A_a = i\delta_c A_a \,, \tag{2.4.1.17}$$

and the injection/pumping of the field is described by

$$\left.\frac{\partial A_a}{\partial t}\right|_{injection} = \frac{\sqrt{T}A_a^{IN}}{\mathscr{L}/c} = \frac{c\sqrt{T}}{\mathscr{L}}A_a^{IN} = \frac{cT}{\mathscr{L}}\frac{A_a^{IN}}{\sqrt{T}} = \kappa A_a^{eq} \,. \tag{2.4.1.18}$$

Including these terms in (2.4.1.15) produces a more robust and realistic equation to govern the evolution of the field amplitude

$$\frac{\partial A_a}{\partial t} = \frac{i\mu\omega_a n}{2\epsilon_0}\langle\sigma_{21}\rangle + (i\delta_c - \kappa)A_a + \kappa A_a^{eq} \ . \tag{2.4.1.19}$$

To be consistent with the scaling for the equations for the population inversion

and the coherence, equations (2.3.1.34) and (2.3.1.35), the scaling terms

$$\bar{\delta}_c = \frac{\delta_c}{\omega_r \rho} \tag{2.4.1.20}$$

$$\bar{\kappa} = \frac{\kappa}{\omega_r \rho}\,, \tag{2.4.1.21}$$

along with those described in equations (2.3.1.28) - (2.3.1.33) are applied to equation (2.4.1.19) to give the scaled form of the equation for the probe field

$$\frac{\partial \bar{A}_a}{\partial \tau} = \langle \sigma_{21} \rangle + (i\bar{\delta}_c - \bar{\kappa})\bar{A}_a + \bar{\kappa}\bar{A}_a^{eq}\ . \tag{2.4.1.22}$$

2.4.2 Optical Bistability

Purely in the interest of demonstrating the evolution of the internal degrees of atomic freedom when the atoms are coupled to the cavity field, a simple bistability result is produced. By using the final values (i.e. the final values for a single iteration of the code, run for a sufficient length of time for the system to reach a steady state) for each variable in the computational model as the initial values for the next iteration, excepting the field amplitude, the bistability of the system was investigated.

While operating close to resonance, the input amplitude was increased incrementally from a low initial value. The output intensity of the system during this phase of operation proceeded along the lower transmission branch until reaching the critical turning point. Increasing the input amplitude beyond that critical point resulted in the transmitted intensity of the system to jump to the upper transmission branch as the system reached saturation point. When the input field was then gradually decreased, the output intensity remained in the upper branch even below the threshold value at which the output field had switched transmission branch. Tuning the field amplitude down further, it eventually reached a second critical turning point at which the system could no longer remain saturated, at which point the output field dropped once again to the lower transmissivity branch. Figure 2.6 demonstrates the results of this process.

By considering the field to be tuned to cavity resonance, $\bar{\delta}_c = 0$ and adiabatically eliminating equation (2.4.1.22) an expression is obtained for the value the optical field assumes at steady state,

$$\bar{A}_a = \frac{1}{\bar{\kappa}} \langle \sigma_{21} \rangle + \bar{A}_a^{eq} \,. \tag{2.4.2.1}$$

It is assumed that the term $\langle \sigma_{21} \rangle$ may be replaced by simply σ_{21} due to stationary atoms behaving in a similar manner. Into the above expression the previously obtained expression for the steady state value of the coherence, equation (2.3.3.6), is substituted to give

$$\bar{A}_a = \frac{1}{\bar{\kappa}} \left(\frac{-2\rho\Gamma_{22}\bar{A}_a D^{eq}(\Gamma_{21} + i\Delta_a)}{(\Gamma_{22}(\Gamma_{21}^2 + \bar{\Delta}_a^2) + 4\rho^2\bar{A}_a^2\Gamma_{21})} \right) + \bar{A}_a^{eq}\,, \tag{2.4.2.2}$$

where A_a, as in the derivation for (2.3.3.6), is again assumed to be purely real. Rearranging the above equation for the pump term A_a^{eq} using $\Delta_a = 0$ gives

$$\bar{A}_a^{eq} = \bar{A}_a + \frac{2\rho D^{eq}\bar{A}_a}{\bar{\kappa}\Gamma_{21}(1 + \frac{4\rho^2\bar{A}_a^2}{\Gamma_{22}\Gamma_{21}})}\,. \tag{2.4.2.3}$$

Making a comparison with equation (32) of [31] for the bistability coefficient or "cooperativity parameter", C, with equation (2.4.2.3) above, the approximation can be made that

$$C \approx \frac{2\rho D^{eq}}{\bar{\kappa}\Gamma_{21}}\,. \tag{2.4.2.4}$$

As can be seen from Figure 2.6, even a small increase in the value of the bistability coefficient gives rise to vast increase in the area over which bistability can occur. It can also be seen that there exists no bistability in Figure 2.6(a), indicating that there exists a threshold value of C which must be exceeded for bistability to occur. This behaviour matches well with the absorptive bistability described in [73], where the threshold value for bistability was $C > 4$. In terms of the above expression for C, this translates to a threshold for bistability of $C > 2$, which matches well with Figure 2.6.

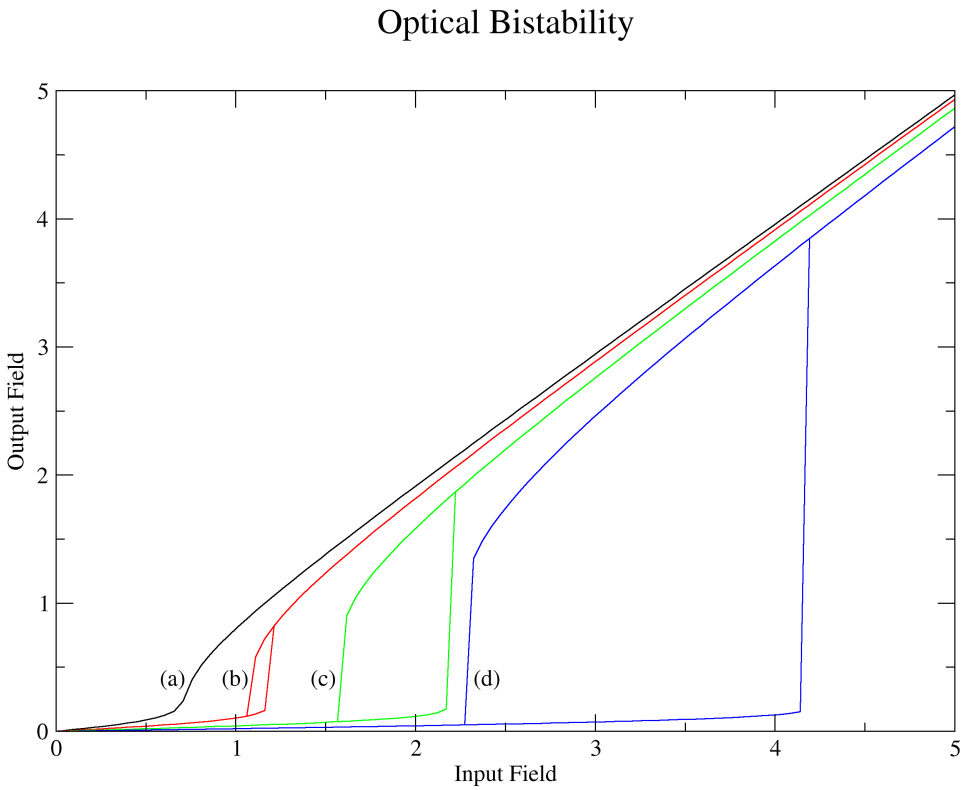

Figure 2.6: The output field for the cooperativity co-efficient C= (a) 2, (b) 4, (c) 8 and (d) 16

2.5 Moving atoms interacting with two counter-propagating, evolving fields

To fully describe the CARL model a second optical field must be added to the computational model, the fields must be allowed to evolve over time and the atoms, which until now have been considered as stationary, must be allowed to move in response to the incident optical fields. The probe beam, which may arise unseeded from noise within an experimental system, is considered to propagate in the forward direction. The pump beam is taken to run counterpropagating to the probe beam. A schematic diagram of this arrangement is shown in Figure 2.7. The total optical electric field in this system may be written as

$$\vec{E} = \left(A_a(t)e^{i(kz-\omega t)} + A_b(t)e^{i(-kz-\omega t)} + c.c.\right)\hat{e}\,. \tag{2.5.0.1}$$

The response of the dipole moment of a two level atom to such an applied field can be assumed to be of the form

$$\vec{d} = \mu\left(\sigma_{21}e^{-i\omega t} + c.c.\right)\hat{e}\,. \tag{2.5.0.2}$$

For this to be consistent with equation (2.3.1.6) then the slowly varying coherence terms $\sigma_{1,2}$ are defined as

$$\begin{aligned} \rho_{21} &= \sigma_{21}e^{-i\omega t} \\ \rho_{12} &= \sigma_{12}e^{i\omega t}\,. \end{aligned} \tag{2.5.0.3}$$

With this taken into consideration the Maxwell-Bloch equations may be derived in much the same manner as before.

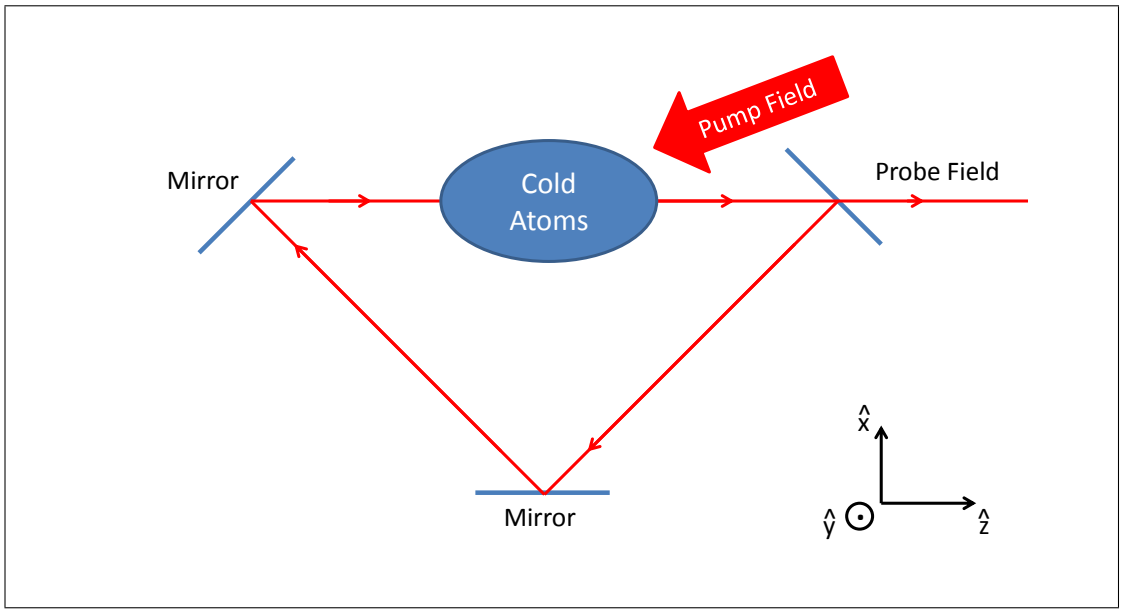

Figure 2.7: Simplified Counter-Propagating Cavity Structure Diagram

2.5.1 The Maxwell-Bloch equations

2.5.1.1 Population inversion

Substituting the expression for the coherence, (2.5.0.3), and the new expression for the field, (2.5.0.1), into (2.3.1.19) gives

$$\begin{aligned}\frac{\partial D}{\partial t} =& -\gamma_{22}\left(D - D^{eq}\right) \\ &+ \frac{i\mu}{\hbar}\left(A_a(t)e^{i(kz-\omega t)} + A_b(t)e^{i(-kz-\omega t)} + c.c.\right) \\ &\left(\sigma_{21}e^{-i\omega t} - \sigma_{12}e^{i\omega t}\right) ,\end{aligned} \tag{2.5.1.1}$$

where the dot product between the terms with polarisations $\hat{e}$ has been taken. Multiplying out the brackets and applying the RWA so that terms with oscillations of the order $e^{\pm ni\omega t}$ (for $n \geq 2$) may be neglected, the equation for the population inversion of an atom under two optical beams takes the form

$$\begin{aligned}\frac{\partial D}{\partial t} =& -\gamma_{22}\left(D - D^{eq}\right) \\ &+ \frac{i\mu}{\hbar}\left(\sigma_{21}\left(A_a^* e^{-ikz} + A_b^* e^{ikz}\right) - \sigma_{12}\left(A_a e^{ikz} + A_b e^{-ikz}\right)\right).\end{aligned} \tag{2.5.1.2}$$

2.5.1.2 Coherences

In a similar fashion the equation for the coherence due to the two applied fields may be obtained by substituting the coherence expression (2.5.0.3), the expression for the total field (2.5.0.1) and the definition of the population inversion (2.3.1.17) into equation (2.3.1.11). By doing so, the equation

$$\begin{aligned}\frac{\partial}{\partial t}\left(\sigma_{21}e^{-i\omega t}\right) =& -\left(\gamma_{21} + i\omega_{21}\right)\left(\sigma_{21}e^{-i\omega t}\right) \\ &+ \frac{i2\mu D}{\hbar}\left(A_a e^{i(kz-\omega t)} + A_b e^{i(-kz-\omega t)} + c.c.\right)\end{aligned} \tag{2.5.1.3}$$

was obtained. The left hand side of this equation may be expanded out using the product rule to give

$$\begin{aligned}&\frac{\partial \sigma_{21}}{\partial t}e^{-i\omega t} - i\omega\sigma_{21}e^{-i\omega t} \\ =& -\left(\gamma_{21} + i\omega_{21}\right)\sigma_{21}e^{-i\omega t} \\ &+ \frac{i2\mu D}{\hbar}\left(A_a e^{i(kz-\omega t)} + A_b e^{i(-kz-\omega t)} + c.c.\right).\end{aligned} \tag{2.5.1.4}$$

The above equation can be rearranging so that the term $-i\omega\sigma_{21}e^{-i\omega t}$ is moved to the right and subsumed into the term $\Delta_a = \omega - \omega_{21}$. By then multiplying through by $e^{i\omega t}$ and applying the RWA as before, the equation for the slowly varying coherence variable, σ_{12} becomes

$$\frac{\partial \sigma_{21}}{\partial t} = -(\gamma_{21} - i\Delta_a)\sigma_{21} + \frac{i2\mu D}{\hbar}\left(A_a e^{ikz} + A_b e^{-ikz}\right) \tag{2.5.1.5}$$

2.5.1.3 Optical fields

The equation for the evolution of the field in the cavity is still given by the wave equation (2.4.1.1), though using the new expression for the total field (2.5.0.1) and (2.5.0.3) produces a more complex result than previously,

$$\begin{aligned}\frac{\partial^2 \vec{E}}{\partial t^2} = \Bigg[&\left(\frac{\partial^2 A_a}{\partial t^2} - 2i\omega\frac{\partial A_a}{\partial t} - \omega^2 A_a\right) e^{i(kz-\omega t)} \\ &\left(\frac{\partial^2 A_b}{\partial t^2} - 2i\omega\frac{\partial A_b}{\partial t} - \omega^2 A_b\right) e^{i(-kz-\omega t)} + c.c.\Bigg]\hat{e}\,.\end{aligned} \tag{2.5.1.6}$$

As was assumed in the case of a single beam, any spatial variations in $A_{a,b}$ or their complex conjugates are negligible and thus may be described by the cavity mode rather than by terms in the wave equation. As was also stated previously, the only evolution of the field which is of concern is that which takes place in the z direction, thus the simplification of $\nabla^2 \approx \frac{\partial^2}{\partial z^2}$ gives the spatial derivative of the field to be

$$\frac{\partial^2 \vec{E}}{\partial z^2} = \left(-k^2 A_a e^{i(kz-\omega t)} - k^2 A_b e^{i(-kz-\omega t)} + c.c.\right)\hat{e}\,. \tag{2.5.1.7}$$

By substituting the two derivative expressions (2.5.1.6) and (2.5.1.7) into the wave equation, (2.4.1.1), the following is produced.

$$\begin{aligned}&\left(-k^2 A_a e^{i(kz-\omega t)} - k^2 A_b e^{i(-kz-\omega t)} + c.c.\right)\hat{e} \\ &-\frac{1}{c^2}\Bigg[\left(\frac{\partial^2 A_a}{\partial t^2} - 2i\omega\frac{\partial A_a}{\partial t} - \omega^2 A_a\right) e^{i(kz-\omega t)} \\ &\qquad\left(\frac{\partial^2 A_b}{\partial t^2} - 2i\omega\frac{\partial A_b}{\partial t} - \omega^2 A_b\right) e^{i(-kz-\omega t)} + c.c.\Bigg]\hat{e} \\ &= \frac{1}{\epsilon_0 c^2}\frac{\partial^2 \vec{P}}{\partial t^2}\end{aligned} \tag{2.5.1.8}$$

As the terms $-k^2A$ and $-\frac{\omega^2}{c^2}A$ cancel due to the dispersion relation, the terms remaining after subsequent application of the SVEA are

$$\left(\frac{2i\omega}{c^2}\frac{\partial A_a}{\partial t}e^{i(kz-\omega t)} + \frac{2i\omega}{c^2}\frac{\partial A_b}{\partial t}e^{i(-kz-\omega t)} + c.c.\right)\hat{e} = \frac{1}{\epsilon_0 c^2}\frac{\partial^2 \vec{P}}{\partial t^2}\,. \tag{2.5.1.9}$$

As for the single evolving field case, the right hand side of the wave equation may be expanded as

$$\begin{aligned}\frac{1}{\epsilon_0 c^2}\frac{\partial^2 \vec{P}}{\partial t^2} =& \frac{1}{\epsilon_0 c^2}\frac{\partial^2}{\partial t^2}\sum_j d_j \delta(r - r_j(t)) \\ =& \frac{1}{\epsilon_0 c^2}\sum_j \frac{\partial^2 d_j}{\partial t^2}\delta(r - r_j(t))\,,\end{aligned} \tag{2.5.1.10}$$

into which may be substituted the expression for the dipole moment, $\vec{d} = \mu\left(\sigma_{21}e^{-i\omega t} + c.c\right)\hat{e}$. When the derivative is taken and the SVEA subsequently applied, the wave equation takes the form

$$\begin{aligned}&\left(\frac{2i\omega}{c^2}\frac{\partial A_a}{\partial t}e^{i(kz-\omega t)} + \frac{2i\omega}{c^2}\frac{\partial A_b}{\partial t}e^{i(-kz-\omega t)} + c.c.\right)\hat{e} \\ &= \frac{1}{\epsilon_0 c^2}\sum_j \mu\left(-\omega^2\sigma_{21}e^{-i\omega t} - \omega^2\sigma_{12}e^{i\omega t}\right)\hat{e}\;\delta(r - r_j(t))\,.\end{aligned} \tag{2.5.1.11}$$

By taking the dot product of both sides with $\hat{e}$, collecting terms and cancelling down where appropriate, the equation is reduced to

$$\begin{aligned}&\left(\frac{\partial A_a}{\partial t}e^{i(kz-\omega t)} + \frac{\partial A_b}{\partial t}e^{i(-kz-\omega t)} - c.c.\right) \\ &= \frac{i\omega\mu}{2\epsilon_0}\sum_j \left(\sigma_{21}e^{-i\omega t} + \sigma_{12}e^{i\omega t}\right)\delta(r - r_j(t))\,.\end{aligned} \tag{2.5.1.12}$$

In this form the evolution of any one individual field may not be easily determined, so the equation must be split in two, one equation for each field. Mul-

tiplying through equation (2.5.1.12) by $e^{i(-kz+\omega t)}$ and applying the RWA results produces

$$\left(\frac{\partial A_a}{\partial t} + \frac{\partial A_b}{\partial t}e^{-2ikz}\right) = \frac{i\omega\mu}{2\epsilon_0}\sum_j \left(\sigma_{21}e^{-ikz}\right)\delta(r - r_j(t))\,. \tag{2.5.1.13}$$

Once again the application of the rotating wave approximation has allowed terms which varied as $e^{\pm ni\omega t}$ for $n \geq 2$ to be considered to average to zero. Integrating this equation over the cavity area $\mathscr{A}$ and the cavity length L eliminates the terms on the left hand side containing $e^{\pm 2ikz}$ and applies the Dirac delta function on the right hand side.

$$\frac{\partial A_a}{\partial t} = \frac{i\omega\mu}{2\epsilon_0}\frac{1}{\mathscr{A}L}\sum_j \left(\sigma_{21}e^{-ikz_j}\right) \tag{2.5.1.14}$$

By multiplying the right hand side by $\frac{N}{N}$, substituting for the atomic density

$$n = \frac{N}{\mathscr{A}L} \tag{2.5.1.15}$$

and defining the average

$$\frac{1}{N}\sum_j^N(\cdots) = <\cdots>\,, \tag{2.5.1.16}$$

and lastly adding detuning, loss and pumping terms as derived for the one field case, then equation (2.5.1.14) takes the form

$$\frac{\partial A_a}{\partial t} = \frac{i\omega\mu n}{2\epsilon_0}\left\langle\sigma_{21}e^{-ikz_j}\right\rangle + (i\delta_c - \kappa)A_a + \kappa A_a^{eq}\,, \tag{2.5.1.17}$$

i.e. the equation describing the evolution of the optical probe beam. By multiplying equation (2.5.1.12) instead by $e^{i(kz+\omega t)}$ and following a similar series of

steps, the equation for the evolution of the optical pump beam is found to be

$$\frac{\partial A_b}{\partial t} = \frac{i\omega\mu n}{2\epsilon_0}\left\langle \sigma_{21} e^{ikz_j} \right\rangle + (i\delta_c - \kappa)A_b + \kappa A_b^{eq}\,. \tag{2.5.1.18}$$

2.5.1.4 Optical force acting on each atom

The rate of change of momentum, i.e. the force, experienced by an atom as a result of the optical fields incident upon it is given simply by

$$\frac{\partial p_j}{\partial t} = F_{zj} = \vec{d_j} \cdot \frac{\partial \vec{E}}{\partial z}\,. \tag{2.5.1.19}$$

By substituting the term for the total field, (2.5.0.1) and the term for the jth atoms dipole moment, (2.5.0.2) into the above and taking the derivative, the equation becomes

$$\begin{aligned}\frac{\partial p_j}{\partial t} =& \mu\left(\sigma_{21}e^{-i\omega t} + \sigma_{12}e^{i\omega t}\right)\hat{e} \\ &\cdot\left(ikA_a e^{i(kz-\omega t)} - ikA_b e^{i(-kz-\omega t)} + c.c.\right)\hat{e}\,.\end{aligned} \tag{2.5.1.20}$$

Upon taking the dot product and applying the RWA, the equation for the force experienced by the jth atom is shown to be

$$\frac{\partial p_j}{\partial t} = ik\mu\Big(\sigma_{12}\left(A_a e^{ikz} - A_b e^{-ikz}\right) - \sigma_{21}\left(A_a^* e^{-ikz} - A_b^* e^{ikz}\right)\Big) \tag{2.5.1.21}$$

2.5.1.5 Evolution of atomic position

The rate of change of position for each atom is simply the velocity at which it is travelling, or rather its momentum divided by its mass

$$\begin{aligned}\frac{\partial z_j}{\partial t} &= \nu_{zj} \\ &= \frac{p_j}{m}\end{aligned} \tag{2.5.1.22}$$

2.5.2 Scaled Maxwell-Bloch equations

Equations (2.5.1.2), (2.5.1.5), (2.5.1.17), (2.5.1.18), (2.5.1.21) and (2.5.1.19) form the Maxwell-Bloch equations for a cold atomic gas interacting with two counter-propagating optical fields. As was the case for stationary atoms, these equations can be numerically solved in their current form, however it is convenient to utilize the scaling terms to rewrite the Maxwell-Bloch equations in a dimensionless scaled form. The dimensionless scaling terms

$$\bar{p}_j = \frac{p_j}{\hbar k \rho} \tag{2.5.2.1}$$

$$\bar{A}_b = -i\sqrt{\frac{2\epsilon_0}{n\hbar\omega\rho}}A_{a,b} \tag{2.5.2.2}$$

$$\theta = 2kz \tag{2.5.2.3}$$

are added to those previously defined in equations (2.3.1.28) - (2.3.1.33), (2.4.1.20), and (2.4.1.21).

When scaled, equations (2.5.1.2), (2.5.1.5), (2.5.1.17), (2.5.1.18), (2.5.1.21) & (2.5.1.22) take the form

$$\frac{\partial D}{\partial t} = -\Gamma_{22}\left(D - D^{eq}\right) + \rho\left(\sigma_{21}\left(\bar{A}_a^* e^{-i\frac{\theta}{2}} + \bar{A}_b^* e^{i\frac{\theta}{2}}\right) + \sigma_{12}\left(\bar{A}_a e^{i\frac{\theta}{2}} + \bar{A}_b e^{-i\frac{\theta}{2}}\right)\right) \tag{2.5.2.4}$$

$$\frac{\partial \sigma_{21}}{\partial \tau} = -(\Gamma_{21} - i\bar{\Delta})\sigma_{21} - 2\rho D\left(\bar{A}_a e^{i\frac{\theta}{2}} + \bar{A}_b e^{-i\frac{\theta}{2}}\right) \tag{2.5.2.5}$$

$$\frac{\partial \bar{A}_a}{\partial \tau} = \left\langle \sigma_{21} e^{-i\frac{\theta_j}{2}} \right\rangle + (i\bar{\delta}_c - \bar{\kappa})\bar{A}_a + \bar{\kappa}\bar{A}_a^{eq} \tag{2.5.2.6}$$

$$\frac{\partial \bar{A}_b}{\partial \tau} = \left\langle \sigma_{21} e^{i\frac{\theta_j}{2}} \right\rangle + (i\bar{\delta}_c - \bar{\kappa})A_b + \bar{\kappa}A_b^{eq} \tag{2.5.2.7}$$

$$\frac{\partial \bar{p}_j}{\partial \tau} = -\left(\sigma_{12}\left(\bar{A}_a e^{i\frac{\theta_j}{2}} - \bar{A}_b e^{-i\frac{\theta_j}{2}}\right) + \sigma_{21}\left(\bar{A}_a^* e^{-i\frac{\theta_j}{2}} - \bar{A}_b^* e^{i\frac{\theta_j}{2}}\right)\right) \tag{2.5.2.8}$$

$$\frac{\partial \theta_j}{\partial \tau} = \bar{p}_j \tag{2.5.2.9}$$

2.5.3 Collective atomic recoil lasing

With the Maxwell-Bloch equations in a scaled notation it is now possible to investigate CARL by solving equations (2.5.2.4), (2.5.2.5), (2.5.2.6), (2.5.2.7), (2.5.2.8) and (2.5.2.9).

On inspection of equations (2.5.2.4) and (2.5.2.5) in particular, it can be seen that when the pump intensity is large, the value of the coherence increases. When the coherence grows, the population inversion moves from its initial ground state value of $^1/_2$ towards zero. The growth of the excited state population and thus the decrease of the population inversion is troublesome for two reasons. Firstly, population in the excited state leads to an increase in spontaneous emission and thus heating of the atomic sample. Secondly, the optical force responsible for the atomic bunching is dependent upon the coherence, which is in turn dependent upon the value of the population inversion. As the population inversion tends towards zero, so too will the coherence and thus the bunching force.

These two factors present good reason for operating CARL with parameter choices which result in negligible growth of the excited state population. To that end it is useful to obtain an expression for the value of pump field amplitude at which a given "saturation" value of the population inversion could be expected.

2.5.3.1 Pump beam saturation value

An equation for the saturation pump amplitude can be obtained by solving the equations for D and σ_{21} in the idealised situation where $\gamma_{21} = \gamma_{22} = 0$, $\bar{A}_a = 0$ and $\frac{\partial\left(\bar{A}_b e^{-ikz}\right)}{\partial\tau} = 0$. In this idealized state, equations (2.5.2.4) and (2.5.2.5) take the form

$$\frac{\partial D}{\partial \tau} = \rho\left(\sigma_{21}F^* + \sigma_{12}F\right) \tag{2.5.3.1}$$

$$\frac{\partial \sigma_{21}}{\partial \tau} = i\bar{\Delta}_a\sigma_{21} - 2\rho DF \tag{2.5.3.2}$$

where $F = \bar{A}_b e^{-ikz}$.

Differentiating the equation for the population difference, (2.5.3.1), produces

$$\begin{aligned}\frac{\partial^2 D}{\partial \tau^2} &= \rho\left(\frac{\partial \sigma_{21}}{\partial \tau}F^* + \frac{\partial \sigma_{12}}{\partial \tau}F\right) \\ &= \rho\left(i\bar{\Delta}_a(\sigma_{21}F^* - \sigma_{12}F) - 4\rho D|F|^2\right)\,, \end{aligned} \tag{2.5.3.3}$$

then when it is differentiated a second time it gives

$$\begin{aligned}\frac{\partial^3 D}{\partial \tau^3} &= \rho\left(i\bar{\Delta}_a\left(\frac{\partial \sigma_{21}}{\partial \tau}F^* - \frac{\partial \sigma_{12}}{\partial \tau}F\right) - 4\rho\frac{\partial D}{\partial \tau}|F|^2\right) \\ &= -\bar{\Delta}_a^2\left(\rho\left(\sigma_{21}F^* + \sigma_{12}F\right)\right) - 4\rho^2\frac{\partial D}{\partial \tau}|F|^2 \\ &= -\left(\bar{\Delta}_a^2 + 4\rho^2|F|^2\right)\frac{\partial D}{\partial \tau}\,. \end{aligned} \tag{2.5.3.4}$$

Looking for solutions to the above equation of the form $D \propto e^{\lambda\tau}$ gives

$$\lambda^3 = -\left(\bar{\Delta}_a^2 + 4\rho^2|F|^2\right)\lambda\,. \tag{2.5.3.5}$$

It is easy to see then that $\lambda = 0$ or $\lambda = \pm i\sqrt{\bar{\Delta}_a^2 + 4\rho^2|F|^2}$. Using these to solve for an equation for D

$$D = Ae^{0\tau} + Bcos(\omega_r\tau) + Csin(\omega_r\tau)\,, \tag{2.5.3.6}$$

where $\omega_r = \sqrt{\bar{\Delta}_a^2 + 4\rho^2|F|^2}$. It follows that at $\tau = 0$ the above expression is

$$D|_{\tau=0} = A + Bcos(0) + Csin(0)\,, \tag{2.5.3.7}$$

so then

$$A = D_0 - B\,. \tag{2.5.3.8}$$

By differentiating (2.5.3.6), the equation takes the form

$$\frac{\partial D}{\partial \tau}|_{\tau=0} = -\omega_r B sin(0) + \omega_r C cos(0)\,. \tag{2.5.3.9}$$

However, as the initial coherence is considered to be zero, $\sigma_{21}|_{\tau=0} = 0$, from (2.5.3.1) it follows that $\frac{\partial D}{\partial \tau}|_{\tau=0} = 0$. Using that value in the above expression it becomes clear that $C = 0$. Differentiating (2.5.3.6) a second time gives

$$\frac{\partial^2 D}{\partial \tau^2}|_{\tau=0} = -\omega_r^2 B cos(0)\,. \tag{2.5.3.10}$$

From equation (2.5.3.3), using $\sigma_{21}|_{\tau=0} = 0$ it follows that

$$\frac{\partial^2 D}{\partial \tau^2}|_{\tau=0} = -4\rho^2|F|^2 D_0 \tag{2.5.3.11}$$

By equating (2.5.3.10) and (2.5.3.10) the value for B is therefore

$$B = \frac{4\rho^2|F|^2 D_0}{\omega_r^2}\,. \tag{2.5.3.12}$$

Collating the values for A and B in (2.5.3.6) gives

$$D = D_0 - \frac{4\rho^2|F|^2 D_0}{\omega_r^2} + \frac{4\rho^2|F|^2 D_0}{\omega_r^2} cos(\omega_r \tau) \tag{2.5.3.13}$$

By averaging out in τ the term $cos(\omega_r \tau)$ disappears, so in substituting for ω_r in the above an expression is obtained for the value of the population as a function of the field, namely

$$D = D_0 \left[1 - \frac{4\rho^2|F|^2}{\bar{\Delta}_a^2 + 4\rho^2|F|^2}\right] \tag{2.5.3.14}$$

Setting $D_0 = \frac{1}{2}$ and defining the "saturation" population inversion value as $D = \frac{1}{4}$ then

$$\frac{1}{4} = \frac{1}{2}\left[1 - \frac{4\rho^2|F|^2}{\bar{\Delta}_a^2 + 4\rho^2|F|^2}\right] \tag{2.5.3.15}$$

Rearranging the above for the pump field, remembering that $F = \bar{A}_b e^{-ikz}$, produces

$$|\bar{A}_b^{sat}| = \frac{|\Delta_a|}{2|\rho|}, \tag{2.5.3.16}$$

where it has been taken that although the term e^{-ikz} may oscillate, considering it as constant at its highest value produces a more useful expression for the saturation value for the pump field. Operating with parameter choices which result in a scaled pump field sufficiently lower than the corresponding saturation pump field value should therefore avoid the risks associated with growth of the excited state population.

2.5.3.2 CARL in the weak pump limit

For a system operating with $\rho = 1$ and $\bar{\Delta}_a = 10$, the saturation condition in equation (2.5.3.16) gives a value for $|\bar{A}_b^{sat}|$, as defined in (2.5.3.16), of 5. A pump field amplitude of $\bar{A}_b = 0.4$ means that the system is operating more than an order of magnitude less than the saturation pump field value. Operating below the pump saturation value in such a manner will be referred to as operating in the weak pump limit.

Numerically solving equations (2.5.2.4), (2.5.2.5), (2.5.2.6), (2.5.2.8) and (2.5.2.9), using the above values, produced Figures 2.8 , 2.9 and 2.10.

The computational model was run with initial values approximating conditions typical for collective atomic recoil lasing. It was assumed that the atoms were initially unexcited, so that the population inversion, D, of each atom was 1/2 at $\tau = 0$. Furthermore the pump field A_b was taken to be considerably

stronger than A_a initially, and the pump field was assumed to remain undepleted throughout the time the CARL instability took to occur. Operating under those assumptions, the equation for the evolution of the pump beam was set to zero, ensuring that the pump amplitude remained constant throughout the length of the run. The atoms were assumed to be evenly spread in the z direction over a distance $\lambda/2$, the period of the optical potential formed by the counterpropagating optical fields. This corresponds to the position variable θ ranging from $0 \rightarrow 2\pi$, so that the magnitude of the bunching parameter, defined as

$$|b| = |\left\langle e^{-i\theta} \right\rangle|, \tag{2.5.3.17}$$

was initially zero. As the force experienced by the atoms are periodic over the range 0 - 2π it was taken that any atom travelling forward past $\theta = 2\pi$ could be accounted for by an identical atom travelling forward past the point $\theta = 0$. Similarly any atom travelling backwards past $\theta = 0$ could be accounted for by an atom travelling backwards from the point $\theta = 2\pi$. Thus the computational model needed only simulate the region between $\theta = 0$ and $\theta = 2\pi$ and could place any atom passing these two limits at the other boundary with its momentum unchanged. The coherence, σ_{21} was taken to be initially zero.

As was explained previously in Section 2.1, in a system which is capable of experiencing the CARL instability the initially stationary atoms first interact with the field through random scattering events. When a photon is scattered counterpropagating with the pump beam, then a weak standing field emerges. This weak standing field, through the action of the dipole force, resulted in the atoms experiencing a push towards the peaks (troughs) of intensity when the field was tuned below (above) atomic resonance [74].

Being the result of a standing field, the peaks and troughs of intensity are periodic over $\frac{\lambda}{2}$, thus the atoms bunch on the same scale. In so bunching, the atoms form a spatial density grating and act in a manner similar to that of a Bragg reflector thus scattering more pump beam photons into the probe beam

[75]. The increased number of photons in the probe beam strengthen the standing wave, which increases the atomic bunching, resulting in a yet stronger "reflection" and more backscattered photons.

This effect can be readily observed in Figure 2.8, in which the probe beam intensity, shown on a log scale in the uppermost graph, experienced gain as a result of the bunching term b, also shown on a log scale in the middle graph, increasing. In Figure 2.9 the graphs shown are phase space plots i.e. atomic momentum against atomic position at three points during the evolution of the CARL instability. It can be seen that atoms to the left of the bunching point gain momentum in the positive direction and atoms on the right of the bunching point gain momentum in the negative direction. The end result being a tendency towards areas of highly bunched atoms with a distinct periodicity.

It is important to note that a similar effect exists where the atoms remain mostly stationary and it is instead the population which varies on a $\frac{\lambda}{2}$ spatial period. This is known as an electromagnetically induced grating (EIG) [76, 77]. As this effect exists, the average population inversion $\langle D \rangle$ has been plotted in Figure 2.10 at the same time points as the graphs shown in Figure 2.9. It can be seen that the scatter plots of atomic population inversion vs. atomic position display no periodic excitation of the population. It can be safely said then that the gain in the probe beam is the result of the CARL instability and not due to an EIG.

Furthermore, it is important to be aware of the population difference experienced by atoms in the system to avoid "washout" of the CARL result. From the definition of D given by (2.3.1.15) it can clearly be seen that when the population in levels 1 and 2 are equal, that D becomes 0. When D experiences a value of zero, the equation for the coherence, σ_{21}, given by equation (2.5.2.5), tends towards zero. As a result, the equation for the probe field, $\bar{A}_a$, equation (2.5.2.6), also tends towards zero.

Figure 2.9 is a scatter plot which shows the momentum of each individual atom plotted against its z-position. In this respect, the number of simulated particles can be thought of as a sampling of the phase space. Running the simulation

with too few particles can introduce numerical noise into the system due to the averaging term $\langle ... \rangle = \frac{1}{n} \sum_{j=1}^{N}$ in equations (2.5.2.6) and (2.5.2.7), which describe the pump and probe field respectively. Running the simulation with too many particles results in runtimes which are prohibitively long. The value of $N = 1000$ was chosen for the number of simulated particles as it was deemed to be sufficiently high to mitigate numerical noise without run times becoming severely protracted.

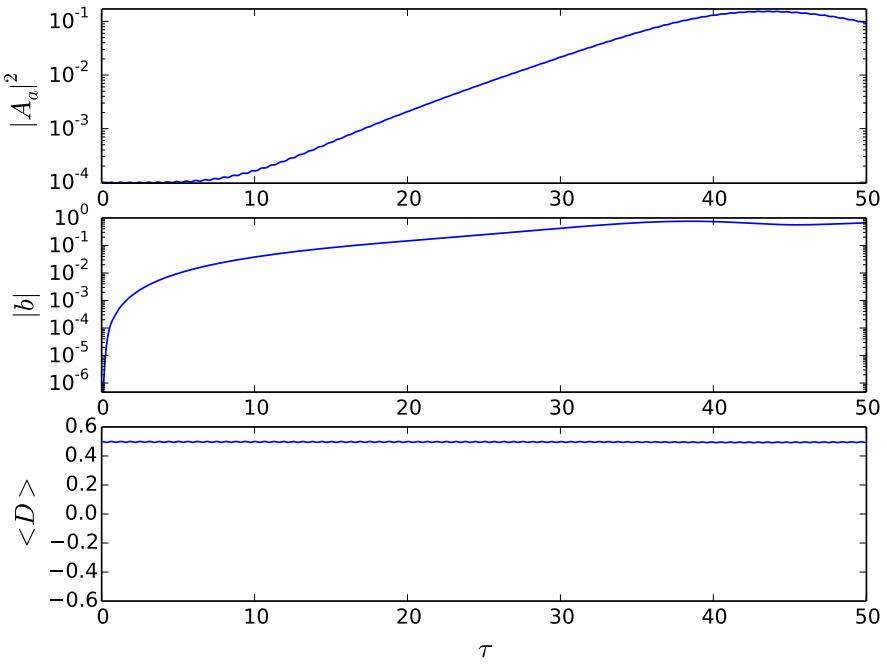

Figure 2.8: Evolution of the magnitude squared of the scaled probe amplitude, $|\bar{A}_a|^2$, bunching parameter, $|b|$, and mean population difference, $\langle D \rangle$ for a case of weak-excitation. Produced by solving equations (2.5.2.4) - (2.5.2.9). Parameters used are $\rho = 1$, $\Delta_{21} = 10$, $\bar{A}_b = 0.4$, $N = 1000$. Top: Exponential growth of the probe beam due to the CARL instability. Middle: Growth of atomic bunching due to the CARL instability. Bottom: Population remains, on average, in the ground state during the instability.

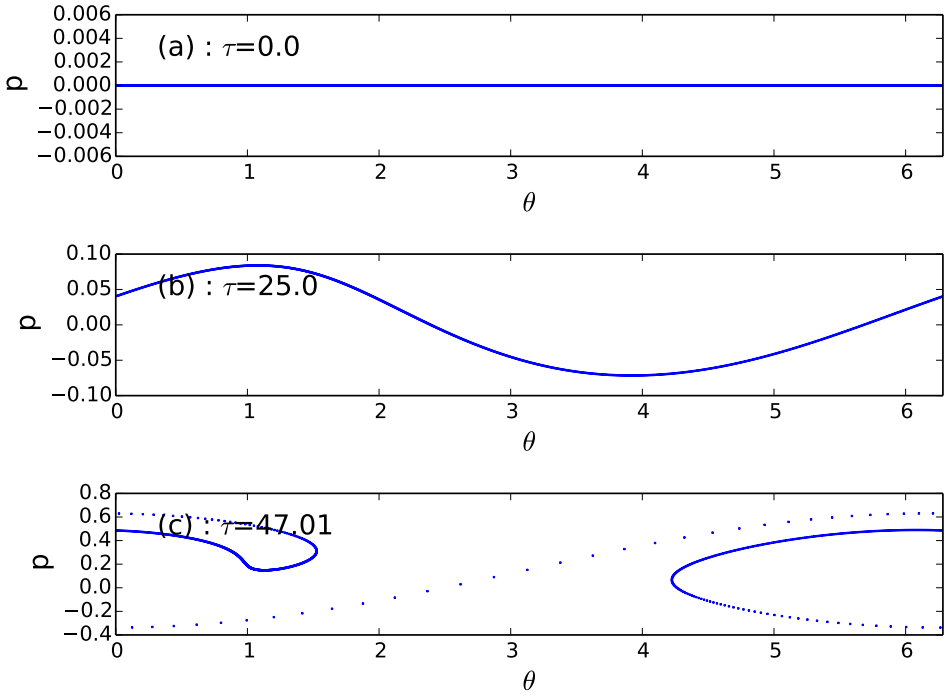

Figure 2.9: Evolution of the momentum, p_j of each atom for a case of weak-excitation at (a)$\tau = 0.0$(a)$\tau = 25.0$ and (c)$\tau = 47.0$. Parameters used and equations solved are as in Figure 2.8. Over the course of the simulation the particles acquire momentum, due to the dipole force, which results in bunching.

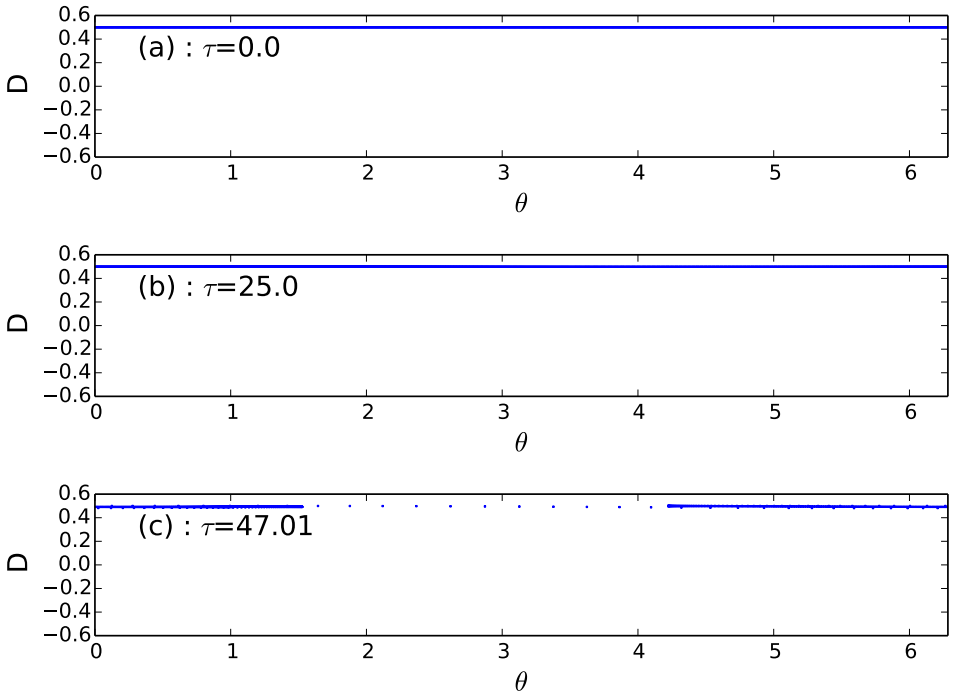

Figure 2.10: Evolution of the population inversion D_j of each atom for a case of weak-excitation at (a)$\tau = 0.0$(a)$\tau = 25.0$ and (c)$\tau = 47.0$. Parameters used and equations solved are as in Figure 2.8. The atoms can be seen to bunch as time progresses, however each atom remains in the ground state due to the low pump intensity.

2.5.3.3 The FEL Limit

It may be shown that, for carefully selected parameter values and through the use of dimensionless scaling terms, the CARL equations take on a form similar to those of a Free Electron Laser [37, 78].

In the limit in which $|A_b|^2 \ll |A_b^{\text{sat}}|^2$, each atom experiences only a weak internal excitation and the population remains almost exclusively in the ground state $|1\rangle$ i.e. $D \to \frac{1}{2}$. In this limit the coherence may be taken to act as a parameter, rather than a variable. With the pump field A_b taken as undepleted with reference to the much weaker probe beam A_a and thus taken as constant, the three remaining unscaled equations governing the system take the form

$$\frac{\partial z_j}{\partial t} = \frac{p_j}{m} \tag{2.5.3.18}$$

$$\frac{\partial p_j}{\partial t} = ik\mu\left(\sigma_{12}\left(A_a e^{ikz} - A_b e^{-ikz}\right) - \sigma_{21}\left(A_a^* e^{-ikz} - A_b^* e^{ikz}\right)\right) \tag{2.5.3.19}$$

$$\frac{\partial A_a}{\partial t} = \frac{i\omega\mu n}{2\epsilon_0}\left\langle \sigma_{21} e^{-ikz_j}\right\rangle - \kappa A_a\,, \tag{2.5.3.20}$$

where the field has been assumed to be sufficient well tuned to the cavity such that the cavity detuning term may be neglected, $\delta_c \approx 0$. Furthermore, the probe beam is not pumped so $A_a^{eq} = 0$. Following a process similar to [78], equations (2.5.3.18) - (2.5.3.20), when written in terms of the scaling variables:

$$\theta = 2kz \tag{2.5.3.21}$$

$$\bar{p} = \frac{p}{\hbar k \rho} \tag{2.5.3.22}$$

$$\tau = \omega_r \rho t \tag{2.5.3.23}$$

$$\bar{A} = iA_a\sqrt{\frac{2\epsilon_0}{n\hbar\omega\rho}} \tag{2.5.3.24}$$

$$\omega_r = \frac{2\hbar k^2}{m} \tag{2.5.3.25}$$

$$\rho^3 = \frac{\omega\mu^4 n A_b^2}{2\hbar^3\epsilon_0\Delta_a^2\omega_r} \tag{2.5.3.26}$$

become the CARL equations in the so-called Free-Electron-Laser (FEL) limit [79]:

$$\frac{d\theta_j}{d\tau} = \bar{p}_j \tag{2.5.3.27}$$

$$\frac{d\bar{p}_j}{d\tau} = -\left(\bar{A}e^{i\theta_j} + c.c.\right) \tag{2.5.3.28}$$

$$\frac{d\bar{a}}{d\tau} = \left\langle e^{-i\theta}\right\rangle - \bar{\kappa}\bar{A}\,. \tag{2.5.3.29}$$

It has been assumed in the above that the system is operating in the far detuned limit, such that $\Delta_a >> \gamma_{21}$). In the scaling terms, θ is the scaled position variable, $\bar{p}$ is the scaled momentum variable, $\bar{A}$ is the scaled probe field variable, τ is the dimensionless time coordinate, $\bar{\kappa}$ is the scaled cavity decay rate, ω_r is the recoil frequency, and lastly ρ is the CARL scaling parameter.

It has been shown in e.g. [37, 80, 79] that equations (2.5.3.27) - (2.5.3.29) display the collective instability described in section 2.5.3.2 in which the initially homogeneous distribution of atomic positions is unstable and the resulting instability involves exponential growth of both the probe field intensity ($|\bar{A}|^2$) and the previously mentioned bunching parameter $|b| = |\left\langle e^{-i\theta}\right\rangle|$, sometimes referred to as the density modulation amplitude or spatial order parameter.

A collective atomic recoil laser is a system of cold, neutral atoms illuminated by a pump beam. A free electron laser is a completely distinct and separate physical system in which a relativistic beam of electrons moves through a magnetostatic undulator. Given the difference between the two systems it is interesting that they both display similar types of self-organising instability when interacting with optical fields.

2.5.3.4 Experimental Setup

As was stated in Section 2.1, in 2003 Kruse et al. [4] produced the first unambiguous experimental proof of the CARL instability. A simple diagram of the experimental setup used in [4] can be seen in Figure 2.11.

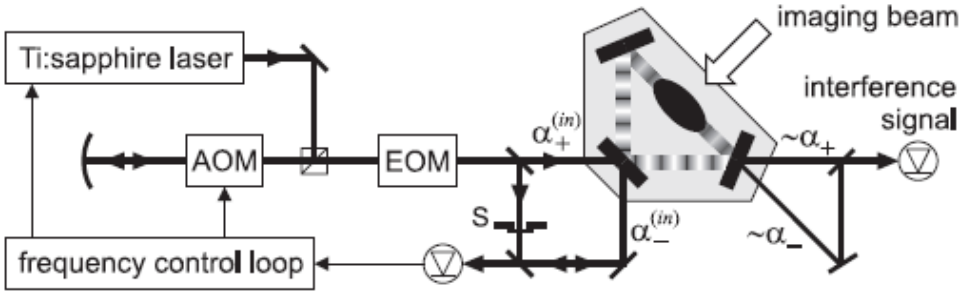

Figure 2.11: Diagram of the experimental setup of Kruse et al. [4]

The experiment consisted of a titanium-sapphire laser (operating at $\lambda = 797nm$) split to form a pump and probe mode, α_+ & α_- respectively, within a high Q ring cavity. The pump and probe modes from [4] correspond closely to the pump and probe beams, α_b & α_a respectively, used in this thesis. The light power exiting the cavity was measured via the fields leaking through one of the cavity mirrors. The power of the light field exciting the cavity was related to the intracavity power by the expression $P_{\pm}^{(out)} = TP_{\pm}^{(cav)} = T\hbar\omega\delta|\alpha_{\pm}|^2$.

A frequency difference between the two cavity modes $\Delta\omega \equiv \omega_+ - \omega_-$ was taken to correspond to a shift in the position of the standing wave node within the cavity. Such a propagation of the standing waves nodes was translated into a variation in the amplitude of the interference signal $P_{beat} = T\hbar\omega\delta|\alpha_+ + \alpha_-|^2$ exiting the cavity. The beat signal was used to monitor the phase dynamics of the pump and probe cavity modes while time-of-flight absorption imaging was used to monitor the density distribution of the atomic sample.

The system was operated initially with no atoms in the cavity. The shutter, shown in Figure 2.11, was used to quickly "switch off" the probe beam (α_-). When the probe beam was switched off the beat signal dropped to $T\hbar\omega\delta|\alpha_+|^2$

within $10\mu s$, a time attributed to the finite closing speed of the shutter.

When atoms were then loaded into the cavity and the experiment repeated, oscillations appeared on the beat signal shortly after the switching off of the probe beam. While the amplitude of the beat signal oscillations dampened rapidly, they continued for a time far in excess of the cavity decay time. Time-of-flight imaging of the atomic sample showed that the atomic cloud's center-of-mass was shifted along the propagation direction of the standing wave.

The experiment was performed again with the finesse of the cavity severely decreased by rotating the polarization of the uncoupled lasers from s to p polarization. In doing so it was verified that the oscillations do not occur in the low finesse limit.

A number of deductions were made based on the above observations. First, the probe mode was fed with light in the presence of the atomic sample, resulting in a standing wave with the pump mode. Second, as the oscillations in the beat signal are due to the relative phase shift of the pump and probe modes, the standing wave was displaced and accelerated by the presence of atoms. Third, the amplitude of the beat signal oscillations reduces in time, fading out after 1.5 ms. And fourth, the atoms were displaced by the moving standing wave.

The above deductions and observations were explained by Kruse et al. as being indications of Collective Atomic Recoil Lasing. The system starts with both pump and probe modes acting upon the atoms, thus the atoms are initially bunched at the anti-nodes of the standing wave cavity field. When the probe field is switched off the atoms which take part in the CARL process scatter photons from the pump mode into the probe mode. In doing so their momentum is shifted by mv, in direction of the pump. The difference in frequency between the two modes is then equal to twice the Doppler shift, $\Delta\omega = 2kv$.

This picture agrees with the experimental observations above where the increasingly Doppler detuned probe beam experiences a decrease in its intensity as its frequency shifts out of cavity resonance by an amount corresponding to $\Delta\omega$.

Kruse et al. then go on to expand the experiment to include a friction force (in the form of optical molasses). This friction force acts upon the atoms to prevent

them being accelerated and frequency shifted from resonance with the pump and probe modes due to the Doppler shift.

The inclusion of the optical molasses has two noteworthy effects. First, it results in the beat signal reaching a steady operating frequency ranging between 100 and 170 kHz. This corresponds to an atomic velocity ranging between 7 and 13 cm/s. The beat signal persist for times longer than 100 ms, with this time mainly limited by the finite size of the molasses region.

The second effect to note is that, as described by von. Cube et al in [38], the optical molasses creates a threshold value for the optical intensity. If the optical modes have intensities below this threshold then the optical dipole force which is responsible for the atomic bunching will be too small to overcome the debunching effect of the finite temperature of the atomic cloud. Without the dipole force forming periodic atomic bunching within the sample, the CARL process cannot take place.

Chapter 3

Three level atoms: ladder configuration

The behaviour of the CARL instability in two-level atoms has been well documented [80, 37, 79, 78, 69]. However, the behaviour of the CARL instability in atoms with three energy levels has not been quite so thoroughly researched.

In this chapter equations are derived which model three level atoms in a ladder configuration. These equations are then used to model two-photon collective atomic recoil lasing and two-photon superfluorescence including recoil.

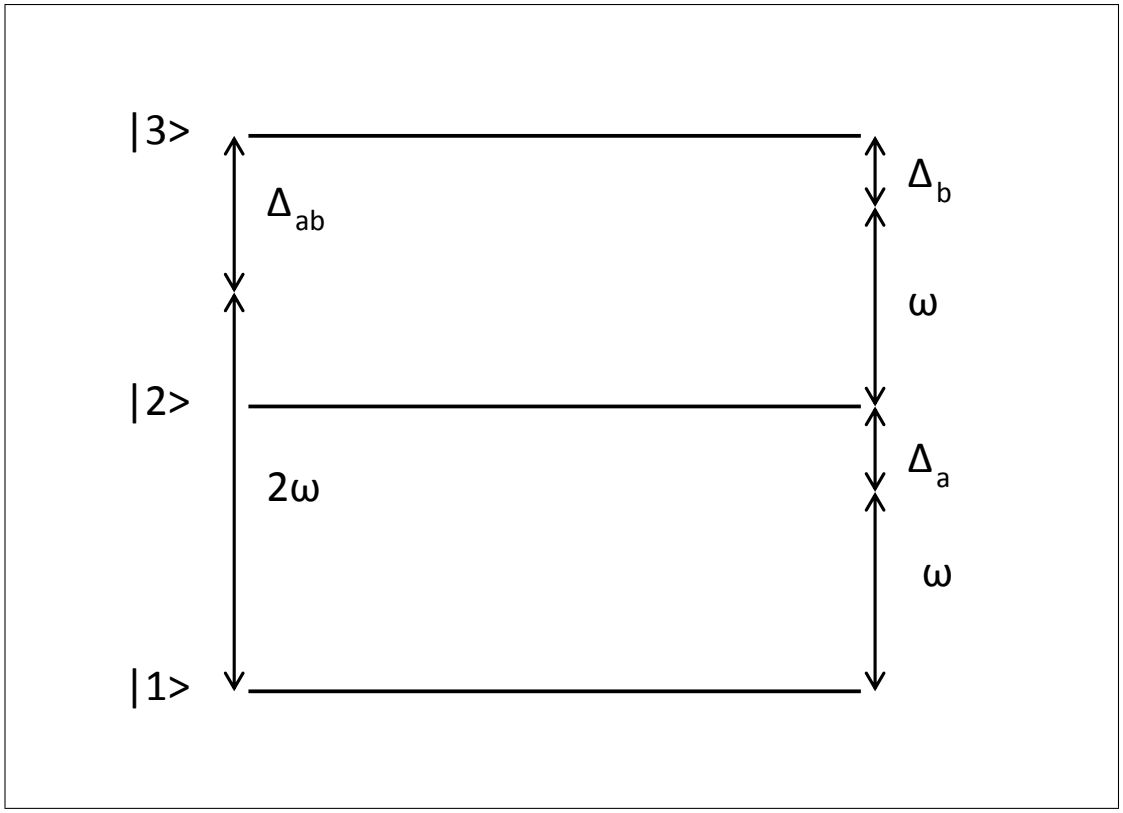

Figure 3.1: Simplified Three Level "Ladder" Energy Level Diagram

3.1 Maxwell-Bloch equations for three-level atoms in ladder configuration

With two counterpropagating fields of degenerate frequency, a pump and a probe beam, the substitution for the field term $\vec{E}$ can be written as

$$\vec{E} = \left(A_a(t)e^{i(kz-\omega t)} + A_b(t)e^{i(-kz-\omega t)} + c.c.\right)\hat{e}\,. \tag{3.1.0.1}$$

The response of each atom's dipole moment to the above field would be expected, therefore, to be of the form

$$\vec{d} = \mu\left(\sigma e^{i(kz-\omega t)} + \sigma e^{i(-kz-\omega t)} + c.c.\right)\hat{e}\,. \tag{3.1.0.2}$$

The dipole moment for the three level system, as it was for the two level system in equation (2.3.1.4), is given by

$$\begin{aligned}\vec{d} &= Trace(\vec{p}\rho)\\ &= Trace\left(\begin{bmatrix}\vec{p}_{11} & \vec{p}_{12} & \vec{p}_{13}\\ \vec{p}_{21} & \vec{p}_{22} & \vec{p}_{23}\\ \vec{p}_{31} & \vec{p}_{32} & \vec{p}_{33}\end{bmatrix}\begin{bmatrix}\rho_{11} & \rho_{12} & \rho_{13}\\ \rho_{21} & \rho_{22} & \rho_{23}\\ \rho_{31} & \rho_{32} & \rho_{33}\end{bmatrix}\right)\\ &= \vec{p}_{11}\rho_{11} + \vec{p}_{12}\rho_{21} + \vec{p}_{13}\rho_{31} + \vec{p}_{21}\rho_{12} + \vec{p}_{22}\rho_{22} + \vec{p}_{23}\rho_{32} + \vec{p}_{31}\rho_{13} + \vec{p}_{23}\rho_{32} + \vec{p}_{33}\rho_{33}\end{aligned} \tag{3.1.0.3}$$

As was the case with a two level atom, the dipole matrix elements with matching indices are always zero as transitions may not occur between the same level, so $\vec{p}_{jj} = 0$. Furthermore, it is assumed that direct transitions between the ground state and the highest energy level are also forbidden, i.e. $p_{31} = p_{13} = 0$. And it has already been assumed that $\rho_{22} = 0$. The dipole moment for a three level atom can therefore be written as

$$\begin{aligned}\vec{d} &= \Big(\vec{p}_{12}\rho_{21} + \vec{p}_{21}\rho_{12} + \vec{p}_{32}\rho_{23} + \vec{p}_{23}\rho_{32}\Big) \\ &= \Big(p_{12}\rho_{21} + p_{21}\rho_{12} + p_{32}\rho_{23} + p_{23}\rho_{32}\Big)\hat{e} \end{aligned} \tag{3.1.0.4}$$

It is assumed that the fields are far detuned, i.e. $|\Delta_a| = |(\omega - \omega_{21})| > 0$ & $|\Delta_b| = |(\omega - \omega_{32})| > 0$, so that the population of the intermediate level, ρ_{22}, can be taken to be approximately zero. By making such an assumption, an effective two level population difference, D, may be defined between the remaining levels in the three level ladder setup. Defining

$$D = \frac{1}{2}(\rho_{11} - \rho_{33}) \tag{3.1.0.5}$$

and remembering that as the system is closed, i.e. $\rho_{11} + \rho_{33} = 1$, the population terms may be replaced by the following terms involving the effective population inversion

$$\rho_{11} = \frac{1}{2} + D, \qquad \rho_{33} = \frac{1}{2} - D\,. \tag{3.1.0.6}$$

As in the case of two level atoms, the equations governing the evolution of the coherence and population terms for each atom may be obtained from equation (2.2.4.14). Substituting for $j, k = 1, 2, 3$, $j \neq k$ in (2.2.4.14) gives the equations for the three coherence terms ρ_{21}, ρ_{32} and ρ_{31} for a three level atom.

3.1.1 Single photon coherences

Using $j = 2$, $k = 1$ in (2.2.4.14) gives

$$\frac{\partial \rho_{21}}{\partial t} = -(\gamma_{21} + i\omega_{21})\rho_{21} + \frac{i\vec{E}}{\hbar} \cdot (\vec{p}_{21}\rho_{11} + \vec{p}_{22}\rho_{21} + \vec{p}_{23}\rho_{31}) - \frac{i\vec{E}}{\hbar} \cdot (\vec{p}_{11}\rho_{21} + \vec{p}_{21}\rho_{22} + \vec{p}_{31}\rho_{23}) \,. \tag{3.1.1.1}$$

Remembering that $\vec{p}_{jj} = 0$, $p_{31} = p_{13} = 0$ and $\rho_{22} = 0$, a number of the terms in the above equation vanish. As was also the case in the two level CARL derivation, the field and dipole matrix elements are assumed for simplicity to have parallel polarizations, such that

$$\vec{p}_{21} = \vec{p}_{12} = \mu_a \hat{e} \tag{3.1.1.2}$$

$$\vec{p}_{32} = \vec{p}_{23} = \mu_b \hat{e} \,. \tag{3.1.1.3}$$

Grouping the terms in equation (3.1.1.1) which remain after applying the above substitutions and using equation (3.1.0.1) to substitute for the field term $\vec{E}$ gives

$$\frac{\partial \rho_{21}}{\partial t} = -(\gamma_{21} + i\omega_{21})\rho_{21} + \frac{i}{\hbar}\left(A_a e^{i(kz-\omega t)} + A_b e^{i(-kz-\omega t)} + c.c.\right) \hat{e} \cdot (\mu_a \rho_{11} + \mu_b \rho_{31})\, \hat{e} \,. \tag{3.1.1.4}$$

When equations (3.1.0.4) and (3.1.0.2) are compared, consistancy requires that the coherence terms may be expressed as

$$\rho_{21} = \sigma_{21} e^{-i\omega t} \tag{3.1.1.5}$$

$$\rho_{32} = \sigma_{32} e^{-i\omega t} \tag{3.1.1.6}$$

$$\rho_{31} = \sigma_{31} e^{-2i\omega t} \,, \tag{3.1.1.7}$$

i.e. the coherence may be expressed as a slowly evolving amplitude multiplied by a oscillating term. Substituting the above expressions for the coherences, substituting for the effective population inversion, (3.1.0.6), and taking the dot

product produces

$$\frac{\partial}{\partial t}\left(\sigma_{21}e^{-i\omega t}\right) = -\left(\gamma_{21}+i\omega_{21}\right)\left(\sigma_{21}e^{-i\omega t}\right) + \frac{i}{\hbar}\left(A_a e^{i(kz-\omega t)} + A_b e^{i(-kz-\omega t)} + c.c.\right)\left(\mu_a\left(\frac{1}{2}+D\right)+\mu_b\sigma_{31}e^{-2i\omega t}\right). \tag{3.1.1.8}$$

So

$$\frac{\partial\sigma_{21}}{\partial t} = -\left(\gamma_{21}-i\left(\omega-\omega_{21}\right)\right)\sigma_{21} + \frac{i}{\hbar}\left(A_a e^{i(kz-\omega t)} + A_b e^{i(-kz-\omega t)} + c.c.\right)\left(\mu_a\left(\frac{1}{2}+D\right)e^{i\omega t}+\mu_b\sigma_{31}e^{-i\omega t}\right). \tag{3.1.1.9}$$

Substituting $\Delta_a = \omega - \omega_{21}$ and applying the RWA gives

$$\frac{\partial\sigma_{21}}{\partial t} = -\left(\gamma_{21}-i\Delta_a\right)\sigma_{21} + \frac{i}{\hbar}\left(\mu_a\left(\frac{1}{2}+D\right)\left(A_a e^{ikz}+A_b e^{-ikz}\right)+\mu_b\sigma_{31}\left(A_a^* e^{-ikz}+A_b^* e^{ikz}\right)\right). \tag{3.1.1.10}$$

In a similar manner to the above, the equations for the other single photon coherence may be shown to be

$$\frac{\partial\sigma_{32}}{\partial t} = -\left(\gamma_{32}-i\Delta_b\right)\sigma_{32} - \frac{i}{\hbar}\left(\mu_b\left(\frac{1}{2}-D\right)\left(A_a e^{ikz}+A_b e^{-ikz}\right)+\mu_a\sigma_{31}\left(A_a^* e^{-ikz}+A_b^* e^{ikz}\right)\right) \tag{3.1.1.11}$$

where, as was stated before, $\Delta_b = \omega - \omega_{32}$. As the fields are assumed far-detuned from one-photon resonance, it is assumed that the coherence terms between the

intermediate level and the excited and ground states may be adiabatically eliminated. Taking equation (3.1.1.10) and adiabatically eliminating, so that $\frac{\partial \sigma_{21}}{\partial t} = 0$, then

$$\sigma_{21} = \frac{i}{\hbar(\gamma_{21} - i\Delta_a)} \left(\mu_a \left(\frac{1}{2} + D \right) \left(A_a e^{ikz} + A_b e^{-ikz} \right) + \mu_b \sigma_{31} \left(A_a^* e^{-ikz} + A_b^* e^{ikz} \right) \right) . \tag{3.1.1.12}$$

The assumption is made that the system operates with single photon detunings much larger than the single photon decay rates, $\Delta_{a,b} >> \gamma_{21,32}$. Operating in such a regime allows the single photon decay rate terms to be neglected, leaving the above equation with the form

$$\sigma_{21} = -\frac{1}{\hbar\Delta_a} \left(\mu_a \left(\frac{1}{2} + D \right) \left(A_a e^{ikz} + A_b e^{-ikz} \right) + \mu_b \sigma_{31} \left(A_a^* e^{-ikz} + A_b^* e^{ikz} \right) \right) . \tag{3.1.1.13}$$

In a similar manner equation (3.1.1.11) may be adiabatically eliminated to give

$$\sigma_{32} = \frac{1}{\hbar\Delta_b} \left(\mu_b \left(\frac{1}{2} - D \right) \left(A_a e^{ikz} + A_b e^{-ikz} \right) + \mu_a \sigma_{31} \left(A_a^* e^{-ikz} + A_b^* e^{ikz} \right) \right) . \tag{3.1.1.14}$$

The two photon detuning term is defined as

$$\begin{aligned}\Delta_{ab} &= \Delta_a + \Delta_b \\ &= (\omega - \omega_{21}) + (\omega - \omega_{32}) \\ &= 2\omega - (\omega_2 - \omega_1) - (\omega_3 - \omega_2) \\ &= 2\omega - (\omega_3 - \omega_1) \\ &= 2\omega - \omega_{31}\,. \end{aligned} \tag{3.1.1.15}$$

It can be seen then that if the one photon detunings are much larger than the two photon detuning, $\Delta_a, \Delta_a >> \Delta_{ab}$, then (3.1.1.15) results in the approximation $\Delta_b \approx -\Delta_a$. Using this in the above equation for the steady state value of σ_{32} gives

$$\sigma_{32} = -\frac{1}{\hbar\Delta_a}\left(\mu_b\left(\frac{1}{2} - D\right)\left(A_a e^{ikz} + A_b e^{-ikz}\right) + \mu_a\sigma_{31}\left(A_a^* e^{-ikz} + A_b^* e^{ikz}\right)\right)\,. \tag{3.1.1.16}$$

3.1.2 Two-photon coherence

By following the same procedure as for the one photon coherence, σ_{21}, the equation for the coherence between the ground state, $|1\rangle$, and the uppermost state, $|3\rangle$, σ_{31} can be shown to be

$$\begin{aligned}\frac{\partial\sigma_{31}}{\partial t} =& -(\gamma_{31} - i\Delta_{ab})\sigma_{31} \\ &+ \frac{i}{\hbar}\left(\mu_b\sigma_{21}\left(A_a e^{ikz} + A_b e^{-ikz}\right) - \mu_a\sigma_{32}\left(A_a e^{ikz} + A_b e^{-ikz}\right)\right)\,. \end{aligned} \tag{3.1.2.1}$$

By substituting the equations for the single photon coherences, (3.1.1.13) & (3.1.1.16), into the above expression, the expression may be written as

$$\begin{aligned}\frac{\partial\sigma_{31}}{\partial t} =& -(\gamma_{31} - i\Delta_{ab})\sigma_{31} \\ &+ \frac{i\left(\mu_a^2 - \mu_b^2\right)}{\hbar^2\Delta_a}\sigma_{31}\left(A_a e^{2ikz} + A_b\right)\left(A_a^* e^{-2ikz} + A_b^*\right) \\ &- \frac{i2\mu_a\mu_b}{\hbar^2\Delta_a}D\left(A_a e^{2ikz} + A_b\right)\left(A_a + A_b e^{-2ikz}\right) \end{aligned} \tag{3.1.2.2}$$

3.1.3 Population terms

By following the same derivation procedure as that which produced equations (3.1.1.10), (3.1.1.11) and (3.1.2.1) for the coherence variables, the equations for the populations of the excited and ground states of the three level system may be found to be

$$\frac{\partial\rho_{11}}{\partial t} = \gamma_{33}\left(\frac{1}{2} - D\right) + \frac{i\mu_a}{\hbar}\left(\sigma_{21}\left(A_a^* e^{-ikz} + A_b^* e^{ikz}\right) - \sigma_{12}\left(A_a e^{ikz} + A_b e^{-ikz}\right)\right) \tag{3.1.3.1}$$

$$\frac{\partial\rho_{33}}{\partial t} = -\gamma_{33}\left(\frac{1}{2} - D\right) + \frac{i\mu_b}{\hbar}\left(\sigma_{23}\left(A_a e^{ikz} + A_b e^{-ikz}\right) - \sigma_{32}\left(A_a^* e^{-ikz} + A_b^* e^{ikz}\right)\right)\,, \tag{3.1.3.2}$$

where it has been assumed that as the population for ρ_{22} is negligible, all population from level $|3\rangle$ decays to level $|1\rangle$ and thus the term $\gamma_{33}\left(\frac{1}{2} - D\right)$ has been added to the equation for the population of the ground state. From (3.1.0.5) it can be seen that

$$\frac{\partial\rho_{11}}{\partial t} - \frac{\partial\rho_{33}}{\partial t} = \frac{\partial}{\partial t}\left(\rho_{11} - \rho_{33}\right) = 2\frac{\partial D}{\partial t}\,. \tag{3.1.3.3}$$

Substituting (3.1.3.1) and (3.1.3.2) into the above gives

$$2\frac{\partial D}{\partial t} = \left(\gamma_{33}\left(\frac{1}{2} - D\right) + \frac{i\mu_a}{\hbar}\left(\sigma_{21}\left(A_a^* e^{-ikz} + A_b^* e^{ikz}\right) - \sigma_{12}\left(A_a e^{ikz} + A_b e^{-ikz}\right)\right)\right) - \left(-\gamma_{33}\left(\frac{1}{2} - D\right) + \frac{i\mu_b}{\hbar}\left(\sigma_{23}\left(A_a e^{ikz} + A_b e^{-ikz}\right) - \sigma_{32}\left(A_a^* e^{-ikz} + A_b^* e^{ikz}\right)\right)\right). \tag{3.1.3.4}$$

Substituting for the one-photon coherences σ_{21} and σ_{32} using equation (3.1.1.13) and (3.1.1.16) respectively , then

$$\frac{\partial D}{\partial t} = -\gamma_{33}\left(D - D^{eq}\right) + \frac{i\mu_a\mu_b}{\hbar^2\Delta_a}\Bigg(\sigma_{13}\left(A_a + A_b e^{-2ikz}\right)\left(A_a e^{2ikz} + A_b\right) - \sigma_{31}\left(A_a^* + A_b^* e^{2ikz}\right)\left(A_a^* e^{-2ikz} + A_b^*\right)\Bigg). \tag{3.1.3.5}$$

3.1.4 Force equation

As for the two level atom case, the dipole force experienced by an atom is given by (2.5.1.19). Substituting (3.1.0.1) for the field and (3.1.0.4) for the dipole moment gives

$$\begin{aligned}\frac{\partial p_j}{\partial t} =& \vec{d_j} \cdot \frac{\partial \vec{E}}{\partial z} \\ =& \left(p_{12}\rho_{21} + p_{21}\rho_{12} + p_{32}\rho_{23} + p_{23}\rho_{32}\right)\hat{e}\cdot \\ & \frac{\partial}{\partial z}\left(A_a(t)e^{i(kz-\omega t)} + A_b(t)e^{i(-kz-\omega t)} + c.c.\right)\hat{e}\,.\end{aligned} \tag{3.1.4.1}$$

Substituting for the dipole matrix elements (3.1.1.2) and (3.1.1.3) using equation (3.1.1.5), along with equation (3.1.1.5) for the coherence, the equation for the force experienced by an atom becomes

$$\frac{\partial p_j}{\partial t} = \left(\mu_a\sigma_{21}e^{-i\omega t} + \mu_a\sigma_{12}e^{i\omega t} + \mu_b\sigma_{23}e^{i\omega t} + \mu_b\sigma_{32}e^{-i\omega t}\right) \left(ikA_ae^{i(kz-\omega t)} - ikA_be^{i(-kz-\omega t)} - ikA_a^*e^{i(-kz+\omega t)} + ikA_b^*e^{i(kz+\omega t)}\right) . \tag{3.1.4.2}$$

Substituting for the one-photon coherence variables, σ_{21} and σ_{32} using equation (3.1.1.13) and (3.1.1.16), then

$$\frac{\partial p_j}{\partial t} = \frac{i2k\mu_a\mu_b}{\hbar\Delta_a}\left[\sigma_{31}\left(A_a^{*2}e^{-2ikz} - A_b^{*2}e^{2ikz}\right) - \sigma_{13}\left(A_a^2e^{2ikz} - A_b^2e^{-2ikz}\right)\right] + \frac{i2k}{\hbar\Delta_a}\left(A_a^*A_be^{-2ikz} - A_aA_b^*e^{2ikz}\right)\left[\frac{1}{2}\left(\mu_a^2+\mu_b^2\right) + D\left(\mu_a^2-\mu_b^2\right)\right] . \tag{3.1.4.3}$$

3.1.5 Position equation

The equation for the position of the jth atom is given again by simply

$$\frac{\partial z_j}{\partial t} = \frac{p_j}{m} . \tag{3.1.5.1}$$

3.1.6 Field equations

The equations for the field amplitudes can be derived once again from the wave equation (2.4.1.1) by substituting for the polarisation using equations (3.1.0.1) & (3.1.0.4). Substituting equation (3.1.0.1) into the left hand side of the wave equation produces the same result as for the two level case, namely

$$\nabla^2\vec{E} - \frac{1}{c^2}\frac{\partial^2\vec{E}}{\partial t^2} = \left(\frac{2i\omega}{c^2}\frac{\partial A_a}{\partial t}e^{i(kz-\omega t)} + \frac{2i\omega}{c^2}\frac{\partial A_b}{\partial t}e^{i(-kz-\omega t)} + c.c.\right)\hat{e} . \tag{3.1.6.1}$$

Substituting equation (3.1.0.4) into the right hand side of the wave equation, using equations (3.1.1.2), (3.1.1.3), (3.1.1.5), (3.1.1.6) and (3.1.1.7), produces

$$\begin{aligned}\frac{\partial^2 \vec{P}}{\partial t^2} &= \frac{\partial^2}{\partial t^2}\left(\sum_j^n \vec{d}_j \delta(r - r_j(t))\right) \\ &= \sum_j^n \frac{\partial^2 \vec{d}_j}{\partial t^2}\delta(r - r_j(t)) \\ &= \sum_j^n \frac{\partial^2}{\partial t^2}\Big(\mu_a \sigma_{21} e^{-i\omega t} + \mu_a \sigma_{32} e^{-i\omega t} + c.c\Big)\hat{e}\ \delta(r - r_j(t))\,. \end{aligned} \tag{3.1.6.2}$$

Expanding the term $\frac{\partial^2 \vec{d}_j}{\partial t^2}$ gives

$$\begin{aligned}\frac{\partial^2 \vec{d}_j}{\partial t^2} &= \frac{\partial^2}{\partial t^2}\Big(\mu_a \sigma_{21} e^{-i\omega t} + \mu_a \sigma_{32} e^{-i\omega t} + c.c\Big)\hat{e} \\ &= \frac{\partial}{\partial t}\left(\mu_a\left(\frac{\partial \sigma_{21}}{\partial t} - i\omega\sigma_{21}\right)e^{-i\omega t} + \mu_b\left(\frac{\partial \sigma_{32}}{\partial t} - i\omega\sigma_{32}\right)e^{-i\omega t} + c.c\right)\hat{e} \\ &= \Big(\mu_a\left(\frac{\partial^2 \sigma_{21}}{\partial t^2} - 2i\omega\frac{\partial \sigma_{21}}{\partial t} - \omega^2\sigma_{21}\right)e^{-i\omega t} \\ &\quad + \mu_b\left(\frac{\partial^2 \sigma_{32}}{\partial t^2} - 2i\omega\frac{\partial \sigma_{32}}{\partial t} - \omega^2\sigma_{32}\right)e^{-i\omega t} + c.c\Big)\hat{e}\,. \end{aligned} \tag{3.1.6.3}$$

Applying the SVEA to the above and substituting into the right hand side of the wave equation gives

$$\begin{aligned}&\left(\frac{2i\omega}{c^2}\frac{\partial A_a}{\partial t}e^{i(kz-\omega t)} + \frac{2i\omega}{c^2}\frac{\partial A_b}{\partial t}e^{i(-kz-\omega t)} + c.c.\right)\hat{e} \\ &= \frac{1}{\epsilon_0 c^2}\sum_j^n \left(-\mu_a\omega^2\sigma_{21}e^{-i\omega t} - \mu_b\omega^2\sigma_{32}e^{-i\omega t} + c.c\right)\hat{e}\ \ \delta(r - r_j(t))\,. \end{aligned} \tag{3.1.6.4}$$

From the above, an equation for the temporal evolution of A_a can be acquired by first multiplying through by $e^{i(-kz+\omega t)}$ and applying the RWA to produce

$$\left(\frac{2i\omega}{c^2}\frac{\partial A_a}{\partial t}+\frac{2i\omega}{c^2}\frac{\partial A_b}{\partial t}e^{-2ikz}\right)\hat{e}$$
$$=\frac{1}{\epsilon_0 c^2}\sum_j^n\left(-\mu_a\omega^2\sigma_{21}e^{-ikz}-\mu_b\omega^2\sigma_{32}e^{-ikz}\right)\hat{e}\ \ \delta(r-r_j(t))\,. \tag{3.1.6.5}$$

Integrating the above over the cavity area $\mathscr{A}$ and the cavity length L, any terms containing $e^{\pm 2ikz}$ on the left hand side are averaged out and eliminated and the Dirac delta function on the right hand side produces

$$\mathscr{A}L\frac{2i\omega}{c^2}\frac{\partial A_a}{\partial t}\hat{e}=\frac{1}{\epsilon_0 c^2}\sum_j^n\left(-\mu_a\omega^2\sigma_{21}e^{-ikz_j}-\mu_b\omega^2\sigma_{32}e^{-ikz_j}\right)\hat{e}\,. \tag{3.1.6.6}$$

By rearranging the constants to the right hand side and cancelling down terms the equation becomes

$$\frac{\partial A_a}{\partial t}\hat{e}=\frac{i\omega}{\mathscr{A}L2\epsilon_0}\sum_j^n\left(\mu_a\sigma_{21}e^{-ikz_j}+\mu_b\sigma_{32}e^{-ikz_j}\right)\hat{e}\,. \tag{3.1.6.7}$$

Multiplying the right hand side by $\frac{N}{N}$, using (2.5.1.16) & (2.5.1.15) and taking the dot product of the equation with $\hat{e}$ the expression for the evolution of the probe beam A_a can be rewritten as

$$\frac{\partial A_a}{\partial t}=\frac{i\omega n}{2\epsilon_0}\left\langle\mu_a\sigma_{21}e^{-ikz_j}+\mu_b\sigma_{32}e^{-ikz_j}\right\rangle\,. \tag{3.1.6.8}$$

Substituting for σ_{21} and σ_{23} using eq. (3.1.1.13) and (3.1.1.16) then

$$\frac{\partial A_a}{\partial t} = \frac{i\omega n}{2\epsilon_0}\Bigg\langle \mu_a e^{-ikz_j}\Bigg[-\frac{1}{\hbar\Delta_a}\Bigg(\mu_a\left(\frac{1}{2}+D\right)\left(A_a e^{ikz}+A_b e^{-ikz}\right) + \mu_b\sigma_{31}\left(A_a^* e^{-ikz}+A_b^* e^{ikz}\right)\Bigg)\Bigg] + \mu_b e^{-ikz_j}\Bigg[-\frac{1}{\hbar\Delta_a}\Bigg(\mu_b\left(\frac{1}{2}-D\right)\left(A_a e^{ikz}+A_b e^{-ikz}\right) + \mu_a\sigma_{31}\left(A_a^* e^{-ikz}+A_b^* e^{ikz}\right)\Bigg)\Bigg]\Bigg\rangle . \quad (3.1.6.9)$$

Collecting terms and adding the detuning, loss and pumping terms derived in Section 2.5.1.3 gives the final form of the equation for the probe field amplitude A_a,

$$\frac{\partial A_a}{\partial t} = \frac{-i\omega n}{2\hbar\epsilon_0\Delta_a}\Bigg\langle \begin{aligned} &2\mu_a\mu_b\sigma_{31}\left(A_a^* e^{-2ikz}+A_b^*\right) \\ &+\frac{1}{2}\left(\mu_a^2+\mu_b^2\right)\left(A_a+A_b e^{-2ikz}\right) \\ &+\left(\mu_a^2-\mu_b^2\right)D\left(A_a+A_b e^{-2ikz}\right) \end{aligned} \Bigg\rangle + (i\delta_c-\kappa)A_a + \kappa A_a^{eq} . \quad (3.1.6.10)$$

In a similar manner, the equation for the amplitude of the pump beam A_b is found to be

$$\frac{\partial A_b}{\partial t} = \frac{-i\omega n}{2\hbar\epsilon_0\Delta_a}\Bigg\langle \begin{aligned} &2\mu_a\mu_b\sigma_{31}\left(A_a^* + A_b^* e^{2ikz}\right) \\ &+\frac{1}{2}\left(\mu_a^2+\mu_b^2\right)\left(A_a e^{2ikz}+A_b\right) \\ &+\left(\mu_a^2-\mu_b^2\right)D\left(A_a e^{2ikz}+A_b\right) \end{aligned} \Bigg\rangle + (i\delta_c-\kappa)A_b + \kappa A_b^{eq} . \quad (3.1.6.11)$$

3.1.7 Describing the AC Stark shift

The AC Stark shift terms within the three level ladder equations derived above result from the small difference between the dipole matrix elements μ_a and μ_b. Prior to scaling, it is convenient to first rearrange the equations to a form where the effects of the AC Stark shift can be easily recognised.

The terms μ_a and μ_b appear in three configurations in the three level ladder equations. Setting $\mu_a = \mu$ and $\mu_b = \mu + \Delta_\mu$, where $\Delta_\mu = \mu_a - \mu_b$ in each of the three configurations gives

$$\mu_a\mu_b = \mu(\mu + \Delta_\mu) = \mu^2(1 + \frac{\Delta_\mu}{\mu})$$
$$\mu_a^2 + \mu_b^2 = \mu^2 + (\mu + \Delta_\mu)^2 = 2\mu^2 + 2\mu\Delta_\mu + \Delta_\mu^2 = \mu^2\left(2 + 2\frac{\Delta_\mu}{\mu} + \left(\frac{\Delta_\mu}{\mu}\right)^2\right)$$
$$\mu_a^2 - \mu_b^2 = \mu^2 - (\mu + \Delta_\mu)^2 = -2\mu\Delta_\mu - \Delta_\mu^2 = -\mu^2\left(\frac{\Delta_\mu}{\mu} + \left(\frac{\Delta_\mu}{\mu}\right)^2\right).$$

Defining

$$\epsilon_\mu = \frac{\Delta_\mu}{\mu} \tag{3.1.7.1}$$

gives

$$\mu_a\mu_b = \mu^2(1 + \epsilon_\mu)$$
$$\mu_a^2 + \mu_b^2 = \mu^2\left(2 + 2\epsilon_\mu + \epsilon_\mu^2\right)$$
$$\mu_a^2 - \mu_b^2 = -\mu^2\left(\epsilon_\mu + \epsilon_\mu^2\right).$$

As the dipole matrix terms μ_a and μ_b are of a similar magnitude, by its very definition, $\Delta_\mu < \mu$, so from (3.1.7.1) it must therefore be true that $\epsilon_\mu << 1$. Likewise $\epsilon_\mu^2 << \epsilon_\mu$. Keeping only the terms with the most significant influence, the AC Stark shift terms above become

$$\mu_a \mu_b = \mu^2 \tag{3.1.7.2}$$

$$\mu_a^2 + \mu_b^2 = 2\mu^2 \tag{3.1.7.3}$$

$$\mu_a^2 - \mu_b^2 = -\mu^2 \epsilon_\mu \,. \tag{3.1.7.4}$$

Substituting equations (3.1.7.2) - (3.1.7.4) into equations (3.1.3.5), (3.1.2.2), (3.1.4.3), (3.1.5.1), (3.1.6.10) & (3.1.6.11) produces the closed set of equations for three-level atoms interacting with two optical fields:

$$\frac{\partial D}{\partial t} = -\gamma_{33}\left(D - D^{eq}\right) + \frac{i\mu^2}{\hbar^2 \Delta_a}\Bigg(\sigma_{13}\left(A_a + A_b e^{-2ikz}\right)\left(A_a e^{2ikz} + A_b\right) - \sigma_{31}\left(A_a^* + A_b^* e^{2ikz}\right)\left(A_a^* e^{-2ikz} + A_b^*\right) \Bigg) \tag{3.1.7.5}$$

$$\begin{aligned} \frac{\partial \sigma_{31}}{\partial t} =& -\left(\gamma_{31} - i\Delta_{ab}\right)\sigma_{31} \\ & - \frac{i\mu^2 \epsilon_\mu}{\hbar^2 \Delta_a}\sigma_{31}\left(A_a e^{2ikz} + A_b\right)\left(A_a^* e^{-2ikz} + A_b^*\right) \\ & - \frac{i2\mu^2}{\hbar^2 \Delta_a} D\left(A_a e^{2ikz} + A_b\right)\left(A_a + A_b e^{-2ikz}\right) \end{aligned} \tag{3.1.7.6}$$

$$\begin{aligned} \frac{\partial p_j}{\partial t} =& \frac{i2k\mu^2}{\hbar \Delta_a}\left[\sigma_{31}\left(A_a^{*2} e^{-2ikz} - A_b^{*2} e^{2ikz}\right) - \sigma_{13}\left(A_a^2 e^{2ikz} - A_b^2 e^{-2ikz}\right)\right] \\ & + \frac{i2k\mu^2}{\hbar \Delta_a}\left(A_a^* A_b e^{-2ikz} - A_a A_b^* e^{2ikz}\right) \end{aligned} \tag{3.1.7.7}$$

$$\frac{\partial z_j}{\partial t} = \frac{p_j}{m} \tag{3.1.7.8}$$

$$\frac{\partial A_a}{\partial t} = \frac{-i\omega\mu^2 n}{2\hbar\epsilon_0\Delta_a}\left\langle 2\sigma_{31}\left(A_a^* e^{-2ikz} + A_b^*\right) + \left(A_a + A_b e^{-2ikz}\right)\right\rangle + (i\delta_c - \kappa)A_a + \kappa A_a^{eq} \tag{3.1.7.9}$$

$$\frac{\partial A_b}{\partial t} = \frac{-i\omega\mu^2 n}{2\hbar\epsilon_0\Delta_a}\left\langle 2\sigma_{31}\left(A_a^* + A_b^* e^{2ikz}\right) + \left(A_a e^{2ikz} + A_b\right)\right\rangle + (i\delta_c - \kappa)A_b + \kappa A_b^{eq} \tag{3.1.7.10}$$

The terms $-\frac{i\mu^2\epsilon_\mu}{\hbar^2\Delta_a}\sigma_{31}\left(A_a e^{2ikz} + A_b\right)\left(A_a^* e^{-2ikz} + A_b^*\right)$ and $i\Delta_{ab}\sigma_{31}$ from the equation for the coherence, equation (3.1.7.6), may be grouped together to produce the term $i\left(\Delta_{ab} - \frac{\mu^2\epsilon_\mu}{\hbar^2\Delta_a}\left(|A_a|^2 + A_a A_b^* e^{2ikz} + A_a^* A_b e^{-2ikz} + |A_b|^2\right)\right)\sigma_{31}$. In such a form it is easy to see the the terms dependent upon the term ϵ_μ act to modify the detuning of the field from atomic resonance. The AC Stark shift may then be thought of as an intensity dependent detuning, or (when multiplied by $\hbar$) as an intensity dependent energy shift.

3.1.8 Scaling the 3 level ladder equations

The equations derived in the above section, (3.1.7.5) - (3.1.7.10), can be rewritten in a manner which more easily lends itself to exploring CARL with three energy levels through use of the common [81, 44, 38, 42, 53] substitution terms

$$\alpha_{a,b} = A_{a,b}\sqrt{\frac{2\epsilon_0 V}{\hbar\omega}} \tag{3.1.8.1}$$

$$g = \mu\sqrt{\frac{\omega}{2\epsilon_0\hbar V}} \tag{3.1.8.2}$$

$$U_0 = \frac{g^2}{\Delta_a}, \tag{3.1.8.3}$$

where U_0 is the dispersive frequency shift due to a single atom, g is the single photon Rabi frequency and $|\alpha_{a,b}|^2$ represents the number of photons in the probe (a) or pump (b) beam.

Substituting the scaling terms (3.1.8.1) - (3.1.8.3) into the closed set of equations for three-level atoms interacting with two optical fields (3.1.7.5) - (3.1.7.10) gives the scaled, two-photon CARL equations

$$\frac{\partial D}{\partial t} = -\gamma_{33}\left(D - D^{eq}\right) + iU_0\Bigg(\sigma_{13}\left(\alpha_a + \alpha_b e^{-2ikz}\right)\left(\alpha_a e^{2ikz} + \alpha_b\right) - \sigma_{31}\left(\alpha_a^* + \alpha_b^* e^{2ikz}\right)\left(\alpha_a^* e^{-2ikz} + \alpha_b^*\right) \Bigg) \tag{3.1.8.4}$$

$$\begin{aligned}\frac{\partial \sigma_{31}}{\partial t} = &-\left(\gamma_{31} - i\Delta_{ab}\right)\sigma_{31} \\ &- i2U_0 D\left(\alpha_a e^{2ikz} + \alpha_b\right)\left(\alpha_a + \alpha_b e^{-2ikz}\right) \\ &- iU_0\epsilon_\mu\sigma_{31}\left(\alpha_a e^{2ikz} + \alpha_b\right)\left(\alpha_a^* e^{-2ikz} + \alpha_b^*\right)\end{aligned} \tag{3.1.8.5}$$

$$\begin{aligned}\frac{\partial p_j}{\partial t} = &\, i2\hbar k U_0\left[\sigma_{31}\left(\alpha_a^{*2} e^{-2ikz} - \alpha_b^{*2} e^{2ikz}\right) - \sigma_{13}\left(\alpha_a^2 e^{2ikz} - \alpha_b^2 e^{-2ikz}\right)\right] \\ &+ i2\hbar k U_0\left(\alpha_a^*\alpha_b e^{-2ikz} - \alpha_a\alpha_b^* e^{2ikz}\right)\end{aligned} \tag{3.1.8.6}$$

$$\frac{\partial z_j}{\partial t} = \frac{p_j}{m} \tag{3.1.8.7}$$

$$\frac{\partial \alpha_a}{\partial t} = -iNU_0\Big\langle 2\sigma_{31}\left(\alpha_a^* e^{-2ikz} + \alpha_b^*\right) + \left(\alpha_a + \alpha_b e^{-2ikz}\right) \Big\rangle + \left(i\delta_c - \kappa\right)\alpha_a + \kappa\alpha_a^{eq} \tag{3.1.8.8}$$

$$\frac{\partial \alpha_b}{\partial t} = -iNU_0 \Big\langle \quad 2\sigma_{31}\left(\alpha_a^* + \alpha_b^* e^{2ikz}\right) + \left(\alpha_a e^{2ikz} + \alpha_b\right) \quad \Big\rangle + (i\delta_c - \kappa)\alpha_b + \kappa\alpha_b^{eq} \tag{3.1.8.9}$$

3.2 Two-photon collective atomic recoil lasing

In what follows, two regimes for two-photon CARL are investigated. A regime of low pump intensity, referred to as the weak pump limit, and a regime of high pump intensity, referred to as the strong pump limit. Both pumping limits are considered for the case where the AC Stark effect is included and neglected. To better highlight the effect being investigated, we will consider an idealised case where there is no incoherent decay of the two-photon coherence or excited state population, i.e. $\gamma_{31} = \gamma_{33} = 0$. It is also assumed that cavity losses are negligible on the timescales considered here ($\kappa \to 0$), that the atoms are initially uniformly distributed in space, and that the atoms are initially sufficiently cold that any thermal dephasing occurs on timescales much longer than the development of the instability ($p_j = 0 \; \forall \; j$).

3.2.1 Including the AC Stark shift

The first step to investigating how the two-photon CARL instability varies with population excitation is to define a reference or "saturation" pump intensity. This can be achieved by solving the equation for the two-photon coherence, (3.1.8.4) and the equation for the population inversion, (3.1.8.5) in the same manner as in section (2.5.3). Solving for D in the limit where $\alpha_a = 0$ we obtain

$$D = \frac{1}{2}\frac{\Delta_{ab}^2}{\Delta_{ab}^2 + 4U_0^2|\alpha_b|^4} + \frac{2U_0^2|\alpha_b|^4}{\Delta_{ab}^2 + 4U_0^2|\alpha_b|^4}\cos\left(\sqrt{\Delta_{ab}^2 + 4U_0^2|\alpha_b|^4}t\right) . \quad (3.2.1.1)$$

By averaging over an oscillation period, this becomes

$$D = \frac{1}{2}\frac{\Delta_{ab}^2}{\Delta_{ab}^2 + 4U_0^2|\alpha_b|^4} . \quad (3.2.1.2)$$

Defining a "saturation" pump intensity as being that for which the average excited-state population, $\langle\rho_{33}\rangle$, is 1/4 i.e. $\langle D\rangle = 1/4$, we can see from the above equation that this occurs when the pump photon number is

$$|\alpha_b|^2 \equiv |\alpha_b|^2_{\text{sat}} = \left|\frac{\Delta_{ab}}{2U_0}\right| . \tag{3.2.1.3}$$

3.2.1.1 Gain in the weak pump limit

A more thorough derivation of the response of the system to the pump and probe beams is performed in Appendix A. It is shown that when the system operates in the weak pump limit and is sufficiently detuned that $\Delta_{ab} >> \gamma_{31}$, the expected gain for the system is approximately

$$Gain = \frac{\sqrt{3}}{2}\sqrt[3]{\frac{2N\hbar k^2|\alpha_b|^2}{m}\left(U_0^2 + \frac{3U_0^3|\alpha_b|^2}{\Delta_{ab}} + \frac{2U_0^4|\alpha_b|^4}{\Delta_{ab}^2}\right)} . \tag{3.2.1.4}$$

The term $\frac{3U_0^3|\alpha_b|^2}{\Delta_{ab}}$, being of an odd power of both U_0 (which is proportional to $^1/_{\Delta_a}$) and Δ_{ab}, is positive when both the single and two photon detuning terms have the same sign. However, for opposing signs of detuning, it should be expected that this term would detract from the gain experienced by the system.

3.2.1.2 The weak excitation limit

We consider first the limit $|\alpha_b|^2 \ll |\alpha_b|^2_{\text{sat}}$ such that each atom experiences only a weak internal excitation and the population remains almost exclusively in the ground state $|1\rangle$ i.e. $D \to \frac{1}{2}$ and $\sigma_{31} \to 0$. In this limit equations (3.1.8.4) - (3.1.8.9) reduce to

$$\frac{dz_j}{dt} = \frac{p_j}{m} \tag{3.2.1.5}$$

$$\frac{dp_j}{dt} = -i2\hbar k U_0\left(\alpha_a\alpha_b^* e^{2ikz_j} - c.c.\right) \tag{3.2.1.6}$$

$$\frac{d\alpha_a(t)}{dt} = -iNU_0\left(\alpha_a + \alpha_b\left\langle e^{-2ikz}\right\rangle\right) + \left(i\delta_c - \kappa\right)\alpha_a , \tag{3.2.1.7}$$

where there is no field for α_a injected into the system, so $\alpha_a^{eq} = 0$. The above, when written in terms of the dimensionless variables:

$$\theta = 2kz \quad , \quad \bar{p} = \frac{2}{\rho}p \quad , \quad \bar{a} = \sqrt{\frac{2}{\rho N}}\alpha_a \,,$$

in a similar manner as to section 2.5.3.3, become the CARL equations originally derived for two-level atoms [37, 80] in what is referred to as the Free-Electron-Laser (FEL) limit [79]:

$$\frac{d\theta_j}{d\tau} = \bar{p}_j \tag{3.2.1.8}$$

$$\frac{d\bar{p}_j}{d\tau} = -\left(\bar{a}e^{i\theta_j} + c.c.\right) \tag{3.2.1.9}$$

$$\frac{d\bar{a}}{d\tau} = \left\langle e^{-i\theta} \right\rangle - \bar{\kappa}\bar{a} \,, \tag{3.2.1.10}$$

where it has been assumed that $\alpha_b = -i|\alpha_b|$ and $\delta_c = NU_0$, that the dimensionless time coordinate $\tau = \omega_r \rho t$, that the cavity decay rate $\bar{\kappa} = \frac{\kappa}{\omega_r \rho}$, that $\omega_r = \frac{2\hbar k^2}{m}$ is the recoil frequency and lastly that the scaling parameter ρ can be defined as

$$\rho = \left(\frac{2NU_0^2|\alpha_b|^4}{\omega_r^2}\right)^{1/3} .$$

As was described previously, in section 2.5.3.3, equations (3.2.1.8)-(3.2.1.10) exhibit a collective instability. The case in which the atoms are equally distributed in the z direction proves to be unstable after spontaneous emission in a direction counter to the pump beam produces a weak standing wave and produces a bunching force. The instability results in exponential growth of the backscattered probe beam $|\bar{a}|^2$ and the bunching parameter $|b| = |\left\langle e^{-i\theta} \right\rangle|$.

Figures 3.2, 3.3 and 3.4 demonstrate the evolution of the system in the weak-excitation regime. Figure 3.2 detail the evolution of the magnitude squared of the probe photon number $|\alpha_a|^2$, bunching parameter $|b|$, and average population difference $\langle D \rangle$ in descending order.

From Figure 3.2 it can be seen that an exponential growth of the number of photons in the probe beam occurs in unison with the growth of the bunching parameter. This behaviour is indicative of a modulation in the atomic density with spacial period $\lambda/2$ occurring within the atomic sample. The same behaviour

in two-level systems is described as the CARL instability [37, 80, 79]. Figure 3.3 provides a clearer look at the development of this density modulation through snapshots of the phase space (θ, p) evolving in time. The behaviour of the atomic motion contrasts with that of the atomic population as can be seen in Figure 3.4 through its snapshots on the atomic population distribution (θ, D) evolving in time. In the snapshots the population differences vary only a tiny amount from their original values, meaning that as the system evolves temporally the population remains almost entirely spatially uniform in the ground state.

Comparing Figure 3.2 back to Figure 2.8 from section 2.5.3.2 shows a high degree of similarity, as would be expected as it has been shown the three level ladder equations can be scaled to match the two level CARL equations in the FEL limit.

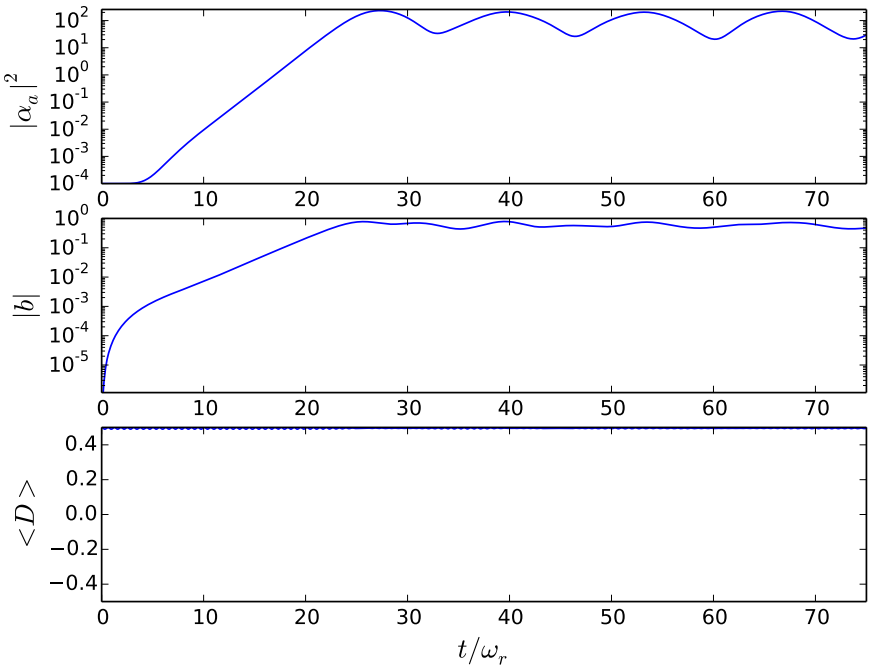

Figure 3.2: Evolution of probe photon number, $|\alpha_a|^2$, bunching parameter, $|b|$, and mean population difference, $\langle D \rangle$ for a case of weak-excitation. Produced by solving equations (3.1.8.9) - (3.1.8.4). Parameters used are $U_0/\omega_r = 5 \times 10^{-5}$, $\Delta_{ab} = 10$, $\alpha_b = 100$, $N = 1000$, $\epsilon_\mu = 0.1$. Top: As was the case for two level CARL, in the three level ladder system the probe beam experiences exponential growth due to the CARL instability. $Gain_{probe} \approx 1$. Middle: Growth of atomic bunching due to the CARL instability. Bottom: Population remains, on average, in the ground state throughout the evolution of the instability.

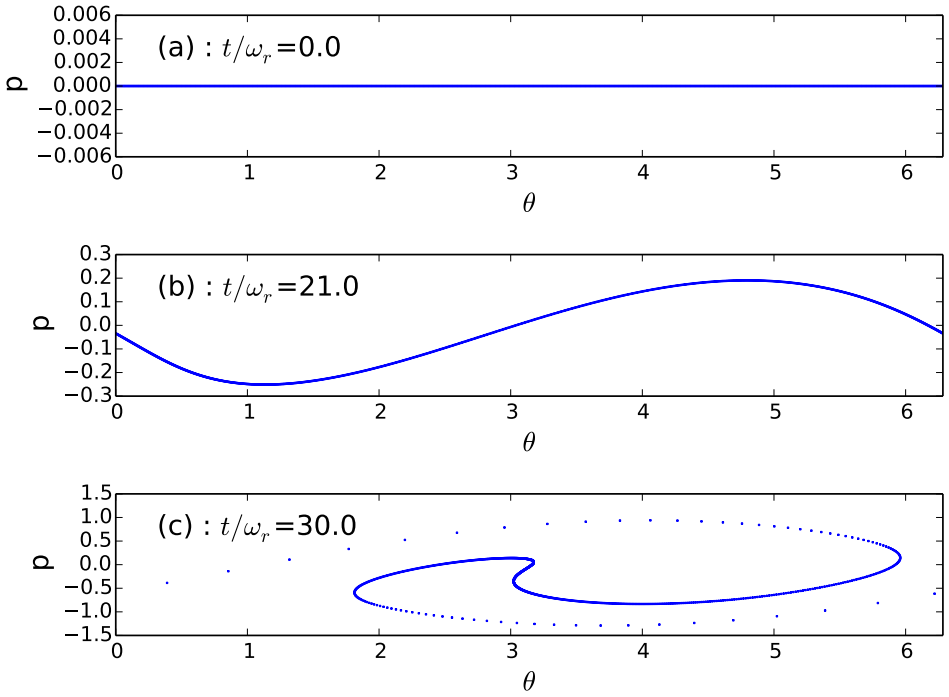

Figure 3.3: Snapshots of momentum distribution (θ_j, p_j) for each atom $j = 1..1000$ when (a) $t = 0\omega_r^{-1}$, (b) $t = 21\omega_r^{-1}$, (c) $t = 30\omega_r^{-1}$ in the case of weak excitation. Parameters used and equations solved are as in Figure 3.2. Similarly to the case of two level CARL, the three level ladder particles acquire momentum due to the dipole force which results in bunching.

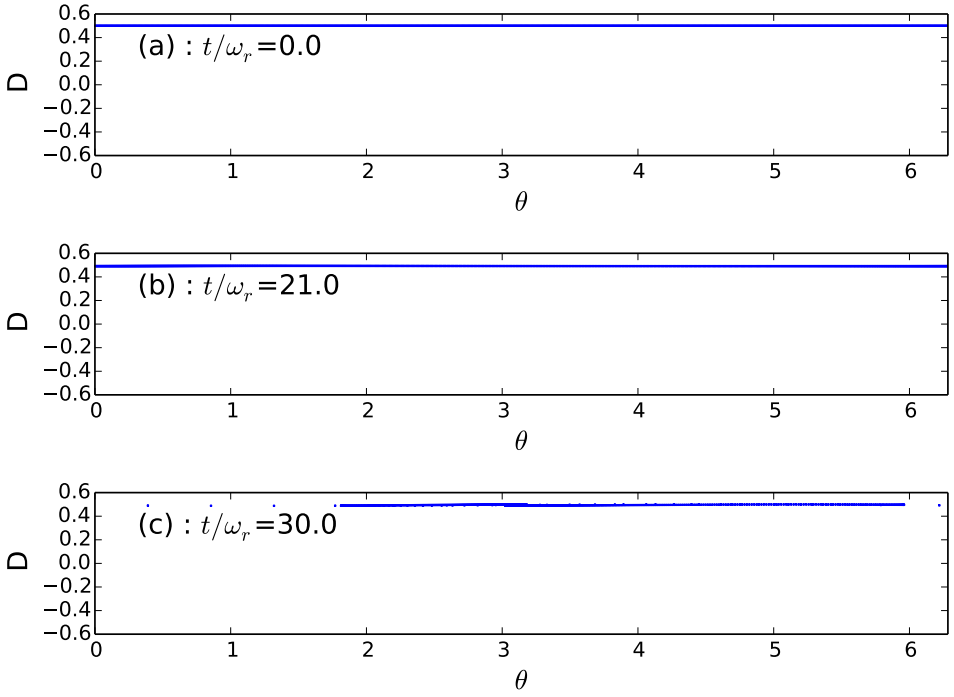

Figure 3.4: Snapshots of population difference distribution (θ_j, D_j) for each atom $j = 1..1000$ when (a) $t = 0\omega_r^{-1}$, (b) $t = 21\omega_r^{-1}$, (c) $t = 30\omega_r^{-1}$ in the case of weak excitation. Parameters used and equations solved are as in Figure 3.2. As was the case in the two level CARL system the atoms bunch as time progresses with each atom remains in the ground state due to the low intensity of the pump field α_b.

Figure 3.2 displays the CARL instability for the case where both the single photon detuning Δ_a (and consequently U_0) and the two photon detuning Δ_{ab} both have positive values and the system is operating in the weak pump regime. As both U_0 and Δ_{ab} are positive, so too is the term $\frac{U_0}{\Delta_{ab}}$ in equation (3.2.1.4) in section 3.2.1.1. As the expression $\frac{U_0}{\Delta_{ab}}$ is also positive when both U_0 and Δ_{ab} are negative, it is to be expected that the when the system operates with those signs the resulting gain should closely match that of Figure 3.2. This prediction is shown to be accurate when the comparison is made between Figures 3.2 and 3.5.

However, when only one of the two detuning terms is negative and the other takes a positive value, the term $\frac{3U_0^3|\alpha_b|^2}{\Delta_{ab}}$ in equation (3.2.1.4) takes a negative value and acts to counter the gain expected in the system. This loss of gain is shown to take place regardless of which detuning is negative when comparing Figures 3.2 and 3.5 to Figures 3.5 and 3.7.

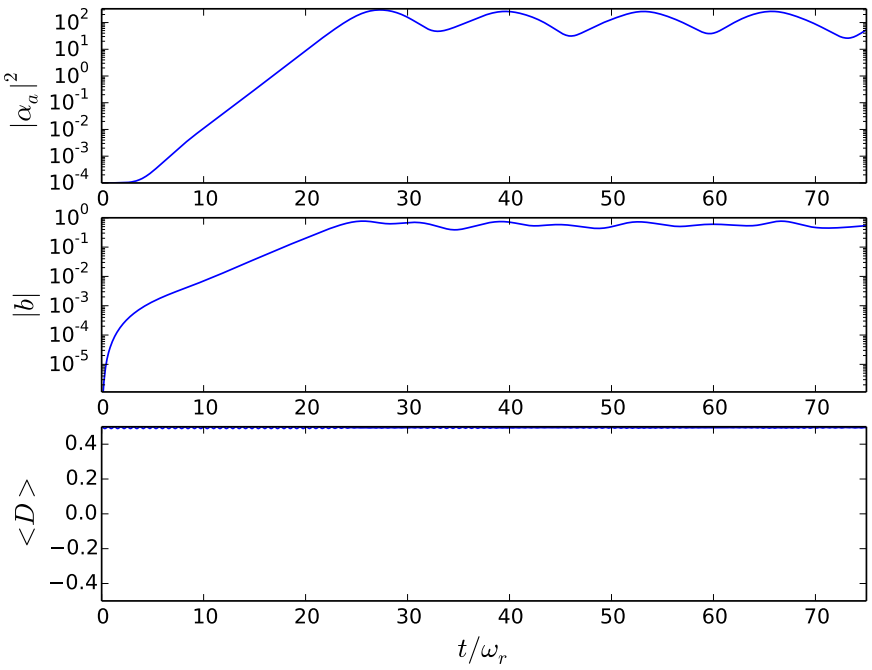

Figure 3.5: Evolution of probe photon number, $|\alpha_a|^2$, bunching parameter, $|b|$, and mean population difference, $\langle D \rangle$ for a case of weak-excitation. Produced by solving equations (3.1.8.9) - (3.1.8.4). Parameters used are $U_0/\omega_r = -5 \times 10^{-5}$, $\Delta_{ab} = -10$, $\alpha_b = 100$, $N = 1000$, $\epsilon_\mu = 0.1$. By changing the terms U_0 and Δ_{ab} from both being positive to both being negative, the term $\frac{U_0}{\Delta_{ab}}$ in the equation for the expected probe beam gain, equation (3.2.1.4), remains positive. Equation (3.2.1.4) remains unchanged then and the gain in the system should remain close to that of the case where both U_0 and Δ_{ab} are positive. This can be seen to be the case when this Figure is compared with Figure 3.2. $Gain_{probe} \approx 1$.

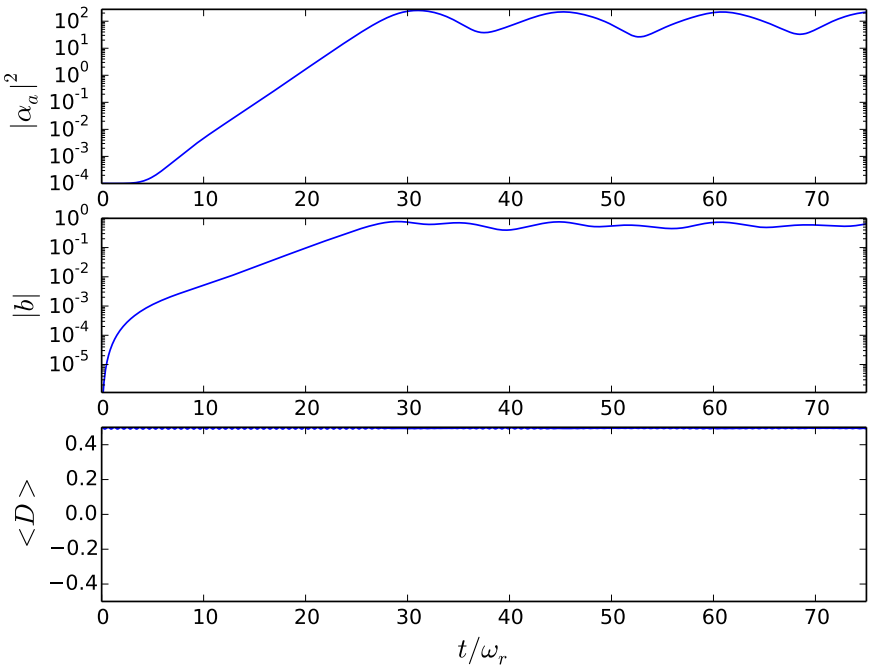

Figure 3.6: Evolution of probe photon number, $|\alpha_a|^2$, bunching parameter, $|b|$, and mean population difference, $\langle D \rangle$ for a case of weak-excitation. Produced by solving equations (3.1.8.9) - (3.1.8.4). Parameters used are $U_0/\omega_r = -5 \times 10^{-5}$, $\Delta_{ab} = 10$, $\alpha_b = 100$, $N = 1000$, $\epsilon_\mu = 0.1$. Allowing U_0 to be negative while Δ_{ab} is positive means that the term $\frac{U_0}{\Delta_{ab}}$ takes a negative value, reducing the resulting value produced by the probe gain equation, equation (3.2.1.4). Comparing this Figure with Figures 3.2 & 3.5 demonstrates this. $Gain_{probe} \approx 0.2$.

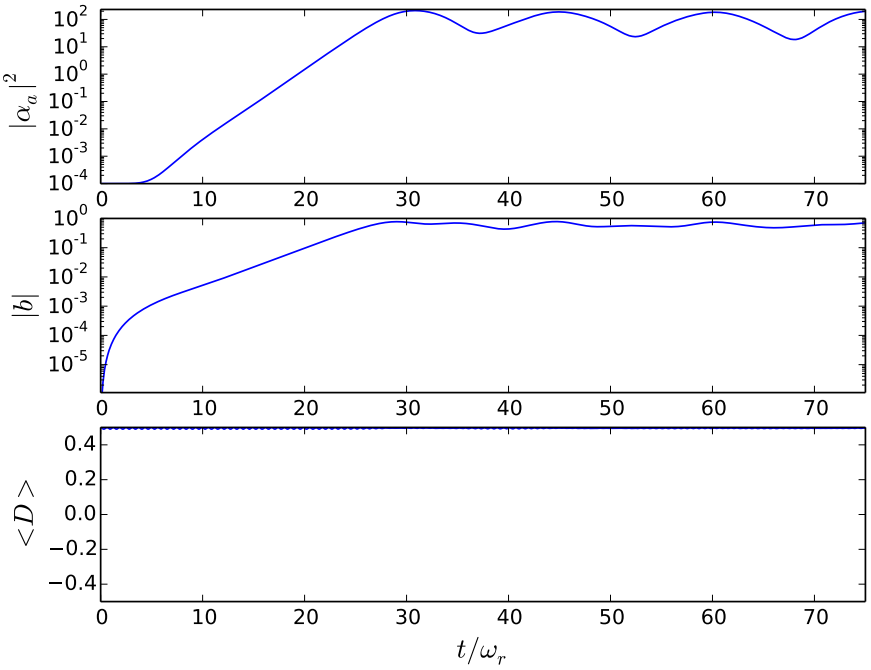

Figure 3.7: Evolution of probe photon number, $|\alpha_a|^2$, bunching parameter, $|b|$, and mean population difference, $\langle D \rangle$ for a case of weak-excitation. Produced by solving equations (3.1.8.9) - (3.1.8.4). Parameters used are $U_0/\omega_r = 5 \times 10^{-5}$, $\Delta_{ab} = -10$, $\alpha_b = 100$, $N = 1000$, $\epsilon_\mu = 0.1$. Allowing U_0 to be positive while Δ_{ab} is negative also produces a reduced value from the probe gain equation, equation (3.2.1.4), in a manner similar to Figure 3.6. It can be seen by comparing this Figure to Figure 3.6 that the gain in the probe beam is similar in both cases, as expected. $Gain_{probe} \approx 0.2$.

3.2.1.3 The strong excitation limit

Figures 3.8, 3.9 and 3.10 show the evolution of the system in the strong-pump limit. It can be seen from Figure 3.8 that once again growth occurs in the cavity field intensity synchronously with the growth of the bunching parameter.

However, from the snapshots of the atomic population distribution (θ, D) shown in Figure 3.10 and the evolution of the average population difference shown in the bottommost graph of Figure 3.8 it can be noted that, in this strong-pump limit, the atomic population difference undergoes a significant deviation from its initial value of $^1/_2$ during the evolution of the instability. This is in stark contrast to the weak-pump limit where the atomic population difference hardly changes from its initial value at all.

In the strong pumping regime the system undergoes initial, rapid, two-photon Rabi oscillations which result in a strongly periodic distribution of atomic population as well as the expected periodic distribution of atomic density. The evolution of the two-photon Rabi oscillations can be seen in Figure 3.8 and the periodic distribution of atomic population can be seen in the snapshots of atomic population distribution (θ, D) in Figure 3.10.

From these figures it can clearly be noted that a significant number of atoms have a value for their population difference in the negative, i.e. their internal population is inverted. In a system of two level atoms, such as that described in Chapter 2, an inversion of the atomic population would result in significant amounts of spontaneous emission. Owing to its stochastic nature, the recoil associated with spontaneous emission would result in a source of heat into the system, however the two-photon/three-level configuration considered in this chapter avoids this, allowing a significant population in the upper state without jeopardizing the coherence of the system.

Additionally, a strong pump value and the resulting population of the upper state would result in $D \to 0$ on average [79], which for a system of two-level atoms would cause the force which bunches the atoms (the dipole force) to vanish. Studying Figure 3.8 it can be observed that the dipole force does not vanish in this three-level case as it contains contributions one-photon coherences ρ_{21}, ρ_{32},

which do not vanish when $D \to 0$, in addition to the two-photon coherence term, σ_{21}. When the value of the probe intensity becomes comparable to the value for the pump intensity the Rabi oscillations begin to dampen, this can be seen in Figure 3.8(c). It is at this point that the position (θ) dependence of the total field which drives the atomic populations becomes significant (see eq. (3.1.8.4) & (3.1.8.5)). As a consequence of this, the spread of momentum which is induced by the CARL instability results in the atoms experiencing different field and thus dephases the Rabi oscillations.

At $t/\omega_r \approx 10$ in the uppermost plot of Figure 3.8 it may be noted that there is a significant dip in the intensity of the probe beam intensity. At $t/\omega_r = 0$ the probe field has some initial phase (i.e. $\alpha_a = \alpha_a^{real} e^{i\phi}$). The bunching instability may, however, require a different probe beam phase. As the rate of change of the probe beam phase is proportional to the inverse of the probe beam amplitude ($\frac{\partial \phi}{\partial t} \propto \frac{1}{\alpha_a^{real}}$), the phase changes more rapidly for smaller values of the field amplitude. The dip in probe field intensity observed at $t/\omega_r \approx 10$ corresponds then to a rapid shift of the probe field phase to facilitate the growth of the bunching instability.

It may be noted that, in Figure 3.9, the particles all evolve to have a negative momentum, i.e. all the particles are moving in the negative z-direction. The particles are pushed in the negative z-direction by the optical scattering force as described in Section 1.1.1.2. The terms $i2\hbar k U_0 \left(\alpha_a^* \alpha_b e^{-2ikz} - \alpha_a \alpha_b^* e^{2ikz}\right)$ in the equation for the atomic momentum, equation (3.1.8.6), are responsible for the optical scattering force. As the intensity of the pump field, α_b is initially much larger than the probe beam, α_a, the terms $i2\hbar k U_0 \left(\alpha_a^* \alpha_b e^{-2ikz} - \alpha_a \alpha_b^* e^{2ikz}\right)$ result in a net force in the negative z-direction.

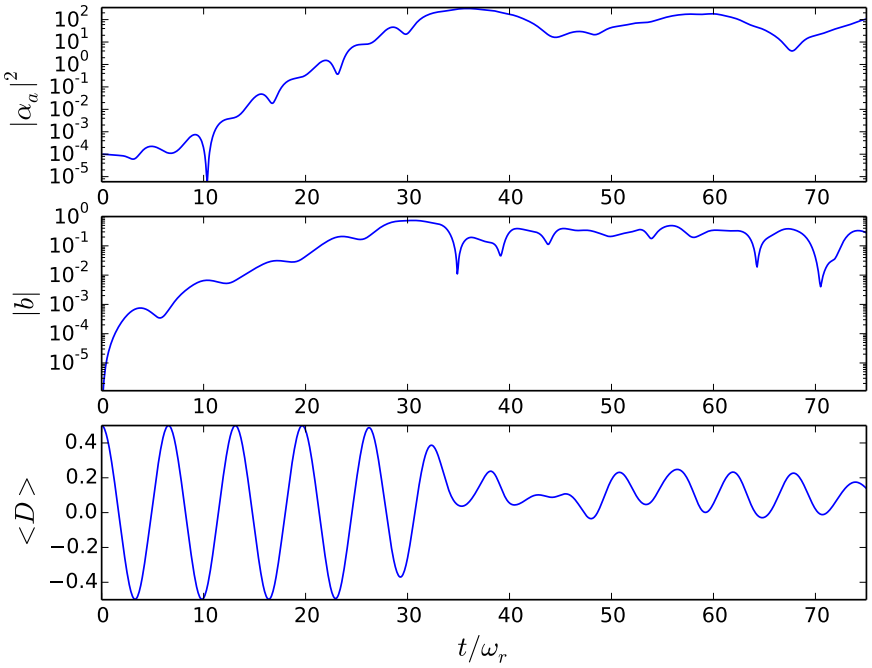

Figure 3.8: Evolution of probe photon number, $|\alpha_a|^2$, bunching parameter, $|b|$, and mean population difference, $\langle D \rangle$ for a case of strong excitation. Produced by solving equations (3.1.8.9) - (3.1.8.4). Parameters used are $U_0/\omega_r = 5 \times 10^{-5}$, $\Delta_{ab} = 1$, $\alpha_b = 100$, $N = 1000$, $\epsilon_\mu = 0.1$. Top: Gain for the probe beam in a three level ladder atomic system due to the CARL instability, despite the system operating at a large value for the pump field amplitude. A similarly large pump value in the two level CARL system would have resulted in the CARL instability being "washed out". Middle: Bunching of the three level atomic sample for a large value of the pump field amplitude. Bottom: Rabi flopping due to the large value for the pump field amplitude, which would have been severely detrimental to the two level CARL process, can be seen here not to destroy the three level ladder cofiguration CARL instability. The Rabi flopping becomes "quenched" when the probe field amplitude approaches that of the pump field. The equal fields result in a spread of momentum, which then causes a spread in population as can be seen in Figure 3.10.

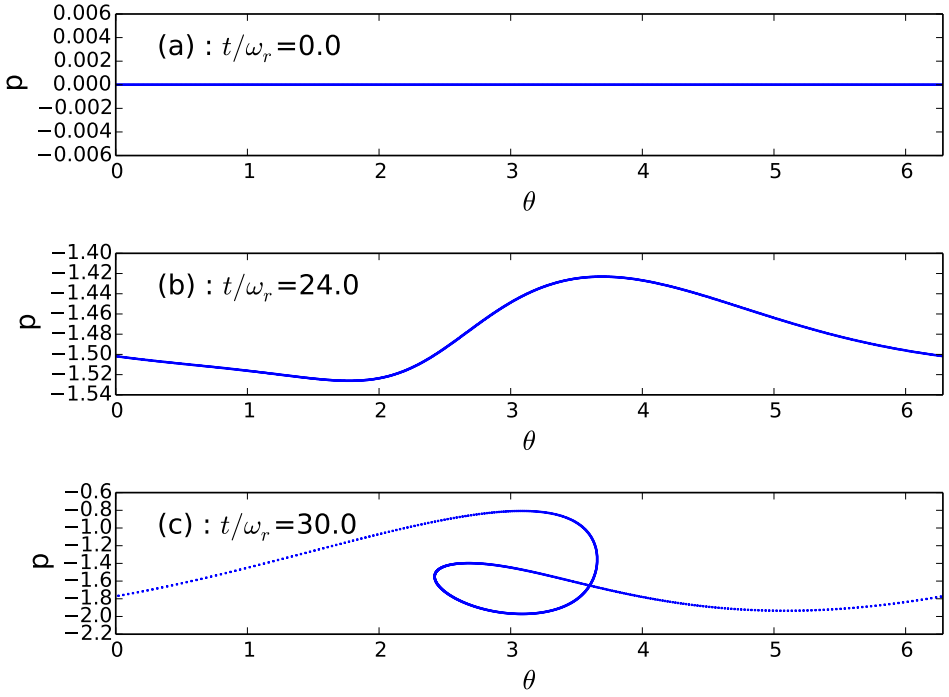

Figure 3.9: Snapshots of momentum distribution (θ_j, p_j) for each atom $j = 1..1000$ when (a) $t = 0\omega_r^{-1}$, (b) $t = 24\omega_r^{-1}$, (c) $t = 30\omega_r^{-1}$ in the case of strong excitation. Parameters used and equations solved are as in Figure 3.8. The atoms in the system under the effects of a strong pump field can be seen to acquire momentum and bunch over time in a similar manner to the system under a weak pump as seen in Figure 3.3.

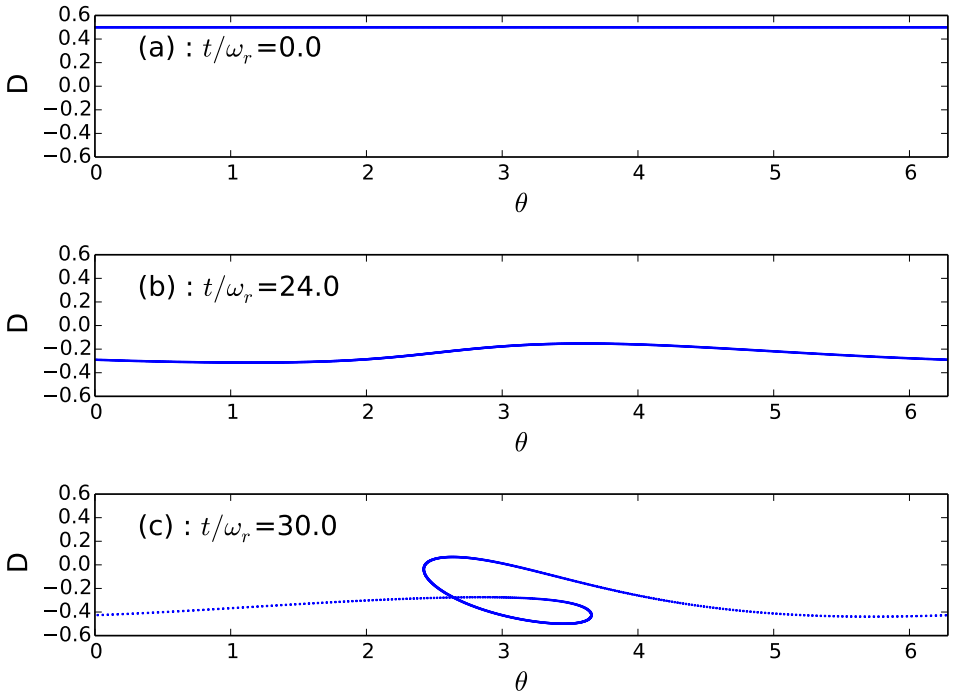

Figure 3.10: Snapshots of population difference distribution (θ_j, D_j) for each atom $j = 1..1000$ when (a) $t = 0\omega_r^{-1}$, (b) $t = 24\omega_r^{-1}$, (c) $t = 30\omega_r^{-1}$ in the case of strong excitation. Parameters used and equations solved are as in Figure 3.8. Unlike the case in which the system is weakly pumped, shown in Figure 3.4, for a strong pump the population experiences significant growth. It can also be seen that, as time progresses, the the atoms experience a spread of population. This spread is responsible for the apparent "quenching" of the population oscillations evident in the bottommost plot of Figure 3.8.

Whilst the gain predicted in section 3.2.1.1 in equation (3.2.1.4) is valid for the weak pump case, it may at least be instructive of what to expect in the strong pump regime. In Figure 3.8 the signs of the detuning terms match, so the gain term $\frac{3U_0^3|\alpha_b|^2}{\Delta_{ab}}$ predicted for the weak pump case is positive. For Figures 3.11 and 3.12 the detuning terms have opposite signs. Thus the term $\frac{3U_0^3|\alpha_b|^2}{\Delta_{ab}}$ is negative and reduces the value of the gain predicted by equation (3.2.1.4). Comparing Figure 3.8 with Figures 3.11 and 3.12 provides good agreement with the predictions for the weak pump gain, though the curves themselves appear less smooth due to the strong pump producing stronger nonlinear effects.

The predictions of the weak pump gain equation (3.2.1.4) break down, however, in Figure 3.13, where the gain of the system is unexpectedly enhanced for the strong excitation limit case in which both detuning terms are negative. As Figure 3.13 demonstrates the gain for the strong excitation limit and equation (3.2.1.4) determines the gain for the weak excitation limit, one does not invalidate the other. A more detailed study of the response of the gain to the detuning in the strong excitation limit will be needed to understand fully the origins of the apparent enhancement seen.

It can be seen that Figure 3.12 shows the same sudden dip in probe field intensity as was seen in Figure 3.8 which marks a rapid change in the probe field phase and the beginning of the CARL bunching instability.

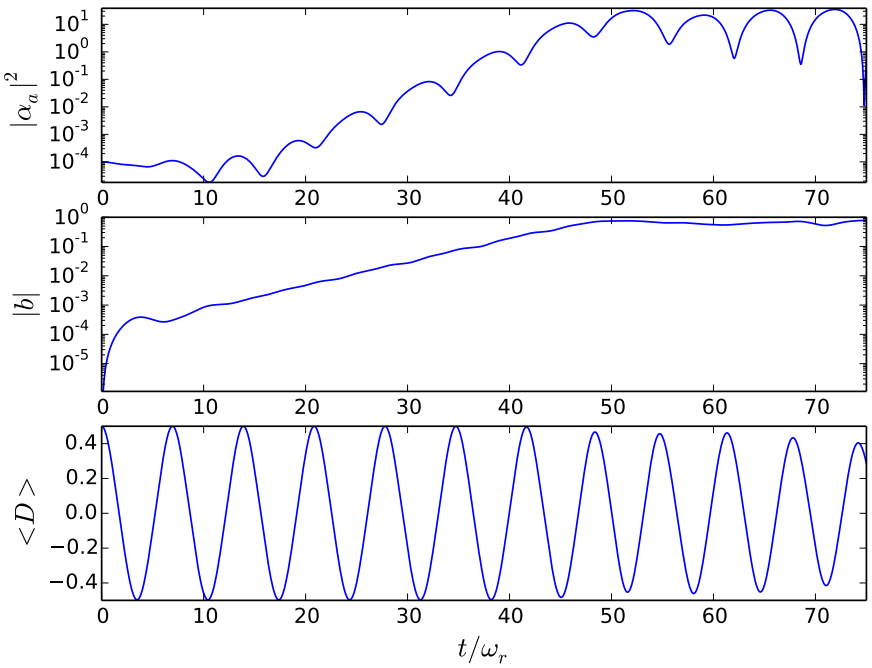

Figure 3.11: Evolution of probe photon number, $|\alpha_a|^2$, bunching parameter, $|b|$, and mean population difference, $\langle D \rangle$ for a case of strong excitation. Produced by solving equations (3.1.8.9) - (3.1.8.4). Parameters used are $U_0/\omega_r = -5 \times 10^{-5}$, $\Delta_{ab} = 1$, $\alpha_b = 100$, $N = 1000$, $\epsilon_\mu = 0.1$. When the value of U_0 is allowed to become negative while Δ_{ab} remains positive, the term $\frac{U_0}{\Delta_{ab}}$ in the equation for the expected probe beam gain, equation (3.2.1.4), becomes negative. The value of gain produced by the expression is therefore smaller than in the cases where the signs of U_0 & Δ_{ab} match. The oscillations in the probe field amplitude make it difficult to produce an accurate value for the probe beam gain, however visual comparison between this Figure and Figures 3.10 and 3.13 shows the gain to be diminished.

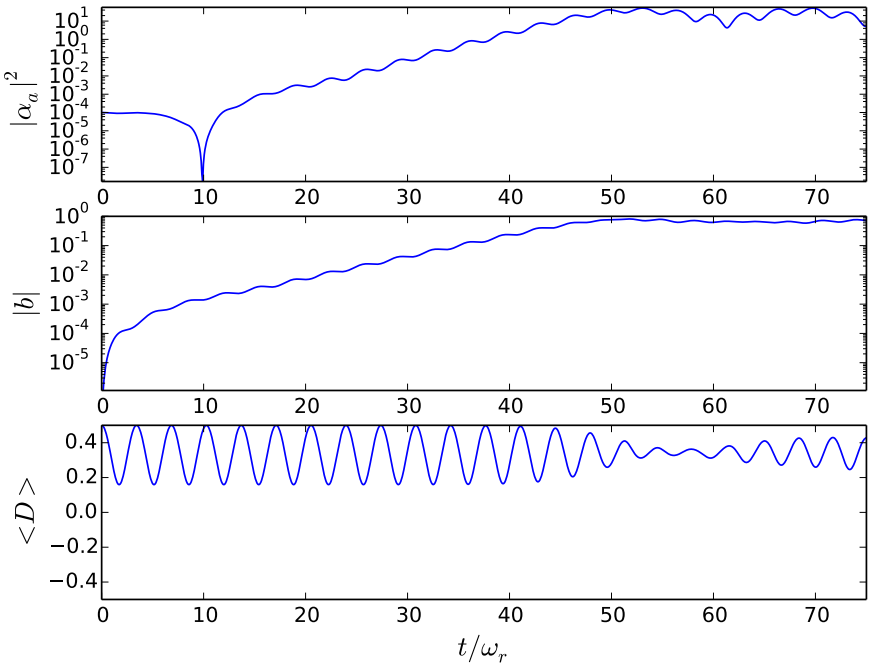

Figure 3.12: Evolution of probe photon number, $|\alpha_a|^2$, bunching parameter, $|b|$, and mean population difference, $\langle D \rangle$ for a case of strong excitation. Produced by solving equations (3.1.8.9) - (3.1.8.4). Parameters used are $U_0/\omega_r = 5 \times 10^{-5}$, $\Delta_{ab} = -1$, $\alpha_b = 100$, $N = 1000$, $\epsilon_\mu = 0.1$. Similarly to Figure 3.11, when the signs of U_0 & Δ_{ab} are flipped the term $\frac{U_0}{\Delta_{ab}}$ remains negative in the equation for the expected probe beam gain, equation (3.2.1.4). Comparing this Figure with Figure 3.11 shows that in each case the gains are similar.

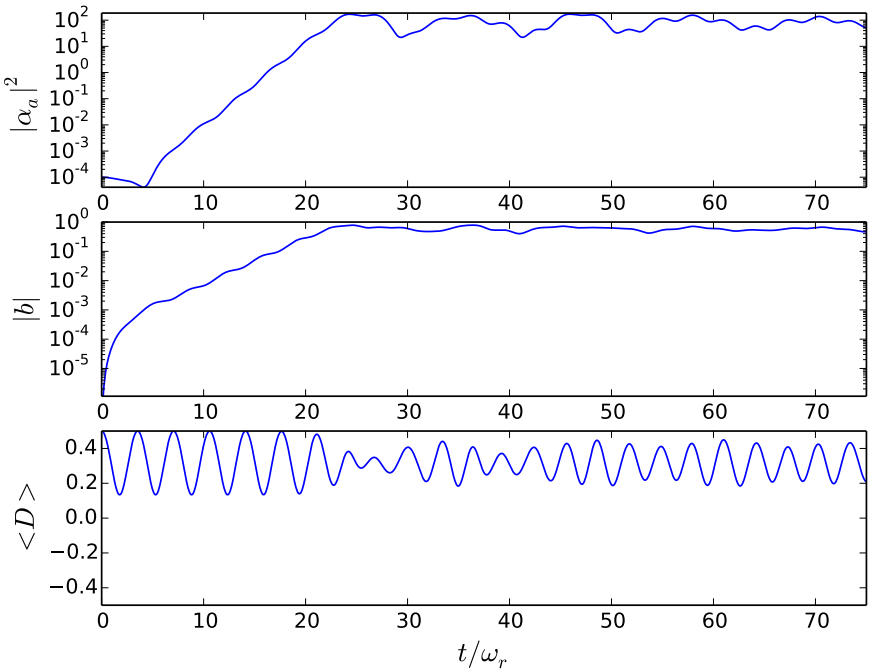

Figure 3.13: Evolution of probe photon number, $|\alpha_a|^2$, bunching parameter, $|b|$, and mean population difference, $\langle D \rangle$ for a case of strong excitation. Produced by solving equations (3.1.8.9) - (3.1.8.4). Parameters used are $U_0/\omega_r = -5 \times 10^{-5}$, $\Delta_{ab} = -1$, $\alpha_b = 100$, $N = 1000$, $\epsilon_\mu = 0.1$. When the signs of U_0 & Δ_{ab} match once again, the term $\frac{U_0}{\Delta_{ab}}$ in the equation for the expected probe beam gain, equation (3.2.1.4), is once again positive, as in Figure 3.8. Comparing this Figure with Figures 3.11 & 3.12 shows once again that matching signs for U_0 & Δ_{ab} results in a larger gain in the probe beam that differing signs.

3.2.2 Neglecting the AC Stark shift

If the assumption is made that $\mu_a = \mu_b$, then the term Δ_{u_0} in the scaled two-photon CARL equations vanishes, ie the position and intensity dependent AC Stark shift is neglected. With such an assumption made, the scaled two-photon CARL equations take the form

$$\frac{\partial D}{\partial t} = \frac{\gamma_{33}}{2}\left(\frac{1}{2} - D\right) + iU_0\Big(\quad \sigma_{13}\left(\alpha_a + \alpha_b e^{-2ikz}\right)\left(\alpha_a e^{2ikz} + \alpha_b\right) \\ -\sigma_{31}\left(\alpha_a^* + \alpha_b^* e^{2ikz}\right)\left(\alpha_a^* e^{-2ikz} + \alpha_b^*\right) \quad \Big) \tag{3.2.2.1}$$

$$\frac{\partial \sigma_{31}}{\partial t} = -(\gamma_{31} - i\Delta_{ab})\sigma_{31} - i2U_0 D\left(\alpha_a e^{2ikz} + \alpha_b\right)\left(\alpha_a + \alpha_b e^{-2ikz}\right) \tag{3.2.2.2}$$

$$\begin{aligned}\frac{\partial p_j}{\partial t} =& i2\hbar k U_0\left[\sigma_{31}\left(\alpha_a^{*2} e^{-2ikz} - \alpha_b^{*2} e^{2ikz}\right) - \sigma_{13}\left(\alpha_a^2 e^{2ikz} - \alpha_b^2 e^{-2ikz}\right)\right] \\ &+ i2\hbar k U_0\left(\alpha_a^* \alpha_b e^{-2ikz} - \alpha_a \alpha_b^* e^{2ikz}\right)\end{aligned} \tag{3.2.2.3}$$

$$\frac{\partial z_j}{\partial t} = \frac{p_j}{m} \tag{3.2.2.4}$$

$$\frac{\partial \alpha_a}{\partial t} = -iN\Big\langle 2U_0\sigma_{31}\left(\alpha_a^* e^{-2ikz} + \alpha_b^*\right) + U_0\left(\alpha_a + \alpha_b e^{-2ikz}\right)\Big\rangle - \kappa_a(\alpha_a - \alpha_a^{eq}) \tag{3.2.2.5}$$

$$\frac{\partial \alpha_b}{\partial t} = -iN\left\langle 2U_0\sigma_{31}\left(\alpha_a^* + \alpha_b^* e^{2ikz}\right) + U_0\left(\alpha_a e^{2ikz} + \alpha_b\right)\right\rangle - \kappa_b(\alpha_b - \alpha_b^{eq}) \tag{3.2.2.6}$$

As before, the "saturation" pump intensity is derived by solving the equations for the population inversion D and the coherence σ_{31}. For the case where the AC Stark shift is neglected that means solving equations (3.2.2.8) and (3.2.2.2). Following the same procedure as previously, where "saturation" is defined to occur when the average excited-state population, ρ_{33} is $\frac{1}{4}$, i.e. $D = \frac{1}{4}$, it can be easily seen that "saturation" occurs when the photon pump number is

$$|\alpha_b| \equiv |\alpha_b|_{\text{sat}} = \sqrt{\left|\frac{\Delta_{ab}}{2U_0}\right|}. \tag{3.2.2.7}$$

3.2.2.1 The weak excitation limit

Again the limit $|\alpha_b|^2 \ll |\alpha_b|^2_{\text{sat}}$ is considered first, such that each atom is only weakly excited internally and almost all the atomic population remains in the ground state, $|1\rangle$ i.e. $D \to \frac{1}{2}$ and $\sigma_{31} \to 0$. In this limit, equations (3.2.2.8)..(3.2.2.6) can be shown to reduce to be identical to (3.2.1.5)..(3.2.1.7).

In the weak-pump limit then, there should be no difference between the case where the AC Stark shift is considered and where it is neglected. This can be confirmed by solving equations (3.1.8.4) - (3.1.8.9) using the same input values as were used to create Figures 3.2 through 3.7 save for the value of the AC Stark shift term reduced to zero ($\epsilon_\mu = 0$). By doing so, Figures 3.14 through 3.18 were created.

Figures 3.2 - 3.7 show plots produced by solving equations (3.1.8.4) - (3.1.8.9) with the AC Stark shift term included ($\epsilon_\mu = 0.1$). Figures 3.14 - 3.18 show plots produced by solving the same equations, using the same input values, with the AC Stark shift term neglected ($\epsilon_\mu = 0$).

By comparing these two sets of figures it can be easily noted that there is

almost no difference between them, i.e. in the weak pump limit the AC Stark shift has little to no effect upon the system. This is to be expected both from the equations in the weak pump limit becoming identical and from the description of the AC Stark shift given in section 3.1.7, wherein the AC Stark shift was described as "an intensity dependent detuning". If the pump field has a low intensity then the AC Stark shift "detuning" will likewise be small.

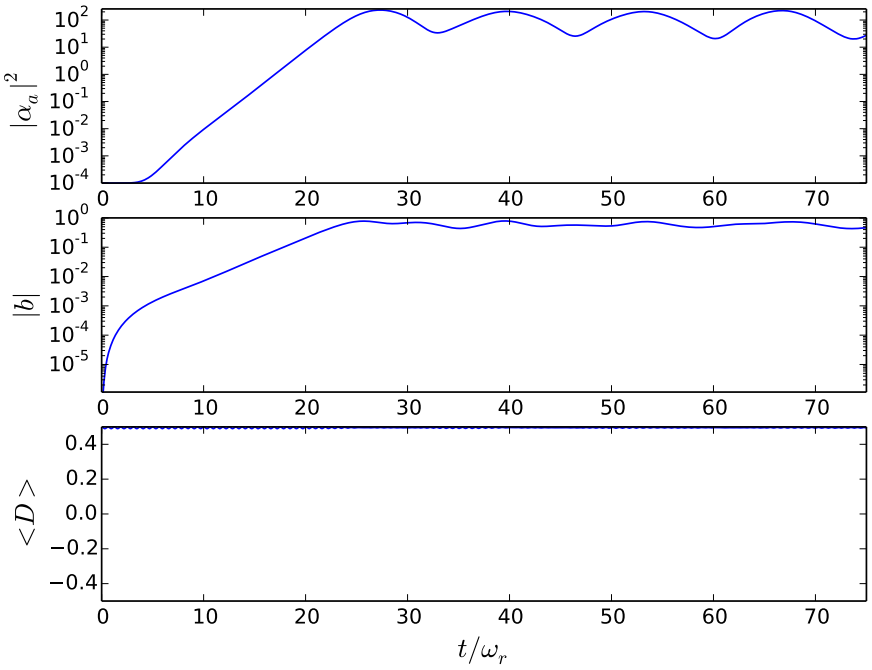

Figure 3.14: Evolution of probe photon number, $|\alpha_a|^2$, bunching parameter, $|b|$, and mean population difference, $\langle D \rangle$ for a case of weak-excitation. Produced by solving equations (3.2.2.8) - (3.2.2.6). Parameters used are $U_0/\omega_r = 5 \times 10^{-5}$, $\Delta_{ab} = 10$, $\alpha_b = 100$, $N = 1000$, $\epsilon_\mu = 0.0$. Top: The probe beam experiencing gain due to the CARL instability in a weakly pumped three level ladder atomic system when the AC Stark shift term ϵ_μ is neglected. The gain experienced by the probe field, $Gain_{probe} \approx 1$, is nearly identical to the case where the AC Stark shift term is included(shown in Figure 3.2). Middle: Bunching of the three level atomic sample due to the CARL instability with ϵ_μ neglected. Bottom: The population remains almost entirely in the ground state throughout the process.

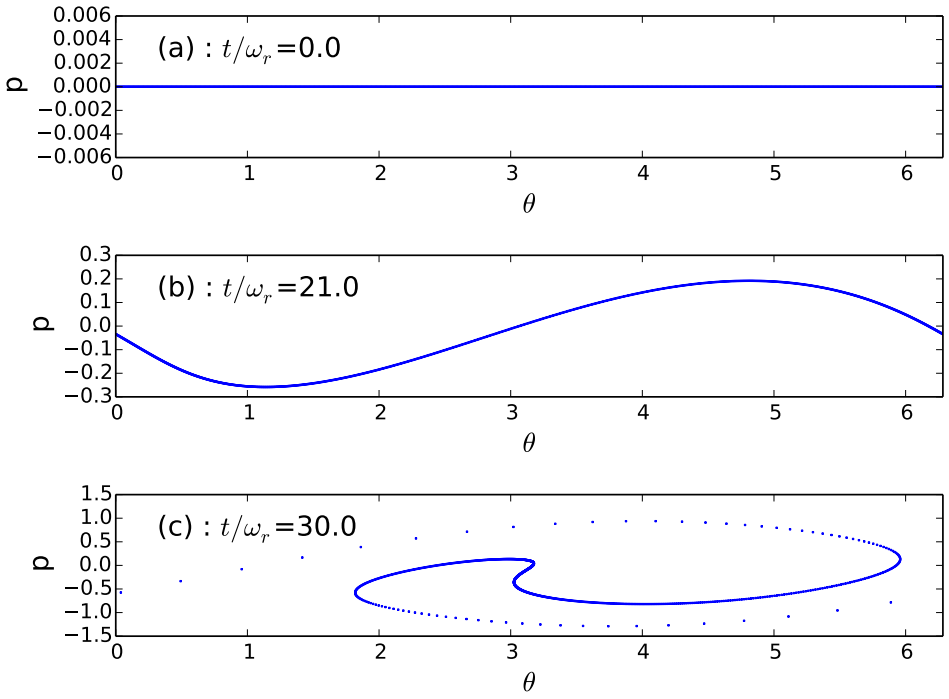

Figure 3.15: Snapshots of momentum distribution (θ_j, p_j) for each atom $j = 1..1000$ when (a) $t = 0\omega_r^{-1}$, (b) $t = 21\omega_r^{-1}$, (c) $t = 30\omega_r^{-1}$ in the case of weak excitation. Parameters used and equations solved are as in Figure 3.14. By comparison with Figure 3.3 it can be seen that when the AC Stark shift term is neglected the weakly pumped atoms in the three level ladder system move almost identically as to when the AC Stark term is included.

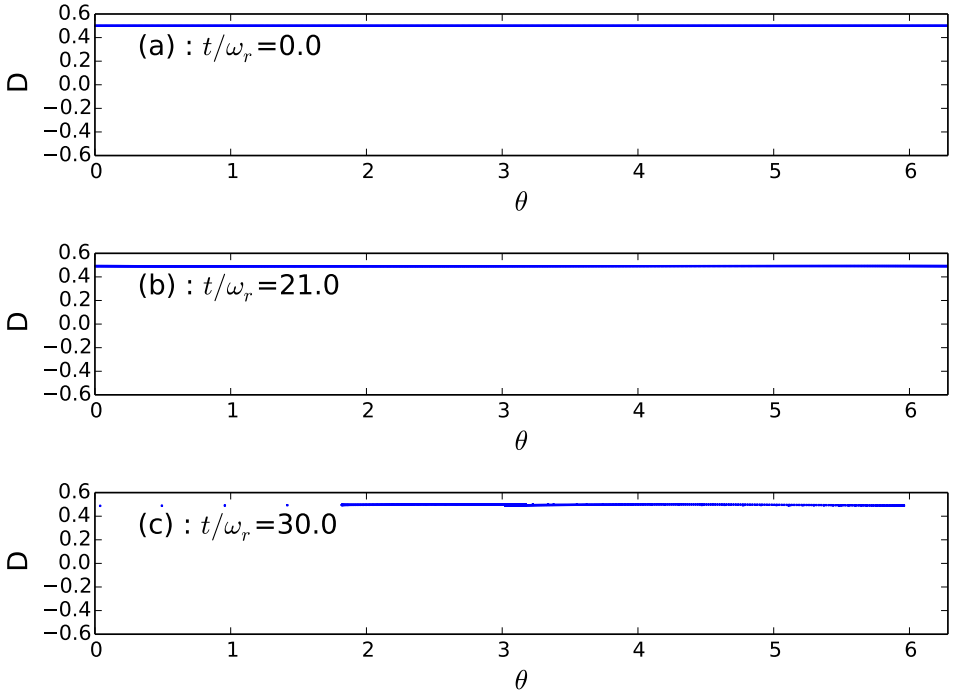

Figure 3.16: Snapshots of population difference distribution (θ_j, D_j) for each atom $j = 1..1000$ when (a) $t = 0\omega_r^{-1}$, (b) $t = 21\omega_r^{-1}$, (c) $t = 30\omega_r^{-1}$ in the case of weak excitation. Parameters used and equations solved are as in Figure 3.14. As was the case when the AC Stark shift was included, the population remains almost entirely constant in the ground state for the weakly pumped case when the AC Stark shift term is neglected.

As was stated previously in section 3.2.1.2, equation (3.2.1.4) allows for the prediction to be made that the gain experienced by the system will not change when the signs of the terms U_0 and Δ_{ab} are exchanged, as doing so leaves their product, $U_0\Delta_{ab}$, unchanged.

Such a prediction is proven to be true when Figure 3.14, in which both U_0 & Δ_{ab} are positive, is compared to Figure 3.17, where the same values have been used but both U_0 & Δ_{ab} are negative. It can easily be seen that Figures 3.14 and 3.17 are identical, confirming the prediction for the case in which the AC Stark shift is neglected.

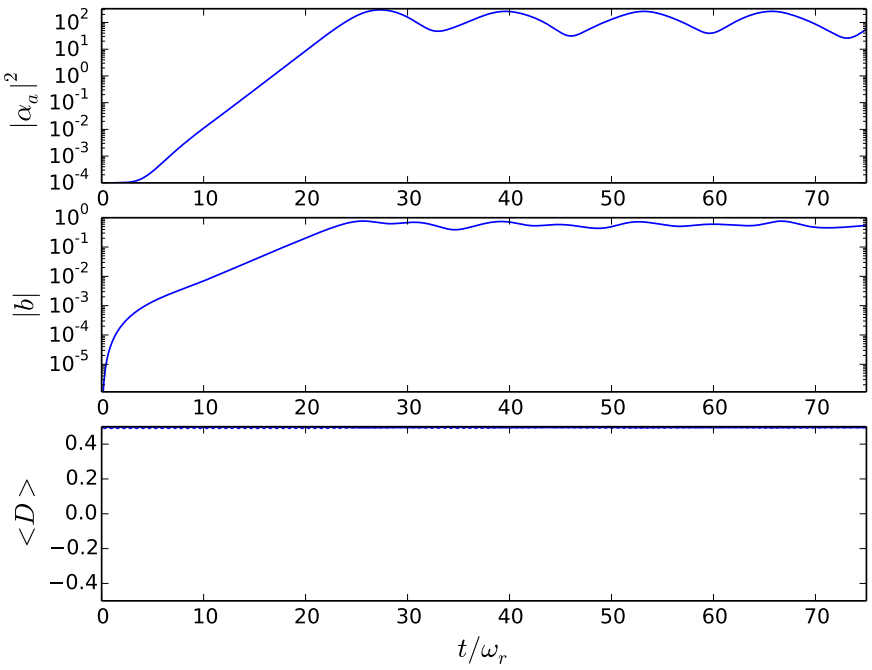

Figure 3.17: Evolution of probe photon number, $|\alpha_a|^2$, bunching parameter, $|b|$, and mean population difference, $\langle D \rangle$ for a case of weak-excitation. Produced by solving equations (3.2.2.8) - (3.2.2.6). Parameters used are $U_0/\omega_r = -5 \times 10^{-5}$, $\Delta_{ab} = -10$, $\alpha_b = 100$, $N = 1000$, $\epsilon_\mu = 0.0$. When the sign of both U_0 & Δ_{ab} are made negative, the same behaviour repeats for the AC Stark neglected case as for when it was included in Figure 3.5. The gain in the probe beam ($Gain_{probe} \approx 1$), remains similar to its value when U_0 & Δ_{ab} are both positive, as in Figure 3.14.

It was explained previously in section 3.2.1.2, wherein the AC Stark shift term was taken to be non zero ($\epsilon_\mu \neq 0$), that when the detuning terms do not share the same sign, i.e. the product $U_0\Delta_{ab}$ is negative, the gain decreases as a result of the term $\frac{3U_0^3|\alpha_b|^2}{\Delta_{ab}}$ in equation (3.2.1.4) being negative.

This is once again the case when the AC Stark shift term is neglected, $\epsilon_\mu = 0$. Figure 3.18 is produced using the same values as in Figures 3.14 and 3.17, only with the signs of the detunings changed so that U_0 has a negative value and Δ_{ab} has a positive value. Consequently, it can be seen that the gain experienced by the system is diminished, as predicted.

Figure 3.19 was produced using the same values as in Figure 3.18, except the signs of U_0 and Δ_{ab} are reversed, so U_0 has a positive value and Δ_{ab} has a negative value.

As stated in section 3.2.1.2, equation (3.2.1.4) should produce an identical value for gain for the case where $U_0 < 0$ & $\Delta_{ab} > 0$ as for the case where $U_0 > 0$ & $\Delta_{ab} < 0$. It should be expected then that Figures 3.19 and 3.18 closely match one another. When compared, it can be seen that the two figures match identically, confirming the prediction of equation (3.2.1.4).

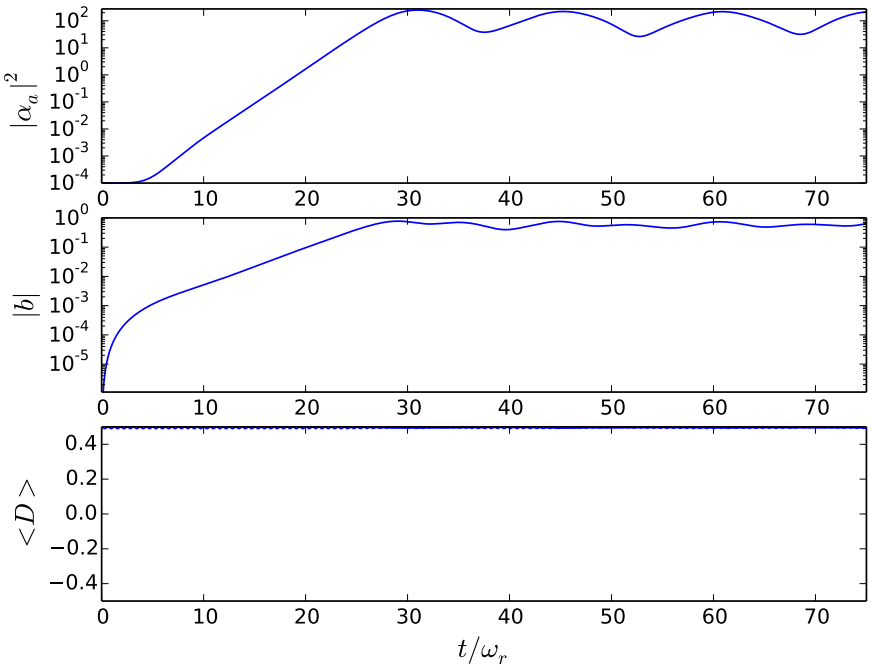

Figure 3.18: Evolution of probe photon number, $|\alpha_a|^2$, bunching parameter, $|b|$, and mean population difference, $\langle D \rangle$ for a case of weak-excitation. Produced by solving equations (3.2.2.8) - (3.2.2.6). Parameters used are $U_0/\omega_r = -5 \times 10^{-5}$, $\Delta_{ab} = 10$, $\alpha_b = 100$, $N = 1000$, $\epsilon_\mu = 0.0$. Allowing the sign of U_0 to remain negative while changing the sign of Δ_{ab} to positive with the AC Stark shift term neglected has the same effect as described in Figure 3.6 wherein the AC Stark shift term is included. When U_0 and Δ_{ab} have opposite signs the term $\frac{U_0}{\Delta_{ab}}$ takes a negative value, reducing the resulting value produced by the probe gain equation, equation (3.2.1.4). This can be seen by comparing this Figure with Figures 3.14 & 3.17. $Gain_{probe} \approx 0.2$.

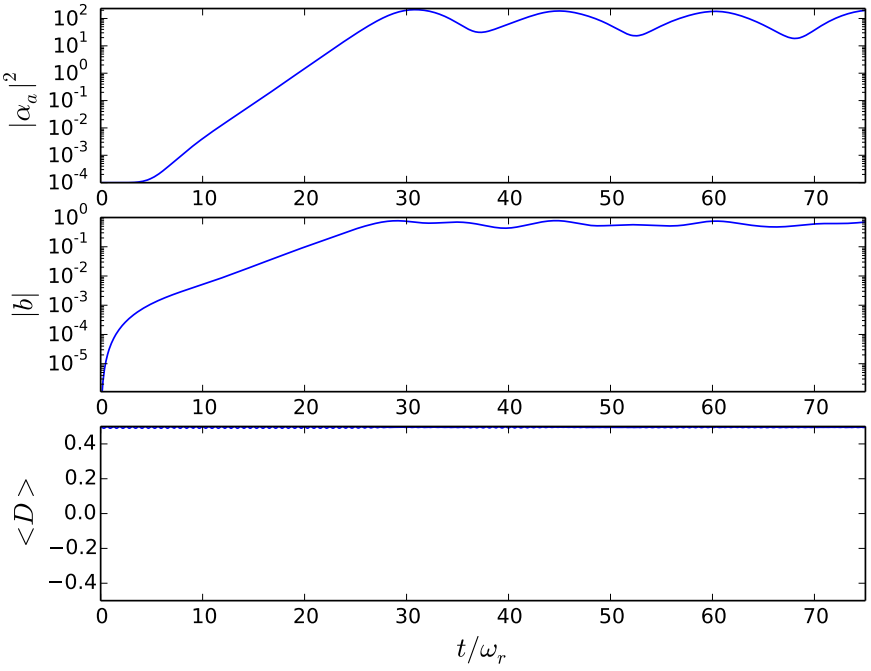

Figure 3.19: Evolution of probe photon number, $|\alpha_a|^2$, bunching parameter, $|b|$, and mean population difference, $\langle D \rangle$ for a case of weak-excitation. Produced by solving equations (3.2.2.8) - (3.2.2.6). Parameters used are $U_0/\omega_r = 5 \times 10^{-5}$, $\Delta_{ab} = -10$, $\alpha_b = 100$, $N = 1000$, $\epsilon_\mu = 0.0$. When U_0 is positive and Δ_{ab} is negative with the AC Stark shift term neglected the system functions the same as when U_0 was negative and Δ_{ab} was positive, as in Figure 3.18. This is due to the term $\frac{U_0}{\Delta_{ab}}$ taking a negative value in the equation for the probe beam gain, equation (3.2.1.4). When this Figure is compared to Figure 3.7 it can be seen that neglecting the AC Stark shift term has negligible effects upon the three level ladder CARL system when the pumping is weak. $Gain_{probe} \approx 0.2$.

3.2.2.2 The strong excitation limit

Figures 3.20, 3.21 and 3.22 show the evolution of the system in the strong-pump limit when the AC Stark shift term ϵ_μ is neglected.

It can be seen from Figure 3.20 that same synchronous growth takes place in the probe field intensity and bunching parameter as in the AC Stark case. The absence of the AC Stark term ϵ_μ seems to have very little effect at all in either the weak or strong excitation regimes. The small differences which do exist seem confined to the highly nonlinear oscillatory region after the probe gain has become equal in magnitude to that of the pump beam.

The same result exist in the case of the AC Stark term being neglected, then. Namely that the two photon terms in the momentum equation remain even when the population tends to zero, $D \to 0$. The CARL instability persists then in regimes with higher pumping intensities than for that of the two level case.

In the lowermost plot of Figure 3.20 it can be seen that the large oscillations population diminish once the optical probe beam amplitude reaches a "saturation" level approximately equal to that of the optical pump beam. From the equation for the evolution of the population inversion, equation (3.2.2.8), it can be seen that when the optical pump and probe beams become approximately equal

$$\frac{\partial D}{\partial t} = \frac{\gamma_{33}}{2}\left(\frac{1}{2} - D\right) + iU_0\Bigg(\sigma_{13}\left(\alpha_a + \alpha_b e^{-2ikz}\right)\left(\alpha_a e^{2ikz} + \alpha_b\right) - \sigma_{31}\left(\alpha_a^* + \alpha_b^* e^{2ikz}\right)\left(\alpha_a^* e^{-2ikz} + \alpha_b^*\right) \Bigg) \quad (3.2.2.8)$$

It may be noted that in Figures 3.21(b) and 3.22(c) that, in bunching, the atoms in the system may take the same z-position with different momentum/population inversion value combinations.

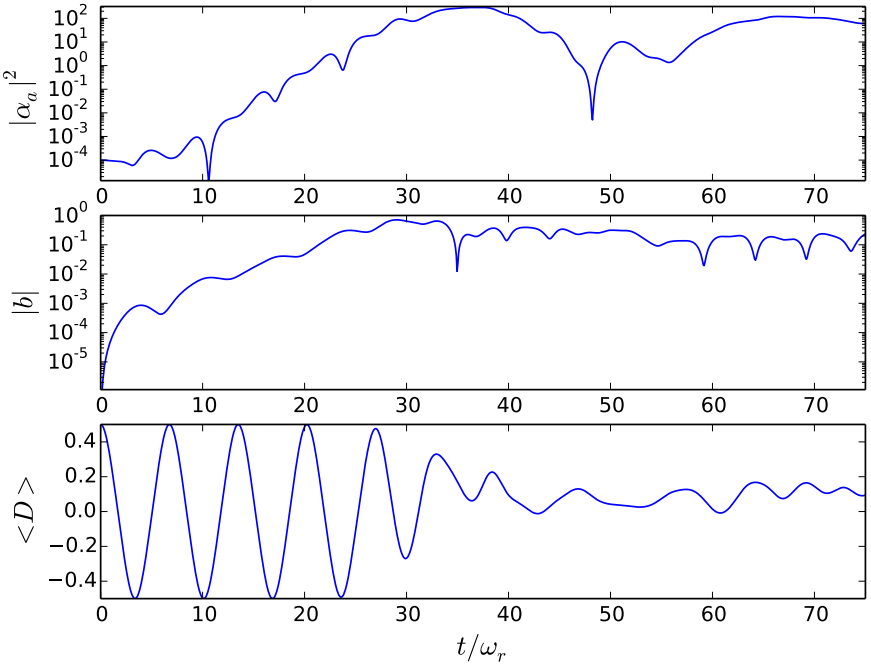

Figure 3.20: Evolution of probe photon number, $|\alpha_a|^2$, bunching parameter, $|b|$, and mean population difference, $\langle D \rangle$ for a case of strong excitation. Produced by solving equations (3.2.2.8) - (3.2.2.6). Parameters used are $U_0/\omega_r = 5 \times 10^{-5}$, $\Delta_{ab} = 1$, $\alpha_b = 100$, $N = 1000$, $\epsilon_\mu = 0.0$. Top: Gain for the probe beam in a three level ladder atomic system due to the CARL instability with the AC Stark shift term neglected, despite the system operating at a large value for the pump field amplitude. Again, a large pump value in the two level CARL system would have resulted in the CARL instability being "washed out". The gain in the probe beam is once again difficult to produce an accurate value for due to the oscillations in the plot. Comparison with Figure 3.8 shows good agreement, however. Middle: Bunching of the three level atomic sample for a large value of the pump field amplitude with the AC Stark shift term neglected. Bottom: Rabi flopping due to the large value for the pump field amplitude, which would have been severely detrimental to the two level CARL process, can be seen here not to destroy the three level ladder configuration CARL instability, regardless of whether the AC Stark shift term is neglected or not. The Rabi flopping becomes "quenched" when the probe field amplitude approaches that of the pump field. The equal fields result in a spread of momentum, which then causes a spread in population as can be seen in Figure 3.22.

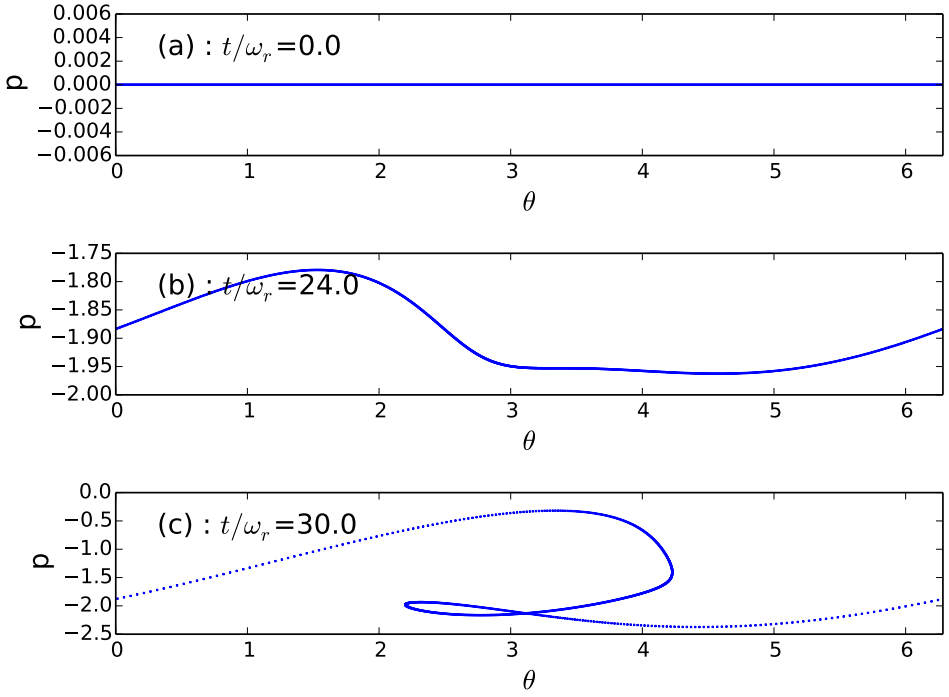

Figure 3.21: Snapshots of momentum distribution (θ_j, p_j) for each atom $j = 1..1000$ when (a) $t = 0\omega_r^{-1}$, (b) $t = 24\omega_r^{-1}$, (c) $t = 30\omega_r^{-1}$ in the case of strong excitation. Parameters used and equations solved are as in Figure 3.20. The atoms in the system under the effects of a strong pump field with the AC Stark shift term neglected can be seen to acquire momentum and bunch over time in the same manner as Figure 3.21, in which the AC Stark shift term was not neglected.

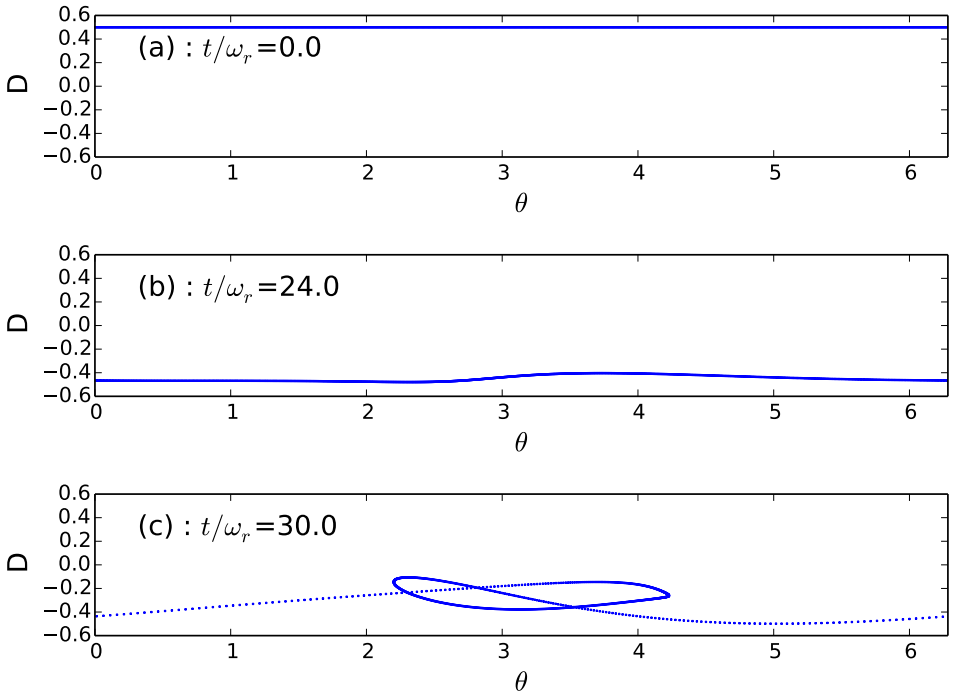

Figure 3.22: Snapshots of population difference distribution (θ_j, D_j) for each atom $j = 1..1000$ when (a) $t = 0\omega_r^{-1}$, (b) $t = 24\omega_r^{-1}$, (c) $t = 30\omega_r^{-1}$ in the case of strong excitation. Parameters used and equations solved are as in Figure 3.20. As was the case for Figure 3.22 where the AC Stark term was included, when it is neglected the population undergoes significant oscillation and as the probe and pump fields draw even with one another the spread of momentum results in a spread of population and the population inversion oscillations become "quenched".

Once again comparison is made between the varying detuning regimes and, as was the case for strong pumping with the AC Stark term ϵ_μ included, there exists a decrease in the gain experienced by the system when the two detuning terms have opposite signs when compared against the case where both detunings have positive sign.

Comparing Figure 3.20, for which both U_0 and Δ_{ab} have positive values, to Figure 3.23, wherein $U_0 < 0$, $\Delta_{ab} > 0$, and Figure 3.24, wherein $U_0 > 0$, $\Delta_{ab} < 0$, it can be seen once more that when the signs of the detunings are opposite one another, that the term $\frac{3U_0^3|\alpha_b|^2}{\Delta_{ab}}$ from equation (3.2.1.4) becomes negative and reduces the gain.

As was also the case in section 3.2.1.3 where the AC Stark term was included, equation (3.2.1.4) predicts that, in the weak pump limit, the gain should be the same for the case where both U_0 & Δ_{ab} are positive and where they are both negative. Comparing Figure 3.20, in which U_0 & Δ_{ab} are both positive, to Figure 3.25, in which U_0 & Δ_{ab} are both negative, shows that in the strong pumping limit the gains do not match. It can be seen that the probe field gain for Figure 3.25 is larger than the gain in the probe beam shown in 3.20. As was stated in section 3.2.1.3, further analysis will be required to better understand the causes for this unexpected enhancement.

By comparing the strong excitation results where the AC Stark term has been neglected to those from section 3.2.1.3 in which the AC Stark term was included, it can easily be noted that the results are almost identical save for in the highly nonlinear region which occurs after the probe beam has reached equal magnitude to that of the pump.

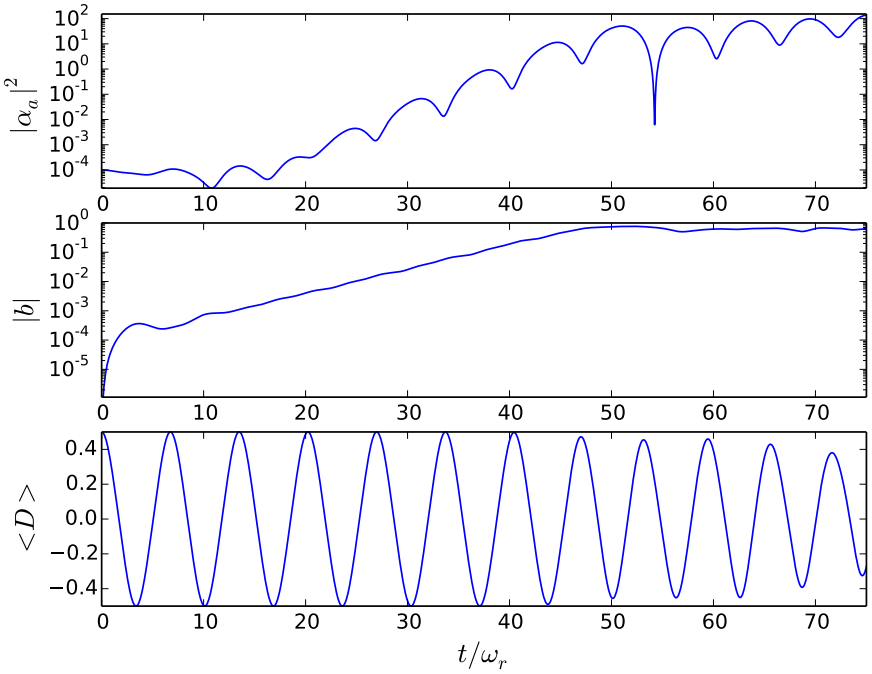

Figure 3.23: Evolution of probe photon number, $|\alpha_a|^2$, bunching parameter, $|b|$, and mean population difference, $\langle D \rangle$ for a case of strong excitation. Produced by solving equations (3.2.2.8) - (3.2.2.6). Parameters used are $U_0/\omega_r = -5 \times 10^{-5}$, $\Delta_{ab} = 1$, $\alpha_b = 100$, $N = 1000$, $\epsilon_\mu = 0.0$. As was the case in Figure 3.11 (where the AC Stark term was included), when the AC Stark term is neglected and the signs of U_0 & Δ_{ab} take negativ and positive signs respectively, term $\frac{U_0}{\Delta_{ab}}$ in the equation for the expected probe beam gain, equation (3.2.1.4), becomes negative. The gain produced by the expression is therefore smaller than in Figure 3.20, where the signs of U_0 & Δ_{ab} match. The oscillations in the probe field amplitude make it difficult to produce an accurate value for the probe beam gain, however visual comparison between this Figure and Figure 3.22 shows the gain to be diminished, as expected.

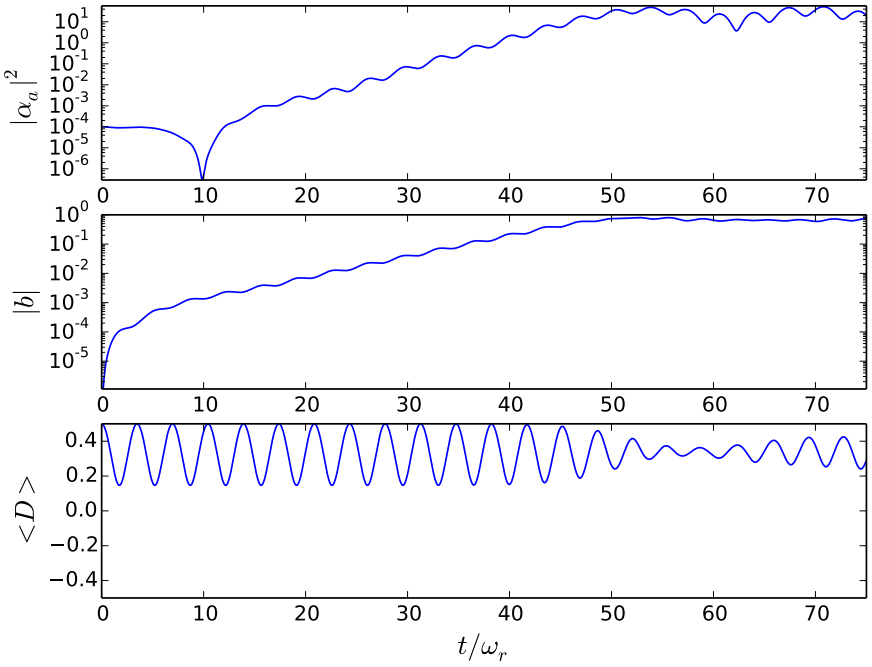

Figure 3.24: Evolution of probe photon number, $|\alpha_a|^2$, bunching parameter, $|b|$, and mean population difference, $\langle D \rangle$ for a case of strong excitation. Produced by solving equations (3.2.2.8) - (3.2.2.6). Parameters used are $U_0/\omega_r = 5 \times 10^{-5}$, $\Delta_{ab} = -1$, $\alpha_b = 100$, $N = 1000$, $\epsilon_\mu = 0.0$. As was the case for 3.23, when the signs of U_0 & Δ_{ab} do not match, as in this Figure where on U_0 is positive and Δ_{ab} is negative, the overall gain of the probe beam is diminished. This is due to the term $\frac{U_0}{\Delta_{ab}}$ in the equations for the probe beam gain, equation (3.2.1.4), being negative and thereby reducing the expected gain. Once more, oscillations in the probe beam plot make calculation of a precise figure for the gain produced difficult. However, comparison of this Figure with Figure 3.23 shows good agreement and comparison with Figure 3.20 shows the expected reduction in gain for the system. Comparing this Figure with Figure 3.12 also shows little difference in the gain, once again suggesting that the AC Stark term being neglected has little overall effect upon the system.

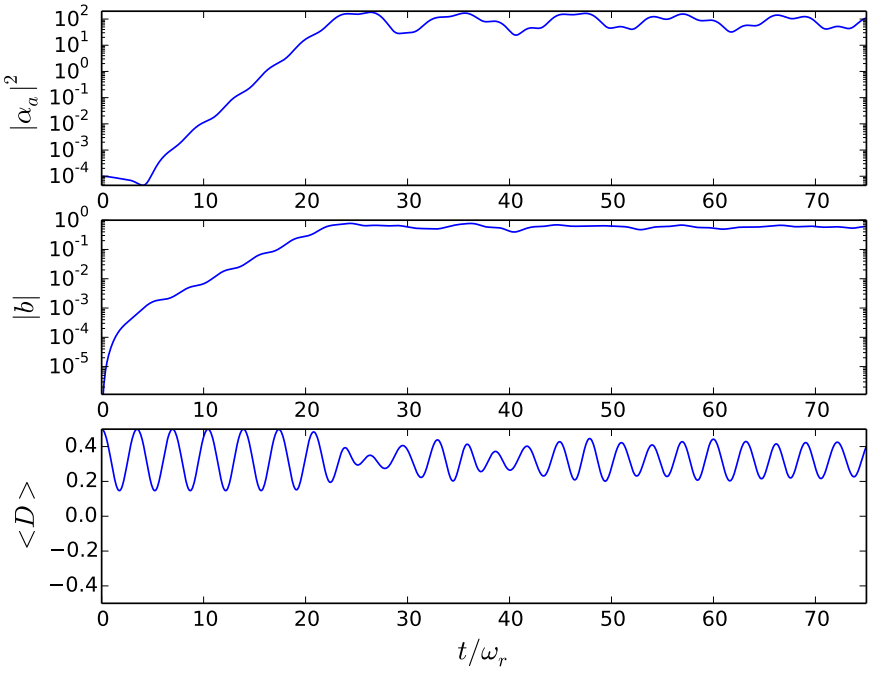

Figure 3.25: Evolution of probe photon number, $|\alpha_a|^2$, bunching parameter, $|b|$, and mean population difference, $\langle D \rangle$ for a case of strong excitation. Produced by solving equations (3.2.2.8) - (3.2.2.6). Parameters used are $U_0/\omega_r = -5 \times 10^{-5}$, $\Delta_{ab} = -1$, $\alpha_b = 100$, $N = 1000$, $\epsilon_\mu = 0.0$. Equation (3.2.1.4) predicts that for the detuning signs used in this Figure, U_0 & Δ_{ab} both negative, that the gain in the probe beam should match that of the system shown in Figure 3.20. This shows the point at which the assumptions used to produce Equation (3.2.1.4) break down, as the gain in the probe beam appears noticeably larger than that of Figure 3.20.

3.3 Two-Photon superfluorescence

It was noted that with careful parameter choice for the cavity detuning δ_c, equations (3.2.2.8) - (3.2.2.6) could be used to investigate a nonlinear optical process very close to that of two-photon superfluorescence (henceforth referred to as simply SF) and effects arising from the inclusion of atomic recoil upon the SF instability.

3.3.1 Linear analysis

To determine the best parameter choices for the investigation of the SF instability a linear analysis was performed. It was very quickly noted, however, that in the case of counterpropagating fields the linear analysis would take a prohibitively large amount of time and effort for the small return in time saved in selecting input parameters. It was subsequently observed that the two-photon CARL equations for the co-propagating case were much easier to perform linear analysis upon and are sufficiently similar to the counter-propagating case to provide at least a first approximation of suitable input parameters.

Using the same scaling as for the counterpropagating case, with the additional assumptions that the decay terms are zero ($\gamma_{33} = \gamma_{31} = 0$), the detuning terms are zero ($\Delta_{ab} = \Delta_a = 0$), the AC Stark shift term is zero ($\epsilon_\mu = 0$), the fields are considered to be equal ($\alpha_a = \alpha_b = \frac{\alpha}{2}$), there is no pumping of the field term ($\alpha^{eq} = 0$), the coherence is scaled as $S = \sigma_{31}e^{-2ikz}$ and recoil is neglected ($p_j = 0$, $\theta_j = \theta_{j_0}$), the equations for the coherence,(3.2.2.2), the population inversion, (3.2.2.8), and the optical (3.2.2.4) field are given by

$$\frac{\partial D}{\partial t} = iU_0\left(\alpha^2 S^* - \alpha^{*2} S\right) \tag{3.3.1.1}$$

$$\frac{\partial S}{\partial t} = -i2U_0\alpha^2 D \tag{3.3.1.2}$$

$$\frac{\partial \alpha_b}{\partial t} = -i2NU_0\alpha^* S - \kappa\alpha \tag{3.3.1.3}$$

3.3.1.1 Rabi oscillations

Differentiating the equation for the evolution of D, (3.3.1.1), gives

$$\frac{\partial^2 D}{\partial t^2} = iU_0\left(\alpha^2\frac{\partial S^*}{\partial t} - \alpha^{*2}\frac{\partial S}{\partial t}\right). \tag{3.3.1.4}$$

Substituting into the above the equation for the coherence, (3.3.1.2) and rearranging produces

$$\begin{aligned}\frac{\partial^2 D}{\partial t^2} &= iU_0\left(\alpha^2[i2U_0\alpha^{*2}D] - \alpha^{*2}[-i2U_0\alpha^2 D]\right)\\ &= -4U_0^2|\alpha|^4 D\\ &= -\left(2U_0|\alpha|^2\right)^2 D\,.\end{aligned} \tag{3.3.1.5}$$

The two-photon Rabi frequency is therefore $2U_0|\alpha|^2$. The rate of change of the magnitude squared of the field is given by

$$\begin{aligned}\frac{\partial|\alpha|^2}{\partial t} &= \frac{\partial\alpha^*\alpha}{\partial t}\\ &= \alpha^*\frac{\partial\alpha}{\partial t} + \alpha\frac{\partial\alpha^*}{\partial t}\\ &= \alpha^*\left[-i2NU_0\alpha^* S - \kappa\alpha\right] + \alpha\left[i2NU_0\alpha S^* - \kappa\alpha^*\right]\\ &= 2N\left[iU_0\left(\alpha^2 S^* - \alpha^{*2}S\right)\right] - 2\kappa|\alpha|^2\,.\end{aligned} \tag{3.3.1.6}$$

Into the above equation may be substituted (3.3.1.1) to produce

$$\frac{\partial|\alpha|^2}{\partial t} = 2N\frac{\partial D}{\partial t} - 2\kappa|\alpha|^2 \tag{3.3.1.7}$$

3.3.1.2 Two-photon area theorem

The two-photon area is defined as

$$\phi = \int_0^t 2U_0|\alpha(t)|^2 dt\,, \tag{3.3.1.8}$$

based on solving (3.3.1.5) for the angle on the Bloch sphere. Expressed in terms of the above term ϕ, the population inversion may be given by

$$D = -\frac{1}{2}\cos(\phi)\,, \tag{3.3.1.9}$$

and consequently

$$\frac{\partial D}{\partial t} = \frac{1}{2}\sin(\phi)\frac{\partial \phi}{\partial t}\,. \tag{3.3.1.10}$$

From its definition in (3.3.1.8), the first and second derivatives of ϕ are

$$\frac{\partial \phi}{\partial t} = 2U_0|\alpha|^2 \tag{3.3.1.11}$$

and

$$\frac{\partial^2 \phi}{\partial t^2} = 2U_0\frac{\partial |\alpha|^2}{\partial t} \tag{3.3.1.12}$$

respectively. The expression in equation (3.3.1.7) followed by equation (3.3.1.10) and (3.3.1.11) may then be substituted into the above expression to produce an equation in terms of ϕ alone,

$$\begin{aligned}\frac{\partial^2\phi}{\partial t^2} &= 2U_0\left[2N\frac{\partial D}{\partial t} - 2\kappa|\alpha|^2\right] \\ &= 4NU_0\left[\frac{1}{2}\sin(\phi)\frac{\partial\phi}{\partial t}\right] - 4U_0\kappa|\alpha|^2 \\ &= 2NU_0\sin(\phi)\frac{\partial\phi}{\partial t} - 2\kappa\left[2U_0|\alpha|^2\right] \\ &= 2NU_0\sin(\phi)\frac{\partial\phi}{\partial t} - 2\kappa\frac{\partial\phi}{\partial t}. \end{aligned} \tag{3.3.1.13}$$

3.3.1.3 Stability Analysis

Using the term $I = \frac{\partial\phi}{\partial t}$ in equation (3.3.1.13) gives it the form

$$\frac{\partial I}{\partial t} = 2NU_0\sin(\phi)I - 2\kappa I\,, \tag{3.3.1.14}$$

from which it is easy to see that the system is stable when I=0. Expanding the two-photon area out as $\phi = \phi_0 + \phi_1$ in (3.3.1.13)

$$\frac{\partial^2(\phi_0+\phi_1)}{\partial t^2} = 2NU_0\sin(\phi_0+\phi_1)\frac{\partial(\phi_0+\phi_1)}{\partial t} - 2\kappa\frac{\partial(\phi_0+\phi_1)}{\partial t}\,. \tag{3.3.1.15}$$

The term ϕ_0 is the initial phase, so time derivatives of this term are zero, leaving only time derivatives of ϕ_1. The term $\sin(\phi_0+\phi_1)\frac{\partial\phi_1}{\partial t}$ expands out to

$$\sin(\phi_0+\phi_1)\frac{\partial\phi_1}{\partial t} = \left(\sin(\phi_0)cos(\phi_1) + \sin(\phi_1)cos(\phi_0)\right)\frac{\partial\phi_1}{\partial t}\,. \tag{3.3.1.16}$$

To first order, $cos(\phi_1) \approx 1 - \frac{\phi_1^2}{2}$, however when multiplied by the term $\frac{\partial\phi_1}{\partial t}$ there are two first order terms multiplied. Such terms may be neglected. Likewise, to first order $\sin(\phi_1) \approx \phi_1 - \frac{\phi_1^3}{6}$, which when multiplied by $\frac{\partial\phi_1}{\partial t}$ may be neglected entirely. The equation is then left as

$$\frac{\partial^2\phi_1}{\partial t^2} = 2NU_0\sin(\phi_0)\frac{\partial\phi_1}{\partial t} - 2\kappa\frac{\partial\phi_1}{\partial t}\,, \tag{3.3.1.17}$$

an expression purely in $\frac{\partial\phi_1}{\partial t}$. Assuming solutions to the above expression may be taken to have the form $\phi_1 \propto e^{\lambda t}$ then the system has solutions of

$$\lambda = 0 \quad or \quad \lambda = 2NU_0\sin(\phi_0) - 2\kappa\,. \tag{3.3.1.18}$$

The SF instability exists when $\lambda > 0$, for this expression to be true then the condition

$$NU_0\sin(\phi_0) > \kappa \tag{3.3.1.19}$$

must be satisfied. The maximum value of the term $2NU_0\sin(\phi_0)$ occurs at $\sin(\phi_0) = 1$, so the condition above becomes

$$NU_0 > \kappa\,, \tag{3.3.1.20}$$

i.e. the SF instability is to be expected in the good cavity limit. This contrasts with, for instance, the case of Superradiant Rayleigh Scattering (SRyS) wherein superradiance is expected in the bad-cavity limit [82][42].

It must also be noted that the term U_0 may be negative, owing to its dependence upon the single photon detuning Δ_a. However, when U_0 takes a negative value, the maximum value of $NU_0\sin(\phi_0)$ occurs at $\sin(\phi_0) = -1$, so the condition described above holds true for both red and blue detuned optical fields.

3.3.2 Two-photon Superfluorescence from stationary atoms

When atoms are stationary and optical forces are neglected it can be seen below in Fig. 3.26 that input parameters which satisfy the SF instability condition described in (3.3.1.20) result in the system producing an optical pulse which closely resembles that of SF.

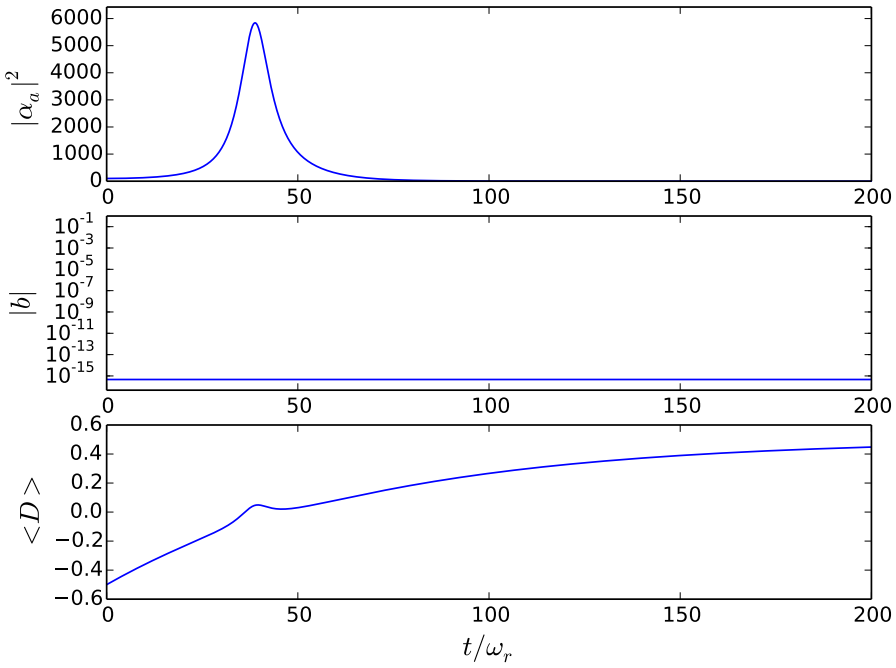

Figure 3.26: Evolution of probe photon number, $|\alpha_a|^2$, bunching parameter, $|b|$, and mean population difference, $\langle D \rangle$ for a case of strong excitation. Produced by solving equations (3.2.2.8) - (3.2.2.6). Parameters used are $U_0/\omega_r = 1 \times 10^{-5}$, $\Delta_{ab} = 0$, $\alpha^{init} = 10$, $N_a = 5 \times 10^4$, $\epsilon_\mu = 0$, $\kappa = 10^{-4}$, $\gamma = 1.5 \times 10^{-2}$, neglecting recoil. Demonstration of Superfluorescent behaviour in the three level ladder system.

One of the characteristic properties of Superfluorescence, and indeed all superemissive effects, is that the peak intensity of the SF pulse is proportional to the square of the number of emitting atoms. Such a proportionality was investigated by running the code for increasing values of N_a and plotting the peak intensity values of the SF curve from each simulation. In doing so, Figure 3.27 was produced and the N^2 dependence of I_{peak} demonstrated.

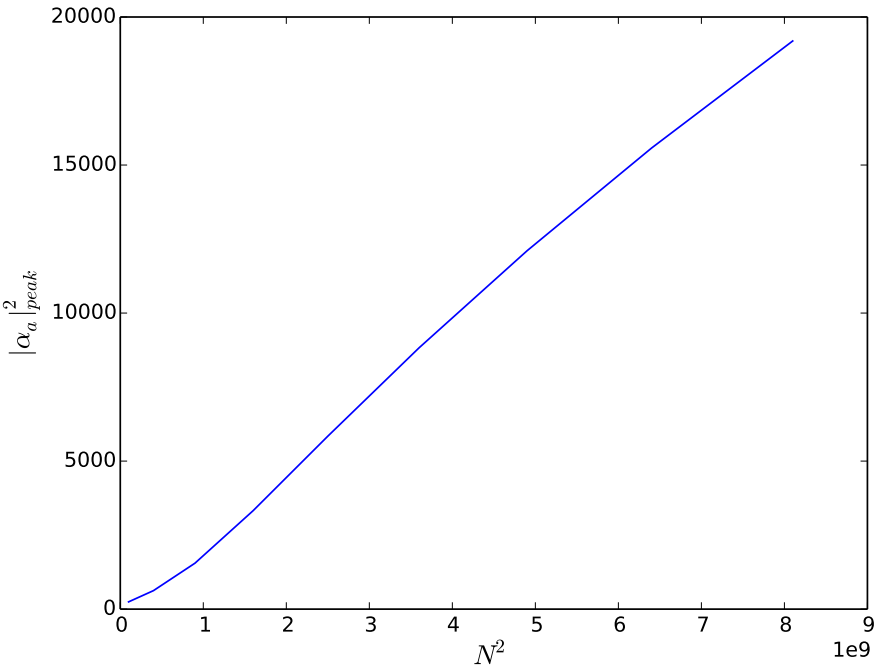

Figure 3.27: Dependence of the probe photon number, $|\alpha_a|^2$ upon the number of atoms, N_a. Produced by solving equations (3.2.2.8) - (3.2.2.6). Parameters used are $U_0/\omega_r = 1 \times 10^{-5}$, $\Delta_{ab} = 0$, $\alpha^{init} = 10$, $\epsilon_\mu = 0$, $\kappa = 10^{-4}$, $\gamma = 1.5 \times 10^{-2}$, neglecting recoil. As this plot shows intensity plotted against the square of the number of atoms, the straight line demonstrates an N^2 depenence of the intensity upon the number of atoms.

Another characteristic of superemissive behaviour is that as the number of atoms emitting increases the width of the emitted pulse decreases. Figure 3.28 shows the curves of intensity evolving with time for increasing numbers of atoms. As can be seen, the width of each pulse grows steadily narrower with increasing number of emitters.

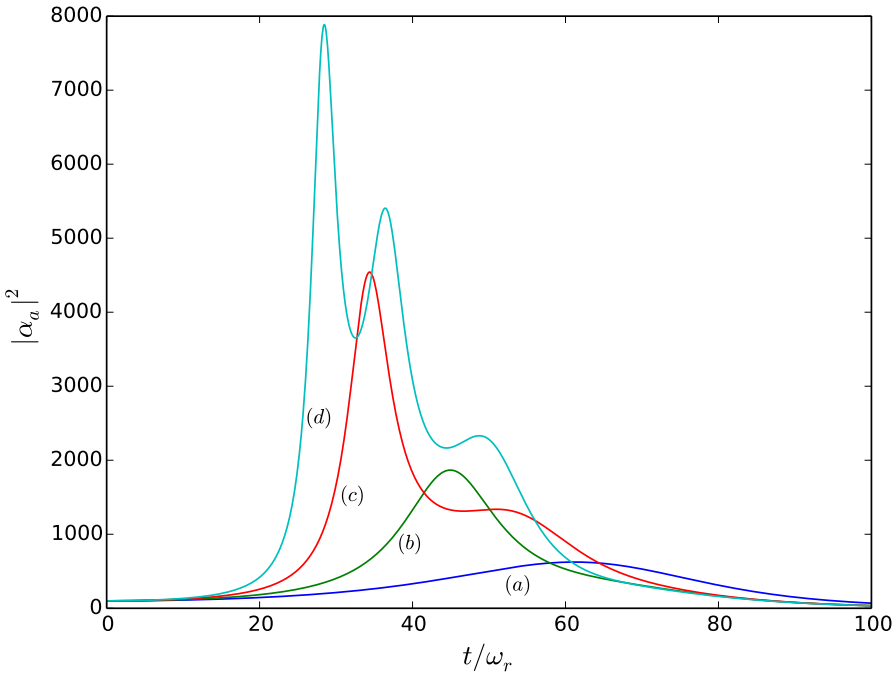

Figure 3.28: Evolution of probe photon number $|\alpha_a|^2$ for the number of atoms in the simulated cavity $N_a =$ (a) 2×10^4, (b) 4×10^4, (c) 6×10^4, (d) 8×10^4. Produced by solving equations (3.2.2.8) - (3.2.2.6). Parameters used are $U_0/\omega_r = 1\times10^{-5}$, $\Delta_{ab} = 0$, $\alpha^{init} = 10$, $\epsilon_\mu = 0$, $\kappa = 10^{-4}$, $\gamma = 1.5\times10^{-2}$, neglecting recoil.

The prediction that two-photon superfluorescence is to be expected only in the good cavity regime is verified when the value for the field losses, κ, is given a value which violated the SF condition described in (3.3.1.20). Running the code with $\kappa = 2 > NU_0 = 0.5$ produced Figure 3.29, which visually demonstrates ordinary fluorescence in the bad cavity limit.

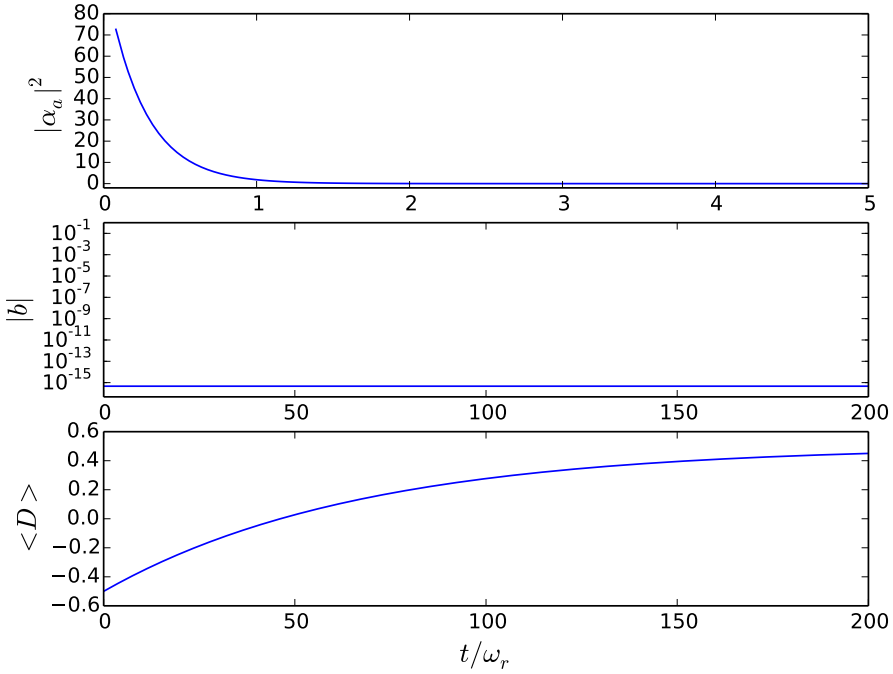

Figure 3.29: Evolution of probe photon number, $|\alpha_a|^2$, bunching parameter, $|b|$, and mean population difference, $\langle D \rangle$ for a case of strong excitation. Produced by solving equations (3.2.2.8) - (3.2.2.6). Parameters used are $U_0/\omega_r = 1 \times 10^{-5}$, $\Delta_{ab} = 0$, $\alpha^{init} = 10$, $N_a = 5 \times 10^4$, $\epsilon_\mu = 0$, $\kappa = 2$, $\gamma = 1.5 \times 10^{-2}$, neglecting recoil. With the condition (3.3.1.20) violated, only ordinary fluorescent decay is evident.

The SF condition (3.3.1.20), predicted that the superfluorescent pulses would exist for both signs of the single photon detuning. This expected behaviour is met when the sign of U_0 is set negative using otherwise identical parameters as to Fig 3.26. The resulting output is shown in Figure 3.30, where the SF instability can not only be easily observed, but matches perfectly with the previous result and confirms the expectation of the SF instability being symmetric in terms of single photon optical detuning.

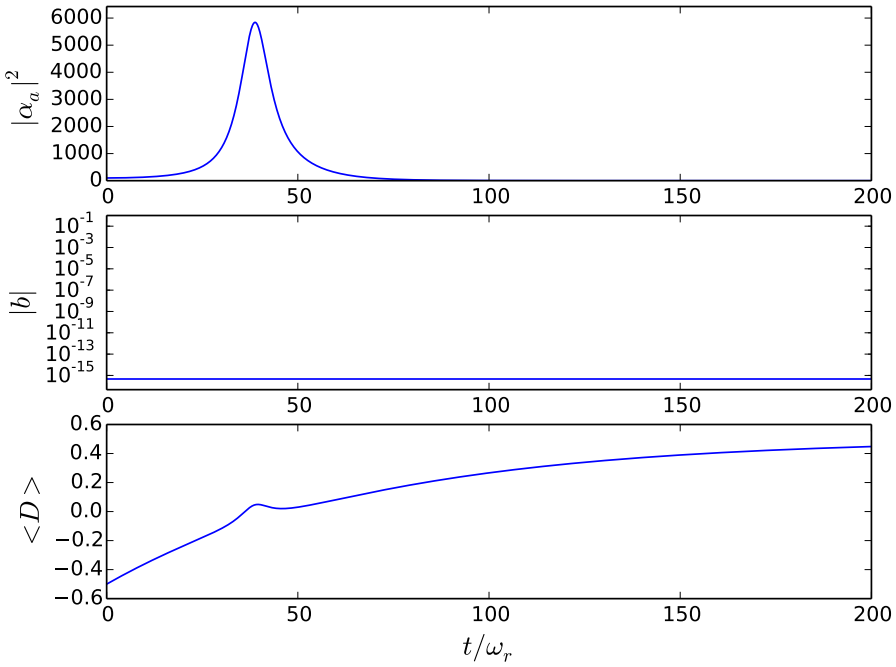

Figure 3.30: Evolution of probe photon number, $|\alpha_a|^2$, bunching parameter, $|b|$, and mean population difference, $\langle D \rangle$ for a case of strong excitation. Produced by solving equations (3.2.2.8) - (3.2.2.6). Parameters used are $U_0/\omega_r = -1 \times 10^{-5}$, $\Delta_{ab} = 0$, $\alpha^{init} = 10$, $N_a = 5 \times 10^4$, $\epsilon_\mu = 0$, $\kappa = 10^{-4}$, $\gamma = 1.5 \times 10^{-2}$, neglecting recoil. Demonstration of Superfluorescent behaviour in the three level ladder system for the alternate sign of the single photon optical detuning.

3.3.3 Two-photon Superfluorescence including recoil

When centre of mass atomic motion is considered, however, the behaviour of the system during emission of light changes.

It can be seen in Figure 3.31 that when recoil is considered for $U_0 > 0$, i.e, $\Delta_a > 0$ that the SF process is retarded both in time and in the value of the intensity peak. This retardation is the result of the atoms in the system bunching at the minima of the standing wave of optical intensity.

It has been shown [36] that for superfluorescence in a gas of cold two level atoms that considering the centre-of-mass atomic recoil results in the detuning symmetry breaking. For a laser which is blue detuned from resonance ($\Delta_a > 0$) the addition of recoil to the two level system lead to enhancement of the superfluorescent pulse, when the laser was red detuned the pulse was diminished.

The explanation for the apparent difference here is that in Section 3.1.1 the assumption was made that, for a sufficiently small two photon detuning Δ_{ab}, the single photon detunings are approximately the same magnitude but of opposite sign $\Delta_a = -\Delta_b$. So when considering the single photon detuning for the lower level transition ($|1\rangle \rightarrow |2\rangle$) Δ_a to be positive, the detuning for the upper level transition ($|2\rangle \rightarrow |3\rangle$) Δ_b is negative. It is the sign of the upper level detuning which must be considered when investigating the SF instability, where the population is initially entirely inverted ($D = -\frac{1}{2}$).

Figure 3.31 then displays "red" detuning ($\Delta_b < 0$) and the consequent hindrance of the SF instability as the atoms bunch at optical intensity minima. It can be seen in in Figure 3.32 that the atoms move and bunch at approximately $\theta = n\pi,\ n = 1, 3, 5, ...$ Observing Figure 3.33 it can be noted that the atoms bunch but the population remains in the uppermost state until the SF pulse begins.

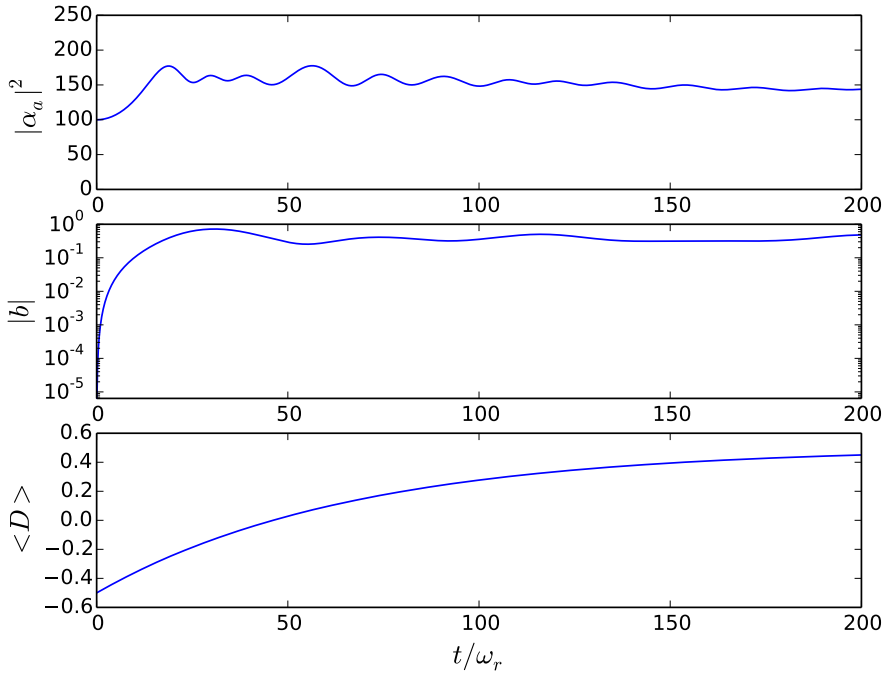

Figure 3.31: Evolution of probe photon number, $|\alpha_a|^2$, bunching parameter, $|b|$, and mean population difference, $\langle D \rangle$ for a case of strong excitation. Produced by solving equations (3.2.2.8) - (3.2.2.6). Parameters used are $U_0/\omega_r = 1 \times 10^{-5}$, $\Delta_{ab} = 0$, $\alpha^{init} = 10$, $N_a = 5 \times 10^4$, $\epsilon_\mu = 0$, $\kappa = 10^{-4}$, $\gamma = 1.5 \times 10^{-2}$, including recoil.

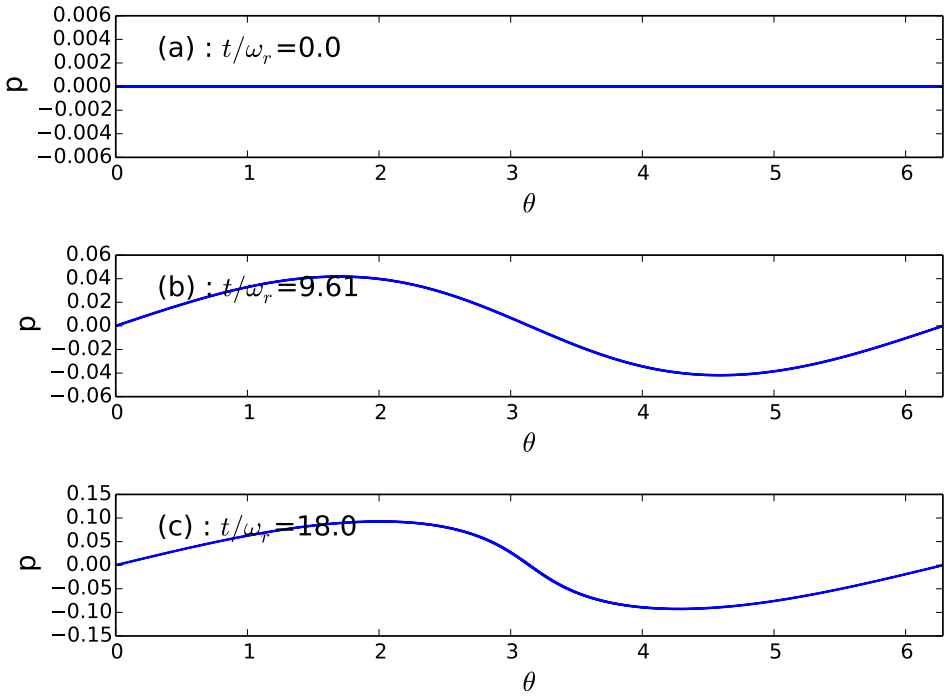

Figure 3.32: Snapshots of momentum distribution (θ_j, p_j) for each atom $j = 1..1000$ when (a) $t = 0\omega_r^{-1}$, (b) $t = 9.61\omega_r^{-1}$, (c) $t = 18.0\omega_r^{-1}$ in the case of strong excitation. Parameters used and equations solved are as in Figure 3.31.

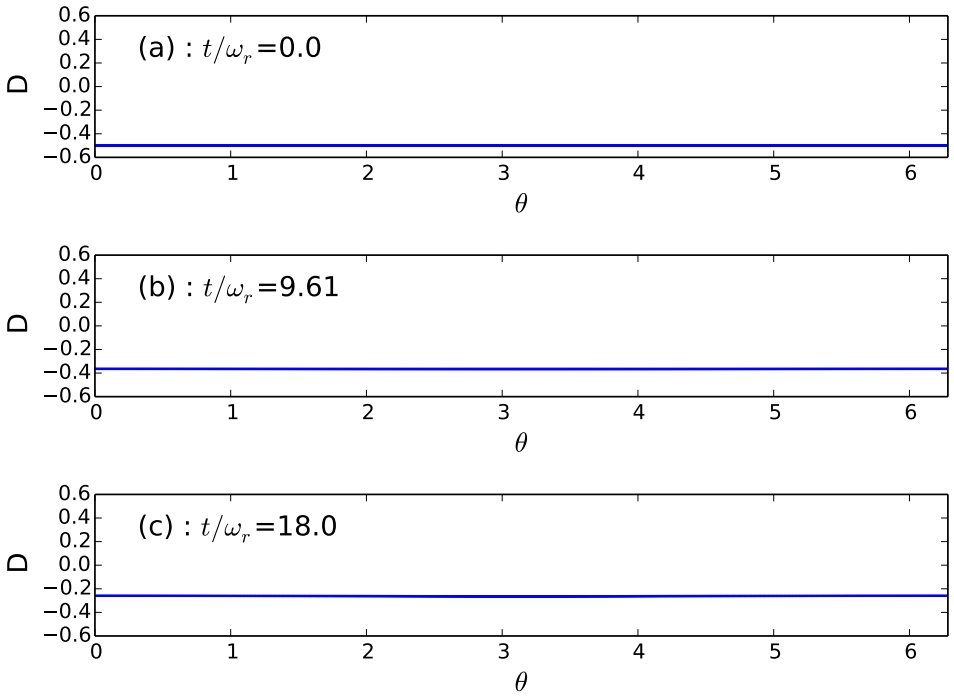

Figure 3.33: Snapshots of population inversion distribution (θ_j, D_j) for each atom $j = 1..1000$ when (a) $t = 0\omega_r^{-1}$, (b) $t = 9.61\omega_r^{-1}$, (c) $t = 18.0\omega_r^{-1}$ in the case of strong excitation. Parameters used and equations solved are as in Figure 3.31.

When the detuning for the upper transition is "blue" ($\Delta_b > 0$), the situation described above is reversed. The atoms bunch at optical field standing wave intensity maxima instead. At optical intensity maxima the optical pulse is enhanced over the red detuned case, achieving a larger a larger intensity peak. This enhancement effect can be observed in Figure 3.34 where the initial optical pulse intensity peak value is greater than that of the opposite detuning sign.

Figure 3.35 shows that the atoms bunch approximately at $\theta = 2n\pi$, $n = 0, 1, 2, 3, ...$, a shift of π from the "red" detuned regime i.e. at the optical field intensity maximum. As before, the population remains in the excited state until decaying and producing the optical pulse.

It should be noted that the intensity of the optical pulses emitted in the recoil included cases cease to exhibit the N^2 dependence, so may not strictly be referred to as superfluorescent. It was discovered that by decreasing the value of the decay term γ that the recoil case could be made superfluorescent. However in such a limit the non recoil case ceased to exhibit superfluorescence. It is possible that this behaviour is due to the narrow linewidth resulting from the condition in equation (3.3.1.20). With further investigation of parameter space it may be possible to uncover conditions under which superfluorescence occurs simultaneously in the cases where atomic centre of mass recoil is both included and neglected.

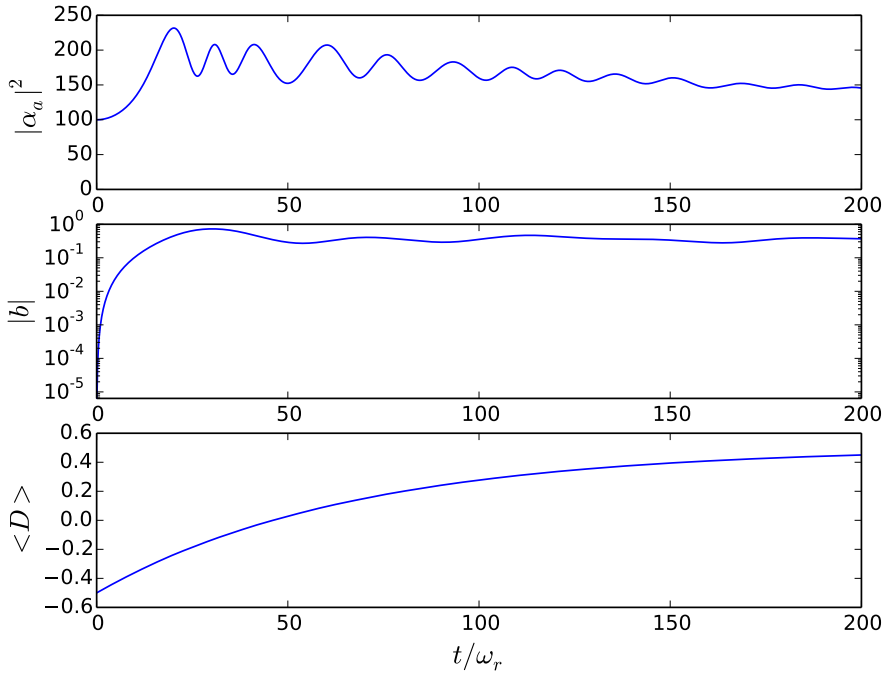

Figure 3.34: Evolution of probe photon number, $|\alpha_a|^2$, bunching parameter, $|b|$, and mean population difference, $\langle D \rangle$ for a case of strong excitation. Produced by solving equations (3.2.2.8) - (3.2.2.6). Parameters used are $U_0/\omega_r = -1 \times 10^{-5}$, $\Delta_{ab} = 0$, $\alpha^{init} = 10$, $N_a = 5 \times 10^4$, $\epsilon_\mu = 0$, $\kappa = 10^{-4}$, $\gamma = 1.5 \times 10^{-2}$, including recoil.

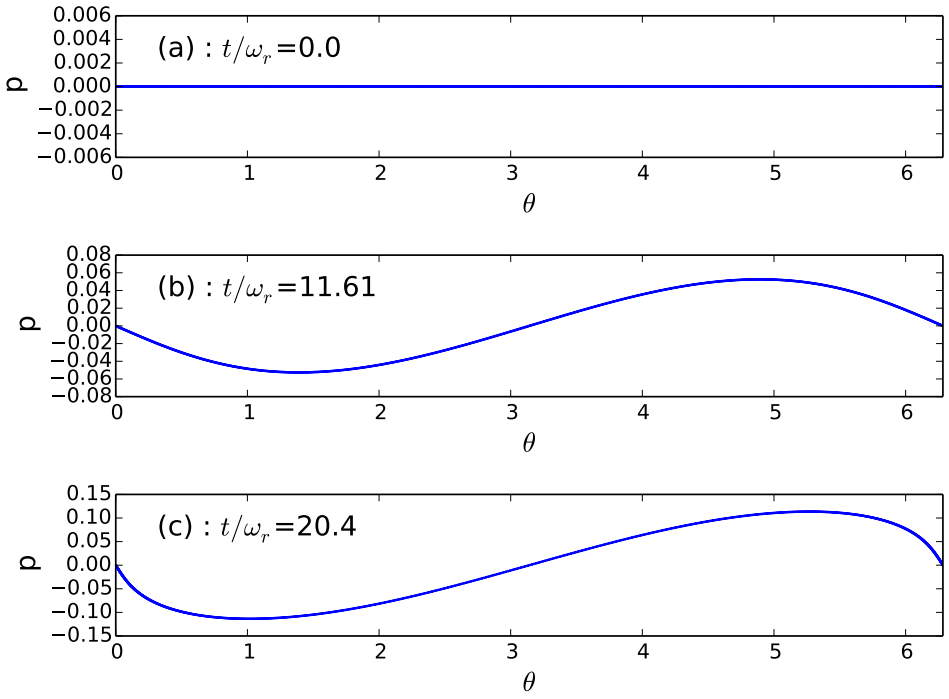

Figure 3.35: Snapshots of momentum distribution (θ_j, p_j) for each atom $j = 1..1000$ when (a) $t = 0\omega_r^{-1}$, (b) $t = 11.61\omega_r^{-1}$, (c) $t = 20.4\omega_r^{-1}$ in the case of strong excitation. Parameters used and equations solved are as in Figure 3.34.

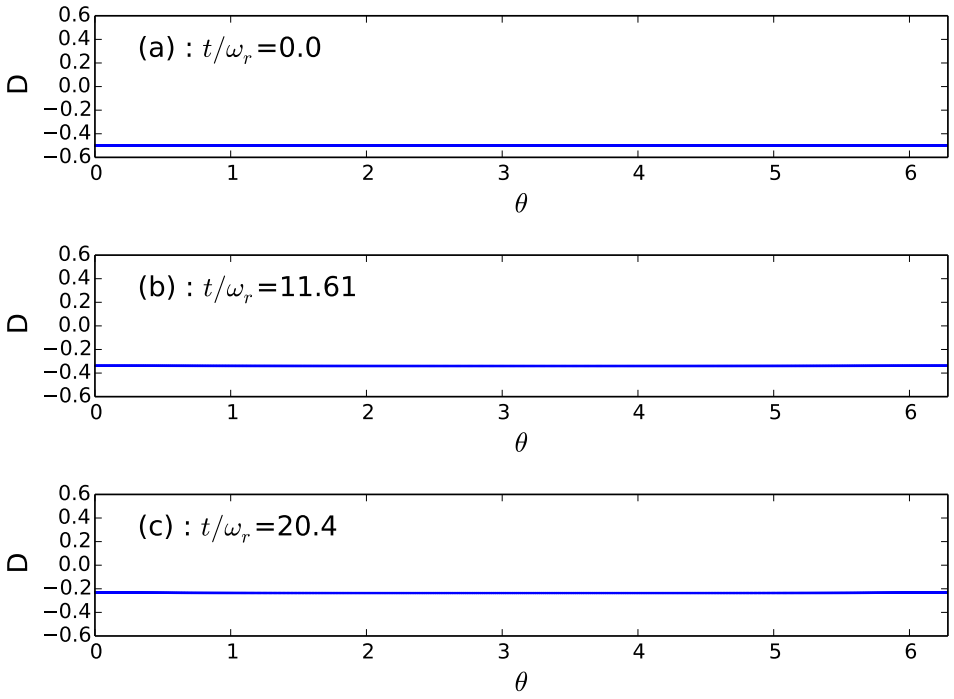

Figure 3.36: Snapshots of population inversion distribution (θ_j, D_j) for each atom $j = 1..1000$ when (a) $t = 0\omega_r^{-1}$, (b) $t = 11.61\omega_r^{-1}$, (c) $t = 20.4\omega_r^{-1}$ in the case of strong excitation. Parameters used and equations solved are as in Figure 3.34.

Chapter 4

Three level atoms: Λ configuration

The ladder configuration considered in Chapter 3 is not the only energy level schema for three level atoms which may yield interesting results when the effects of atomic motion are considered. There exist interesting results also for the case of a three level "Lambda" (Λ) configuration, wherein there exist two relatively close energy levels which share a common transition to a third much higher energy level, as shown schematically in Figure 4.1.

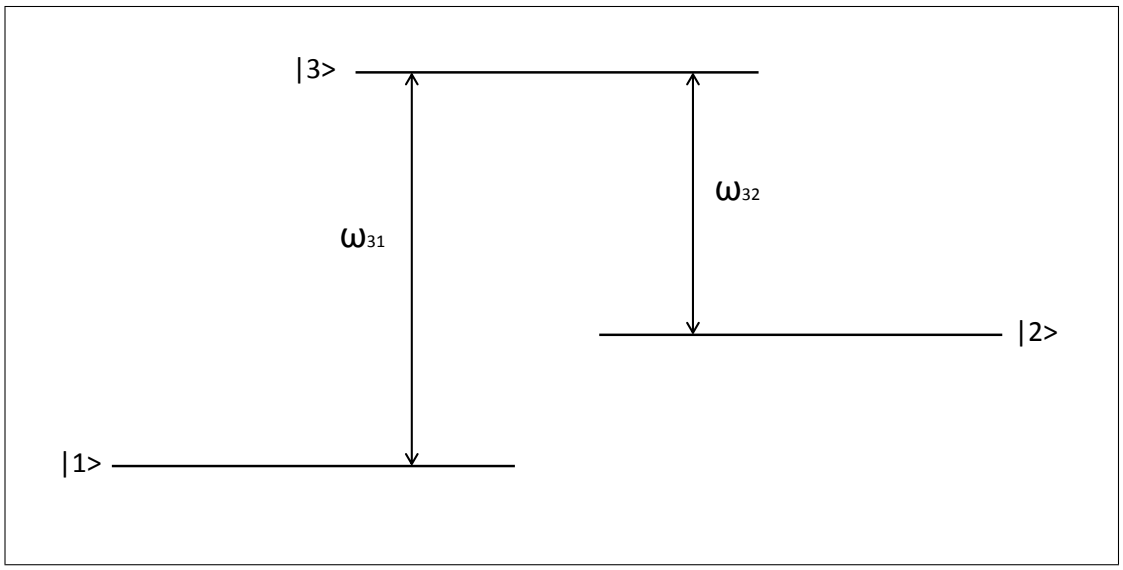

Figure 4.1: Simplified Three level Λ Energy Level Diagram

4.1 Three level Maxwell-Bloch equations in a Λ configuration

As was the case for the ladder configuration, two counterpropagating fields of degenerate frequency are used in the Λ system as well. The optical electric field, $\vec{E}$ can once again be written as

$$\vec{E} = \left(A_a(t)e^{i(kz-\omega t)} + A_b(t)e^{i(-kz-\omega t)} + c.c.\right)\hat{e}\,, \tag{4.1.0.1}$$

to which the response of each atom's dipole moment to the above field would to be of the form

$$\vec{d} = \left(\mu_a\sigma_{31}e^{i(kz-\omega t)} + \mu_b\sigma_{32}e^{i(-kz-\omega t)} + c.c.\right)\hat{e}. \tag{4.1.0.2}$$

The dipole moment for the Λ three level system is given once again by equation (3.1.0.3). As was the case with both two level atoms and three level ladder configuration atoms, the dipole matrix terms with matching indices are always zero, so $\vec{p}_{jj} = 0$. It is also assumed that direct transitions between $|1\rangle$ and $|2\rangle$ are also forbidden, i.e. $p_{21} = p_{12} = 0$. Furthermore, it has been assumed that the pump and probe optical beams are both sufficiently detuned from resonance that the highest energy level $|3\rangle$ has negligible population, so that we may write $\rho_{33} = 0$. Lastly, it is once again assumed that the dipole matrix terms may be taken to be real, with any complex quantity absorbed into the density matrix elements. We may then write

$$\vec{p}_{13} = \vec{p}_{31} = \mu_a\hat{e} \quad \& \quad \vec{p}_{23} = \vec{p}_{32} = \mu_b\hat{e}\,, \tag{4.1.0.3}$$

where the polarisation of the dipole moment has been taken to be parallel to that of the optical pump and probe beams, i.e. $\hat{e}$. The dipole moment for a three level atom can therefore be rewritten as

$$\vec{d} = \left(\mu_a\rho_{31} + \mu_b\rho_{32} + c.c.\right)\hat{e} \tag{4.1.0.4}$$

Again, as was the case in both the two level atom and three level ladder configuration, substituting integer values into (2.2.4.14) produces equations for the coherence and population terms for the system.

4.1.1 Coherence terms

Substituting $j = 3$ & $k = 1$ into (2.2.4.14) produces the first of the three level, Λ configuration coherence equations

$$\frac{\partial \rho_{31}}{\partial t} = -(\gamma_{31} + i\omega_{31})\rho_{31} + \frac{i\vec{E}}{\hbar} \cdot (\vec{p}_{31}\rho_{11} + \vec{p}_{32}\rho_{21} + \vec{p}_{33}\rho_{31}) - \frac{i\vec{E}}{\hbar} \cdot (\vec{p}_{11}\rho_{31} + \vec{p}_{21}\rho_{32} + \vec{p}_{31}\rho_{33}) \,. \tag{4.1.1.1}$$

Remembering our previous statements that $\rho_{jj} = \rho_{21} = \rho_{12} = 0$, $\vec{p}_{13} = \vec{p}_{31} = \mu_a \hat{e}$ & $\vec{p}_{23} = \vec{p}_{32} = \mu_b \hat{e}$ the above simplifies to

$$\frac{\partial \rho_{31}}{\partial t} = -(\gamma_{31} + i\omega_{31})\rho_{31} + \frac{i\vec{E}}{\hbar} \cdot (\mu_a \rho_{11} + \mu_b \rho_{21})\, \hat{e} \,. \tag{4.1.1.2}$$

In comparing (4.1.0.4) to (4.1.0.2) we see that for both conditions to hold true, we must be able to equate terms such that

$$\rho_{31} = \sigma_{31} e^{-i\omega t} \tag{4.1.1.3}$$

$$\rho_{32} = \sigma_{32} e^{-i\omega t} \tag{4.1.1.4}$$

$$\rho_{21} = \sigma_{21} \,. \tag{4.1.1.5}$$

Substituting for ρ in the above using (4.1.1.3) gives

$$\frac{\partial \left(\sigma_{31} e^{-i\omega t}\right)}{\partial t} = -(\gamma_{31} + i\omega_{31})\sigma_{31} e^{-i\omega t} + \frac{i\vec{E}}{\hbar} \cdot (\mu_a \rho_{11} + \mu_b \sigma_{21})\, \hat{e} \tag{4.1.1.6}$$

and consequently

$$\frac{\partial \sigma_{31}}{\partial t} = -(\gamma_{31} - i(\omega - \omega_{31}))\sigma_{31} + \frac{i\vec{E}}{\hbar} \cdot \left(\mu_a \rho_{11} e^{i\omega t} + \mu_b \sigma_{21} e^{i\omega t}\right) \hat{e}\,. \qquad (4.1.1.7)$$

Defining the detuning as $\Delta_a = \omega - \omega_{31}$ and substituting for $\vec{E}$ using (4.1.0.1) gives

$$\begin{aligned}\frac{\partial \sigma_{31}}{\partial t} =& -(\gamma_{31} - i\Delta_a)\sigma_{31} \\ &+ \frac{i}{\hbar}\left(A_a e^{i(kz-\omega t)} + A_b e^{i(-kz-\omega t)} + c.c.\right)\hat{e} \cdot \left(\mu_a \rho_{11} e^{i\omega t} + \mu_b \sigma_{21} e^{i\omega t}\right)\hat{e}\,,\end{aligned} \qquad (4.1.1.8)$$

which, after applying the RWA (which once again eliminates terms which vary as $\pm e^{in\omega t}$ for $n > 1$), reduces to

$$\begin{aligned}\frac{\partial \sigma_{31}}{\partial t} =& -(\gamma_{31} - i\Delta_a)\sigma_{31} \\ &+ \frac{i}{\hbar}\left(A_a e^{ikz} + A_b e^{-ikz}\right)\left(\mu_a \rho_{11} + \mu_b \sigma_{21}\right)\,.\end{aligned} \qquad (4.1.1.9)$$

As the system is assumed to be closed, i.e. $\rho_{11} + \rho_{22} = 1$ (where we have already stated that the population of the highest energy level is taken to be approximately zero, $\rho_{33} \approx 0$), we can define the population difference of the three level Λ configuration system to be

$$D = \frac{1}{2}(\rho_{11} - \rho_{22})\,. \qquad (4.1.1.10)$$

From this definition substitutions for the two population terms may be produced, i.e.

$$\rho_{11} = \frac{1}{2} + D \quad \& \quad \rho_{22} = \frac{1}{2} - D\,. \tag{4.1.1.11}$$

Substituting the above into (4.1.1.12) gives the equation for the evolution of the coherence between level $|1\rangle$ and $|3\rangle$

$$\begin{aligned}\frac{\partial \sigma_{31}}{\partial t} =& -(\gamma_{31} - i\Delta_a)\sigma_{31} \\ &+ \frac{i}{\hbar}\left(A_a e^{ikz} + A_b e^{-ikz}\right)\left(\mu_a\left(\frac{1}{2} + D\right) + \mu_b \sigma_{21}\right).\end{aligned} \tag{4.1.1.12}$$

Following the same derivation steps, the equations for the coherences between levels $|2\rangle$ and $|3\rangle$ and $|1\rangle$ and $|2\rangle$ can be shown to be

$$\begin{aligned}\frac{\partial \sigma_{32}}{\partial t} =& -(\gamma_{32} - i\Delta_b)\sigma_{31} \\ &+ \frac{i}{\hbar}\left(A_a e^{ikz} + A_b e^{-ikz}\right)\left(\mu_a \sigma_{12} + \mu_b\left(\frac{1}{2} - D\right)\right)\end{aligned} \tag{4.1.1.13}$$

and

$$\begin{aligned}\frac{\partial \sigma_{21}}{\partial t} =& -(\gamma_{21} - i\Delta_{ab})\sigma_{21} \\ &+ \frac{i}{\hbar}\left(\left(A_a^* e^{-ikz} + A_b^* e^{ikz}\right)\mu_b \sigma_{31} - \left(A_a e^{ikz} + A_b e^{-ikz}\right)\mu_a \sigma_{23}\right).\end{aligned} \tag{4.1.1.14}$$

In the three level ladder configuration the intermediate level $|2\rangle$ was assumed to have negligible population, thus coherence terms for transitions involving that level were adiabatically eliminated under the assumption that such coherences would respond rapidly to changes in the two-photon coherence. A similar situation is assumed to be the case here, where coherences for transitions involving the highest energy level $|3\rangle$, which has negligible population, are assumed to respond rapidly to the coherence term σ_{21} and thus may be adiabatically eliminated to

produce

$$\sigma_{31} = \frac{-1}{\hbar\Delta_a}\left(A_a e^{ikz} + A_b e^{-ikz}\right)\left(\mu_a\left(\frac{1}{2} + D\right) + \mu_b\sigma_{21}\right) \tag{4.1.1.15}$$

$$\sigma_{32} = \frac{-1}{\hbar\Delta_b}\left(A_a e^{ikz} + A_b e^{-ikz}\right)\left(\mu_a\sigma_{12} + \mu_b\left(\frac{1}{2} - D\right)\right) . \tag{4.1.1.16}$$

Where, as we are operating in the far detuned regime, we have neglected the coherence decay terms as $\Delta_a >> \gamma_{31}$ & $\Delta_b >> \gamma_{32}$. Substituting the two adiabatically eliminated coherence terms into the equation for the coherence term σ_{21} gives

$$\begin{aligned}\frac{\partial\sigma_{21}}{\partial t} =& -(\gamma_{21} - i\Delta_{ab})\sigma_{21} \\ &+ \frac{i\mu_b}{\hbar}\left(A_a^* e^{-ikz} + A_b^* e^{ikz}\right)\left[\frac{-1}{\hbar\Delta_a}\left(A_a e^{ikz} + A_b e^{-ikz}\right)\left(\mu_a\left(\frac{1}{2} + D\right) + \mu_b\sigma_{21}\right)\right] \\ &- \frac{i\mu_a}{\hbar}\left(A_a e^{ikz} + A_b e^{-ikz}\right)\left[\frac{-1}{\hbar\Delta_b}\left(A_a e^{ikz} + A_b e^{-ikz}\right)\left(\mu_a\sigma_{12} + \mu_b\left(\frac{1}{2} - D\right)\right)\right] ,\end{aligned} \tag{4.1.1.17}$$

which may be rearranged and simplified to

$$\begin{aligned}\frac{\partial\sigma_{21}}{\partial t} =& -(\gamma_{21} - i\Delta_{ab})\sigma_{21} \\ &- \frac{i}{\hbar^2\Delta_a\Delta_b}|\left(A_a e^{ikz} + A_b e^{-ikz}\right)|^2\mu_a\mu_b\left(D\left(\Delta_a + \Delta_b\right) - \frac{1}{2}\Delta_{ab}\right) \\ &- \frac{i}{\hbar^2\Delta_a\Delta_b}|\left(A_a e^{ikz} + A_b e^{-ikz}\right)|^2\left(\Delta_b\mu_b^2 - \Delta_a\mu_a^2\right)\sigma_{21} .\end{aligned} \tag{4.1.1.18}$$

4.1.2 Population terms

Substituting $j\,\&\,k = 1$ and $j\,\&\,k = 2$ into (2.2.4.14) and following a similar procedure to that used for the coherence terms produces the equations governing

the evolution of the two population terms ρ_{11} & ρ_{22}

$$\frac{\partial \rho_{11}}{\partial t} = \frac{i\mu_a}{\hbar}\left(\left(A_a^* e^{-ikz} + A_b^* e^{ikz}\right)\sigma_{31} - \left(A_a e^{ikz} + A_b e^{-ikz}\right)\sigma_{13}\right) \qquad (4.1.2.1)$$

$$\frac{\partial \rho_{22}}{\partial t} = \frac{i\mu_b}{\hbar}\left(\left(A_a^* e^{-ikz} + A_b^* e^{ikz}\right)\sigma_{32} - \left(A_a e^{ikz} + A_b e^{-ikz}\right)\sigma_{23}\right) . \qquad (4.1.2.2)$$

It may be noted that population decay terms $\gamma_{33,22,11}$ are absent from the above expressions. In Chapter 2 the population can decay from the excited state $|2\rangle$ to the ground state $|1\rangle$ directly through spontaneous emission. This is encapsulated by the term $\gamma_{22}\rho_{22}$. In Chapter 3, the population may decay from the excited state $|3\rangle$ through the intermediate state $|2\rangle$ to the ground state $|1\rangle$, a process described by inclusion of the term $\gamma_{33}\rho_{33}$ in the population equations. Direct decay from level $|3\rangle$ to level $|1\rangle$ in the ladder configuration is forbidden under the selection rules. So it is with direct transitions from level $|2\rangle$ to level $|1\rangle$ in the three level Λ configuration. As it is assumed that the system is far enough detuned from field atom resonance that the upper state population ρ_{33} remains effectively zero, no spontaneous emission or associated decay in population may take place, thus $\gamma_{33,22,11} = 0$.

From the definition of the population difference for the three level Λ configuration given in (4.1.1.10) it can easily be seen that $\frac{\partial D}{\partial t} = \frac{1}{2}\left(\frac{\partial \rho_{11}}{\partial t} - \frac{\partial \rho_{22}}{\partial t}\right)$. Plugging (4.1.2.1) and (4.1.2.2) into this relation gives

$$\begin{aligned}\frac{\partial D}{\partial t} = \frac{1}{2}\Bigg(& \frac{i\mu_a}{\hbar}\left(\left(A_a^* e^{-ikz} + A_b^* e^{ikz}\right)\sigma_{31} - \left(A_a e^{ikz} + A_b e^{-ikz}\right)\sigma_{13}\right) \\ & -\frac{i\mu_b}{\hbar}\left(\left(A_a^* e^{-ikz} + A_b^* e^{ikz}\right)\sigma_{32} - \left(A_a e^{ikz} + A_b e^{-ikz}\right)\sigma_{23}\right) \Bigg) \end{aligned} \qquad (4.1.2.3)$$

which, after substitution of the one-photon coherence terms σ_{32}, σ_{31} gives

$$\begin{aligned}\frac{\partial D}{\partial t} =&\frac{i\mu_a}{2\hbar}\left(A_a^* e^{-ikz} + A_b^* e^{ikz}\right)\left[\frac{-1}{\hbar\Delta_a}\left(A_a e^{ikz} + A_b e^{-ikz}\right)\left(\mu_a\left(\frac{1}{2}+D\right)+\mu_b\sigma_{21}\right)\right]\\ &-\frac{i\mu_a}{2\hbar}\left(A_a e^{ikz} + A_b e^{-ikz}\right)\left[\frac{-1}{\hbar\Delta_a}\left(A_a^* e^{-ikz} + A_b^* e^{ikz}\right)\left(\mu_a\left(\frac{1}{2}+D\right)+\mu_b\sigma_{12}\right)\right]\\ &-\frac{i\mu_b}{2\hbar}\left(A_a^* e^{-ikz} + A_b^* e^{ikz}\right)\left[\frac{-1}{\hbar\Delta_b}\left(A_a e^{ikz} + A_b e^{-ikz}\right)\left(\mu_b\left(\frac{1}{2}-D\right)+\mu_a\sigma_{12}\right)\right]\\ &+\frac{i\mu_b}{2\hbar}\left(A_a e^{ikz} + A_b e^{-ikz}\right)\left[\frac{-1}{\hbar\Delta_b}\left(A_a^* e^{-ikz} + A_b^* e^{ikz}\right)\left(\mu_b\left(\frac{1}{2}-D\right)+\mu_a\sigma_{21}\right)\right],\end{aligned} \tag{4.1.2.4}$$

which can be further simplified to the form

$$\frac{\partial D}{\partial t} = \frac{-i\mu_a\mu_b}{2\hbar\Delta_a\Delta_b}(\Delta_a+\Delta_b)|\left(A_a e^{ikz} + A_b e^{-ikz}\right)|^2(\sigma_{21}-\sigma_{12}). \tag{4.1.2.5}$$

4.1.3 Momentum and position equations

The force experienced by the jth atom is once more given by

$$\frac{\partial p_j}{\partial t} = \vec{d}\cdot\frac{\partial\vec{E}}{\partial z}\,. \tag{4.1.3.1}$$

Substituting for ρ in equation (4.1.0.4) using (4.1.1.3) allows the equation for an atom's dipole moment to be written as

$$\vec{d} = \left(\mu_a\sigma_{31}e^{-i\omega t} + \mu_b\rho_{32}e^{-i\omega t} + c.c.\right)\hat{e}\,. \tag{4.1.3.2}$$

Substituting for the optical electric field, $\vec{E}$, using equation (4.1.0.1), and the atomic dipole, $\vec{d_j}$, using equation (4.1.3.2), in the above equation for the force, equation (4.1.3.1), and applying the RWA gives

$$\frac{\partial p_j}{\partial t} = -ik\Big(\quad \mu_a \left(A_a^* e^{-ikz} - A_b^* e^{ikz}\right)\sigma_{31} - \mu_a \left(A_a e^{ikz} - A_b e^{-ikz}\right)\sigma_{13} \\ +\mu_b \left(A_a^* e^{-ikz} - A_b^* e^{ikz}\right)\sigma_{32} - \mu_b \left(A_a e^{ikz} - A_b e^{-ikz}\right)\sigma_{23} \quad \Big) . \tag{4.1.3.3}$$

By substituting for the coherence terms, σ_{32} & σ_{31}, the equation for the momentum of the jth atom becomes

$$\frac{\partial p_j}{\partial t} = \frac{ik}{\hbar\Delta_a\Delta_b}\Big(- \mu_a\mu_b\Delta_{ab}\left(|A_a|^2 - |A_b|^2\right)\left(\sigma_{21} - \sigma_{12}\right) \\ + \left(A_a^* A_b e^{-2ikz} - A_a A_b^* e^{2ikz}\right)\Big[\Delta_b\mu_a^2 + \Delta_a\mu_b^2 + 2D\left(\Delta_b\mu_a^2 - \Delta_a\mu_b^2\right) \\ + \mu_a\mu_b\left(\Delta_a + \Delta_b\right)\left(\sigma_{21} + \sigma_{12}\right)\Big] \quad \Big) . \tag{4.1.3.4}$$

The position equation is given by the same equation as for the three level ladder configuration

$$\frac{\partial z_j}{\partial t} = \frac{p_j}{m} . \tag{4.1.3.5}$$

4.1.4 Field equations

The equations describing the evolution of the field amplitudes for the optical pump and probe beams are derived in the same manner as for the three level ladder configuration, by solving the wave equation

$$\nabla^2\vec{E} - \frac{1}{c^2}\frac{\partial^2\vec{E}}{\partial t^2} = \frac{1}{\epsilon_0 c^2}\frac{\partial^2\vec{P}}{\partial t^2} . \tag{4.1.4.1}$$

As the expression for $\vec{E}$, i.e. equation (4.1.0.1) for the three level Λ configuration

is identical to that of both the two level and three level ladder terms (equations (2.4.1.2) and (3.1.0.1) respectively), the left hand of the wave equation produces the same result as before, namely

$$\nabla^2\vec{E} - \frac{1}{c^2}\frac{\partial^2\vec{E}}{\partial t^2} = \left(\frac{2i\omega}{c^2}\frac{\partial A_a}{\partial t}e^{i(kz-\omega t)} + \frac{2i\omega}{c^2}\frac{\partial A_b}{\partial t}e^{i(-kz-\omega t)} + c.c.\right)\hat{e}\,. \qquad (4.1.4.2)$$

Substituting the dipole moment (4.1.3.2) into the right hand side of this wave equation produces

$$\begin{aligned}\frac{\partial^2\vec{P}}{\partial t^2} &= \frac{\partial^2}{\partial t^2}\left(\sum_j^n \vec{d_j}\delta(r-r_j(t))\right)\\ &= \sum_j^n \frac{\partial^2\vec{d_j}}{\partial t^2}\delta(r-r_j(t))\\ &= \sum_j^n \frac{\partial^2}{\partial t^2}\Big(\mu_a\sigma_{31}e^{-i\omega t} + \mu_b\sigma_{32}e^{-i\omega t} + c.c\Big)\hat{e}\;\delta(r-r_j(t))\,, \qquad (4.1.4.3)\end{aligned}$$

and expanding the term $\frac{\partial^2\vec{d_j}}{\partial t^2}$ gives

$$\begin{aligned}\frac{\partial^2\vec{d_j}}{\partial t^2} &= \frac{\partial^2}{\partial t^2}\Big(\mu_a\sigma_{31}e^{-i\omega t} + \mu_a\sigma_{32}e^{-i\omega t} + c.c\Big)\hat{e}\\ &= \frac{\partial}{\partial t}\left(\mu_a\left(\frac{\partial\sigma_{31}}{\partial t} - i\omega\sigma_{31}\right)e^{-i\omega t} + \mu_b\left(\frac{\partial\sigma_{32}}{\partial t} - i\omega\sigma_{32}\right)e^{-i\omega t} + c.c\right)\hat{e}\\ &= \Bigg(\quad \mu_a\left(\frac{\partial^2\sigma_{31}}{\partial t^2} - 2i\omega\frac{\partial\sigma_{31}}{\partial t} - \omega^2\sigma_{31}\right)e^{-i\omega t}\\ &\qquad + \mu_b\left(\frac{\partial^2\sigma_{32}}{\partial t^2} - 2i\omega\frac{\partial\sigma_{32}}{\partial t} - \omega^2\sigma_{32}\right)e^{-i\omega t} + c.c\;\Bigg)\hat{e}\,. \qquad (4.1.4.4)\end{aligned}$$

Applying the SVEA to the above and substituting it in to the right hand side of (4.1.4.1) gives

$$\left(\frac{2i\omega}{c^2}\frac{\partial A_a}{\partial t}e^{i(kz-\omega t)} + \frac{2i\omega}{c^2}\frac{\partial A_b}{\partial t}e^{i(-kz-\omega t)} + c.c.\right)\hat{e}$$
$$= -\frac{1}{\epsilon_0 c^2}\sum_j^n \left(\mu_a\omega^2\sigma_{31}e^{-i\omega t} + \mu_b\omega^2\sigma_{32}e^{-i\omega t} + c.c\right)\delta(r - r_j(t))\,\hat{e}\,. \qquad (4.1.4.5)$$

Taking the dot product of both sides with $\hat{e}$, multiplying through by $e^{i(-kz+\omega t)}$, rearranging constant terms to the right hand side and applying the RWA leaves

$$\left(\frac{\partial A_a}{\partial t} + \frac{\partial A_b}{\partial t}e^{-2ikz}\right) = \frac{i\omega}{2\epsilon_0}\sum_j^n \left(\mu_a\omega^2\sigma_{31}e^{-ikz} + \mu_b\omega^2\sigma_{32}e^{-ikz}\right)\delta(r - r_j(t))\,. \qquad (4.1.4.6)$$

By integrating this expression over the length L and area $\mathscr{A}$ of the atomic sample, then the Dirac delta function on the right hand side is applied, the expression $\frac{\partial A_b}{\partial t}e^{-2ikz}$ averages out to zero and the term $\frac{\partial A_a}{\partial t}$, which has been assumed not to vary, becomes $\mathscr{A}L\frac{\partial A_a}{\partial t}$. By then multiplying the right hand side by $\frac{N}{N}$, using the definitions $n = \frac{N}{\mathscr{A}L}$, $\frac{1}{N}\sum_j^n$ and rearranging terms an expression for the evolution of the probe amplitude is given

$$\frac{\partial A_a}{\partial t} = \frac{i\omega n}{2\epsilon_0}\left\langle \mu_a\omega^2\sigma_{31}e^{-ikz} + \mu_b\omega^2\sigma_{32}e^{-ikz}\right\rangle\,. \qquad (4.1.4.7)$$

The steady state values for the coherence terms σ_{31} and σ_{32}, equations (4.1.1.15) and (4.1.1.16) respectively, are then substituted into the above expression. By re-organising terms and extracting common factors, the expression for the evolution of the probe beam becomes

$$\frac{\partial A_a}{\partial t} = -\frac{i\omega n}{2\hbar\epsilon_0\Delta_a\Delta_b}\Big\langle \left(A_a + A_b e^{-2ikz}\right)\Big(\frac{1}{2}\left(\Delta_b\mu_a^2 + \Delta_a\mu_b^2\right) + D\left(\Delta_b\mu_a^2 - \Delta_a\mu_b^2\right) + \mu_a\mu_b\left(\Delta_b\sigma_{21} + \Delta_a\sigma_{12}\right)\Big)\Big\rangle . \quad (4.1.4.8)$$

As was done for the the two level and three level ladder cases, the assumption is made that the field amplitudes evolve on a timescale much longer than the time taken for a cavity round-trip so that the effects of losses, field injection and detuning from cavity resonance can be represented by introduction of the terms $+(i\delta_c - \kappa)A_a + \kappa A_a^{eq}$. With these terms added to (4.1.4.9), the equation for the evolution of the probe beam field becomes

$$\frac{\partial A_a}{\partial t} = -\frac{i\omega n}{2\hbar\epsilon_0\Delta_a\Delta_b}\Big\langle \left(A_a + A_b e^{-2ikz}\right)\Big(\frac{1}{2}\left(\Delta_b\mu_a^2 + \Delta_a\mu_b^2\right) + D\left(\Delta_b\mu_a^2 - \Delta_a\mu_b^2\right) + \mu_a\mu_b\left(\Delta_b\sigma_{21} + \Delta_a\sigma_{12}\right)\Big)\Big\rangle + (i\delta_c - \kappa)A_a + \kappa A_a^{eq} \quad (4.1.4.9)$$

By multiplying equation (4.1.4.5) through by $e^{i(kz+\omega t)}$ and following a similar process to the once just described an expression for the evolution of the pump amplitude can also be found

$$\frac{\partial A_b}{\partial t} = -\frac{i\omega n}{2\hbar\epsilon_0\Delta_a\Delta_b}\Big\langle \left(A_a e^{2ikz} + A_b\right)\Big(\frac{1}{2}\left(\Delta_b\mu_a^2 + \Delta_a\mu_b^2\right) + D\left(\Delta_b\mu_a^2 - \Delta_a\mu_b^2\right) + \mu_a\mu_b\left(\Delta_b\sigma_{21} - \Delta_a\sigma_{12}\right)\Big)\Big\rangle + (i\delta_c - \kappa)A_b + \kappa A_b^{eq} \quad (4.1.4.10)$$

4.2 CARL in a three level Λ configuration

So as to make the results for the three level Λ configuration consistent with those of the three level ladder configuration, it is convenient to use the same scaling. However, the equations derived above contain the term $\frac{1}{\Delta_b}$, a term which was taken to be approximately equal to $\frac{-1}{\Delta_a}$ in the ladder equations. There exist two detuning regimes for which it is simple to substitute the detuning term Δ_b for an approximately equivalent expression in terms of Δ_a.

The first of these regimes is where the two lower state energy levels $|1\rangle$ & $|2\rangle$ are sufficiently close together and the detunings Δ_a and Δ_a are sufficiently large that the assumption is made that $\omega_{21} = -\Delta_{ab} = \Delta_b - \Delta_a \approx 0$ and so $\Delta_b \approx \Delta_a$. A simplified energy level diagram for such a system is displayed in Figure 4.2. This detuning schema will be referred to as the degenerate Λ configuration.

The second detuning regime in which it is simple to substitute out for Δ_b, is that in which the two ground state energy levels are split relativly far apart from one another. If the magnitude of the detuning of the degenerate pump and probe fields from the transition frequencies ω_{31} & ω_{32} are equal, i.e. $|\Delta_a| \approx |\Delta_b|$, then it can be assumed that $\Delta_b \approx -\Delta_a$ and $\Delta_{ab} \approx 2\Delta_a$. A simplified energy level diagram for this second detuning system is displayed in Figure 4.15. This detuning schema will be referred to as the non-degenerate Λ configuration.

Both the degenerate and non-degenerate Λ configurations allow for the detuning term to be substituted out, leaving only one additional hurdle before the scaling terms (3.1.8.1) - (3.1.8.3) may be applied. In the three level ladder model, the terms μ_a and μ_b were expressed in the form $\mu_a\mu_b = \mu^2$, $\mu_a^2 + \mu_b^2 = 2\mu^2$ and $\mu_a^2 - \mu_b^2 = -\mu^2\epsilon_\mu$. In doing so the governing equations for the ladder model were given a form where the scaling terms in equations (3.1.8.1) - (3.1.8.3) could be applied. Performing similar substitutions for μ_a and μ_b in the Λ three level equations (4.2.1.2), (4.1.2.5), (4.1.3.4), (4.1.3.5), (4.1.4.9), & (4.1.4.10) allows them to be scaled in the same manner.

4.2.1 Accounting for the AC Stark Shift

Defining

$$\mu_a = \mu + \frac{1}{2}\Delta_\mu \quad \& \quad \mu_b = \mu - \frac{1}{2}\Delta_\mu \,, \tag{4.2.1.1}$$

then for the Λ CARL equations the AC Stark shift term is

$$\epsilon_\mu = \frac{\Delta_\mu}{\mu} \,. \tag{4.2.1.2}$$

Substituting the above expressions into the three level Λ equations (4.2.1.2), (4.1.2.5), (4.1.3.4), (4.1.3.5), (4.1.4.9), & (4.1.4.10) with the assumption that $\epsilon_\mu << 1$ gives them the form

$$\begin{aligned}\frac{\partial \sigma_{21}}{\partial t} =& -(\gamma_{21} - i\Delta_{ab})\sigma_{21} \\ & - \frac{i\mu^2}{\hbar^2 \Delta_a \Delta_b} |\left(A_a e^{ikz} + A_b e^{-ikz}\right)|^2 \left(D\left(\Delta_a + \Delta_b\right) - \frac{1}{2}\Delta_{ab}\right) \\ & - \frac{i\mu^2}{\hbar^2 \Delta_a \Delta_b} |\left(A_a e^{ikz} + A_b e^{-ikz}\right)|^2 \big(\Delta_{ab} + \epsilon_\mu \left(\Delta_a + \Delta_b\right)\big)\sigma_{21}\end{aligned} \tag{4.2.1.3}$$

$$\frac{\partial D}{\partial t} = \frac{-i\mu^2}{2\hbar \Delta_a \Delta_b}(\Delta_a + \Delta_b)|\left(A_a e^{ikz} + A_b e^{-ikz}\right)|^2(\sigma_{21} - \sigma_{12}) \tag{4.2.1.4}$$

$$\begin{aligned}\frac{\partial p_j}{\partial t} = \frac{i\mu^2 k}{\hbar \Delta_a \Delta_b}\Big(& -\Delta_{ab}\left(|A_a|^2 - |A_b|^2\right)(\sigma_{21} - \sigma_{12}) \\ & + \left(A_a^* A_b e^{-2ikz} - A_a A_b^* e^{2ikz}\right)\Big[(\Delta_a + \Delta_b)(1 + 2D\epsilon_\mu + \sigma_{21} + \sigma_{12}) \\ & - \Delta_{ab}(2D + \epsilon_\mu)\Big] \quad \Big)\end{aligned} \tag{4.2.1.5}$$

$$\frac{\partial z_j}{\partial t} = \frac{p_j}{m} \tag{4.2.1.6}$$

$$\begin{aligned}\frac{\partial A_a}{\partial t} = -\frac{i\omega\mu^2 n}{2\hbar\epsilon_0\Delta_a\Delta_b}\Big\langle \left(A_a + A_b e^{-2ikz}\right)\Big(& \frac{1}{2}\left(\left(\Delta_b + \Delta_a\right) - \Delta_{ab}\epsilon_\mu\right) \\ & + D\left(\left(\Delta_b + \Delta_a\right)\epsilon_\mu - \Delta_{ab}\right) \\ & + \left(\Delta_b\sigma_{21} + \Delta_a\sigma_{12}\right)\Big)\Big\rangle \\ & + (i\delta_c - \kappa)A_a + \kappa A_a^{eq}\end{aligned} \tag{4.2.1.7}$$

$$\begin{aligned}\frac{\partial A_b}{\partial t} = -\frac{i\omega\mu^2 n}{2\hbar\epsilon_0\Delta_a\Delta_b}\Big\langle \left(A_a e^{2ikz} + A_b\right)\Big(& \frac{1}{2}\left(\left(\Delta_b + \Delta_a\right) - \Delta_{ab}\epsilon_\mu\right) \\ & + D\left(\left(\Delta_b + \Delta_a\right)\epsilon_\mu - \Delta_{ab}\right) \\ & + \left(\Delta_b\sigma_{21} + \Delta_a\sigma_{12}\right)\Big)\Big\rangle \\ & + (i\delta_c - \kappa)A_b + \kappa A_b^{eq}\end{aligned} \tag{4.2.1.8}$$

4.2.2 Degenerate Λ configuration

The first configuration considered is that in which the two energy levels $|1\rangle$ and $|2\rangle$ are approximately degenerate, i.e. $\hbar\omega_{31} \approx \hbar\omega_{32}$. In such a system $\omega_{21} = -\Delta_{ab} \approx 0$, $\omega_{31} \approx \omega_{32}$ and thus by definition $\Delta_b \approx \Delta_a$. In this configuration the Λ three level equations take the form

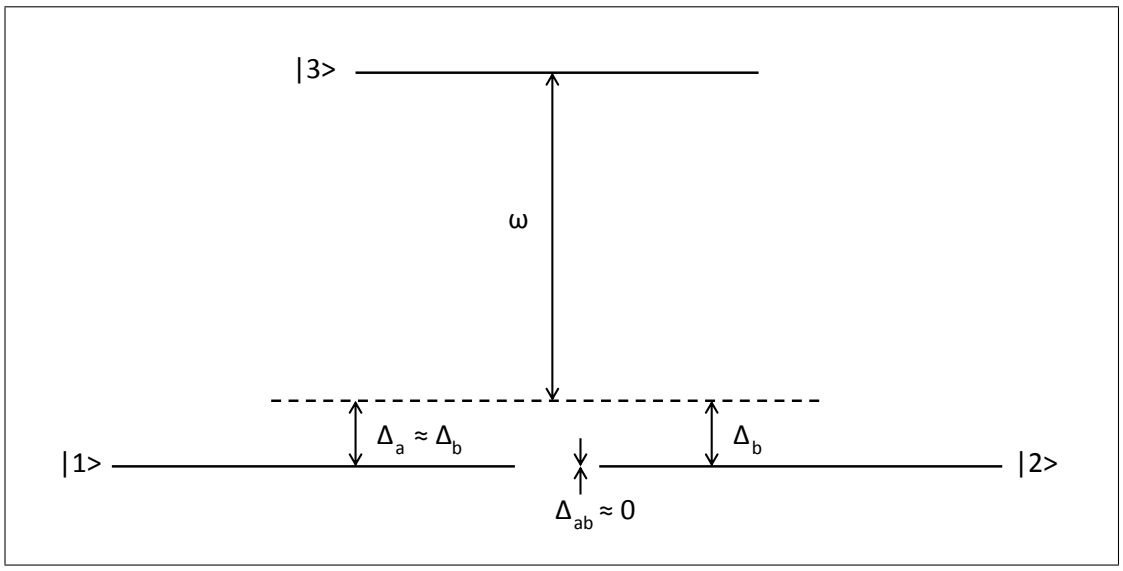

Figure 4.2: Simplified Three Level Λ Energy Level Diagram: The Λ energy level structure for the case where the two lower energy levels are approximately degenerate, so the single transition detunings are also approximately equal.

$$\frac{\partial \sigma_{21}}{\partial t} = -\gamma_{21}\sigma_{21} - \frac{i2\mu^2}{\hbar^2\Delta_a}|\left(A_a e^{ikz} + A_b e^{-ikz}\right)|^2 \left(D - \epsilon_\mu \sigma_{21}\right) \tag{4.2.2.1}$$

$$\frac{\partial D}{\partial t} = -\frac{i\mu^2}{\hbar\Delta_a}|\left(A_a e^{ikz} + A_b e^{-ikz}\right)|^2 (\sigma_{21} - \sigma_{12}) \tag{4.2.2.2}$$

$$\frac{\partial p_j}{\partial t} = \frac{i2\mu^2 k}{\hbar\Delta_a}\left(A_a^* A_b e^{-2ikz} - A_a A_b^* e^{2ikz}\right)(1 + 2\epsilon_\mu D + \sigma_{21} + \sigma_{12}) \tag{4.2.2.3}$$

$$\frac{\partial z_j}{\partial t} = \frac{p_j}{m} \tag{4.2.2.4}$$

$$\begin{aligned}\frac{\partial A_a}{\partial t} = &-\frac{i\omega\mu^2 n}{2\hbar\epsilon_0\Delta_a}\left\langle \left(A_a + A_b e^{-2ikz}\right)(1 + 2\epsilon_\mu D + \sigma_{21} + \sigma_{12}) \right\rangle \\ &+ (i\delta_c - \kappa)A_a + \kappa A_a^{eq}\end{aligned} \tag{4.2.2.5}$$

$$\begin{aligned}\frac{\partial A_b}{\partial t} = &-\frac{i\omega\mu^2 n}{2\hbar\epsilon_0\Delta_a\Delta_b}\left\langle \left(A_a e^{2ikz} + A_b\right)(1 + 2\epsilon_\mu D + \sigma_{21} + \sigma_{12}) \right\rangle \\ &+ (i\delta_c - \kappa)A_b + \kappa A_b^{eq}\end{aligned} \tag{4.2.2.6}$$

4.2.2.1 Scaling the three level Λ equations

In the above form, the Λ equations can now be scaled using the same method as for the three level ladder configuration. Substituting the scaling terms (3.1.8.1) - (3.1.8.3) into the above equations (4.2.2.1) - (4.2.2.6) gives them the form

$$\frac{\partial \sigma_{21}}{\partial t} = -\gamma_{21}\sigma_{21} - iU_0|\left(\alpha_a e^{ikz} + \alpha_b e^{-ikz}\right)|^2 \left(D - \epsilon_\mu \sigma_{21}\right) \tag{4.2.2.7}$$

$$\frac{\partial D}{\partial t} = -iU_0|\left(\alpha_a e^{ikz} + \alpha_b e^{-ikz}\right)|^2 (\sigma_{21} - \sigma_{12}) \tag{4.2.2.8}$$

$$\frac{\partial p_j}{\partial t} = i2\hbar k U_0 \left(\alpha_a^* \alpha_b e^{-2ikz} - \alpha_a \alpha_b^* e^{2ikz}\right)(1 + 2\epsilon_\mu D + \sigma_{21} + \sigma_{12}) \tag{4.2.2.9}$$

$$\frac{\partial z_j}{\partial t} = \frac{p_j}{m} \tag{4.2.2.10}$$

$$\frac{\partial \alpha_a}{\partial t} = -iNU_0 \left\langle \left(\alpha_a + \alpha_b e^{-2ikz}\right)(1 + 2\epsilon_\mu D + \sigma_{21} + \sigma_{12}) \right\rangle + (i\delta_c - \kappa)\alpha_a + \kappa \alpha_a^{eq} \tag{4.2.2.11}$$

$$\frac{\partial \alpha_b}{\partial t} = -iNU_0 \left\langle \left(\alpha_a e^{2ikz} + \alpha_b\right)(1 + 2\epsilon_\mu D + \sigma_{21} + \sigma_{12}) \right\rangle + (i\delta_c - \kappa)\alpha_b + \kappa \alpha_b^{eq} \tag{4.2.2.12}$$

4.2.2.2 Solving for the population inversion

By following the same procedure as for the two level and three level ladder configuration, an expression can be produced for the value of the population inversion, D, for a given pump field by solving equations (4.2.2.7) and (4.2.2.8). Assuming idealised conditions where $\gamma_{21} = 0$, $\alpha_a = 0$ and $\frac{\partial \alpha_b}{\partial t} = 0$, the equations become

$$\frac{\partial \sigma_{21}}{\partial t} = -iU_0|\alpha_b|^2 \left(D - \epsilon_\mu \sigma_{21}\right) \tag{4.2.2.13}$$

$$\frac{\partial D}{\partial t} = -iU_0|\alpha_b|^2(\sigma_{21} - \sigma_{12})\,. \tag{4.2.2.14}$$

Differentiating this equation for D gives

$$\begin{aligned}
\frac{\partial^2 D}{\partial t^2} &= -iU_0|\alpha_b|^2 \left(\frac{\partial \sigma_{21}}{\partial t} - \frac{\partial \sigma_{12}}{\partial t}\right) \\
&= -iU_0|\alpha_b|^2 \Big(\Big[-iU_0|\alpha_b|^2 \left(D - \epsilon_\mu \sigma_{21}\right) \Big] - \Big[iU_0|\alpha_b|^2 \left(D - \epsilon_\mu \sigma_{12}\right) \Big] \Big) \\
&= -iU_0^2|\alpha_b|^4 \Big(2D - \epsilon_\mu(\sigma_{21} + \sigma_{12}) \Big)\,.
\end{aligned} \tag{4.2.2.15}$$

Differentiating this again yields

$$\begin{aligned}
\frac{\partial^3 D}{\partial t^3} &= -iU_0^2|\alpha_b|^4 \left(2\frac{\partial D}{\partial t} - \epsilon_\mu \left(\frac{\partial \sigma_{21}}{\partial t} + \frac{\partial \sigma_{12}}{\partial t}\right)\right) \\
&= -iU_0^2|\alpha_b|^4 \left(2\frac{\partial D}{\partial t} - \epsilon_\mu \left(\Big[-iU_0|\alpha_b|^2 \left(D - \epsilon_\mu \sigma_{21}\right) \Big] + \Big[iU_0|\alpha_b|^2 \left(D - \epsilon_\mu \sigma_{12}\right) \Big]\right)\right) \\
&= -iU_0^2|\alpha_b|^4 \left(2\frac{\partial D}{\partial t} - iU_0|\alpha_b|^2(\sigma_{21} - \sigma_{12})\epsilon_\mu^2\right) \\
&= -iU_0^2|\alpha_b|^4 \left(2\frac{\partial D}{\partial t} + \epsilon_\mu^2 \frac{\partial D}{\partial t}\right) \\
&= -iU_0^2|\alpha_b|^4 \left(2 + \epsilon_\mu^2\right) \frac{\partial D}{\partial t}\,.
\end{aligned} \tag{4.2.2.16}$$

Assuming a solution for the above of the form $D \propto e^{\lambda t}$ it can be seen that either

$$\begin{aligned} &\lambda = 0 \\ &or \\ &\lambda = \pm i\sqrt{U_0^2|\alpha_b|^4\,(2+\epsilon_\mu)}\,, \end{aligned} \tag{4.2.2.17}$$

so,

$$D = Ae^0 + B\cos(\omega_r t) + c\sin(\omega_r t)\,, \tag{4.2.2.18}$$

where $\omega_r = \sqrt{U_0^2|\alpha_b|^4\,(2+\epsilon_\mu)}$. At $t = 0$,

$$D = D_0 \Rightarrow D_0 = A + B \Rightarrow A = D_0 - B\,. \tag{4.2.2.19}$$

Furthermore, $\sigma_{21}|_{t=0} = 0$, so $\frac{\partial D}{\partial t}\big|_{t=0} = 0$. Therefore

$$\begin{aligned} &\frac{\partial D}{\partial t} = -\omega_r B\sin(\omega_r t) + \omega_r C\cos(\omega_r t) \\ &\left.\frac{\partial D}{\partial t}\right|_{t=0} = \omega_r C = 0 \\ &\Rightarrow C = 0\ . \end{aligned} \tag{4.2.2.20}$$

Using $C = 0$ in the second derivative of D, it can be seen that

$$\begin{aligned} &\frac{\partial^2 D}{\partial t^2} = -\omega_r^2 B\cos(\omega_r t) \\ &\left.\frac{\partial^2 D}{\partial t^2}\right|_{t=0} = -\omega_r^2 B\,. \end{aligned} \tag{4.2.2.21}$$

Equating the above with equation (4.2.2.15) at $t = 0$ it can then be seen that

$$\begin{aligned} -\omega_r^2 B &= -2U_0^2|\alpha_b|^4 D_0 \\ B &= \frac{2U_0^2|\alpha_b|^4}{\omega_r^2} D_0 \,. \end{aligned} \tag{4.2.2.22}$$

The solution for D is therefore

$$D = D_0 - \frac{2U_0^2|\alpha_b|^4}{\omega_r^2} D_0 + \frac{2U_0^2|\alpha_b|^4}{\omega_r^2} D_0 \cos(\omega_r t) \,. \tag{4.2.2.23}$$

Averaging over t, the term $\cos(\omega_r t)$ vanishes, reducing the expression to

$$\begin{aligned} D &= \left(1 - \frac{2U_0^2|\alpha_b|^4}{\omega_r^2}\right) D_0 \\ &= \left(1 - \frac{2U_0^2|\alpha_b|^4}{U_0^2|\alpha_b|^4\,(2+\epsilon_\mu)}\right) D_0 \\ &= \left(1 - \frac{2}{(2+\epsilon_\mu)}\right) D_0 \\ &= \left(1 - \frac{1}{\left(1+\frac{\epsilon_\mu}{2}\right)}\right) D_0 \\ &= \left(1 - \left(1+\frac{\epsilon_\mu}{2}\right)^{-1}\right) D_0 \,. \end{aligned} \tag{4.2.2.24}$$

The term $\left(1+\frac{\epsilon_\mu}{2}\right)^{-1}$ may be expanded using $(1+x)^n \approx 1 + xn$. This means that the above expression may be written as

$$\begin{aligned} D &= \left(1 - \left(1 - \frac{\epsilon_\mu}{2}\right)\right) D_0 \\ &= \frac{\epsilon_\mu}{2} D_0 \,. \end{aligned} \tag{4.2.2.25}$$

From this equation it can be seen that, for the limit described above, the population inversion, D, is not dependent upon the intensity of the pump field.

4.2.2.3 Decoupling of internal and external degrees of freedom

In the somewhat idealised case wherein $\gamma_{21} = 0$ & $\epsilon_\mu = 0$, the equation for the evolution σ_{21} (4.2.2.7) simplifies to

$$\frac{\partial \sigma_{21}}{\partial t} = -iU_0 | \left(\alpha_a e^{ikz} + \alpha_b e^{-ikz}\right) |^2 D \,. \tag{4.2.2.26}$$

The terms U_0, $| \left(\alpha_a e^{ikz} + \alpha_b e^{-ikz}\right) |^2$ and D are all real at every point in time. As a consequence of this the coherence, σ_{21}, will be purely imaginary at all points in time ($Re(\sigma_{21}) = 0$). Equations (4.2.2.9), (4.2.2.11) and (4.2.2.12) contain terms $\sigma_{21} + \sigma_{12} = 2Re(\sigma_{21})$, which will be zero in this limit as a result of the coherence being always imaginary. These equations then take the form

$$\frac{\partial p_j}{\partial t} = i2\hbar k U_0 \left(\alpha_a^* \alpha_b e^{-2ikz} - \alpha_a \alpha_b^* e^{2ikz}\right) \tag{4.2.2.27}$$

$$\frac{\partial \alpha_a}{\partial t} = -iNU_0 \left\langle \left(\alpha_a + \alpha_b e^{-2ikz}\right) \right\rangle + (i\delta_c - \kappa)\alpha_a + \kappa \alpha_a^{eq} \tag{4.2.2.28}$$

$$\frac{\partial \alpha_b}{\partial t} = -iNU_0 \left\langle \left(\alpha_a e^{2ikz} + \alpha_b\right) \right\rangle + (i\delta_c - \kappa)\alpha_b + \kappa \alpha_b^{eq} \tag{4.2.2.29}$$

Looking at the equation for the atomic momentum, equation (4.2.2.27), it can be seen that for this configuration the evolution of both the position and momentum of each atom has been decoupled from the internal degrees of freedom, i.e. the coherence and population difference variables D & σ_{21}. As a consequence of this, when the atoms become excited to the point that the population inversion (and as a consequence the coherence) approaches zero, the bunching force experienced by the atoms does not similarly tend towards zero, in contrast to the case of two-level atoms described in Chapter 2.

Furthermore, in section 4.2.2.2 it was predicted that the population inversion, and consequently the coherence, would experience oscillations as the system evolved. The decoupling of the momentum from D & σ_{21} prevents oscillations from influencing the evolution of the atomic momentum.

Figures 4.3 - 4.8 display the CARL instability in the Λ configuration for initial values of the population inversion of $D_0 = 1/2$ and $D_0 = -1/2$, which correspond to initial population entirely in level $|1\rangle$ and $|2\rangle$ respectively. Figures 4.4 and 4.7 display the evolution of the atomic momentum, once again demonstrating the atomic bunching which is at the heart of the CARL instability. The oscillations predicted in section 4.2.2.2 can be observed in Figures 4.5(c) and 4.8(c)

However, the result of most interest for this configuration is shown in Figures 4.9, 4.10 and 4.11. It can be seen clearly in Figures 4.9 and 4.10 that for an initial value for the population inversion of D_0, the population does not evolve away from the initial value. More importantly, and in contrast to two level CARL, it can be seen from Fig. 4.9 that even with a constant value of zero for the population inversion the system still experiences the CARL instability.

4.2.2.4 Linear analysis

In the limit discussed in the last section where the terms $\gamma_{21} = \epsilon_\mu = \kappa = 0$, the equations for the atomic position, atomic momentum and probe field are given by equations (4.2.2.27) (4.2.2.10) and (4.2.2.28) respectively. The stability of the system can be understood better through the consideration of the growth of small perturbation terms. Substituting the perturbation terms

$$z = z_0 + \delta z(t) \tag{4.2.2.30}$$

$$p = \delta p(t) \tag{4.2.2.31}$$

$$\alpha_a = \delta\alpha_a(t) \tag{4.2.2.32}$$

into the aforementioned equations gives:

For the equation for atomic position

$$\frac{\partial\left(z_0+\delta z\right)}{\partial t}=\frac{\delta p}{m}, \tag{4.2.2.33}$$

which simplifies to

$$\frac{\partial \delta z}{\partial t}=\frac{\delta p}{m} \tag{4.2.2.34}$$

as z_0 is constant.

For the equation for atomic momentum

$$\frac{\partial \delta p}{\partial t}=i2\hbar kU_0\left(\delta\alpha_a^*\alpha_b e^{-2ik(z_0+\delta z)}-\delta\alpha_a\alpha_b^* e^{2ik(z_0+\delta z)}\right) \tag{4.2.2.35}$$

$$=i2\hbar kU_0\left(\delta\alpha_a^*\alpha_b e^{-2ikz_0}e^{-2ik\delta z}-\delta\alpha_a\alpha_b^* e^{2ikz_0}e^{2ik\delta z}\right). \tag{4.2.2.36}$$

As the perturbation term δz is small, $1>>\delta z$, when the terms $e^{\pm 2ik\delta z}$ are expanded out using the Maclaurin series, only the first term need be retained, so that $e^{\pm 2ik\delta z}\approx 1\pm 2ik\delta z$. The above equation therefore becomes

$$\frac{\partial \delta p}{\partial t}=i2\hbar kU_0\left(\delta\alpha_a^*\alpha_b e^{-2ikz_0}\left(1-2ik\delta z\right)-\delta\alpha_a\alpha_b^* e^{2ikz_0}\left(1+2ik\delta z\right)\right). \tag{4.2.2.37}$$

Retaining only terms linear in the perturbation variables, the linear equation for the evolution of the momentum perturbation term becomes

$$\frac{\partial \delta p}{\partial t}=i2\hbar kU_0\left(\delta\alpha_a^*\alpha_b e^{-2ikz_0}-\delta\alpha_a\alpha_b^* e^{2ikz_0}\right). \tag{4.2.2.38}$$

For the equation for the probe field

$$\frac{\partial \delta\alpha_a}{\partial t} = -iNU_0\Big\langle \delta\alpha_a + \alpha_b e^{-2ik(z_0+\delta z)}\Big\rangle + i\delta_c\delta\alpha_a \tag{4.2.2.39}$$

$$= -iNU_0\Big(\delta\alpha_a + \alpha_b\left\langle e^{-2ikz_0}e^{-2ik\delta z}\right\rangle\Big) + i\delta_c\delta\alpha_a\,. \tag{4.2.2.40}$$

Making the same expansion of the term $e^{-2ik\delta z}$ as before gives

$$\frac{\partial \delta\alpha_a}{\partial t} = -iNU_0\Big(\delta\alpha_a + \alpha_b\left\langle e^{-2ikz_0}\right\rangle - i2k\alpha_b\left\langle \delta z e^{-2ikz_0}\right\rangle\Big) + i\delta_c\delta\alpha_a\,. \tag{4.2.2.41}$$

As the atoms are initially uniformly spaced, the term $\alpha_b\langle e^{-2ikz_0}\rangle$ averages to zero, leaving

$$\frac{\partial \delta\alpha_a}{\partial t} = -iNU_0\Big(\delta\alpha_a - i2k\alpha_b\left\langle \delta z e^{-2ikz_0}\right\rangle\Big) + i\delta_c\delta\alpha_a\,. \tag{4.2.2.42}$$

The equations for the three perturbation terms are then (4.2.2.34), (4.2.2.38) and (4.2.2.42). The evolution of the probe field perturbation term can be more readily understood through defining two additional terms describing bunching and momentum fluctuations respectively i.e.

$$b = -i\langle \delta z e^{-2ikz_0}\rangle \tag{4.2.2.43}$$

and

$$P = \left\langle \frac{\delta p}{m} e^{-2ikz_0}\right\rangle\,. \tag{4.2.2.44}$$

Substituting for b in (4.2.2.42) leaves

$$\frac{\partial \delta\alpha_a}{\partial t} = -iNU_0\Big(\delta\alpha_a + 2k\alpha_b b\Big) + i\delta_c\delta\alpha_a \ . \tag{4.2.2.45}$$

Differentiating the equation for b produces

$$\frac{\partial b}{\partial t} = -i\left\langle \frac{\partial \delta z}{\partial t} e^{-2ikz_0} \right\rangle \tag{4.2.2.46}$$

into which may then be substituted the equation for the spatial perturbation term, equation (4.2.2.34), to give

$$\frac{\partial b}{\partial t} = -i\left\langle \frac{\delta p}{m} e^{-2ikz_0} \right\rangle \ . \tag{4.2.2.47}$$

Substituting for P using equation (4.2.2.44) simplifies the equation to

$$\frac{\partial b}{\partial t} = -iP \ . \tag{4.2.2.48}$$

The evolution of P is then described by

$$\frac{\partial P}{\partial t} = \frac{1}{m}\left\langle \frac{\partial \delta p}{\partial t} e^{-2ikz_0} \right\rangle \ . \tag{4.2.2.49}$$

The term $\frac{\partial \delta p}{\partial t}$ is then substituted for using equation (4.2.2.38) to give

$$\begin{aligned} \frac{\partial P}{\partial t} &= \frac{1}{m}\Big\langle \Big(i2\hbar k U_0 \Big(\delta\alpha_a^* \alpha_b e^{-2ikz_0} - \delta\alpha_a \alpha_b^* e^{2ikz_0} \Big) \Big) e^{-2ikz_0} \Big\rangle \\ &= \frac{i2\hbar k U_0}{m} \left(\delta\alpha_a^* \alpha_b \left\langle e^{-4ikz_0} \right\rangle - \delta\alpha_a \alpha_b^* \right) \ . \end{aligned} \tag{4.2.2.50}$$

The term e^{-4ikz_0} averages out to zero as the atoms are initially evenly spaced, so the equation simplifies to

$$\frac{\partial P}{\partial t} = -\frac{i2\hbar k U_0 \alpha_b^*}{m}\delta\alpha_a \,. \tag{4.2.2.51}$$

To investigate the growth of the probe field perturbation term, other perturbation terms must first be eliminated and an equation produced depending only upon $\delta\alpha_a$. To accomplish this, it is assumed that the cavity detuning term may be set such that $\delta_c = NU_0$ so that the term $-iNU_0\delta\alpha_a$ is cancelled out, as in [4]. The equation for the probe field perturbation term, equation (4.2.2.45), is then differentiated to produce

$$\frac{\partial^2 \delta\alpha_a}{\partial t^2} = -i2kNU_0\alpha_b\frac{\partial b}{\partial t} \,. \tag{4.2.2.52}$$

Substituting for $\frac{\partial b}{\partial t}$ using equation (4.2.2.48) in the above produces

$$\frac{\partial^2 \delta\alpha_a}{\partial t^2} = -2kNU_0\alpha_b P \,, \tag{4.2.2.53}$$

which, after further differentiation and substitution using equation (4.2.2.51), produces

$$\frac{\partial^3 \delta\alpha_a}{\partial t^3} = \frac{i4N\hbar k^2 U_0^2 |\alpha_b|^2}{m}\delta\alpha_a \,. \tag{4.2.2.54}$$

Looking for solutions of the form $\delta\alpha_a \propto e^{\lambda t}$ it can be seen that

$$\lambda^3 = \frac{i4N\hbar k^2 U_0^2 |\alpha_b|^2}{m} \,, \tag{4.2.2.55}$$

or,

$$\lambda = \sqrt[3]{\frac{i4N\hbar k^2 U_0^2 |\alpha_b|^2}{m}}\,. \tag{4.2.2.56}$$

The system experiences gain when the real component of λ is both nonzero and positive. The cube root of i, $\sqrt[3]{i}$, has three possible solutions: $-i$, $e^{5\pi/6}$ and $e^{\pi/6}$. The first solution, $-i$, has no real component, it is purely imaginary and will thus not result in gain. The second solution, $e^{5\pi/6}$, does have a real component as $e^{5\pi/6} = \cos(5\pi/6) + i\sin(5\pi/6)$. However, as $\cos(5\pi/6) = -\sqrt{3}/2$ this yields a negative value for the real component and will also not produce gain. The third solution $e^{\pi/6}$ may be expanded out as $\cos(\pi/6) + i\sin(\pi/6)$, the real part of which takes the value $\cos(\pi/6) = \sqrt{3}/2$. As a real, nonzero, positive value, this term will result in gain for the system. The gain experienced by the system should then be given by the expression

$$Gain = \frac{\sqrt{3}}{2}\sqrt[3]{\frac{4N\hbar k^2 U_0^2 |\alpha_b|^2}{m}} \tag{4.2.2.57}$$

4.2.2.5 Degenerate Λ Configuration Results

Equation (4.2.2.57) predicts a very similar gain as to that for the two-photon CARL gain equation (3.2.1.4), from Chapter 3. The key difference in need of highlighting between the two-photon CARL gain equation and the degenerate Λ CARL equation, is how the evolution of the population inversion affects each system, which becomes important in the nonlinear regime of the interaction.

For the case of two level CARL, a significant increase in the population inversion leads to spontaneous emission and the subsequent heating of the sample which results due to the stochastic nature of spontaneous emission events. Heating of the atomic sample reduces the effectiveness of the dipole force at bunching the atoms and inhibits the gain mechanism as a result. Furthermore, for a strong pump, the population inversion will average out to zero, resulting in decay of the coherence and a drop in the bunching force itself, as shown in the force equation for a two-level atom (equation (2.5.2.8)).

As was stated previously, in the case of the two-photon CARL system, the growth of the population inversion poses less of a concern than in 2 level CARL because the dipole force contains contributions from the single-photon coherences σ_{32}^{ladder} and σ_{21}^{ladder} in addition to the two-photon coherence σ_{31}^{ladder}. Thus, even if the two-photon population inversion averages to zero, the dipole force which bunches the atoms may be diminished but will not tend to zero.

For the degenerate Λ three level configuration the population inversion does not define a difference in population between an excited state energy level and a ground state energy level, but rather the difference in population between two approximately degenerate ground state levels. The heating associated with spontaneous emission should therefore be greatly reduced. Furthermore, as discussed in section 4.2.2.3, the equation for internal and external degrees of freedom have become decoupled. With the equation for the atomic bunching no longer dependent upon the coherence of the system, and by extension the population inversion, even if D does tend towards zero, the force on the atoms (and consequently the atomic bunching) will remain unaffected.

The lack of dependence of the CARL gain instability upon the population

inversion is demonstrated by numerically solving equations (4.2.2.7) - (4.2.2.12) and plotting the results for initial values of the population inversion of $D_0 = {}^1\!/_2$, $D_0 = 0$ and $D_0 = -{}^1\!/_2$, which correspond to the atomic population being initially entirely in level $|1>$, initially entirely in level $|2>$, and initially equally distributed between levels $|1\rangle$ and $|2\rangle$, respectively.

Figure 4.3 plots (a) the pump intensity, $|\alpha|^2$, (b) the bunching term, $|b|$, and (c) the average population inversion, $\langle D\rangle$ for the case of $D_0 = {}^1\!/_2$. As expected, the bunching parameter and field intensity grow smoothly despite large Rabi oscillations in the population inversion.

Figure 4.4 shows snapshots of the momentum vs position of each atom at various times throughout the evolution of the instability. Comparing it with Figure 4.3 illustrates the bunching effect responsible for the CARL instability.

Figure 4.5 displays snapshots of the population inversion vs. position of each atom. It can be clearly seen that the Rabi oscillations shown in Figure 4.3 are the result of each atoms population oscillating almost in unison, i.e. no substantial population grating forms and the atoms experience identical evolution of the population until the system reaches the oscillatory region following the initial gain curve.

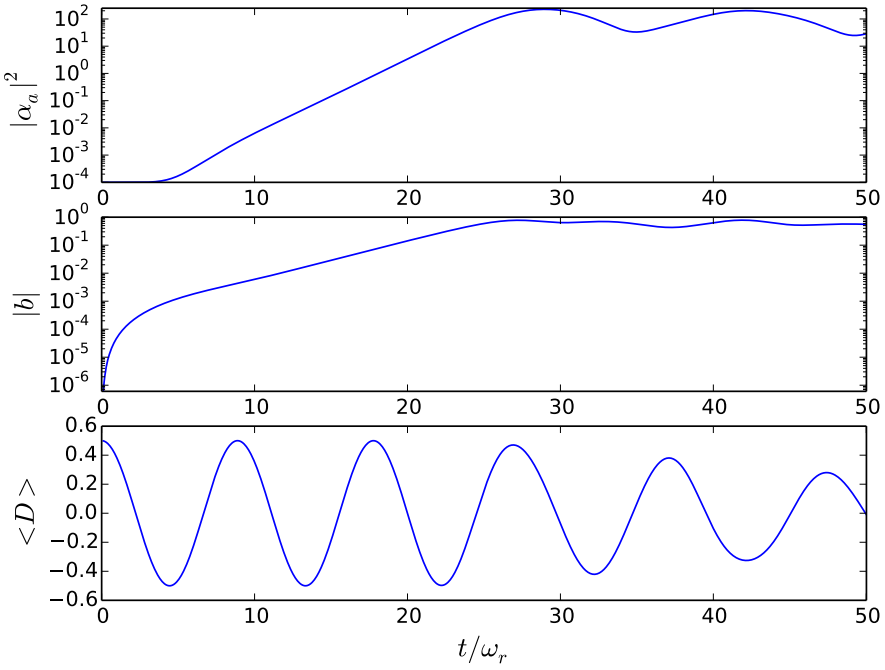

Figure 4.3: Evolution of probe photon number, $|\alpha_a|^2$, bunching parameter, $|b|$, and mean population difference, $\langle D \rangle$, for the case where the two transition detunings are equal, $\Delta_a = \Delta_b$, and the population of the system is initially in state $|1\rangle$, $D_0 = 1/2$. Produced by solving equations (4.2.2.1) - (4.2.2.6). Parameters used are $U_0/\omega_r = 5 \times 10^{-5}$, $\alpha_b = 100$, $N = 1000$, $\epsilon_\mu = 0$. It can be seen that, for the degenerate Λ configuration, the probe beam experiences gain and that the atoms bunch, both due to the CARL instability, despite the presence of large Rabi oscillations in the population which would be problematic in a two level system.

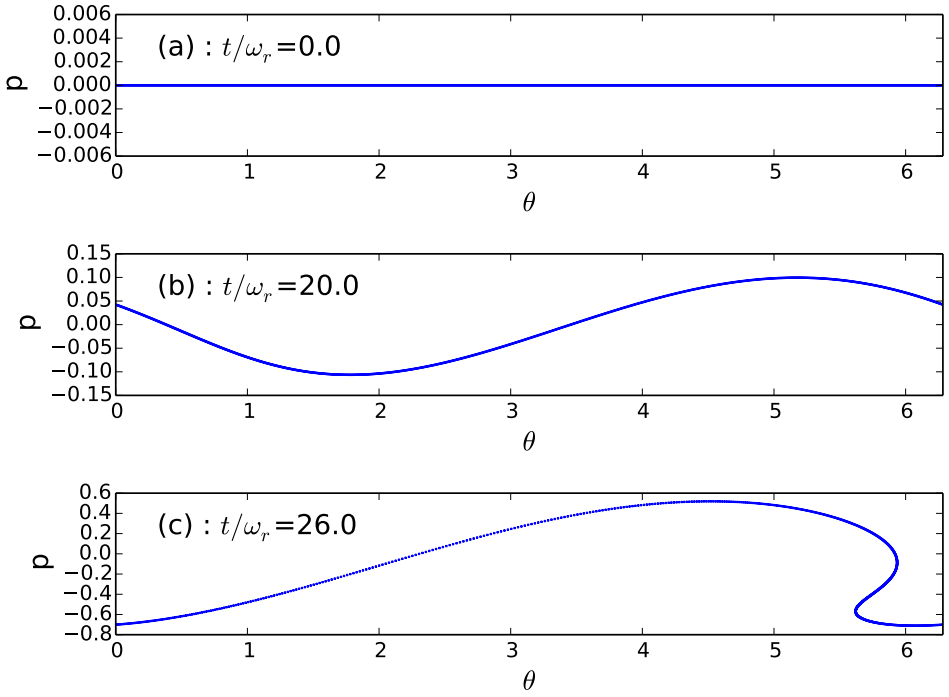

Figure 4.4: Snapshots of momentum distribution (θ_j, p_j) for each atom $j = 1..1000$ when (a) $t = 0\omega_r^{-1}$, (b) $t = 20\omega_r^{-1}$, (c) $t = 26\omega_r^{-1}$. Parameters used and equations solved are as in Figure 4.3. The atoms aquire momentum and are bunched by the dipole forces.

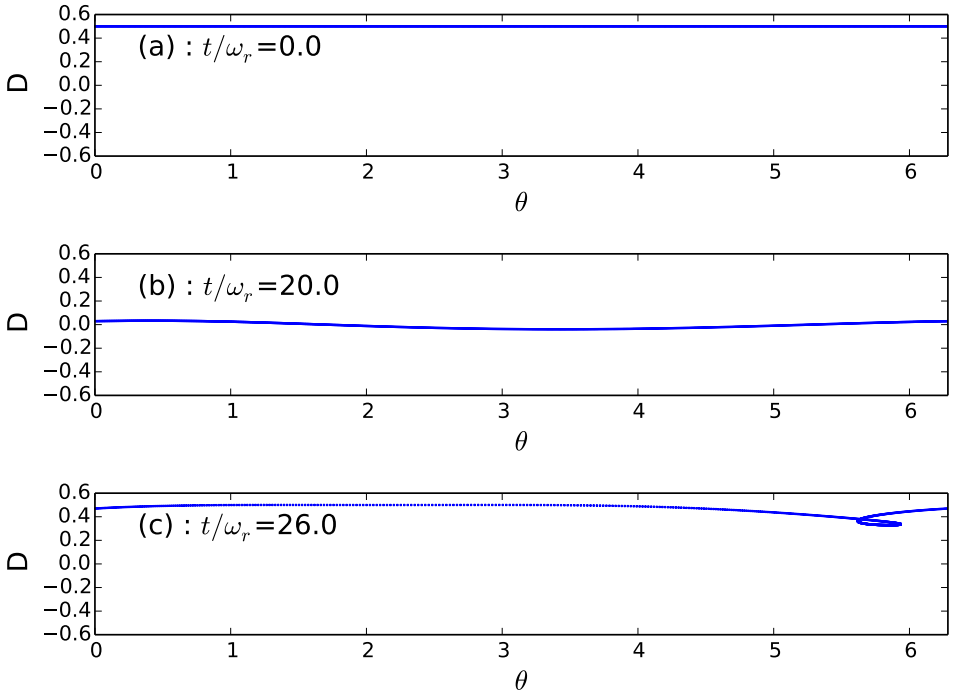

Figure 4.5: Snapshots of population difference distribution (θ_j, D_j) for each atom $j = 1..1000$ when (a) $t = 0\omega_r^{-1}$, (b) $t = 20\omega_r^{-1}$, (c) $t = 26\omega_r^{-1}$. Parameters used and equations solved are as in Figure 4.3. The population experiences almost uniform oscillations in the population.

Figures 4.3, 4.4 and 4.5 shows the evolution of the system when the population inversion has an initial value of one half ($D_0 = {}^1/_2$), i.e. initially the population is uniformly in the $|1\rangle$ ground state as defined by Figure 4.2.

The equation for the gain in the probe beam which may be expected from the system, equation (4.2.2.57), has no dependence upon the population inversion, D. The system should then show no change in probe gain even when the simulation is run for the same values but for the population entirely in ground state $|2\rangle$ (as defined by Figure 4.2).

Figure 4.6 shows the evolution of (a) the pump intensity, $|\alpha|^2$, (b) the bunching term, $|b|$, and (c) the average population inversion, $\langle D\rangle$ for the case of $D_0 = -{}^1/_2$. Comparing Figure 4.6, for which the population is initially entirely in state $|2\rangle$, with Figure 4.3, for which the population is initially entirely in state $|1\rangle$, it can be seen that the probe fields behave identically, as expected. Furthermore, as was the case for the system when $D_0 = {}^1/_2$, for $D_0 = -{}^1/_2$ the field intensity and bunching parameter once again grow smoothly despite the presence of large Rabi oscillations in the population inversion.

Figure 4.7 displays the snapshots of the momentum vs. position of each atom at various times throughout the evolution of the instability. By comparing Figure 4.7, for which $D_0 = -{}^1/_2$, with Figure 4.6, for which $D_0 = -{}^1/_2$, it can be seen that the atoms move in an identical manner when only the initial value of the population inversion is altered.

Figure 4.8 displays snapshots of the population inversion vs. position of each atom. Although the population begins exclusively in level $|2\rangle$, it undergoes similar oscillations to the case where the population begins exclusively in state $|1\rangle$, shown in Figure 4.5. Again it can be seen that the atomic populations oscillate almost in unison, so that no population grating forms.

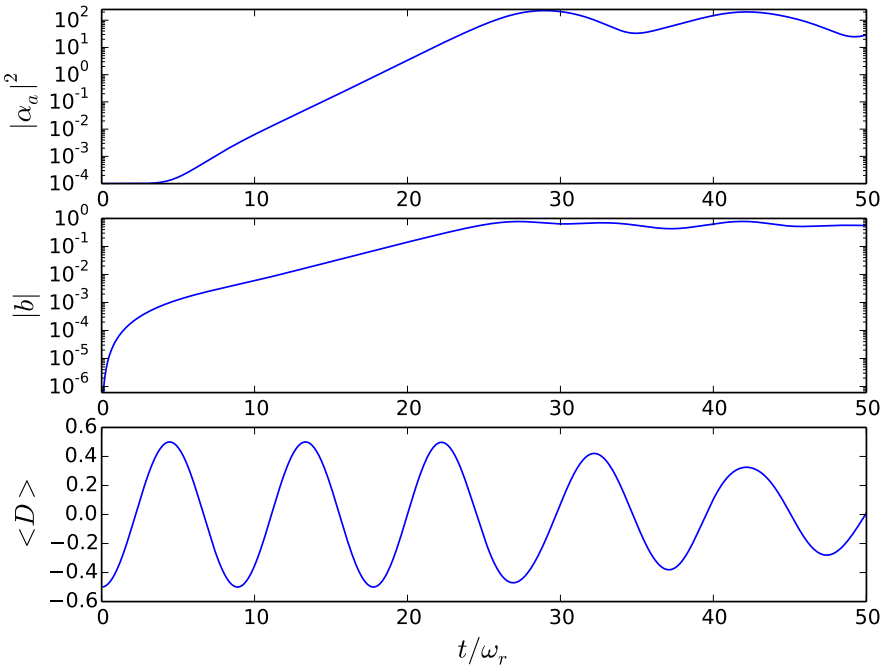

Figure 4.6: Evolution of probe photon number, $|\alpha_a|^2$, bunching parameter, $|b|$, and mean population difference, $\langle D \rangle$, for the case where the two transition detunings are equal, $\Delta_a = \Delta_b$, and the population of the system is initially in state $|2\rangle$, $D_0 = -1/2$. Produced by solving equations (4.2.2.1) - (4.2.2.6). Parameters used are $U_0/\omega_r = 5 \times 10^{-5}$, $\alpha_b = 100$, $N = 1000$, $\epsilon_\mu = 0$. When compared with Figure 4.3 it can be seen that changing the initial value of the population inversion from $D = {}^1/_2$ to $D = -{}^1/_2$ has no effect upon the evolution of the system or the gain in the probe beam.

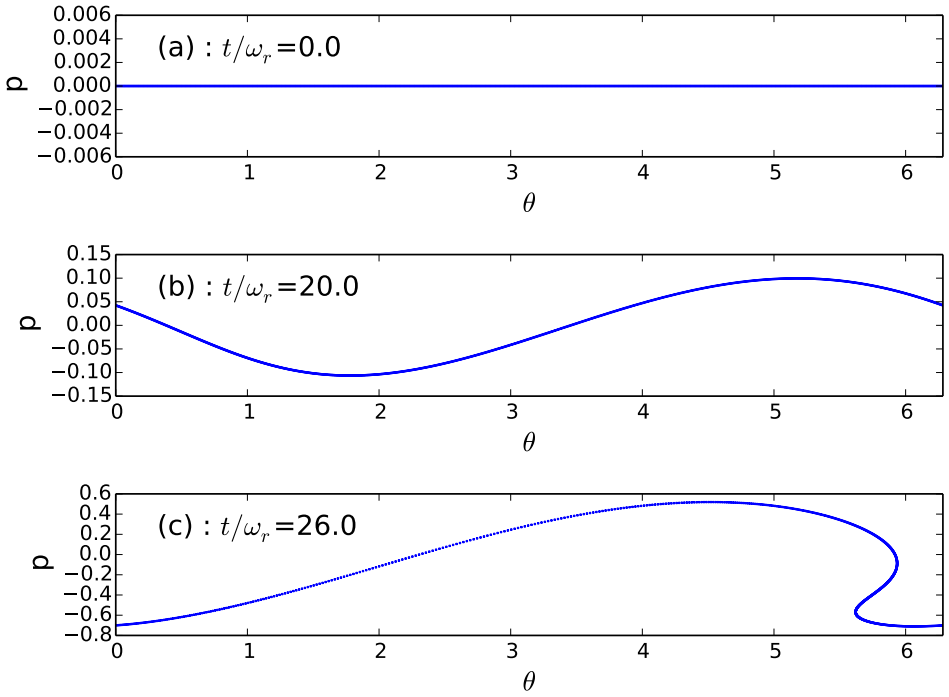

Figure 4.7: Snapshots of momentum distribution (θ_j, p_j) for each atom $j = 1..1000$ when (a) $t = 0\omega_r^{-1}$, (b) $t = 20\omega_r^{-1}$, (c) $t = 26\omega_r^{-1}$. Parameters used and equations solved are as in Figure 4.6. When compared with 4.4 it can be seen that changing the initial value of the population inversion from $D = {}^1/_2$ to $D = -{}^1/_2$ has no effect upon the evolution of each atom's momentum.

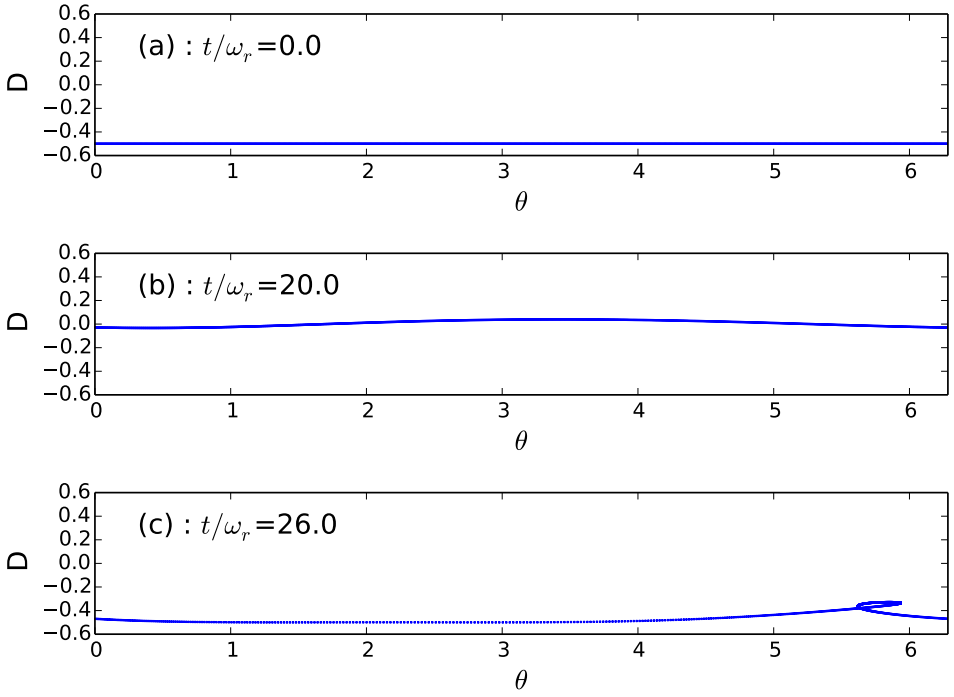

Figure 4.8: Snapshots of population difference distribution (θ_j, D_j) for each atom $j = 1..1000$ when (a) $t = 0\omega_r^{-1}$, (b) $t = 20\omega_r^{-1}$, (c) $t = 26\omega_r^{-1}$. Parameters used and equations solved are as in Figure 4.6. When compared with 4.5 it can be seen that changing the initial value of the population inversion from $D = {}^1/_2$ to $D = -{}^1/_2$ simply mirrors the behaviour of each atom's population inversion on the y axis.

Figure 4.9 plots (a) the pump intensity, $|\alpha|^2$, (b) the bunching term, $|b|$, and (c) the average population inversion, $\langle D \rangle$ for the case of $D_0 = 0$. Once again the bunching parameter and field intensity grow smoothly, however in this instance the population does not display Rabi oscillations. Instead the average population inversion remains constant at zero and never evolves.

This behaviour is easily understood when equations (4.2.2.13) and (4.2.2.14) are taken into consideration for ϵ_μ. For an initial value of D_0, equation (4.2.2.13) at t=0 is equal to zero itself. If the coherence is also initially zero, then (4.2.2.14) never evolves from zero itself, hence no Rabi-oscillations.

Figure 4.10 then displays snapshots of momentum vs position for each atom at various times throughout the evolution of the instability. Comparison between Figure 4.7 and Figure 4.6 shows the bunching effect responsible for the CARL instability once more.

Figure 4.11 displays snapshots of the population inversion vs. position for each atom. As was explained above, not one of the atoms experiences any change in population. The population remains equally spread across the two ground state levels $|1\rangle$ and $|2\rangle$.

Figures 4.9, 4.10 and 4.11 demonstrate most clearly the decoupling of the internal and external degrees of freedom for the degenerate Λ three level configuration, as the CARL gain instability proceeds with absolutely no evolution of the population.

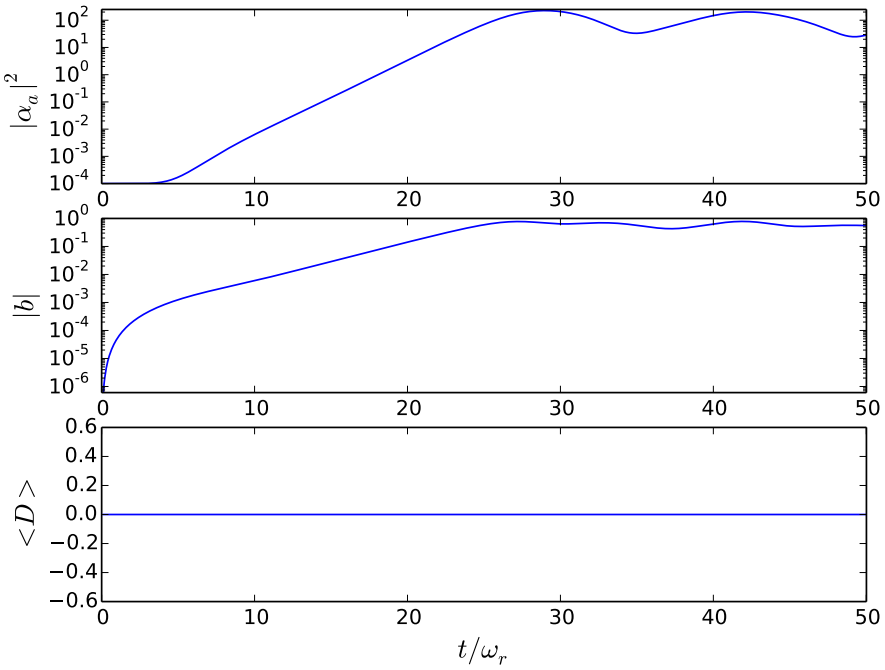

Figure 4.9: Evolution of probe photon number, $|\alpha_a|^2$, bunching parameter, $|b|$, and mean population difference, $\langle D \rangle$, for the case where the two transition detunings are equal, $\Delta_a = \Delta_b$, and the population of the system is initially equally distributed between states $|1\rangle$ and $|2\rangle$, $D_0 = 0$. Produced by solving equations (4.2.2.1) - (4.2.2.6). Parameters used are $U_0/\omega_r = 5 \times 10^{-5}$, $\alpha_b = 100$, $N = 1000$, $\epsilon_\mu = 0$. When compared with Figures 4.3 & 4.6 it can again be seen that changing the initial value of the population inversion from $D = {}^1/_2$ or $D = -{}^1/_2$ to $D = 0$ has no effect upon the evolution of the system or the gain in the probe beam.

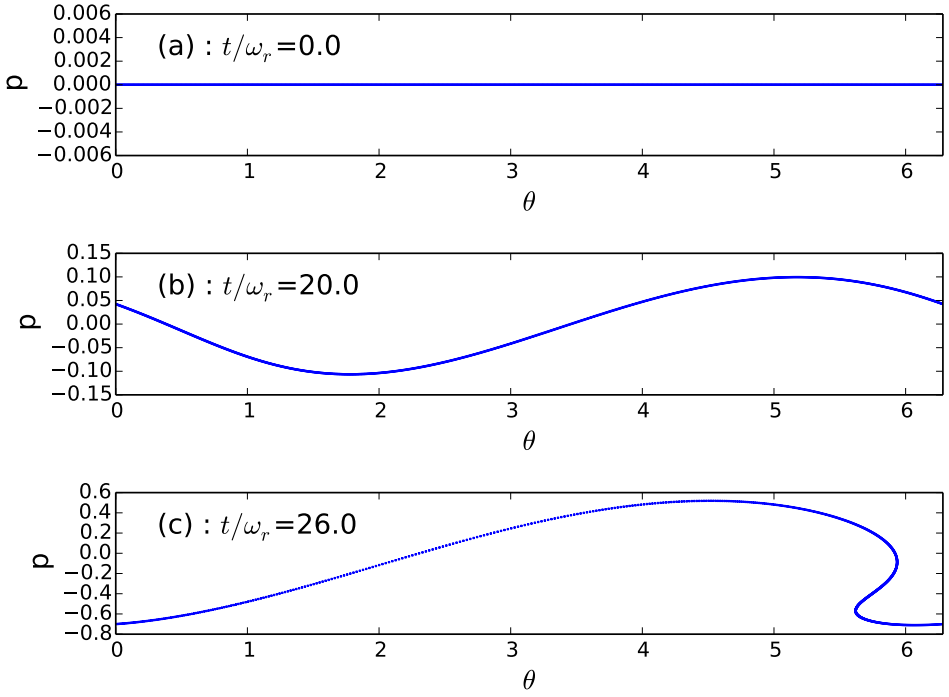

Figure 4.10: Snapshots of momentum distribution (θ_j, p_j) for each atom $j = 1..1000$ when (a) $t = 0\omega_r^{-1}$, (b) $t = 20\omega_r^{-1}$, (c) $t = 26\omega_r^{-1}$. Parameters used and equations solved are as in Figure 4.9. When compared with Figures 4.4 & 4.7 it can again be seen that changing the initial value of the population inversion from $D = {}^1/_2$ or $D = -{}^1/_2$ to $D = 0$ has no effect upon the evolution of each atom's momentum.

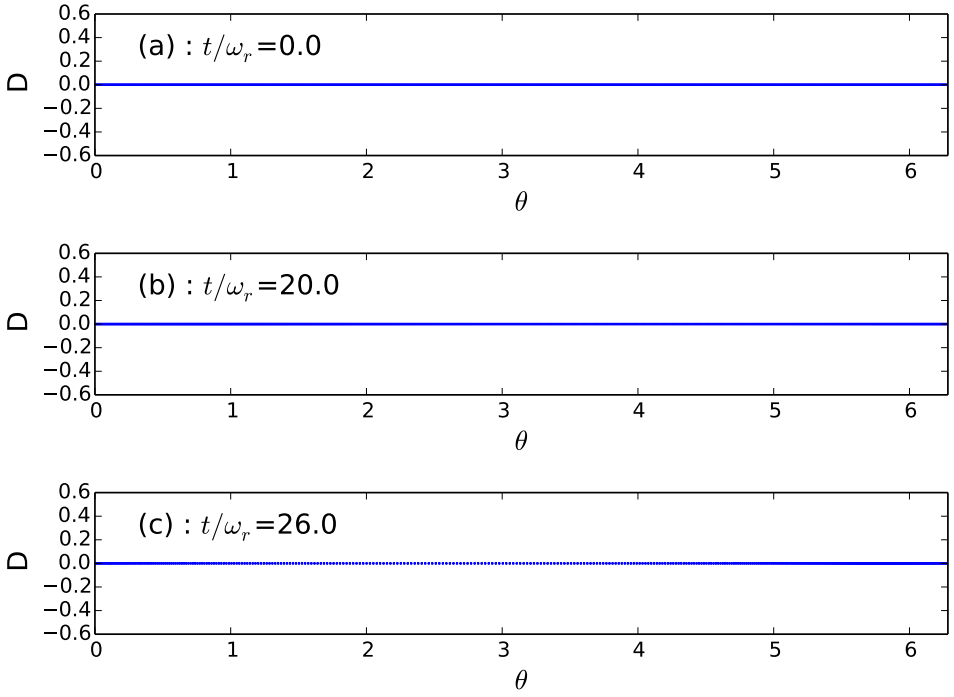

Figure 4.11: Snapshots of population difference distribution (θ_j, D_j) for each atom $j = 1..1000$ when (a) $t = 0\omega_r^{-1}$, (b) $t = 20\omega_r^{-1}$, (c) $t = 26\omega_r^{-1}$. Parameters used and equations solved are as in Figure 4.9. It can be seen that without an initial value for the population inversion, the oscillations observed in Figures 4.5 & 4.8 do not occur. If the population inversion has an initial value of zero then it does not evolve away from its initial value.

The preceding Figures, 4.3 - 4.11, demonstrate results for positive values of the detuning Δ_a. Equation (4.2.2.57), which describes the gain which may be expected in the probe beam, varies as $\sqrt[3]{U_0^2}$. As a result, the gain for the optical probe beam should be symmetric in the sign of the detuning term Δ_a, due to $U_0 \propto \frac{1}{\Delta_a}$.

It may be expected then that using the same values as in Figures 4.3, 4.6 and 4.9 save for a change in the sign of U_0 should produce identical results. This is seen to be the case when the aforementioned Figures 4.3, 4.6 and 4.9 are compared to Figures 4.12, 4.13 and 4.14 respectively.

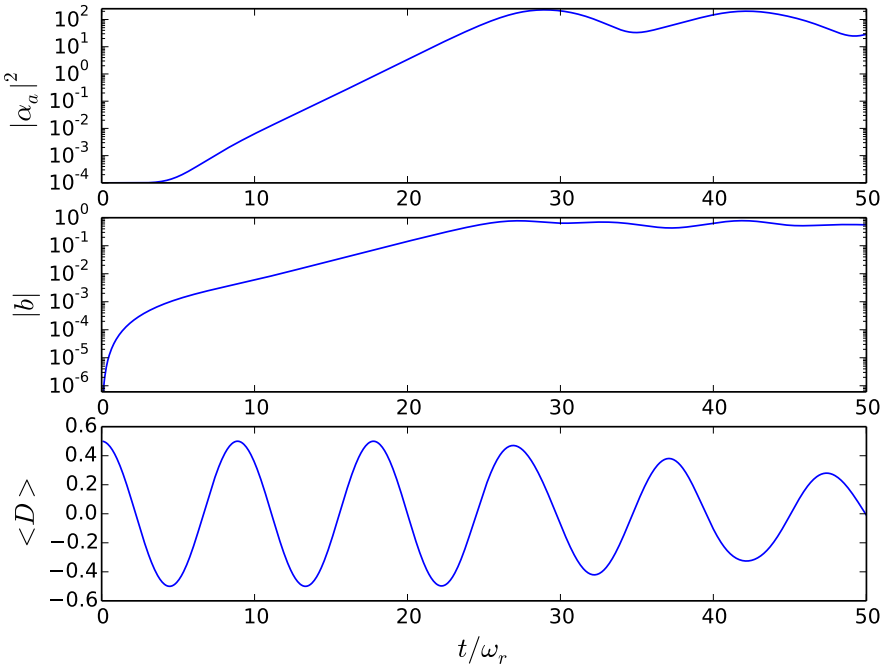

Figure 4.12: Evolution of probe photon number, $|\alpha_a|^2$, bunching parameter, $|b|$, and mean population difference, $\langle D \rangle$, for the case where the two transition detunings are equal, $\Delta_a = \Delta_b$, and the population of the system is initially in state $|1\rangle$, $D_0 = 1/2$. Produced by solving equations (4.2.2.1) - (4.2.2.6). Parameters used are $U_0/\omega_r = -5 \times 10^{-5}$, $\alpha_b = 100$, $N = 1000$, $\epsilon_\mu = 0$. When compared with Figure 4.3 it can be seen that the sign of U_0 has no effect upon the output of the system.

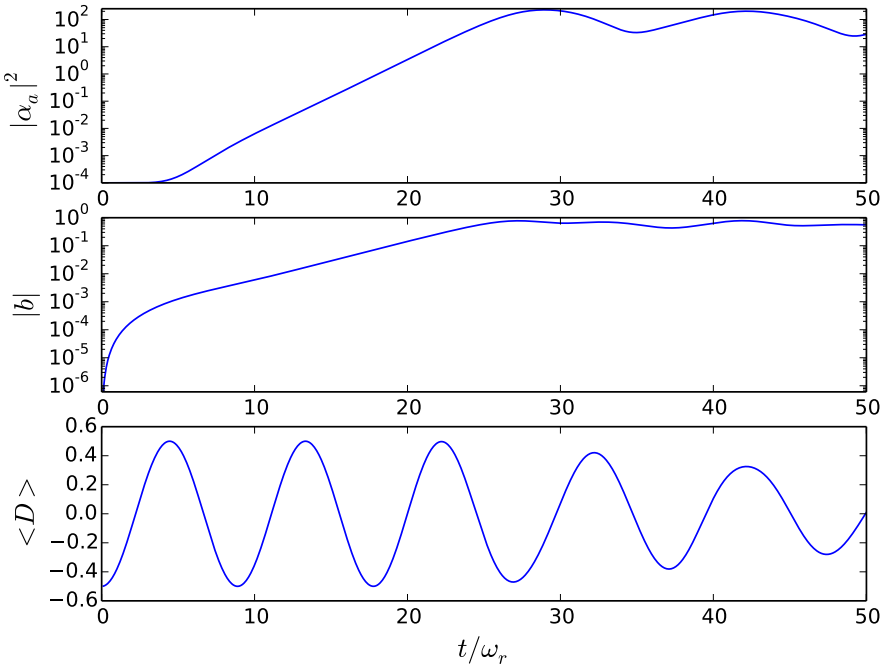

Figure 4.13: Evolution of probe photon number, $|\alpha_a|^2$, bunching parameter, $|b|$, and mean population difference, $\langle D \rangle$, for the case where the two transition detunings are equal, $\Delta_a = \Delta_b$, and the population of the system is initially in state $|1\rangle$, $D_0 = -1/2$. Produced by solving equations (4.2.2.1) - (4.2.2.6). Parameters used are $U_0/\omega_r = -5 \times 10^{-5}$, $\alpha_b = 100$, $N = 1000$, $\epsilon_\mu = 0$. When compared with Figure 4.6 it can be seen that the sign of U_0 has no effect upon the output of the system.

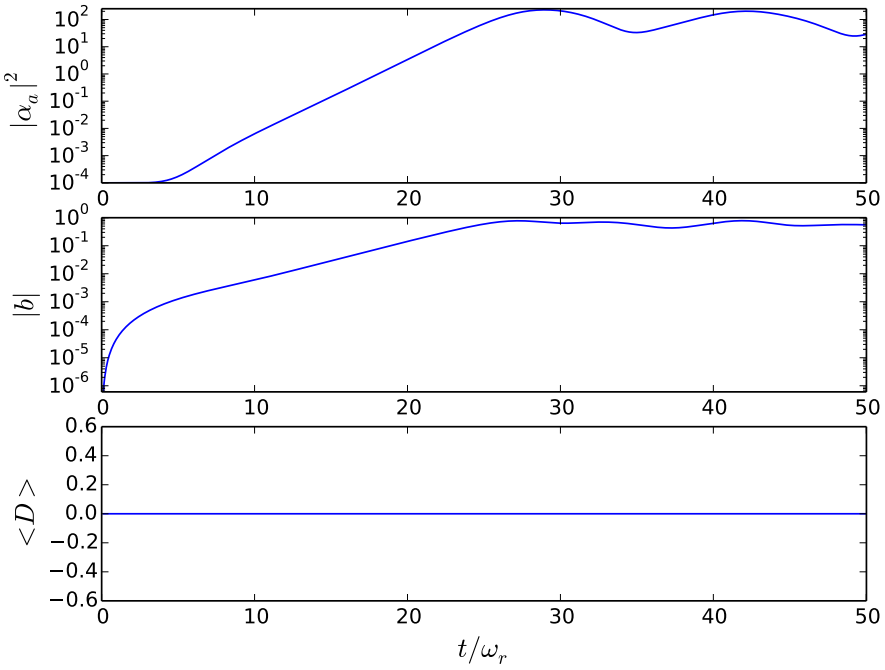

Figure 4.14: Evolution of probe photon number, $|\alpha_a|^2$, bunching parameter, $|b|$, and mean population difference, $\langle D \rangle$, for the case where the two transition detunings are equal, $\Delta_a = \Delta_b$, and the population of the system is initially in state $|1\rangle$, $D_0 = 0$. Produced by solving equations (4.2.2.1) - (4.2.2.6). Parameters used are $U_0/\omega_r = -5 \times 10^{-5}$, $\alpha_b = 100$, $N = 1000$, $\epsilon_\mu = 0$. When compared with Figure 4.9 it can be seen that the sign of U_0 has no effect upon the output of the system.

4.2.3 Non-degenerate Λ configuration

The second configuration considered is that in which the energy levels $|1\rangle$ and $|2\rangle$ are non-degenerate. Instead the levels are separated and the optical pump and probe field frequencies are tuned half way between the two levels, such that $\Delta_b = -\Delta_a$ and $\Delta_{ab} = 2\Delta_a$. Using these substitutions in equations (4.2.1.3) - (4.2.1.8) gives them the form

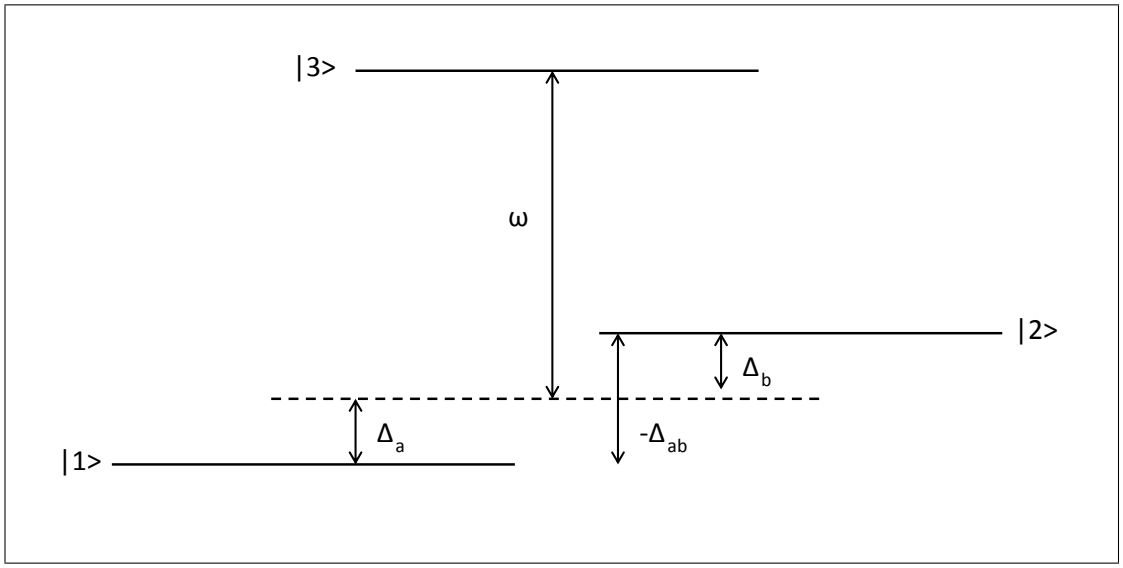

Figure 4.15: Simplified Three Level Λ Energy Level Diagram: The Λ energy level structure for the lower energy states are non-degenerate.

$$\frac{\partial \sigma_{21}}{\partial t} = -(\gamma_{21} - i2\Delta_a)\sigma_{21} - \frac{i\mu^2}{\hbar^2 \Delta_a} | \left(A_a e^{ikz} + A_b e^{-ikz} \right) |^2 (1 - 2\sigma_{21}) \qquad (4.2.3.1)$$

$$\frac{\partial D}{\partial t} = 0 \qquad (4.2.3.2)$$

$$\frac{\partial p_j}{\partial t} = \frac{i2\mu^2 k}{\hbar \Delta_a} \Big(\left(|A_a|^2 - |A_b|^2 \right) (\sigma_{21} - \sigma_{12}) + \left(A_a^* A_b e^{-2ikz} - A_a A_b^* e^{2ikz} \right) (\epsilon_\mu + 2D) \Big) \qquad (4.2.3.3)$$

$$\frac{\partial z_j}{\partial t} = \frac{p_j}{m} \qquad (4.2.3.4)$$

$$\frac{\partial A_a}{\partial t} = -\frac{i\omega\mu^2 n}{2\hbar\epsilon_0 \Delta_a} \Big\langle \left(A_a + A_b e^{-2ikz} \right) (\epsilon_\mu + 2D + \sigma_{21} - \sigma_{12}) \Big\rangle \quad + (i\delta_c - \kappa) A_a + \kappa A_a^{eq} \qquad (4.2.3.5)$$

$$\frac{\partial A_b}{\partial t} = -\frac{i\omega\mu^2 n}{2\hbar\epsilon_0 \Delta_a} \Big\langle \left(A_a e^{2ikz} + A_b \right) (\epsilon_\mu + 2D + \sigma_{21} - \sigma_{12}) \Big\rangle \quad + (i\delta_c - \kappa) A_b + \kappa A_b^{eq} \qquad (4.2.3.6)$$

4.2.3.1 Scaling the three level Λ equations

With the term Δ_b substituted for $-\Delta_a$, equations 4.2.3.1 can be scaled in a similar manner to Section 4.2.2.1, by substituting the terms (3.1.8.1) - (3.1.8.3) to produce

$$\frac{\partial \sigma_{21}}{\partial t} = -(\gamma_{21} - i2\Delta_a)\sigma_{21} - iU_0|\left(\alpha_a e^{ikz} + \alpha_b e^{-ikz}\right)|^2 (1 - 2\sigma_{21}) \tag{4.2.3.7}$$

$$\frac{\partial D}{\partial t} = 0 \tag{4.2.3.8}$$

$$\frac{\partial p_j}{\partial t} = i2\hbar k U_0 \Big(\left(|\alpha_a|^2 - |\alpha_b|^2\right)(\sigma_{21} - \sigma_{12}) + \left(\alpha_a^* \alpha_b e^{-2ikz} - \alpha_a \alpha_b^* e^{2ikz}\right)(\epsilon_\mu + 2D) \Big) \tag{4.2.3.9}$$

$$\frac{\partial z_j}{\partial t} = \frac{p_j}{m} \tag{4.2.3.10}$$

$$\frac{\partial \alpha_a}{\partial t} = -iNU_0 \Big\langle \left(\alpha_a + \alpha_b e^{-2ikz}\right)(\epsilon_\mu + 2D + \sigma_{21} - \sigma_{12}) \Big\rangle + (i\delta_c - \kappa)\alpha_a + \kappa \alpha_a^{eq} \tag{4.2.3.11}$$

$$\frac{\partial \alpha_b}{\partial t} = -iNU_0 \Big\langle \left(\alpha_a e^{2ikz} + \alpha_b\right)(\epsilon_\mu + 2D + \sigma_{21} - \sigma_{12}) \Big\rangle + (i\delta_c - \kappa)\alpha_b + \kappa \alpha_b^{eq} \tag{4.2.3.12}$$

4.2.3.2 Decoupling the coherence from the momentum and field equations

In Section 4.2.2.3 it was shown that the internal and external degrees of freedom may become decoupled for certain parameter choices. Making the assumption that the detuning is sufficiently larger than the decay rate, $2\Delta_a >> \gamma_{21}$, so that the decay may be neglected in equation (4.2.3.7), which gives it the form

$$\frac{\partial \sigma_{21}}{\partial t} = i2\Delta_a\sigma_{21} - iU_0|\left(\alpha_a e^{ikz} + \alpha_b e^{-ikz}\right)|^2\left(1 - 2\sigma_{21}\right) . \tag{4.2.3.13}$$

By adiabatically eliminating σ_{21} from the above equation it can be seen that the coherence takes the value

$$\sigma_{21} = \frac{1}{2\left(1 + \frac{\Delta_a}{U_0|\left(\alpha_a e^{ikz} + \alpha_b e^{-ikz}\right)|^2}\right)} , \tag{4.2.3.14}$$

which will always be real. As a result, it may be expected that in the limit $2\Delta_a >> \gamma_{21}$ any terms $\sigma_{21} - \sigma_{12} = i2Im(\sigma_{21}) \approx 0$. The equations for the atomic momentum and the two fields in this limit are

$$\frac{\partial p_j}{\partial t} = i2\hbar k U_0\left(\alpha_a^* \alpha_b e^{-2ikz} - \alpha_a \alpha_b^* e^{2ikz}\right)\left(\epsilon_\mu + 2D\right) \tag{4.2.3.15}$$

$$\frac{\partial \alpha_a}{\partial t} = -iNU_0\Big\langle \left(\alpha_a + \alpha_b e^{-2ikz}\right)\left(\epsilon_\mu + 2D\right) \Big\rangle + (i\delta_c - \kappa)\alpha_a + \kappa\alpha_a^{eq} \tag{4.2.3.16}$$

$$\frac{\partial \alpha_b}{\partial t} = -iNU_0\Big\langle \left(\alpha_a e^{2ikz} + \alpha_b\right)\left(\epsilon_\mu + 2D\right) \Big\rangle + (i\delta_c - \kappa)\alpha_b + \kappa\alpha_b^{eq} . \tag{4.2.3.17}$$

In a similar turn of events to the degenerate Λ configuration, the equations for

atomic motion have been decoupled from the coherence. In contrast to the previous configuration however, for the non-degenerate configuration the atomic movement still has a dependence upon the population inversion D. As can be seen from equation (4.2.3.8), the population will never evolve away from its initial value D_0, so in this schema the population inversion acts more as a parameter than a variable.

4.2.3.3 Linear stability analysis

To determine the gain to be expected for this configuration it is useful to undertake a linear analysis of the system. Assuming that $\kappa = \epsilon_\mu = 0$, the equations for the atomic momentum, atomic position and probe field amplitude take the form

$$\frac{\partial p_j}{\partial t} = i4\hbar k U_0 D_0 \left(\alpha_a^* \alpha_b e^{-2ikz} - \alpha_a \alpha_b^* e^{2ikz}\right) \tag{4.2.3.18}$$

$$\frac{\partial z_j}{\partial t} = \frac{p_j}{m} \tag{4.2.3.19}$$

$$\frac{\partial \alpha_a}{\partial t} = -i2NU_0 \Big\langle \left(\alpha_a + \alpha_b e^{-2ikz}\right) D_0 \Big\rangle + i\delta_c \alpha_a \tag{4.2.3.20}$$

To study the stability of the system, the perturbation terms

$$z = z_0 + \delta z(t) \tag{4.2.3.21}$$

$$p = \delta p(t) \tag{4.2.3.22}$$

$$\alpha_a = \delta \alpha_a(t) \tag{4.2.3.23}$$

are introduced.

Substituting the perturbation terms into equations (4.2.3.18) - (4.2.3.18) gives:

First

$$\frac{\partial\left(z_0+\delta z\right)}{\partial t}=\frac{\delta p}{m}\,, \tag{4.2.3.24}$$

which as z_0 is constant simplifies to

$$\frac{\partial \delta z}{\partial t}=\frac{\delta p}{m}\,. \tag{4.2.3.25}$$

Second,

$$\frac{\partial \delta p}{\partial t}=i4\hbar k U_0 D_0\left(\delta\alpha_a^*\alpha_b e^{-2ik(z_0+\delta z)}-\delta\alpha_a\alpha_b^* e^{2ik(z_0+\delta z)}\right) \tag{4.2.3.26}$$

$$=i4\hbar k U_0 D_0\left(\delta\alpha_a^*\alpha_b e^{-2ikz_0}e^{-2ik\delta z}-\delta\alpha_a\alpha_b^* e^{2ikz_0}e^{2ik\delta z}\right)\,. \tag{4.2.3.27}$$

As the perturbation term δz is small, $1>>\delta z$, then $e^{\pm 2ik\delta z}\approx 1\pm 2ik\delta z$. The above equation therefore becomes

$$\frac{\partial \delta p}{\partial t}=i4\hbar k U_0 D_0\left(\delta\alpha_a^*\alpha_b e^{-2ikz_0}\left(1-2ik\delta z\right)-\delta\alpha_a\alpha_b^* e^{2ikz_0}\left(1+2ik\delta z\right)\right)\,. \tag{4.2.3.28}$$

Retaining only terms which are linear in the perturbation variables, the equation for the evolution of the momentum perturbation term becomes

$$\frac{\partial \delta p}{\partial t}=i4\hbar k U_0 D_0\left(\delta\alpha_a^*\alpha_b e^{-2ikz_0}-\delta\alpha_a\alpha_b^* e^{2ikz_0}\right)\,. \tag{4.2.3.29}$$

Third, the equation for the field perturbation term becomes

$$\frac{\partial \delta\alpha_a}{\partial t} = -i2NU_0\Big\langle \left(\delta\alpha_a + \alpha_b e^{-2ik(z_0+\delta z)}\right) D_0 \Big\rangle + i\delta_c\delta\alpha_a \tag{4.2.3.30}$$

$$= -i2NU_0\Big\langle \left(\delta\alpha_a + \alpha_b e^{-2ikz_0}e^{-2ik\delta z}\right) D_0 \Big\rangle + i\delta_c\delta\alpha_a\,. \tag{4.2.3.31}$$

Making the same expansion of the term $e^{-2ik\delta z}$ as before gives

$$\frac{\partial \delta\alpha_a}{\partial t} = -i2NU_0\Big\langle \left(\delta\alpha_a + \alpha_b e^{-2ikz_0} - i2k\delta z\alpha_b e^{-2ikz_0}\right) D_0 \Big\rangle + i\delta_c\delta\alpha_a\,. \tag{4.2.3.32}$$

As the atoms are initially uniformly spaced, the term $\langle\alpha_b e^{-2ikz_0}\rangle$ averages to zero, leaving

$$\frac{\partial \delta\alpha_a}{\partial t} = -i2NU_0\Big\langle \left(\delta\alpha_a - i2k\delta z\alpha_b e^{-2ikz_0}\right) D_0 \Big\rangle + i\delta_c\delta\alpha_a\,. \tag{4.2.3.33}$$

Defining $b = -i\langle\delta z e^{-2ikz_0}\rangle$ so that

$$\frac{\partial b}{\partial t} = -i\left\langle \frac{\partial \delta z}{\partial t} e^{-2ikz_0} \right\rangle \tag{4.2.3.34}$$

into which may then be substituted the equation for the spacial perturbation term, equation (4.2.3.25), to give

$$\frac{\partial b}{\partial t} = -i\left\langle \frac{\delta p}{m} e^{-2ikz_0} \right\rangle\,. \tag{4.2.3.35}$$

The probe field perturbation equation may then be written as

$$\frac{\partial \delta\alpha_a}{\partial t} = -i2NU_0 D_0\big(\delta\alpha_a + 2k\alpha_b b\big) + i\delta_c\delta\alpha_a\,. \tag{4.2.3.36}$$

Going on then to define $P = \left\langle \frac{\delta p}{m} e^{-2ikz_0} \right\rangle$ means that the equation for the

evolution of the bunching parameter b simplifies to

$$\frac{\partial b}{\partial t} = -iP\,. \tag{4.2.3.37}$$

The equation for P is then given by

$$\frac{\partial P}{\partial t} = \frac{1}{m}\left\langle \frac{\partial \delta p}{\partial t} e^{-2ikz_0} \right\rangle\,, \tag{4.2.3.38}$$

into which is then substituted equation (4.2.3.29) to give

$$\frac{\partial P}{\partial t} = \frac{1}{m}\left\langle \left(i4\hbar k U_0 D_0 \left(\delta\alpha_a^* \alpha_b e^{-2ikz_0} - \delta\alpha_a \alpha_b^* e^{2ikz_0}\right)\right) e^{-2ikz_0} \right\rangle \tag{4.2.3.39}$$

$$= \frac{1}{m}\left\langle \left(i4\hbar k U_0 D_0 \left(\delta\alpha_a^* \alpha_b e^{-4ikz_0} - \delta\alpha_a \alpha_b^*\right)\right)\right\rangle\,. \tag{4.2.3.40}$$

The term e^{-4ikz_0} averages out to zero as the atoms were initially evenly spaced, so the equation simplifies to

$$\frac{\partial P}{\partial t} = -\frac{i4\hbar k U_0 D_0 \alpha_b^*}{m}\delta\alpha_a\,. \tag{4.2.3.41}$$

To investigate the growth of the probe field perturbation term, other perturbation terms must first be eliminated and an equation produced depending only upon $\delta\alpha_a$. To accomplish this, it is assumed that the cavity detuning term may be set such that $\delta_c = 2NU_0D_0$ so that the term $-2iNU_0D_0\delta\alpha_a$ is cancelled out, as in [4]. The equation for the probe field perturbation term, equation (4.2.3.36), is then differentiated and equation (4.2.3.37) is substituted into it to produce

$$\frac{\partial^2 \delta\alpha_a}{\partial t^2} = -4kNU_0D_0\alpha_b P\,. \tag{4.2.3.42}$$

Differentiating a second time and substituting equation (4.2.3.41) for $\frac{\partial P}{\partial t}$ produces

$$\frac{\partial^3 \delta\alpha_a}{\partial t^3} = \frac{i16N\hbar k^2 U_0^2 D_0^2 |\alpha_b|^2}{m}\delta\alpha_a \,. \tag{4.2.3.43}$$

The end result is an equation solely dependent upon $\delta\alpha_a$. Looking for solutions to this equation of the form $\delta\alpha_a \propto e^{\lambda t}$ it can be seen that

$$\lambda^3 = \frac{i16N\hbar k^2 U_0^2 |\alpha_b|^2 D_0^2}{m}\,, \tag{4.2.3.44}$$

or simply

$$\lambda = \sqrt[3]{\frac{i16N\hbar k^2 U_0^2 |\alpha_b|^2 D_0^2}{m}}\,. \tag{4.2.3.45}$$

As was stated in Section 4.2.2.4 , the system experiences gain when the real component of λ is both nonzero and positive. Once again $\sqrt[3]{i}$ has three possible solutions: $-i$, $e^{5\pi/6}$ and $e^{\pi/6}$, with only the third expression possessing a positive nonzero real component of $Re(e^{\pi/6}) = \sqrt{3}/2$. The gain for the system is then given by the expression

$$Gain = \frac{\sqrt{3}}{2}\sqrt[3]{\frac{16N\hbar k^2 U_0^2 |\alpha_b|^2 D_0^2}{m}} \tag{4.2.3.46}$$

4.2.3.4 Non-degenerate Λ Configuration Results

It may be noted that in the instance where $D_0 = \pm 1/2$ the above solution matches that of the gain for the degenerate Λ configuration given by equation (4.2.2.57). It would be expected, then, that for those values of D the gain curves for α_a in the degenerate and non-degenerate configurations would match exactly. This is shown to be the case when Figures 4.16(a) and 4.19(a) are compared to their counterparts from the degenerate Λ configuration, 4.3(a) and 4.6(a).

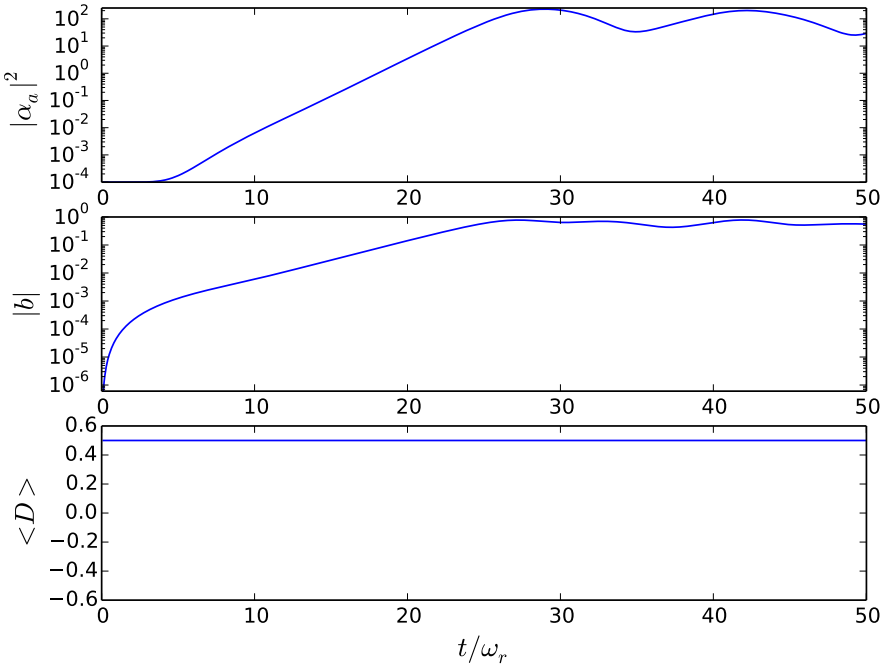

Figure 4.16: Evolution of probe photon number, $|\alpha_a|^2$, bunching parameter, $|b|$, and mean population difference, $\langle D \rangle$, for the case where the two transition detunings are equal in magnutide but opposite in sign, $\Delta_a = -\Delta_b$, and the population of the system is initially in state $|1\rangle$, $D_0 = 1/2$. Produced by solving equations (4.2.3.7) - (4.2.3.12). Parameters used are $U_0/\omega_r = 5 \times 10^{-5}$, $\Delta_{ab} = 10$, $\alpha_b = 100$, $N = 1000$, $\epsilon_\mu = 0$.

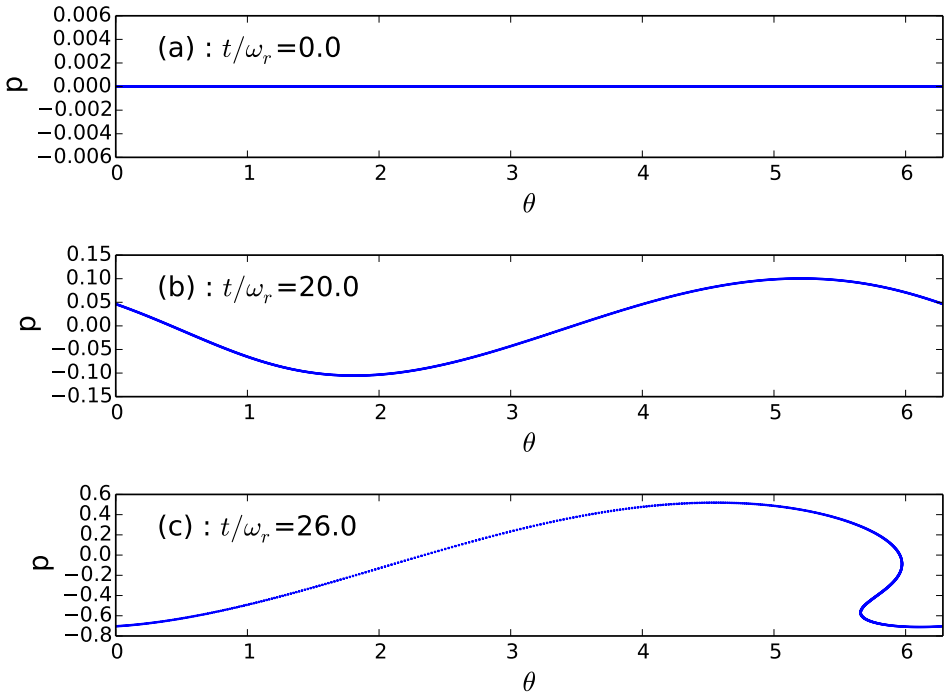

Figure 4.17: Snapshots of momentum distribution (θ_j, p_j) for each atom $j = 1..1000$ when (a) $t = 0\omega_r^{-1}$, (b) $t = 20\omega_r^{-1}$, (c) $t = 26\omega_r^{-1}$. Parameters used and equations solved are as in Figure 4.16.

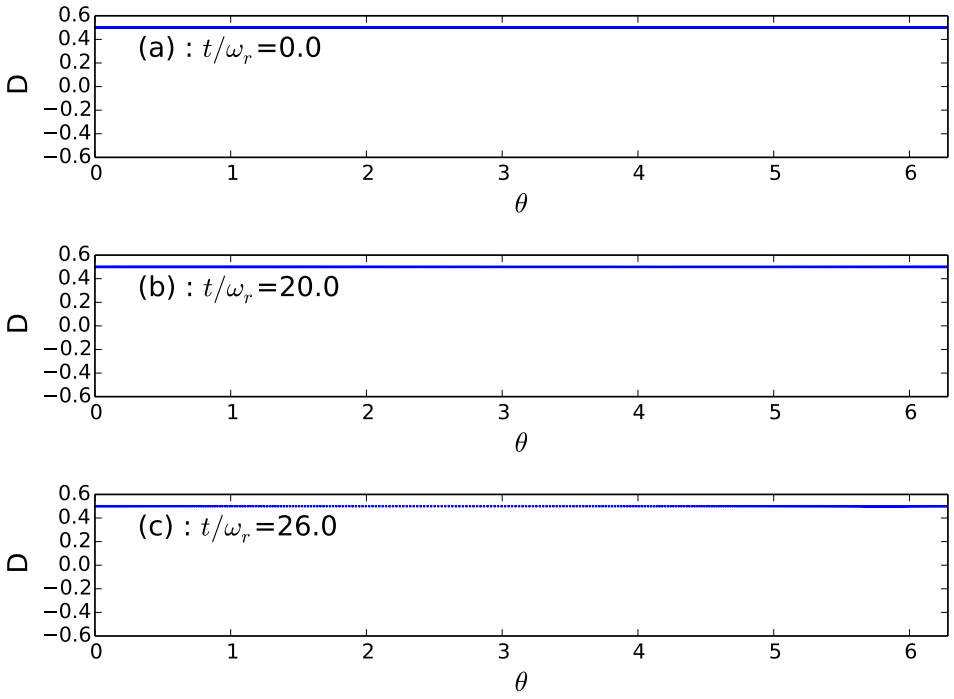

Figure 4.18: Snapshots of population difference distribution (θ_j, D_j) for each atom $j = 1..1000$ when (a) $t = 0\omega_r^{-1}$, (b) $t = 20\omega_r^{-1}$, (c) $t = 26\omega_r^{-1}$. Parameters used and equations solved are as in Figure 4.16.

As was also the case for the degenerate Λ configuration, equation (4.2.3.46) predicts equal gain for both signs of the population inversion in the non-degenerate configuration. This is shown to be true in comparing Figures 4.16 and 4.19.

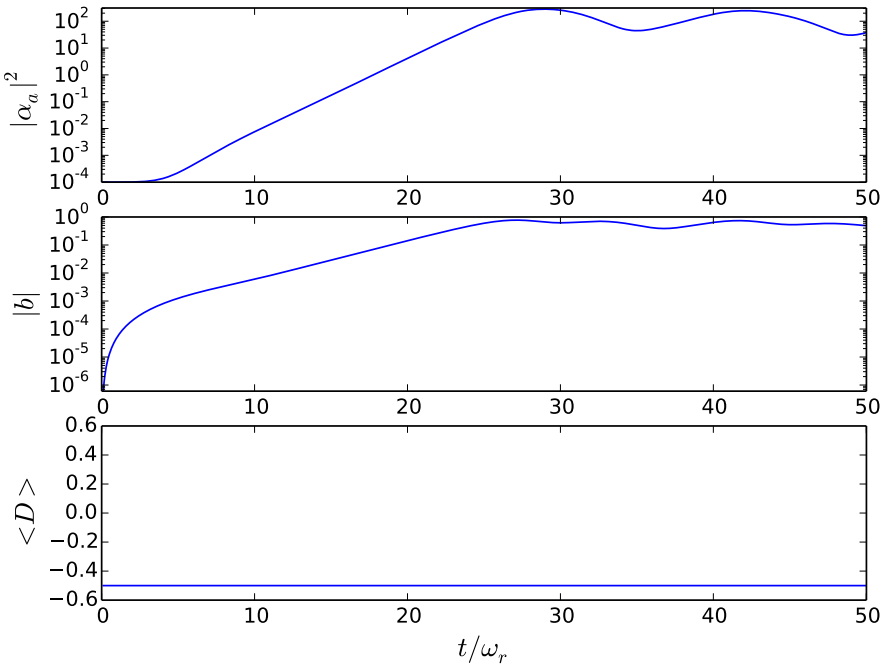

Figure 4.19: Evolution of probe photon number, $|\alpha_a|^2$, bunching parameter, $|b|$, and mean population difference, $\langle D \rangle$, for the case where the two transition detunings are equal in magnutide but opposite in sign, $\Delta_a = -\Delta_b$, and the population of the system is initially in state $|2\rangle$, $D_0 = -1/2$. Produced by solving equations (4.2.3.7) - (4.2.3.12). Parameters used are $U_0/\omega_r = 5 \times 10^{-5}$, $\Delta_{ab} = 10$, $\alpha_b = 100$, $N = 1000$, $\epsilon_\mu = 0$.

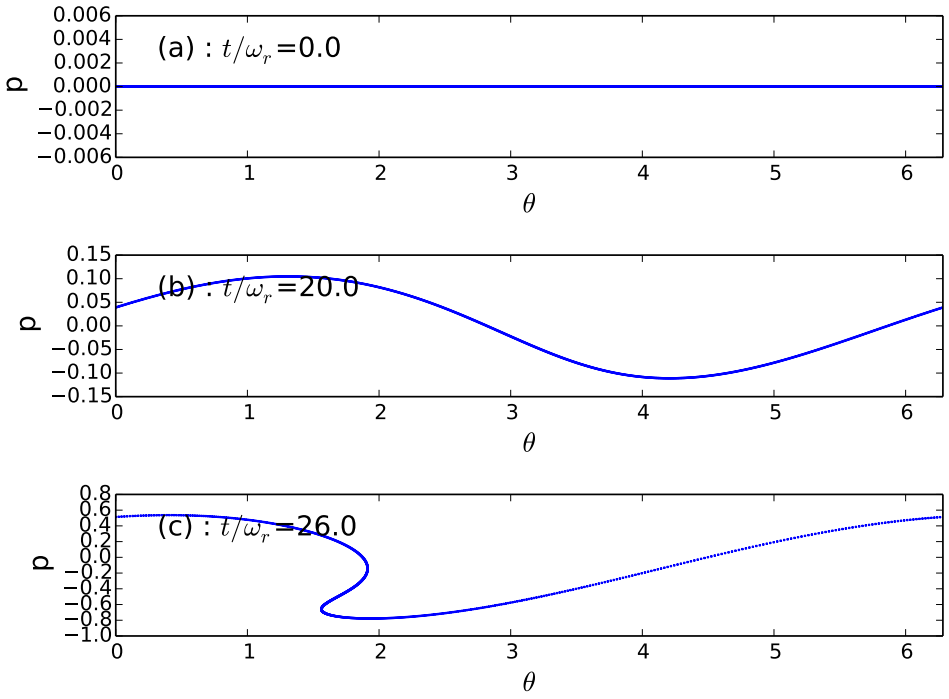

Figure 4.20: Snapshots of momentum distribution (θ_j, p_j) for each atom $j = 1..1000$ when (a) $t = 0\omega_r^{-1}$, (b) $t = 20\omega_r^{-1}$, (c) $t = 26\omega_r^{-1}$. Parameters used and equations solved are as in Figure 4.19.

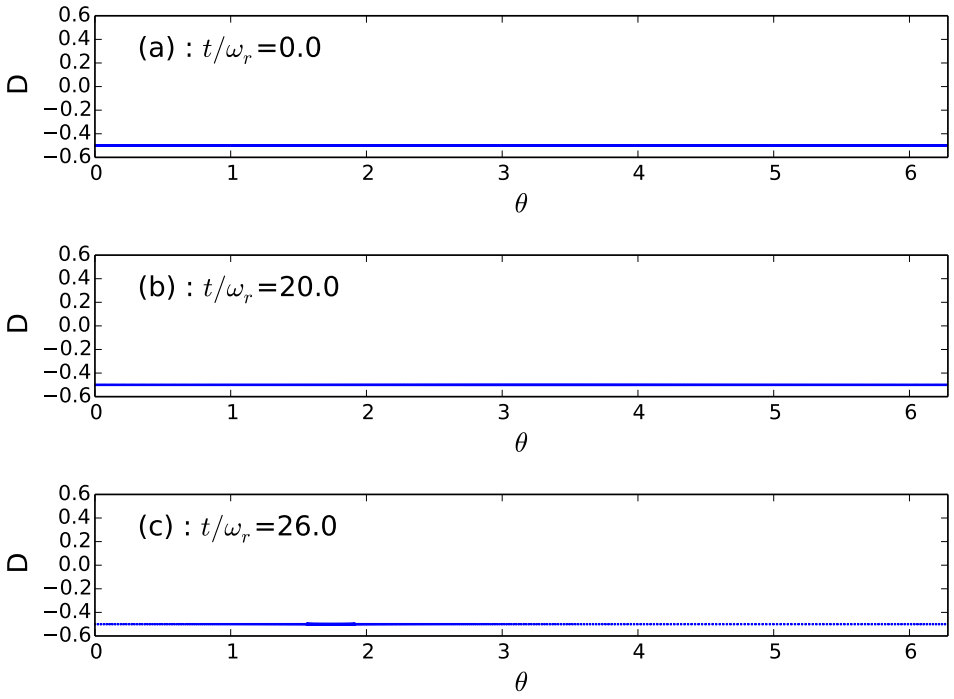

Figure 4.21: Snapshots of population difference distribution (θ_j, D_j) for each atom $j = 1..1000$ when (a) $t = 0\omega_r^{-1}$, (b) $t = 20\omega_r^{-1}$, (c) $t = 26\omega_r^{-1}$. Parameters used and equations solved are as in Figure 4.19.

The previously mentioned similarities between the non-degenerate Λ and degenerate Λ configurations break down, however, when comparisons are made between the results for the $D_0 = 0$ case. Comparing 4.22(a) to 4.9(a) shows that although the degenerate Λ configuration case allows the CARL gain mechanism to continue even with equally distributed population between the two lower levels, the non-degenerate Λ configuration does not.

As was the case in Figures 4.16 & 4.19, (where the initial values for the population inversion, D_0 were $^1/_2$ and $-^1/_2$ respectively), when the population is equally split between levels $|1\rangle$ and $|2\rangle$, i.e. $D_0 = 0$, the population remains constant at its initial value, as can be seen from Figure 4.24.

However, contrary to the cases where $D_0 \neq 0$, when the initial value is $D_0 = 0$, equation (4.2.3.18) for the force experience by an atom experiences a zero value. With zero force acting upon the atoms they remain uniformly spread and stationary, i.e. no atomic bunching takes place, as can be seen in Figure 4.23. As atomic bunching is the root cause of the CARL instability, the probe field remains at its initial seed value.

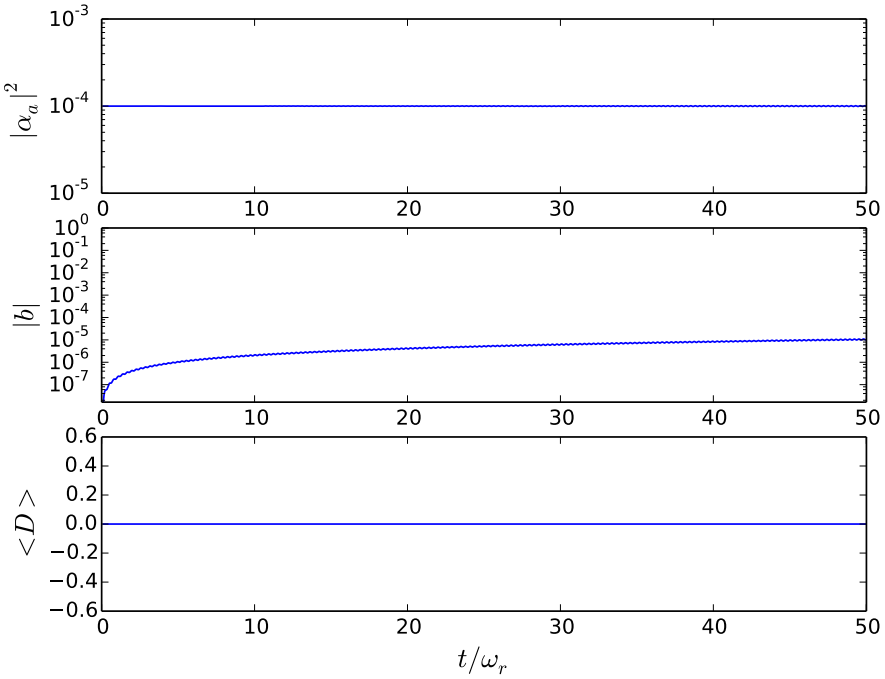

Figure 4.22: Evolution of probe photon number, $|\alpha_a|^2$, bunching parameter, $|b|$, and mean population difference, $\langle D \rangle$, for the case where the two transition detunings are equal in magnutide but opposite in sign, $\Delta_a = -\Delta_b$, and the population of the system is initially equally distributed between states $|1\rangle$ and $|2\rangle$, $D_0 = 0$. Produced by solving equations (4.2.3.7) - (4.2.3.12). Parameters used are $U_0/\omega_r = 5 \times 10^{-5}$, $\Delta_{ab} = 10$, $\alpha_b = 100$, $N = 1000$, $\epsilon_\mu = 0$.

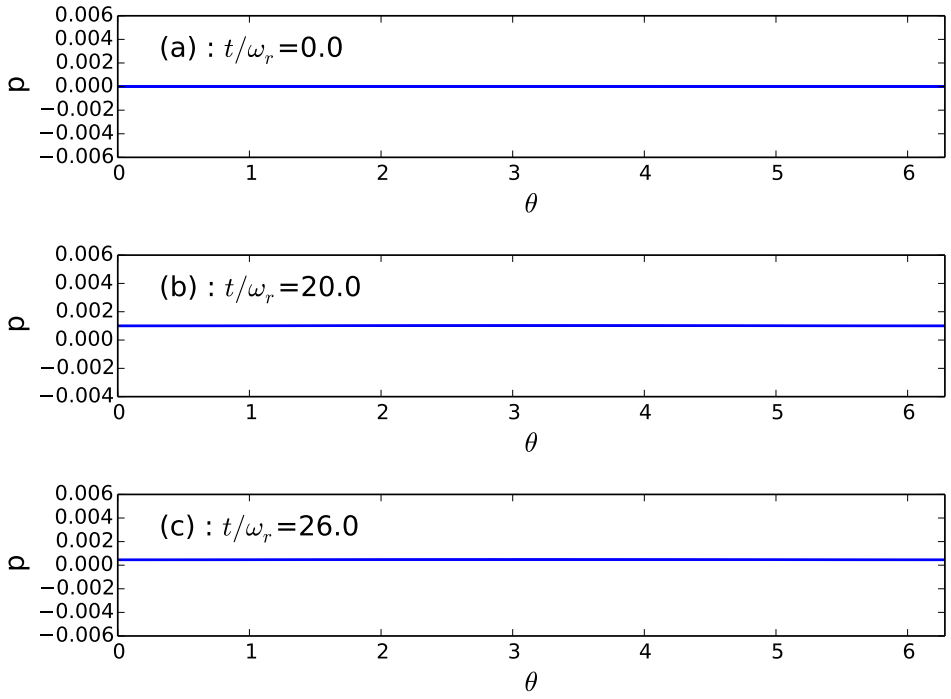

Figure 4.23: Snapshots of momentum distribution (θ_j, p_j) for each atom $j = 1..1000$ when (a) $t = 0\omega_r^{-1}$, (b) $t = 20\omega_r^{-1}$, (c) $t = 26\omega_r^{-1}$. Parameters used and equations solved are as in Figure 4.22.

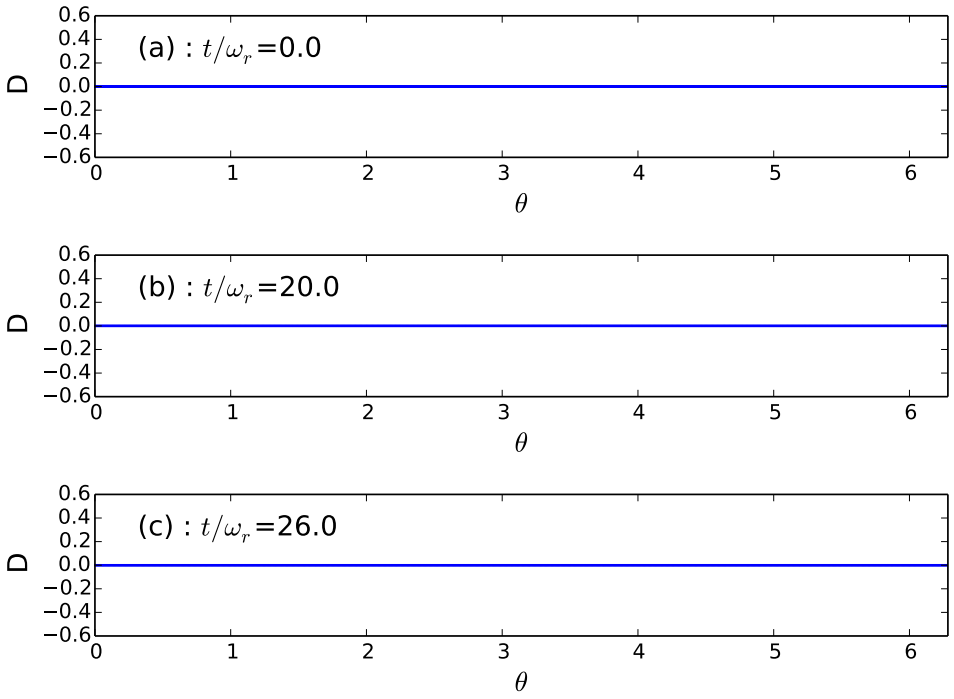

Figure 4.24: Snapshots of population difference distribution (θ_j, D_j) for each atom $j = 1..1000$ when (a) $t = 0\omega_r^{-1}$, (b) $t = 20\omega_r^{-1}$, (c) $t = 26\omega_r^{-1}$. Parameters used and equations solved are as in Figure 4.22.

Equation (4.2.3.46) also suggests that the gain in the optical probe beam, $|\alpha_a|^2$, should be identical regardless of the sign of the detuning used. This is shown to be true when comparison is made between Figures 4.16, 4.19 and 4.22 above, in which $U_0 = \frac{g^2}{\Delta_a} > 0$, to Figures 4.25, 4.26 and 4.27, in which $U_0 = \frac{g^2}{\Delta_a} < 0$. It can be seen that the gain curves experience little to no change when the sign of the detuning is inverted, as well as very little change when the sign of the population inversion is altered.

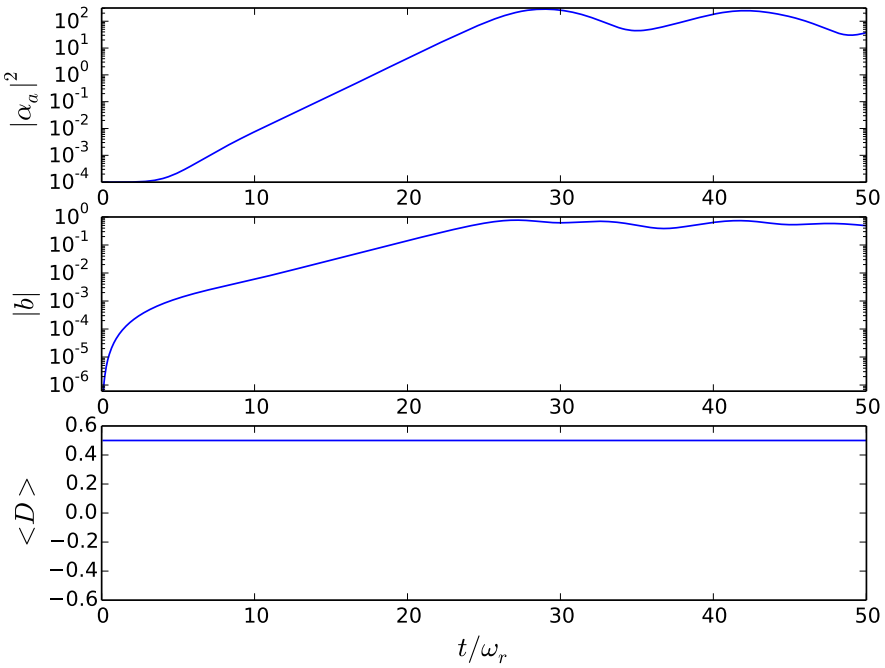

Figure 4.25: Evolution of probe photon number, $|\alpha_a|^2$, bunching parameter, $|b|$, and mean population difference, $\langle D \rangle$, for the case where the two transition detunings are equal in magnutide but opposite in sign, $\Delta_a = -\Delta_b$, and the population of the system is initially in state $|1\rangle$, $D_0 = 1/2$. Produced by solving equations (4.2.3.7) - (4.2.3.12). Parameters used are $U_0/\omega_r = -5 \times 10^{-5}$, $\Delta_{ab} = 10$, $\alpha_b = 100$, $N = 1000$, $\epsilon_\mu = 0$.

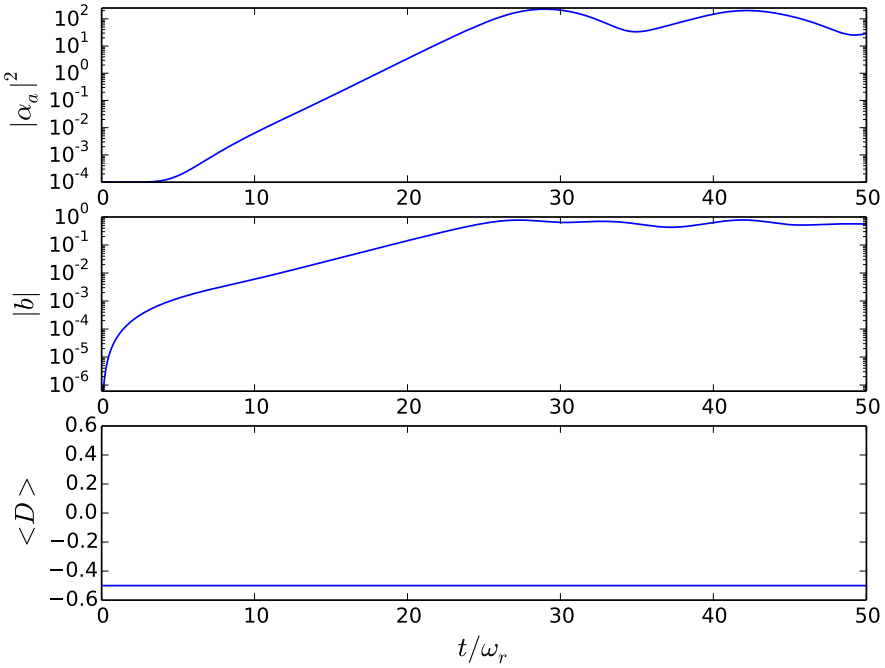

Figure 4.26: Evolution of probe photon number, $|\alpha_a|^2$, bunching parameter, $|b|$, and mean population difference, $\langle D \rangle$, for the case where the two transition detunings are equal in magnutide but opposite in sign, $\Delta_a = -\Delta_b$, and the population of the system is initially in state $|1\rangle$, $D_0 = -1/2$. Produced by solving equations (4.2.3.7) - (4.2.3.12). Parameters used are $U_0/\omega_r = -5 \times 10^{-5}$, $\Delta_{ab} = 10$, $\alpha_b = 100$, $N = 1000$, $\epsilon_\mu = 0$.

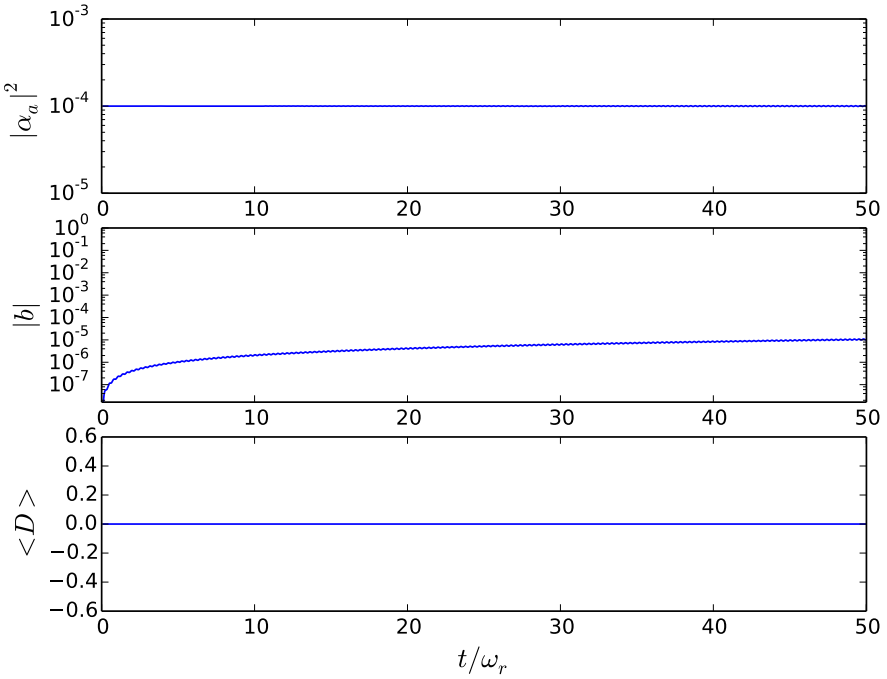

Figure 4.27: Evolution of probe photon number, $|\alpha_a|^2$, bunching parameter, $|b|$, and mean population difference, $\langle D \rangle$, for the case where the two transition detunings are equal in magnutide but opposite in sign, $\Delta_a = -\Delta_b$, and the population of the system is initially in state $|1\rangle$, $D_0 = 0$. Produced by solving equations (4.2.3.7) - (4.2.3.12). Parameters used are $U_0/\omega_r = -5 \times 10^{-5}$, $\Delta_{ab} = 10$, $\alpha_b = 100$, $N = 1000$, $\epsilon_\mu = 0$.

Chapter 5

Conclusion

5.1 Summary

This thesis has presented numerical results related to the study of centre of mass atomic motion in multilevel cold atomic gases of various internal energy level configurations. Below I give a brief summary of the main results from each chapter followed by an overall summary of the work described in the thesis.

5.1.1 Chapter 2 Summary

In Chapter 2 the Maxwell-Bloch equations for a cloud of cold two level atoms were derived over three stages. Firstly, equations were produced which described the evolution of the internal degrees of freedom of two level atoms in response to a single incident static field. Those equations were used to demonstrate Rabi oscillations in the atomic population and the variation of susceptibility with field-atom detuning.

The equations were then extended to allow the incident field to evolve with time. In doing so it was shown that the system exhibited bistable properties.

Further extending the model to include atomic centre of mass motion produced Maxwell-Bloch equations for an ultracold cloud of two level atoms interacting with two counterpropagating, temporally evolving optical fields. It was shown that such equations could demonstrate the CARL instability. In CARL it was

shown that the initial homogeneous spread of atomic positions was unstable and the atoms in the system were induced to bunch by formation of a standing wave between the pump and probe beams. The growth of the atomic bunching term $|b| = |\langle e^{i\theta} \rangle|$ was shown to proceed synchronously with the probe beam, as the bunching of atoms resulted in backscattering of the pump field into the probe field.

It was shown that when the pump amplitude exceeded a saturation threshold, the population within the atoms could become sufficiently excited that the population inversion approached zero, which in turn caused the forces bunching the atoms to quench and tend towards zero.

5.1.2 Chapter 3 Summary

In Chapter 3 the model from Chapter 2 was extended to describe a system of three level atoms in a ladder configuration. Two nonlinear optical processes were investigated using the three level ladder equations:

In the first process, two photon CARL, two expressions of note were derived; a condition for when the three level ladder system was in the high or low pump regime, and an expression for the gain expected from the system in the low pump regime.

Those two expressions were employed to compare the system in the low and high pump intensity regimes. It was demonstrated, when both including and neglecting the AC Stark shift term ϵ_μ, that in contrast with the two level CARL system of chapter 2, the three level CARL instability persisted into the high pump intensity regime. This was due to terms in the force equation which did not tend to zero with the population inversion term.

The second process investigated was that of two-photon superfluorescence. It was demonstrated that, as was the case for single photon fluorescence[36], introduction of centre of mass movement and atomic bunching resulted in symmetry breaking in the sign of detuning from field-atom resonance.

When the emitting atoms were set stationary, the two-photon SF pulse showed no dependence upon the sign of detuning. When centre of mass motion was

included, the atoms bunched at maxima (minima) of intensity when the field was red (blue) detuned from field-atom resonance. When the atoms bunched at the maxima of optical standing wave intensity, the emitted optical pulse was enhanced over the case in which the atoms bunched at the point of intensity minima, wherein the optical pulse was suppressed.

5.1.3 Chapter 4 Summary

In Chapter 4 Maxwell-Bloch equations were derived which modelled the evolution of a cloud of atoms with a three level "lambda" atomic energy level configuration. Two subcategories of the Λ configuration were investigated: one in which the two lower energy levels were degenerate, the degenerate Λ configuration, and one where the two lower energy levels were non-degenerate, the non-degenerate Λ configuration.

It was demonstrated in the degenerate configuration that, for particular values of field-atom detuning, it was possible to decouple the atomic centre of mass equations from the internal atomic degrees of freedom.

It was then shown that in the non-degenerate configuration that there exists a field-atom detuning regime in which the atomic motion becomes decoupled from the atomic coherence but not the atomic population. The population difference remained constant throughout the interaction, so the population inversion $D(t = 0)$ acted instead as a parameter in the equation for the force experienced by the atoms.

It was therefore demonstrated that both the degenerate and non-degenerate Λ configurations lend themselves towards operation of the CARL instabilities at higher pump intensities than for the case of two-level atoms. In particular the non-degenerate Λ configuration offered a particularly attractive prospect for CARL gain, as the apparent trapping of the population at its initial state, $D(t = 0)$, offered a system in which spontaneous emission may be impeded.

5.2 Overall Summary

In this thesis the theory of CARL has been extended from 2-level atoms to 3-level atoms with ladder and Λ configurations. It has been demonstrated that the additional internal energy level allows a variety of schemes involving CARL. Some of these new schemes have features which appear promising for enhancing CARL instabilities.

5.3 Future Work

A number of potential avenues may be explored following the work described in this thesis.

5.3.1 Effects of centre of mass atomic recoil on non-linear optical processes in three and four level atoms

Numerous non-linear processes occur in multi-level atomic systems. Continuing from the research presented here many of these processes may produce interesting results when centre of mass atomic recoil is introduced.

For example, [72] demonstrates that a system of light on a cloud of cold atoms can produce dispersive bistability for properly chosen parameters. With centre of mass movement included in the model, it is shown that blue detuned light results in the formation of an atomic density grating. The density grating leads to a change in the dispersive properties of the cloud and causes the pump transmission to jump from the lower transmission state to the upper transmission state.

Studies could be undertaken investigating dispersive optical bistability in a three level system, such as that described in Chapter 3. Similar changes to the dispersive properties of a cloud of three level atoms which exhibit two-photon bistability may occur, leading to the pump transmission to change transmission state.

5.3.2 Enhancement of CARL through use of EIT in three and four level atoms

Electromagnetically Induced Transparency (EIT) [83, 84] is a coherent nonlinear optical process in which destructive quantum interference between transition probability amplitudes results in the creation of a "window" of reduced, or even negated, absorption within the susceptibility profile of a physical media. In addition to the window created in the absorption portion of the atomic sample's susceptibility curve, a large value for the dispersive portion of the susceptibility is also formed as a result of EIT. EIT can take place in atoms with ladder, Λ or "V" three level energy level structures[85].

As has been explained in this thesis, collective atomic recoil lasing is dependent upon the dispersive properties of an atomic sample for the bunching force which is the root cause of the CARL instability. Furthermore, atomic absorption can hinder the CARL instability. The window of reduced absorption and enhanced dispersion may then prove to be a useful method of enhancing CARL.

5.3.3 Sum-frequency generation from CARL using four level ladder configuration atoms

It has been predicted in [86] that four wave mixing and frequency up conversion are possible in four level ladder configuration CARL. The benefit of using CARL for frequency up conversion is that the complicated phase matching required by traditional methods, which utilise nonlinear crystals, is handled as a natural consequence of the bunching process.

In [86] assumptions are made which reduce the complete four level Maxwell-Bloch equations describing the system to the CARL equations in the FEL limit, similar to the reductions made in sections 2.5.3.3 and 3.2.1.2 of this thesis. Investigations may be made into the behaviour of such a system outside of the FEL limit.

5.3.4 Investigation of parameter space for two-photon superfluorescence including recoil

As was stated in section 3.3.3, when recoil is introduced to the superfluorescent system, for the parameters selected, the emitted optical pulse ceases to be superfluorescent. As it is possible to create superfluorescent pulses where recoil has been included, for sufficiently small values of the decay rate γ, it may be possible to discover parameters in which the superfluorescent behaviour exists in both the recoil included and recoil neglected cases for otherwise identical input values.

5.3.5 Proposed experimental test of results from this thesis

In Section 2.5.3.4 an experimental setup used by Kruse et al. [4] and von. Cube et al. [38] to investigate CARL in the laboratory using samples of two level atoms was described. A diagram of the experimental setup used by these experiments is shown in Figure 2.11. A similar laboratory setup could be used to investigate the results shown in this thesis.

For the case of three level atoms in a ladder configuration, either ^{87}Sr [18] or ^{171}Yb [19] may be useful as a replacement for the ^{85}Rb used in [4, 38].

For investigating the results shown for three level atoms with a Λ energy level configuration, the ^{87}Rb D1 line including magnetic sublevels has been used, for example in [87], as an atom with a Λ energy level configuration. A tunable magnetic field may be used to split the ground state energy energy levels via the Zeeman effect, allowing for the creation of an energy level structure which may be used to investigate the non-degenerate Λ energy level configuration discussed in Section 4.2.3.

Other alkali metals such as sodium or caesium may also be suitable for use as three level Λ configuration atom samples through use of similar methods.

Appendix A

Three level CARL Linear Analysis

Performing a linear analysis upon equations (3.2.2.8), (3.2.2.2), (3.2.2.3), (3.2.2.4), (3.2.2.5) and (3.2.2.6). It is assumed that the pump field α_b remains undepleted throughout the course of the instability and thus may be treated as a constant, with (3.2.2.6) set equal to zero. At steady state the equations for the population and coherence of the system are given by

$$D = {}^1\!/_2 + iU_0\Big(\quad \sigma_{13}\left(\alpha_a + \alpha_b e^{-2ikz}\right)\left(\alpha_a e^{2ikz} + \alpha_b\right) \\ -\sigma_{31}\left(\alpha_a^* + \alpha_b^* e^{2ikz}\right)\left(\alpha_a^* e^{-2ikz} + \alpha_b^*\right) \quad \Big) \tag{A.0.0.1}$$

$$\sigma_{31} = \frac{2U_0 D(\Delta_{ab} - i\gamma_{31})}{(\gamma_{31}^2 + \Delta_{ab}^2)}\left(\alpha_a e^{2ikz} + \alpha_b\right)\left(\alpha_a + \alpha_b e^{-2ikz}\right) \tag{A.0.0.2}$$

By substituting the above expression for the coherence, σ_{21}, into the steady state expression for the population inversion and defining the terms

$$F = \left(\alpha_a + \alpha_b e^{-2ikz}\right)\left(\alpha_a e^{2ikz} + \alpha_b\right) = \alpha_a^2 e^{2ikz} + 2\alpha_a\alpha_b + \alpha_b^2 e^{-2ikz} \tag{A.0.0.3}$$

and

$$H = \frac{4\gamma_{31}U_0^2}{\gamma_{33}(\gamma_{31}^2 + \Delta_{ab}^2)} \tag{A.0.0.4}$$

gives a expression for D devoid of any other varying terms, namely

$$D = \frac{1}{2(1 + H|F|^2)}\,. \tag{A.0.0.5}$$

Substituting the expressions for the population inversion, (A.0.0.5) into the expression for the steady state coherence produces

$$\sigma_{31} = \frac{U_0 F(\Delta_{ab} - i\gamma_{31})}{(1 + H|F|^2)(\gamma_{31}^2 + \Delta_{ab}^2)}\,. \tag{A.0.0.6}$$

Substituting the above expression for the value the coherence takes in the weak regime into the remaining equations of the system gives

$$\begin{aligned}\frac{dp_j}{dt} = {} & i2\hbar k U_0 \Bigg[\frac{U_0}{(1 + H|F|^2)(\gamma_{31}^2 + \Delta_{ab}^2)} \Bigg(\\ & \Delta_{ab} \Big(2\left(\alpha_a^{*2}\alpha_b^2 e^{-4ikz} - \alpha_a^2 \alpha_b^{*2} e^{4ikz}\right) \\ & \quad + \left(|\alpha_a|^2 + |\alpha_b|^2\right)\left(\alpha_a^*\alpha_b e^{-2ikz} - \alpha_a\alpha_b^* e^{2ikz}\right) \Big) \\ & - \gamma_{31} \Big(|\alpha_a|^4 - |\alpha_b|^4 + \left(|\alpha_a|^2 - |\alpha_b|^2\right)\left(\alpha_a^*\alpha_b e^{-2ikz} + \alpha_a\alpha_b^* e^{2ikz}\right) \Big) \Bigg) \Bigg] \\ & + i2\hbar k U_0 \left(\alpha_a^*\alpha_b e^{-2ikz} - \alpha_a\alpha_b^* e^{2ikz}\right)\end{aligned} \tag{A.0.0.7}$$

$$\frac{dz_j}{dt} = \frac{p_j}{m} \tag{A.0.0.8}$$

$$\frac{\partial \alpha_a}{\partial t} = -iNU_0\Bigg(\frac{2U_0(\Delta_{ab} - i\gamma_{31})}{(\gamma_{31}^2 + \Delta_{ab}^2)} \left\langle \frac{(|\alpha_a|^2\alpha_a + 2|\alpha_a|^2\alpha_b e^{-2ikz} + \alpha_a^*\alpha_b^2 e^{-4ikz})}{(1 + H|F|^2)} \right\rangle + \frac{2U_0(\Delta_{ab} - i\gamma_{31})}{(\gamma_{31}^2 + \Delta_{ab}^2)} \left\langle \frac{(\alpha_a^2\alpha_b^* e^{2ikz} + 2\alpha_a|\alpha_b|^2 + |\alpha_b|^2\alpha_b e^{-2ikz})}{(1 + H|F|^2)} \right\rangle + \alpha_a + \alpha_b\langle e^{-2ikz}\rangle \Bigg) + (i\delta_c - \kappa)\alpha_a + \kappa\alpha_a^{eq} \tag{A.0.0.9}$$

By studying the evolution of small perturbation terms, defined as

$$z = z_0 + \delta z(t) \tag{A.0.0.10}$$

$$p = \delta p(t) \tag{A.0.0.11}$$

$$\alpha_a = \delta\alpha_a(t)\,, \tag{A.0.0.12}$$

the gain response of the system may be investigated. The assumption is made that the field is well tuned with the cavity and that there are minimal losses from the field, so that $\delta_c = \kappa = 0$. Substituting the above perturbation terms into the equations for the system (A.0.0.7) - (A.0.0.9), keeping only those terms which remain linear in perturbation terms gives equations

$$\frac{\partial \delta p_j}{\partial t} = i2\hbar k U_0 \Bigg[\left(1 + \frac{\Delta_{ab}U_0|\alpha_b|^2}{(\gamma_{31}^2 + \Delta_{ab}^2)(1 + H|\alpha_b|^4)}\right)\left(\delta\alpha_a^*\alpha_b e^{-2ikz_0} - \delta\alpha_a\alpha_b^* e^{2ikz_0}\right) + \frac{i\gamma_{31}U_0|\alpha_b|^2}{(\gamma_{31}^2 + \Delta_{ab}^2)(1 + H|\alpha_b|^4)}\left(|\alpha_b|^2 + \delta\alpha_a^*\alpha_b e^{-2ikz_0} + \delta\alpha_a\alpha_b^* e^{2ikz_0}\right)\Bigg] \tag{A.0.0.13}$$

$$\frac{\partial \delta z_j}{\partial t} = \frac{\delta p_j}{m} \tag{A.0.0.14}$$

$$\frac{\partial \delta\alpha_a}{\partial t} = -iNU_0\Bigg(\delta\alpha_a \left(1 + \frac{4U_0|\alpha_b|^2(\Delta_{ab} - i\gamma_{31})}{(\gamma_{31}^2 + \Delta_{ab}^2)(1 + H|\alpha_b|^4)}\right) - i2k\alpha_b \left(1 + \frac{2U_0|\alpha_b|^2(\Delta_{ab} - i\gamma_{31})}{(\gamma_{31}^2 + \Delta_{ab}^2)(1 + H|\alpha_b|^4)}\right) \langle \delta z e^{-2ikz_0}\rangle \Bigg) \tag{A.0.0.15}$$

where it has been assumed that as δz is small, $1 >> \delta z$, when the terms $e^{\pm 2ik\delta z}$ are expanded out using the Maclaurin series, only the first term need be retained, so that $e^{\pm 2ik\delta z} \approx 1 \pm 2ik\delta z$. Further to this, as the atoms are initially equally distributed any terms $\langle e^{\pm ikz}\rangle$ are assumed to average out to zero. Considering the system to be running sufficiently detuned that $\Delta_{ab} >> \gamma_{31}$, the approximation may be made that $\gamma_{31} \approx 0$. Under this assumption the term H in the above equations is also approximately zero, so the equations take the form

$$\frac{\partial \delta p_j}{\partial t} = i2\hbar k U_0 \left(1 + \frac{U_0|\alpha_b|^2}{\Delta_{ab}}\right)\left(\delta\alpha_a^*\alpha_b e^{-2ikz_0} - \delta\alpha_a\alpha_b^* e^{2ikz_0}\right) \tag{A.0.0.16}$$

$$\frac{\partial \delta z_j}{\partial t} = \frac{\delta p_j}{m} \tag{A.0.0.17}$$

$$\frac{\partial \delta\alpha_a}{\partial t} = -iNU_0\left(\delta\alpha_a \left(1 + \frac{4U_0|\alpha_b|^2}{\Delta_{ab}}\right) - i2k\alpha_b \left(1 + \frac{2U_0|\alpha_b|^2}{\Delta_{ab}}\right)\langle \delta z e^{-2ikz_0}\rangle\right) \tag{A.0.0.18}$$

It is convenient to define

$$b = -i\langle \delta z e^{-2ikz_0}\rangle \tag{A.0.0.19}$$

and

$$P = \left\langle \frac{\delta p_j}{m} e^{-2ikz_0} \right\rangle \tag{A.0.0.20}$$

as intermediate variables for substitution into the field equation. From the above definitions it is easy to see that

$$\begin{aligned}\frac{db}{dt} &= -i\left\langle \frac{\partial \delta z_j}{\partial t} e^{-2ikz_0} \right\rangle \\ &= -i\left\langle \frac{\delta p_j}{m} e^{-2ikz_0} \right\rangle \\ &= -iP \end{aligned} \tag{A.0.0.21}$$

and

$$\begin{aligned}\frac{dP}{dt} &= \left\langle \frac{1}{m}\frac{\partial \delta p_j}{\partial t} e^{-2ikz_0} \right\rangle \\ &= -\frac{i2\hbar k U_0}{m}\left(1 + \frac{U_0|\alpha_b|^2}{\Delta_{ab}}\right)\alpha_b^* \delta\alpha_a \,, \end{aligned} \tag{A.0.0.22}$$

where once again it has been taken that the initial even distribution of the atoms means that terms $\langle e^{\pm ikz} \rangle$ may be assumed to average to zero. Substituting for the term b using (A.0.0.19) in (A.0.0.18) and differentiating gives

$$\frac{d^2\delta\alpha_a}{dt^2} = -iNU_0\left(\left(1 + \frac{4U_0|\alpha_b|^2}{\Delta_{ab}}\right)\frac{d\delta\alpha_a}{dt} + 2k\alpha_b\left(1 + \frac{2U_0|\alpha_b|^2}{\Delta_{ab}}\right)\frac{db}{dt}\right). \tag{A.0.0.23}$$

Substituting for $\frac{\partial b}{\partial t}$ using (A.0.0.21) then differentiating a second time gives

$$\frac{d^3\delta\alpha_a}{dt^3} = -iNU_0\left(\left(1 + \frac{4U_0|\alpha_b|^2}{\Delta_{ab}}\right)\frac{d^2\delta\alpha_a}{dt^2} - i2k\alpha_b\left(1 + \frac{2U_0|\alpha_b|^2}{\Delta_{ab}}\right)\frac{dP}{dt}\right). \tag{A.0.0.24}$$

By substituting for $\frac{dP}{dt}$ using (A.0.0.22) and grouping terms, an expression purely in terms of field variables is obtained, namely

$$\frac{d^3\delta\alpha_a}{dt^3} = -iNU_0\Bigg(\left(1+\frac{4U_0|\alpha_b|^2}{\Delta_{ab}}\right)\frac{d^2\delta\alpha_a}{dt^2} - \frac{2\hbar k^2 U_0|\alpha_b|^2}{m}\left(1+\frac{3U_0|\alpha_b|^2}{\Delta_{ab}}+\frac{2U_0^2|\alpha_b|^4}{\Delta_{ab}^2}\right)\delta\alpha_a\Bigg) \quad \text{(A.0.0.25)}$$

At this point it is convenient to reintroduce a detuning between the field and cavity of $\delta_c \approx iNU_0\left(1+\frac{4U_0|\alpha_b|^2}{\Delta_{ab}}\right)$. In doing so it is possible to cancel the first term in the above equation, making the solution far simpler. Looking for solutions of the form $\delta\alpha_a \propto e^{\lambda t}$ gives

$$\lambda^3 = \frac{i2N\hbar k^2 U_0^2|\alpha_b|^2}{m}\left(1+\frac{3U_0|\alpha_b|^2}{\Delta_{ab}}+\frac{2U_0^2|\alpha_b|^4}{\Delta_{ab}^2}\right). \quad \text{(A.0.0.26)}$$

Gain is to be expected where the real component of λ is both nonzero and positive. The cubed root of i, $\sqrt[3]{i}$, has three possible solutions: $-i$, $e^{5\pi/6}$ and $e^{\pi/6}$. The first solution, $-i$, has no real component, it is purely imaginary and will thus not result in gain. The second solution, $e^{5\pi/6}$, does have a real component as $e^{5\pi/6} = \cos(5\pi/6) + i\sin(5\pi/6)$. However, as $\cos(5\pi/6) = -\sqrt{3}/2$ this yields a negative value for the real component and will also not produce gain. The third solution $e^{\pi/6}$ may be expanded out as $\cos(\pi/6)+i\sin(\pi/6)$, the real part of which takes the value $\cos(\pi/6) = \sqrt{3}/2$. As a real, nonzero, positive value, this term will result in gain for the system. The gain experienced by the system should then be given by the expression

$$Gain = \frac{\sqrt{3}}{2}\sqrt[3]{\frac{2N\hbar k^2|\alpha_b|^2}{m}\left(U_0^2+\frac{3U_0^3|\alpha_b|^2}{\Delta_{ab}}+\frac{2U_0^4|\alpha_b|^4}{\Delta_{ab}^2}\right)}. \quad \text{(A.0.0.27)}$$

Bibliography

[1] M. J. Pritchard, *Manipulation of ultracold atoms using magnetic and optical fields*. PhD thesis, University of Durham, 2006.

[2] S. A. Collins, Jr., and K. C. Wasmundt, "Optical feedback and bistability: a review," *Opt. Eng.*, vol. 19, pp. 478–487, 1980.

[3] M. Gross, and S. Haroche, "Superradiance: An essay on the theory of collective spontaneous emission," *Physics Reports*, vol. 93, pp. 301–396, 1982.

[4] D. Kruse, C. von Cube, C. Zimmermann, and Ph. W. Courteille, "Observation of lasing mediated by collective atomic recoil," *Phys. Rev. Lett.*, vol. 91, p. 183601, 2003.

[5] Sir I. Newton, *Opticks: or, A treatise of the reflections, refractions, inflections and colours of light*. London : Printed for William Innys at the West-End of St. Paul's, 1704.

[6] J. C. Maxwell, *A Treatise on Electricity and Magnetism*. Oxford : Clarendon Press, 1873.

[7] P. N. Lebedev, "Experimental examination of light pressure," *Ann. der Physik*, vol. 6, pp. 433–458, 1901.

[8] E. F. Nichols and G. F. Hull, "Experimental examination of light pressure," *Phys. Rev.*, vol. 17, pp. 26–50, 1903.

[9] A. Einstein, "The quantum theory of radiation," *Phys. Z.*, vol. 18, pp. 318–323, 1917.

[10] O. R. Frisch, "Experimenteller nachweis des einsteinschen strahlungsrückstoßes," *Phys. Z.*, vol. 86, pp. 42–48, 1933.

[11] S. Chu, "Laser manipulation of atoms and particles," *Science*, vol. 253, pp. 861–866, 1991.

[12] A. Ashkin, "Acceleration and trapping of particles by radiation pressure," *Phys. Rev. Lett.*, vol. 24, pp. 156–159, 1970.

[13] A. Ashkin, "Trapping of atoms by resonance radiation pressure," *Phys. Rev. Lett.*, vol. 40, pp. 729–732, 1978.

[14] A. Ashkin, "Applications of laser radiation pressure," *Science*, vol. 210, pp. 1081–1088, 1980.

[15] T. W. Hänsch and A. L. Schawlow, "Cooling of gases by laser radiation," *Opt. Comm.*, vol. 13, pp. 68–69, 1975.

[16] S. Chu, L. Hollberg, J. E. Bjorkholm, A. Cable, and A. Ashkin, "Three-dimensional viscous confinement and cooling of atoms by resonance radiation pressure," *Phys. Rev. Lett.*, vol. 55, pp. 48–51, 1985.

[17] J. Dalibard, and C. Cohen-Tannoudji, "Laser cooling below the doppler limit by polarization gradients: simple theoretical models," *J. Opt. Soc. Am. B*, vol. 6, pp. 2023–2045, 1989.

[18] H. Katori, M. Takamoto, V. G. Pal'chikov, and V. D. Ovsiannikov, "Ultrastable optical clock with neutral atoms in an engineered light shift trap," *Phys. Rev. Lett.*, vol. 91, p. 173005, 2003.

[19] A. D. Ludlow, N. M. Hinkley, J. A. Sherman, N. B. Phillips, M. Schioppo, N. D. Lemke, K. P. Beloy, M. Pizzocaro, C. W. Oates, "An atomic clock with 10^{-18} instability," *Science*, vol. 341, pp. 1215–1218, 2013.

[20] A. Ashkin and J. M. Dziedzic, "Optical trapping and manipulation of viruses and bacteria," *Science*, vol. 235, pp. 1517–1520, 1987.

[21] H. Yim, Wang, M. D., Svoboda, K., Landick, R., Block, S. M., and Gelles, J., "Transcription against an applied force," *Science*, vol. 270, pp. 1653–1657, 1995.

[22] A. Ashkin, "Optical trapping and manipulation of neutral particles using lasers," *Proc. Natl. Acad. Sci.*, vol. 94, pp. 4853–4859, 1997.

[23] W. D. Phillips, "Laser cooling and trapping of neutral atoms*," *Rev. Mod. Phys.*, vol. 70, pp. 721–741, 1998.

[24] S. Chu, "The manipulation of neutral particles*," *Rev. Mod. Phys.*, vol. 70, pp. 685–706, 1998.

[25] S. Inouye, A. P. Chikkatur, D. M. Stamper-Kurn, J. Stenger, D. E. Pritchard, and W. Ketterle, "Superradiant rayleigh scattering from a bose-einstein condensate," *Science*, vol. 285, pp. 571–574, 1999.

[26] J. P. Gordon and A. Ashkin, "Motion of atoms in a radiation trap," *Phys. Rev. A*, vol. 21, pp. 1606–1617, 1980.

[27] H. J. Metcalf and P. van der Straten, *Laser Cooling and Trapping*. Springer-Verlag New York, Inc., 1999.

[28] A. Szöke, V. Daneu, J. Goldhar, and N. A. Kurnit, "Bistable optical element and its applications," *Appl. Phys. Lett.*, vol. 15, pp. 376–379, 1969.

[29] H. M. Gibbs, S. L. McCal, and T. N. C. Venkatesan, "Differential gain and bistability using a sodium-filled fabry-perot interferometer," *Phys. Rev. Lett.*, vol. 36, pp. 1135–1138, 1976.

[30] R. W. Boyd, *Nonlinear Optics*. Academic Press, 2008.

[31] L. A. Lugiato, "Theory of optical bistability," in *Progress in Optics XXI*, pp. 42–440, Elsevier Science Publishers, 1984.

[32] D. J. Gauthier, "Two-photon lasers," *Progress in Optics*, vol. 45, 2003.

[33] R. H. Dicke, "Coherence in spontaneous radiation processes," *Phys. Rev.*, vol. 93, pp. 99–110, 1954.

[34] R. Bonifacio, P. Schwendimann, and F. Haake, "Quantum statistical theory of superradiance. i*," *Phys. Rev. A*, vol. 4, pp. 302–313, 1971.

[35] R. Bonifacio, L. A. Lugiato, "Cooperative radiation processes in two-level systems: Superfluorescence," *Phys. Rev. A*, vol. 11, pp. 1507–1521, 1975.

[36] G. R. M. Robb, B. W. J. McNeil, and R. Bonifacio, "Recoil-induced symmetry breaking in superfluorescence," *Phys. Rev. A*, vol. 61, p. 031801, 2000.

[37] R. Bonifacio, L. De Salvo, "Collective atomic recoil laser (carl) optical gain without inversion by collective atomic recoil and self-bunching of two-level atoms," *Nucl. Instrum. and Meth. in Phys. Res.*, vol. 341, pp. 360–362, 1994.

[38] C. von Cube, S. Slama, D. Kruse, C. Zimmermann, Ph. W. Courteille, G. R. M. Robb, N. Piovella, and R. Bonifacio, "Self-synchronization and dissipation-induced threshold in collective atomic recoil lasing," *Phys. Rev. Lett.*, vol. 93, p. 083601, 2004.

[39] P. R. Hemmer, N. P. Bigelow, D. P. Katz, M. S. Shahriar, L. DeSalvo, and R. Bonifacio, "Self-organization, broken symmetry, and lasing in an atomic vapor: The interdependence of gratings and gain," *Phys. Rev. Lett.*, vol. 77, pp. 1468–1471, 1996.

[40] J. -Y. Courtois, G. Grynberg, B. Lounis and P. Verkerk, "Recoil-induced resonances in cesium: An atomic analog to the free-electron laser," *Phys. Rev. Lett.*, vol. 72, pp. 3017–3020, 1994.

[41] G. L. Lippi, G. P. Barozzi, S. Barbay, and J. R. Tredicce, "Spontaneous generation of a longitudinal atomic density grating in sodium vapor," *Phys. Rev. Lett.*, vol. 76, pp. 2452–2455, 1996.

[42] S. Slama, S. Bux, G. Krenz, C. Zimmermann, and Ph.W. Courteille, "Superradiant rayleigh scattering and collective atomic recoil lasing in a ring cavity," *Phys. Rev. Lett.*, vol. 98, p. 053603, 2007.

[43] M. G. Moore, and P. Meystre, "Theory of superradiant scattering of laser light from bose-einstein condensates," *Phys. Rev. Lett*, vol. 83, pp. 5202–5205, 1999.

[44] M. Gangl, H. Ritsch, "Cold atoms in a high-q ring cavity," *Phys. Rev. A*, vol. 61, p. 043405, 2000.

[45] N. Piovella, M. Gatelli, and R. Bonifacio, "Quantum effects in the collective light scattering by coherent atomic recoil in a bose−einstein condensate," *Opt. Comm.*, vol. 194, pp. 167–173, 2001.

[46] D. Schneble, Y. Torii, M. Boyd, E.W. Streed, D.E. Pritchard, and W. Ketterle, "The onset of matter-wave amplification in a superradiant bose-einstein condensate," *Science*, vol. 300, pp. 475–478, 2003.

[47] B. Nagorny, Th. Elsässer, and A. Hemmerich, "Collective atomic motion in an optical lattice formed inside a high finesse cavity," *Phys. Rev. Lett.*, vol. 91, p. 153003, 2003.

[48] Y. Yoshikawa, Y. Torii, and T. Kuga, "Superradiant light scattering from thermal atomic vapors," *Phys. Rev. Lett.*, vol. 94, p. 083602, 2005.

[49] L. Fallani, C. Fort, N. Piovella, M. M. Cola, F. S. Cataliotti, M. Inguscio, and R. and Bonifacio, "Collective atomic recoil in a moving bose-einstein condensate: From superradiance to bragg scattering," *Phys. Rev. A*, vol. 71, p. 033612, 2005.

[50] J. K. Asboth. P. Domokos, H. Ritsch, and A. Vukics, "Self-organization of atoms in a cavity field: Threshold, bistability, and scaling laws," *Phys. Rev. A*, vol. 72, p. 053417, 2005.

[51] D. Nagy, J. K. Asboth, P. Domokos, H. and Ritsch, "Self-organization of a laser-driven cold gas in a ring cavity," *Europhys. Lett.*, vol. 74, p. 254, 2006.

[52] S. Fernandez-Vidal, G. De Chiara, J. Larson, and G. Morigi, "Quantum ground state of self-organized atomic crystals in optical resonators," *Phys. Rev. A*, vol. 81, p. 043407, 2010.

[53] J. Keeling, M. J. Bhaseen, B. D. and Simons, "Collective dynamics of bose-einstein condensates in optical cavities," *Phys. Rev. Lett.*, vol. 105, p. 043001, 2010.

[54] S. Bux, C. Gnahm, R. A. W. Maier, C. Zimmermann and Ph. W. Courteille, "Cavity-controlled collective scattering at the recoil limit," *Phys. Rev. Lett.*, vol. 106, p. 203601, 2011.

[55] J. A. Greenberg, B. L. Schmittberger, and D. J. Gauthier, "Bunching-induced optical nonlinearity and instability in cold atoms," *Opt. Express*, vol. 19, pp. 22535–22549, 2011.

[56] B. L. Schmittberger, and D. J. Gauthier, "Enhancing light-atom interactions via atomic bunching," *Phys. Rev. A*, vol. 90, p. 013813, 2014.

[57] D. Schmidt, H. Tomczyk, S. Slama, and C. Zimmermann, "Dynamical instability of a bose-einstein condensate in an optical ring resonator," *Phys. Rev. Lett.*, vol. 112, p. 115302, 2014.

[58] H. Kessler, J. Klinder, M. Wolke, A. and Hemmerich, "Steering matter wave superradiance with an ultranarrow-band optical cavity," *Phys. Rev. Lett.*, vol. 113, p. 070404, 2014.

[59] J. Keeling, M. J. Bhaseen, and B. D. Simons, "Fermionic superradiance in a transversely pumped optical cavity," *Phys. Rev. Lett.*, vol. 112, p. 143002, 2014.

[60] P. Domokos, and H. Ritsch, "Collective cooling and self-organization of atoms in a cavity," *Phys. Rev. Lett.*, vol. 89, p. 253003, 2002.

[61] H. W. Chan, A. T. Black, and V. Vuletic, "Observation of collective-emission-induced cooling of atoms in an optical cavity," *Phys. Rev. Lett.*, vol. 90, p. 063003, 2003.

[62] A. T. Black, H. W. Chan, and V. Vuletic, "Observation of collective friction forces due to spatial self-organization of atoms: from rayleigh to bragg scattering," *Phys. Rev. Lett.*, vol. 91, p. 203001, 2003.

[63] M. Saffman, and Y. Wang, "Collective focusing and modulational instability of light and cold atoms," *Lect. Notes Phys.*, vol. 751, pp. 1–20, 2008.

[64] E. Tesio, G. R. M. Robb, T. Ackemann, W. J. Firth, and G.–L. Oppo, "Spontaneous optomechanical pattern formation in cold atoms," *Phys. Rev. A*, vol. 86, p. 031801, 2012.

[65] E. Tesio, G. R. M. Robb, T. Ackemann, W. J. Firth, and G.–L. Oppo, "Kinetic theory for transverse optomechanical instabilities," *Phys. Rev. Lett.*, vol. 112, p. 043901, 2014.

[66] G. Labeyrie, E. Tesio, P. M. Gomes, G.–L. Oppo, W. J. Firth, G. R. M. Robb, A. S. Arnold, R. Kaiser, and T. Ackemann , "Optomechanical self-structuring in a cold atomic gas," *Nat. Phot.*, vol. 8, pp. 321–325, 2014.

[67] G. R. M. Robb, E. Tesio, G.–L. Oppo, W. J. Firth, T. Ackemann, and R. Bonifacio, "Quantum threshold for optomechanical self-structuring in a bose-einstein condensate," *Phys. Rev. Lett.*, vol. 114, p. 173903, 2015.

[68] R. Bonifacio, L. De Salvo, "Collective resonant compton scattering by two-level particles," *Opt. Comm.*, vol. 115, pp. 505–510, 1995.

[69] R. Bonifacio, L. De Salvo, and W. A. Barletta, "Relativistic theory of the collective atomic recoil laser," *Nucl. Instrum. and Meth. in Phys. Res. A*, vol. 384, pp. 337–341, 1997.

[70] J. V. Moloney and A. C. Newell, *Nonlinear Optics*. Westview Press, 2004.

[71] P. C. W. Davies, *Quantum Mechanics*. Routledge & Kegan Paul, 1984.

[72] G. R. M. Robb, B. W. J. McNeil, R. Bonifacio and N. Piovella, "Dispersive optical bistability in cold atomic vapours," *Opt. Comm.*, vol. 194, pp. 151–165, 2001.

[73] R. Bonifacio, B. W. J. McNeil, N. Piovella, and G. R. M. Robb, "Recoil-induced effects in absorptive optical bistability," *Phys. Rev. A*, vol. 61, p. 023807, 2000.

[74] R. Grimm, M. Weidemûller, and Y. B. Ovchinnikov, "Optical dipole traps for neutral atoms," *Advances in Atomic, Molecular and Optical Physics*, vol. 42, pp. 95–170, 2000.

[75] A. T. Black, J. K. Thompson, and V. Vuletić, "Collective light forces on atoms in resonators," *Journal of Physics B: Atomic, Molecular and Optical Physics*, vol. 38, pp. 605–615, 2005.

[76] W. J. Brown, J. R. Gardner, D. J. Gauthier, and R. Vilaseca, "Amplification of laser beams counterpropagating through a potassium vapor: The effects of atomic coherence," *Phys. Rev, A*, vol. 56, pp. 3255–3261, 1997.

[77] M. Mitsunaga and N. Imoto, "Observation of an electromagnetically induced grating in cold sodium atoms," *Phys. Rev. A*, vol. 59, pp. 4773–4776, 1999.

[78] R. Bonifacio, G. R. M. Robb, and B. W. J. McNeil, "Propagation, cavity, and doppler-broadening effects in the collective atomic recoil laser," *Phys. Rev. A*, vol. 56, pp. 912–924, 1997.

[79] R. Bonifacio, L. De Salvo, "Analytical theory of the collective atomic recoil laser in the fel limit," *Appl. Phys. B*, vol. 60, pp. 233–239, 1995.

[80] R. Bonifacio, L. De Salvo, L. M. Narducci and E. J. D'Angelo, "Exponential gain and self-bunching in a collective atomic recoil laser," *Phys. Rev. A*, vol. 50, pp. 1716–1724, 1994.

[81] P. Domokos, and H. Ritsch, "Mechanical effects of light in optical resonators," *J. Opt. Soc. Am. B*, vol. 20, pp. 1098–1130, 2003.

[82] G. R. M. Robb, N. Piovella, A. Ferraro, R. Bonifacio, Ph.W. Courteille, and C. Zimmermann, "Collective atomic recoil lasing including friction and diffusion effects," *Phys. Rev. A*, vol. 69, p. 041403, 2004.

[83] A. Imamoglu, S. E. Harris, "Lasers without inversion: Interference of dressed lifetime-broadened states," *Opt. Lett.*, vol. 14, pp. 1344–1346, 1989.

[84] K.-J. Boller, A. Imamoglu, S.E. Harris, "Observation of electromagnetically induced transparency," *Phys. Rev. Lett.*, vol. 66, pp. 2593–2596, 1991.

[85] M. Yan, E. G. Rickey, and Y. Zhu, "Electromagnetically induced transparency in cold rubidium atoms," *J. Opt. Soc. Am. B*, vol. 18, pp. 1057–1062, 2001.

[86] G. R. M. Robb and B. W. J. McNeil, "Four-wave mixing with self-phase matching due to collective atomic recoil," *Phys. Rev. Lett.*, vol. 94, p. 023901, 2005.

[87] Y.-q. Li and M. Xiao, "Electromagnetically induced transparency in a three-level lambda-type system in rubidium atoms," *Phys. Rev. A*, vol. 51, pp. 2703–2706, 1995.